Freie Universität Berlin

Modelling NO_x concentrations at urban scales: model sensitivity, emissions and applications

Dissertation

zur Erlangung des Grades

eines Doktors der Naturwissenschaften

am Fachbereich Geowissenschaften

der Freien Universität Berlin

vorgelegt von

Friderike Kuik

Berlin, 2018

What would we have known about our atmosphere if it had not been polluted?
(Paul Crutzen, 2013)

Zusammenfassung

Luftverschmutzung durch Stickoxide ($NO_x = NO_2 + NO$) verusacht Atem- und Herz-Kreislauf-Erkrankungen. Stickoxide sind gleichzeitig eine wichtige Vorläufersubstanz für troposphärisches Ozon (O_3). Dieses widerum schädigt ebenso die menschliche Gesundheit, Ökosysteme und trägt zur Erwärmung des Klimas bei. Seit europäische Grenzwerte für NO_2 in 2010 eingeführt wurden, wurden sie regelmäßig überschritten, vor allem in Deutschland. Zudem halten Automobilhersteller, teilweise mutwillig durch den Einsatz von manipulierter Software, die NO_x-Emissions-Grenzwerte für Dieselautos nicht ein. Zusammengenommen machen die Grenzwertüberschreitungen und Emissionsgrenzwert-Missachtung es notwendig, weiterführende Maßnahmen zu treffen, um NO_x-Konzentrationen zu reduzieren und Emissionen besser zu kontrollieren. Darüberhinaus bestehen Wissenslücken in Bezug auf die weitergehenden Auswirkungen hoher städtischer NO_x-Konzentrationen auf die Luftqualität.

Um die oben genannten Fragen zur Luftqualiät zu beantworten und Maßnahmen zur Emissionskontrolle zu untersuchen, spielen Forschung und insbesondere Modellstudien eine wichtige Rolle. Diese Arbeit trägt auf verschiedenen Ebenen zur Literatur bei: Sie leistet einen Beitrag zur Weiterentwicklung der Modellwerkzeuge, die benötigt werden, um Luftqualität im städtischen Raum zu untersuchen. Weiterhin analysiert sie, inwiefern NO_x-Emissionen aus dem Straßenverkehr - die wichtigste NO_x-Emissionsquelle im städtischen Raum - in einem gängigen Emissionsinventar unterschätzt werden könnten. Der entwickelte Modellaufbau kommt dann zur Anwendung, um zu untersuchen, inwieweit NO_2-Konzentrationen reduziert werden könnten, wenn Emissionsgrenzwerte im Verkehr eingehalten würden. Weiterhin wird in dieser Arbeit analysiert, wie viel Emissionen biogener flüchtiger organischer Substanzen (VOCs, volatile organic compounds) - eine weitere Vorläufersubstanz von O_3 - in der Stadt zu städtischen O_3-Konzentrationen während einer Hitzewelle beitragen. Die Ergebnisse sind in vier publizierten Artikeln präsentiert, die alle auf Modellstudien mit der Chemie-Version des "Weather Research and Forecasting Model" (WRF-Chem) basieren und den Großraum Berlin-Brandenburg als Fallstudie betrachten.

Der erste Artikel stellt den verwendeten WRF-Chem-Modellaufbau für Berlin-Brandenburg vor und evaluiert ihn, als Basis für die weiteren Artikel dieser Arbeit. Modellsimulationen zeigen, dass eine horizontale Modellauflösung von 3kmx3km sowohl die simulierte Meteorologie als auch die Chemie verbessert, im Vergleich zu einer Auflösung von 15kmx15km. Die Ergebnisse der Studie weisen weiterhin darauf hin, dass eine detailierte Beschreibung der städtischen Gegebenheiten (z.B. Landnutzung, Stadtstruktur) basierend auf lokal verfügbaren Daten die modellierte Meteorologie und Luftchemie verbessert. Modellierte NO_x -Konzentrationen und deren räumliche Verteilung können verbessert werden, wenn die Auflösung der Emissions-Eingangsdaten der hohen Model-

lauflösung angepasst wird. Dennoch zeigen die Ergebnisse auch, dass die simulierten NO_x-Konzentrationen die Messwerte insbesondere tagsüber an Wochentagen unterschätzen.

Diese Ergebnisse sowie auch eine Analyse im zweiten Artikel basierend auf gemessenen NO_x-Konzentrationen und Verkehrszählungen weisen darauf hin, dass Verkehrsemissionen unterschätzt werden und eine der Hauptfehlerquellen der NO_x-Unterschätzung im Modell darstellen. Im zweiten Artikel wird dann ein Korrekturfaktor für NO_x-Emissionen aus dem Straßenverkehr berechnet, wobei auch andere mögliche Fehlerquellen wie beispielsweise eine tagsüber zu starke Durchmischung der Atmosphäre berücksichtigt werden. Laut den Berechnungen werden NO_x-Emissionen aus dem Straßenverkehr tagsüber und an Wochentagen um ca. einen Faktor 3 im städtischen Kernbereich unterschätzt. Über die ganze Woche gemittelt entspricht dies einer Unterschätzung der NO_x-Verkehrsemissionsn von ca. einem Faktor 2, und einer Unterschätzung von NO_x-Emissionen insgesamt von ca. einem Faktor 1.5. Eine Anwendung dieses Faktors auf die Emissions-Eingangsdaten verbessert die modellierten NO_x-Konzentrationen im Kerngebiet der Stadt sowie auch in den in Windrichtung gelegenen vorstädtischen Gebieten. Insgesamt weisen die Ergebnisse darauf hin, dass weitere Studien notwendig sind, um NO_x-Emissionsfaktoren für den Verkehr präziser zu bestimmen und offizielle Emissionsdatenbanken - die hier als Eingangsdaten dienen - zu verbessern.

Der dritte Artikel wendet den entwickelten und evaluierten Modellaufbau sowie auch einen Modellaufbau mit gröberer Auflösung an und präsentiert Sensitivitäts-Studien. Diese analysieren, inwieweit NO_2-Konzentrationen gesenkt werden könnten, wenn Emissionsgrenzwerte im Verkehr eingehalten würden. Die Modellstudien werden kombiniert mit einer auf Messungen basierenden Analyse. Die Ergebnisse beider Ansätze sind konsistent und weisen darauf hin, dass NO_2-Konzentrationen im städtischen Hintergrund um 1.2 - 2.7 μg m^{-3} und entlang von Straßen um 9.0 - 23.0 μg m^{-3} verbessert werden könnten, würden die strengsten Standards der US EPA eingehalten. Deutliche Verbesserungen wären allerdings auch zu erwarten, würden europäische Standards eingehalten.

Im vierten Artikel geht es um weitergehende Konsequenzen hoher städtischer NO_x-Konzentrationen. Die Studie quantifiziert den Beitrag von biogenen VOC-Emissionen aus städtischer Vegetation zu O_3-Kontentrationen während einer Hitzewelle. Laut den Modellergebnissen tragen biogene VOC-Konzentrationen an einzelnen Tagen während der Hitzewelle bis zu 60% zur Ozon-Entwicklung bei, im Vergleich zu einem Beitrag von im Schnitt 17%-20% während des gesamten Monats. Dies zeigt, dass Umweltmaßnahmen in der Stadt in ihrer Ganzheit betrachtet werden müssen, damit Städte auch ganzheitlich davon profitieren können. Die Begrünung von Städten, beispielsweise, ist vorteilhafter für die Luftqualität wenn gleichzeitig anthropogene Ozon-Vorläufersubstanzen (NO_x, VOCs) reduziert werden, beispielsweise im Verkehrsbereich.

Abstract

Nitrogen oxides ($NO_x = NO_2 + NO$) cause respiratory and cardiovascular diseases, and are an important precursor of tropospheric ozone (O_3), in turn damaging human health, ecosystems and warming the climate. Since the introduction of European NO_2 limit values in 2010, these have been frequently exceeded, especially in Germany. In addition, car manufacturers do not comply with NO_x emission limit values for diesel cars, with some of them having implemented defeat devices to suggest compliance. Together, the exceedance of limit values and non-compliance with emission thresholds make action on reducing NO_x concentrations and more stringent NO_x emission control policies necessary. Beyond that, knowledge gaps exist concerning the broader consequences of high urban NO_x concentrations for overall urban air quality.

Research and in particular modelling play an important role for assessing above-mentioned air quality issues and emission control measures in their context. This thesis contributes to the literature in several ways: it contributes to the development of the modelling tools needed for studying air quality at urban scales and assesses the potential underestimation of traffic NO_x emissions - the most important source of NO_x emissions in urban areas - in a commonly used emission inventory. It then applies the developed model setup, analyzing to what extent urban NO_2 concentrations could be reduced if vehicle emission standards were met. It also assesses the contribution of urban biogenic volatile organic compound (VOC) emissions - another important precursor of O_3 - to O_3 concentrations during a heat wave. The research is presented in four published articles, all based on modelling studies using the chemistry version of the Weather Research and Forecasting model (WRF-Chem), and using the Berlin-Brandenburg area as a case study.

The first article presents and evaluates a WRF-Chem setup for Berlin-Brandenburg, building the basis for the other articles in this thesis. It finds that a horizontal model resolution of 3km x 3km improves both modeled meteorology and chemistry compared to a 15km x 15km horizontal resolution. The article further finds that when modelling air quality in urban areas at high resolution, a detailed description of the urban area based on locally available input data is beneficial. For modelling NO_x concentrations, the study finds a better representation of local pollution patterns when downscaling the emission inventory to the model resolution. However, modelled NO_x concentrations are underestimated compared to observations, particularly on weekdays during daytime.

The results from the model evaluation as well as an analysis based on observed NO_x concentrations and traffic counts in the second article suggest that an underestimation of traffic emissions is one of the main sources of the model bias. Also taking into account other potential sources of model bias such as too strong mixing during daytime, the study

then calculates a correction factor for traffic NO_x emissions. It finds that traffic NO_x emissions are underestimated by a factor of ca. 3 during daytime on weekdays in the core urban area, corresponding to an underestimation of weekly mean traffic NO_x emissions in the core urban area of ca. a factor of 2 and an underestimation of total NO_x emissions in the city centre by a factor of ca. 1.5. Applying this correction factor improves modelled NO_x concentrations in the core urban area as well as downwind of the city. The results suggest that further research is needed in order to better specify NO_x emission factors used for officially reported emissions.

The third article applies the WRF-Chem setup, as well as a coarser setup covering a larger domain, and presents sensitivity simulations looking at how much NO_2 concentrations could be improved if vehicle emission standards were met. It combines the model-based assessment with an analysis based on measurement data. The results from the different approaches are consistent and suggest that NO_2 concentrations could be improved by 1.2 - 2.7 μg m^{-3} in the urban background and 9.0 - 23.0 μg m^{-3} at the roadside if the strictest US EPA standards were met. Considerable improvements of urban air quality could also be expected if car manufacturers would comply with European emission limits.

The fourth article looks at broader consequences of high urban NO_x concentrations, and is aimed at quantifying the contribution of VOC emissions from urban vegetation to O_3 concentrations during a heatwave. The results suggest that on specific days during the analyzed heatwave period the contribution of biognic VOCs to ozone formation reaches up to 60%, compared to average contributions of 17% to 20% during the month of the heatwave. This shows that urban environmental measures need to be assessed comprehensively in order for cities to fully benefit from them. For example, urban tree planting campaigns would have to be accompanied by a reduction of anthropogenic sources of O_3 precursors (NO_x, VOCs), e.g. in the area of road transport.

Contents

1. Introduction

1.1. Air pollution: a threat for human health, climate and ecosystems

1.1.1. NO$_x$ air pollution in Europe

In May 2018, the European Commission announced legal action against seven European countries, who continue to breach EU law on air pollution limit values and disregard rules on vehicle type approvals concerning air pollutant emissions. Amongst them is Germany, which the European Commission is referring to the European Court of Justice for disrespecting air quality limit values for nitrogen dioxides (NO$_2$) whilst failing to take suitable measures to keep exceedances to short periods. In addition, the European Commission has formally informed Germany about non-compliance with vehicle type approval rules, which should hinder car manufacturers from breaking EU laws on emission thresholds.[1]

The EU limit value for annual mean NO$_2$ concentrations of 40 μg m^{-3} has been in force since 2010, and has since been exceeded regularly at many measurement stations. In 2015, the limit value was exceeded at 10.5% of all EU NO$_2$ monitoring stations. On average, EU measurement stations recorded the highest values in Germany (EEA, 2017). In the EU, 98% of the NO$_2$ limit value exceedances take place in urban areas and particularly at roadside measurement stations (EEA, 2017), which is linked to the main source sector of NO$_x$ (= NO$_2$ + NO) emissions: road transport. While gasoline vehicles emit only a small amount of NO$_x$, diesel vehicles are the main contributors to traffic NO$_x$ emissions (see Section 1.2.1).

Though emissions of NO$_x$ are generally decreasing in Europe (Stocker et al., 2013), annual limit values would still be exceeded at 7% of the measurement stations in 2020 if the current trend was extrapolated (EEA, 2016). In addition, NO$_x$ emissions have recently shifted back into the public debate, triggered by the discovery of the large-scale use of defeat devices in diesel cars by research of the West Virginia University (Thompson et al., 2014). Through the use of defeat devices, emissions under test conditions are intentionally reduced

---

[1] `http://europa.eu/rapid/press-release_IP-18-3450_en.htm`, last access: 1 July 2018.

compared to what would be emitted under real-world driving conditions. However, actual emissions measured under real-driving conditions are also higher than those measured in the lab without the use of defeat devices, due to deficiencies in testing procedures (Bishop and Stedman, 2015), and official emission inventories already assume higher emissions per kilometer driven (emission factors, see Section 1.2.1) than those that are legally allowed. Overall, studies find a difference between NO_x emissions measured in the lab and on road of up to a factor of 4-20 (depending on the car type, e.g. EMEP/EEA, 2014; Fontaras et al., 2014; Hagman et al., 2015).

The impact of NO_x concentrations is both direct and indirect: exposure to NO_2 (both long-term and short-term) is associated with respiratory and cardiovascular effects, and increases in all-cause mortality (Faustini et al., 2014; Mills et al., 2015). On the other hand, NO_x is a precursor for other air pollutants, including particulate matter (PM) and tropospheric ozone (O_3), which also impact health, damage ecosystems and contribute to climate change (see Section 1.1.2).

Overall, air pollution is the single largest environmental factor of premature deaths both worldwide and in Europe (OECD, 2012). The estimates for premature deaths caused by air pollution have consistently increased, with most recent studies attributing about 6.5 mio. premature deaths worldwide to ambient air pollution in 2015 (Landrigan et al., 2017). Up to 400 000 premature deaths are attributed to air pollution in Europe (EEA, 2015), and ca. 38 000 premature death are attributed to increased $PM_{2.5}$ and O_3 concentrations through excess diesel NO_x emissions only (Anenberg et al., 2017).

In view of its detrimental impacts, the exceedance of limit values and non-compliance with emission thresholds make action on reducing NO_x concentrations and emissions necessary. While the implementation and surveillance of emission reduction measures is under the responsibility of policy makers, research and in particular modelling plays an important role for assessing air quality issues (e.g. Giordano et al., 2015) and emission control measures in their context.

This thesis contributes to the literature by further developing and evaluating some of the tools and data available for studying urban NO_x air pollution and its impacts, and by applying the developed model setup to analyze the impact of non-compliance with diesel emission limits and to assess broader air quality consequences of high urban NO_x emissions. Specifically, a setup of the frequently used chemistry version of the Weather Research and Forecasting model (WRF-Chem, Fast et al., 2006; Grell et al., 2005; Skamarock et al., 2008) is evaluated. In contrast to most studies published in the literature, the model is used here at very high spatial resolutions, and it is then tested what resolution and level of detail in the input data is needed in order to simulate urban air quality. In a top-down approach, the model is then used to estimate the potential underestimation of

traffic NO_x emissions in a commonly used inventory based on officially reported emissions. The applications of the developed setup presented in this thesis include an assessment of how much air quality could be improved if emission standards were met by diesel vehicles, and an analysis of the effect of VOC emissions from urban vegetation on air quality during a heatwave. The Berlin-Brandenburg urban area is used as a case study throughout the thesis.

The research topics are introduced in more detail in the remainder of this introduction: it first broadens the view on air pollution, then elaborates on the sources, chemistry and physics of air pollutants and in particular NO_x, and gives an introduction to air quality modelling. The research questions are then further specified in Section 1.4, and an overview of the articles contributing to this thesis is presented.

1.1.2. Air pollution and its broader context

"For the past three centuries, the effects of humans on the global environment have escalated" (Crutzen, 2002). Anthropogenic emissions of NO_x and resulting air pollutant concentrations that harm human health are only part of that picture. More broadly, air pollution is intimately linked to human-made climate change and different areas of sustainable development.

Air pollution and climate change are linked in several ways (e.g., Melamed et al., 2016; Schmale et al., 2014; Shindell et al., 2012; von Schneidemesser et al., 2015). Firstly, air pollutants and greenhouse gases have the same sources. For example, NO_x is emitted during combustion processes, e.g. burning of fossil fuel in cars or industrial processes - the same processes emit CO_2, the main driver of anthropogenic climate change. Secondly, many substances in the atmosphere act both as air pollutants and climate forcers. Ozone, for example, has detrimental impacts for human health as an air pollutant, but also a positive radiative forcing and thus warms the climate. Other air pollutants, however, cool the earth's surface and thus mask a warming atmosphere (e.g., Ramanathan and Feng, 2009), which may lead to a dilemma when considering measures to reduce air pollution or climate change. Thirdly, a changing climate might also impact air pollution, either directly through the physical and chemical impacts, or indirectly via changed emission patterns due to a changing climate. For example, a changing climate, with (amongst others) warmer and more frequent heat waves, might increase O_3 production or the emission of O_3 precursors (see Section 1.2.3).

Air pollution is also linked to sustainable development and quality of life, as for example recognized in the UN Sustainable Development Goals[2]. One important example are urban areas, already now home to more than half of the world's population. Both emissions and impacts of air pollution are often particularly concentrated in cities. This means that the urban population is often most exposed to adverse health impacts of air pollution, but also influences emissions through (voluntary or policy-motivated) behavior changes. Beyond that, sources of air pollution in cities have other adverse effects. For example, road transport also causes noise pollution, disturbs habitable spaces and can cause death and injuries. At the same time, road infrastructure is vital for citizens' quality of life and economic development (Schmale et al., 2015), and emission reduction measures might unequally impact parts of the population that are already socially disadvantaged.

These examples illustrate the relevance of air pollution in the context of global environmental and societal changes. In the case of air pollution, many problems have been recognized long ago. However, the examples given above show that not enough progress has been made in designing and implementing effective mitigation measures. As introduced in Section 1.1.1, this poses a challenge to both science and policy, or collaborative efforts of both at their interface. However, existing literature suggests that the science-policy interface so far seems inadequate to address these challenges, and that new approaches are needed (see, e.g., Kates et al., 2001). An inter- or transdisciplinary research approach, integrating scientific, expert and other types of knowledge, might be a solution for addressing air pollution in its context (see Section 2.3).

1.2. Sources, chemistry and physics of air pollution

1.2.1. Emissions of NO_x

Nitrogen oxides are mainly produced during combustion, through two processes. Oxidation of organic nitrogen contained in fuel, and oxidation of molecular nitrogen from air. The latter happens at high temperatures, where oxygen (O_2) thermolyzes, and O reacts with nitrogen (N_2) to produce NO (Jacob, 1999):

$$O_2 \quad \overset{heat}{\Longleftrightarrow} \quad O + O \tag{1.1}$$

$$O + N_2 \quad \Longleftrightarrow \quad NO + N \tag{1.2}$$

$$N + O_2 \quad \Longleftrightarrow \quad NO + O \tag{1.3}$$

[2]In particular it is linked to goals 3, 6, 7, 11, 12, 13 and 15; `https://www.un.org/sustainabledevelopment/sustainable-development-goals/`

NO_x formation during combustion is increased with increasing temperature, as the equilibria are shifted to the right at high temperature (Jacob, 1999). NO_x is mainly emitted as NO, but rapidly reacts with oxygen-containing species in the atmosphere to form NO_2 (e.g. Jacob, 1999):

$$NO + O_3 \rightarrow NO_2 + O_2 \tag{1.4}$$

$$NO + HO_2 \rightarrow NO_2 + OH \tag{1.5}$$

Primary NO_2 is normally produced at comparably small quantities during combustion processes. Its engine-internal formation mechanisms are less well known, but assumed to exclusively take place via NO (Rößler et al., 2017). Beyond that, a recently observed increase in the primary NO_2 fraction in diesel exhaust is associated with the use of exhaust after treatment technologies such as particulate traps and oxidation catalysts (e.g. Grice et al., 2009).

Beyond road transport, the main emission source sectors of NO_x in urban areas are the production and distribution of energy, industrial combustion, non-road transport and residential combustion (see Fig. 1.1 for the example of Berlin). Globally, anthropogenic sources contribute more than 75% to total (tropospheric) NO_x emissions (Seinfeld and Pandis, 2016).

Emissions are estimated from a combination of activity data (e.g. fuel burnt) and emission factors. Emission factors for road transport emissions depend on the fuel type and the car type (heavy duty or light duty, exhaust treatment) as well as on the driving conditions including road type and speed (e.g. Hausberger and Matzer, 2017). While activity data are only assumed to have an uncertainty of ca. 5%-10%, the emission factor is more difficult to quantify in many cases (Kuenen et al., 2014, and references therein). Emission factors for road transport, for example, may have an error range between 50% and 200%, while emission factors for energy industry emissions are much better constrained with an error range between 20% and 60% (Kuenen et al., 2014).

The individual contribution of the different NO_x sources varies throughout the year, week and day as well as with their emission height (also see Section 2.1.3). For example, industry and energy production emit NO_x from factory stacks higher above ground level, potentially leaving a comparably greater role of traffic emissions for surface NO_x concentrations. With traffic being the main emission source of NO_x in urban areas, emissions follow a distinct temporal pattern, with higher emissions during weekdays and traffic rush hours in the morning and evening. This temporal pattern can also be observed in NO_x concentrations at roadside measurement stations. Consequently, these variations are important to take into account when modelling NO_x concentrations.
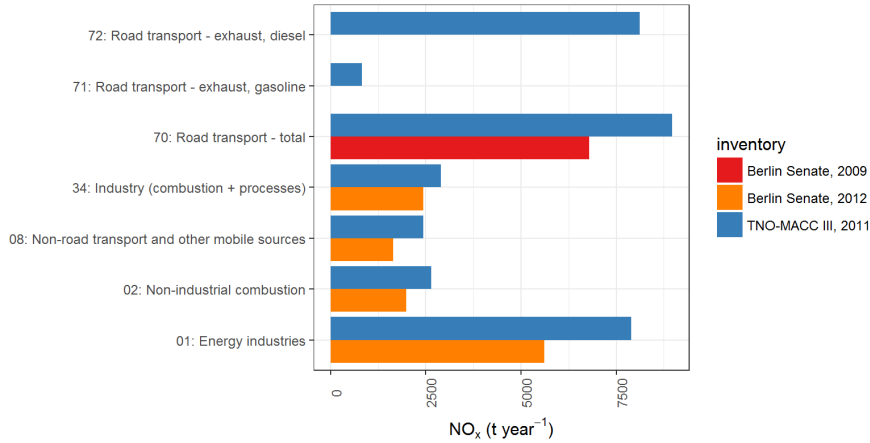
Figure 1.1.: NO$_x$ emissions in Berlin calculated from the TNO-MACC III inventory (Kuenen et al., 2014) and inventories of the Berlin Senate Department for the Environment, Transport and Climate (Berlin Senate Department for the Environment and Protection). The emissions shown for TNO-MACC III are downscaled to a horizontal resolution of 1km x 1km based on local proxy data (see Section 2.1.3). Categories with comparably negligible NO$_x$ emissions in Berlin are not shown in this figure, they include the extraction and distribution of fossil fuels, waste treatment, agriculture and road transport exhaust emissions from other fuels.

1.2.2. The role of NO$_x$ and VOCs for O$_3$ formation

Once emitted, NO$_x$ has an atmospheric lifetime in the troposphere of ca. 1 day and plays an important role for atmospheric chemistry (Seinfeld and Pandis, 2016). Of major importance for air quality is its role as one of the two major precursors of O$_3$, leading to the formation of O$_3$ in the presence of sunlight:

$$NO_2 + h\nu \quad \rightarrow \quad NO + O \tag{1.6}$$
$$O + O_2 \quad \rightarrow \quad O_3 \tag{1.7}$$

The photochemical cycle of NO, NO$_2$ and O$_3$ is closed by reaction of O$_3$ with NO (Equation 1.4). If no sunlight is present, Equation 1.4 leads to the destruction of O$_3$ if NO is present (termed NO$_x$ titration, Sillman, 1999).

The other major class of O$_3$ precursors are volatile organic compounds (VOCs), which are emitted both by anthropogenic and biogenic sources (e.g. plants). VOCs lead to O$_3$ production by reaction with a hydroxyl radical (OH), leading to the formation of an organic peroxy radical (RO$_2$), and subsequently to the formation of HO$_2$ and NO$_2$:

$$VOC + OH + O_2 \quad \rightarrow \quad RO_2 + H_2O \tag{1.8}$$

$$RO_2 + NO + O_2 \quad \rightarrow \quad secondary VOC + HO_2 + NO_2 \tag{1.9}$$

Then, HO_2 reacts with NO to produce NO_2 via Equation 1.5. As a net reaction, two molecules of NO_2 are thus produced, leading to the formation of O_3 via Reactions 1.6 and 1.7. Whether Reactions 1.8 and 1.9 dominate the process of O_3 formation depends on the availability of odd hydrogen radicals (HO_x = OH + HO_2 + RO_2). These are removed via the following reactions:

$$HO_2 + HO_2 \quad \rightarrow \quad H_2O_2 + O_2 \tag{1.10}$$

$$RO_2 + HO_2 \quad \rightarrow \quad ROOH + O_2 \tag{1.11}$$

$$OH + NO_2 \quad \rightarrow \quad HNO_3 \tag{1.12}$$
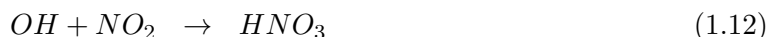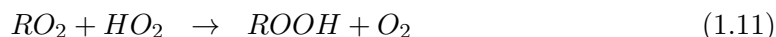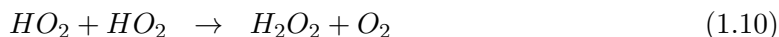
If the dominant sink for odd hydrogen is nitric acid (HNO_3), OH decreases with increasing NO_x, and O_3 formation is controlled by Reaction 1.9: O_3 increases with increasing VOC and decreases with increasing NO_x (Sillman, 1999).

Thus, O_3 concentrations and its changes depend on the ratio of VOC to NO_x concentrations in the atmosphere. At a high ratio of VOC to NO_x (low-NO_x), O_3 production increases linearly with NO concentrations (NO_x-limited or NO_x-sensitive regime). At a low ratio of VOC to NO_x (high-NO_x), O_3 increases with VOCs, but decreases with increasing NO_x (NO_x-saturated or VOC-sensitive regime, Reactions 1.8 and 1.9) (Seinfeld and Pandis, 2016; Sillman, 1999). Consequently, urban areas with high NO_x emissions are often VOC-sensitive, with O_3 concentrations in these areas being sensitive to changes in VOC emissions.

This complex relationship illustrates that the broader consequences of high urban NO_x concentrations go beyond the adverse effects of NO_x itself. For air pollution control strategies, this implies that measures targeting the reduction of NO_x will not successfully reduce O_3 concentrations in a VOC-sensitive regime. Both NO_x and VOC emissions need to be controlled when aiming at reducing overall air pollution, and knowledge of the chemical regime of an area is necessary in order to reduce air pollution by both NO_x and O_3 (Jacob, 1999). Thus, the broader consequences of high urban NO_x concentrations need to be investigated with air quality modelling, which however requires reliable information of NO_x and VOC emissions.

1.2.3. The influence of atmospheric dynamics on air pollution

During their lifetime in the atmosphere, air pollutants are strongly influenced by meteorological conditions, including temperature and solar radiation, but also by wind speed and direction, humidity, precipitation, and the evolution of the planetary boundary layer. With constant emissions, the influence of meteorological conditions can determine whether the air at a given time is "clean" or "polluted" (e.g. Seinfeld and Pandis, 2016).

Planetary boundary layer and atmospheric stability

Vertical mixing of air pollutants depends on the stability of the atmosphere in the planetary boundary layer or mixed layer, which includes the lowest few hundred meters of the troposphere. Atmospheric stability can be described by considering the motion of an air parcel in the atmosphere: motion in the atmosphere (e.g. turbulence) displaces the air parcel upward or downward. Upon displacement, the parcel can either continue moving in the same direction of displacement (unstable atmosphere), stay at the new position (neutral atmosphere) or return to the old position (stable atmosphere). The stability of the atmosphere depends on the sign of the potential temperature[3] gradient of the atmosphere: it is unstable if the potential temperature gradient is negative, neutral if the gradient is zero and stable if the gradient is positive (Seinfeld and Pandis, 2016).

The exact depth of the mixed layer varies diurnally, as does atmospheric stability. The diurnal variations are caused by the heating of the ground due to solar radiation during the day, and radiative cooling at night. With sunrise, the earth's surface warms, and subsequently the lower layers of the atmosphere are warmed up. The subsequently warming atmosphere leads to convective mixing and a deepening of the mixed layer, with an unstable atmosphere in which an air parcel can continue to rise. After sunset, the earth's surface cools more rapidly than the atmosphere, cooling the lowest layers of the atmosphere. As a consequence, the temperature of the atmosphere increases with height (temperature inversion) and the atmosphere is stable. The inversion is then broken up during the morning hours with the warming of the atmosphere as described above (Seinfeld and Pandis, 2016).

In addition, atmospheric stability might also be influenced by larger scale circulation patterns. A subsidence inversion is related to sinking air masses in a high pressure cell, warming as a result of the downward motion and that way reaching a higher temperature than the air masses below (Seinfeld and Pandis, 2016).

---

[3]The potential temperature is the temperature of an air parcel brought adiabatically from its position to the surface

Atmospheric stability is crucial for the mixing of air pollutants: emissions mix more efficiently and are thus diluted into a larger volume under unstable atmospheric conditions (e.g. during daytime). Under stable atmospheric conditions (e.g. in the early morning hours or at nighttime), air pollutants are trapped below the inversion layer and accumulate, leading to increased concentrations. Thus, besides activity-related variations in emissions discussed in Section 1.2.1, the diurnal (and seasonal, e.g. due to differences in solar radiation in summer and winter) variations of the planetary boundary layer strongly influence air pollutant concentrations. As an example, combining both effects - a stable atmosphere in early morning hours or evening hours with peak rush hour emissions from traffic - may lead to particularly high levels of NO_x air pollution at those times.

Temperature, wind and precipitation

Temperature and solar radiation impact atmospheric chemistry in several ways: first, as just discussed, the atmospheric temperature profile determines the stability of the atmosphere and thus the extent to which air pollutants are vertically mixed. Second, air chemistry, most importantly O_3 production, is temperature- (Coates et al., 2016) and irradiation-dependent (Reaction 1.6). Third, air pollutant emissions themselves are temperature-dependent, e.g. with higher emissions from residential combustion (heating) in winter, and even diesel NO_x emissions depending on temperature - with an increase in emissions with decrease in temperature (Hausberger and Matzer, 2017). This temperature-dependence of emissions influences the temporal variations of emissions discussed in Section 1.2.1.

Wind speed and direction influence the horizontal transport of air pollutants (Brunner et al., 2015), and thus also air pollutant concentrations close to the emission sources. Depending on the atmospheric lifetime of the species, they can be transported on spatial scales from a few kilometers (e.g. NO_x), a few hundred to thousands of kilometers (e.g. O_3) to global scales (e.g. methane). Similarly, wind speed and direction influence pollution hot spots: for example, O_3 concentrations downwind of the main NO_x emission sources are often higher than directly at the source, as less NO is available for O_3 destruction (Reaction 1.4, e.g. Rodes and Holland, 1981).

Humidity influences the aqueous phase chemistry of the atmosphere, including the formation of particles and cloud droplets. Precipitation, on the other hand, is important for the (wet) removal of water soluble air pollutants and particles (Brunner et al., 2015).

Processes in the urban area

In urban areas, the meteorological processes just discussed depend in addition on the city itself. Cities are usually warmer than the surrounding areas due to the urban heat island effect, with anthropogenic heat sources such as industrial facilities or air conditioning warming the air. At the same time, buildings and paved surfaces store heat during the day and emit it during the night, which may lead to particularly large differences in air temperature between cities and the surrounding areas at nighttime (Grimmond, 2007).

High temperatures in cities, especially if the urban heat island effect is reinforced by a heat wave, can impact air quality. An important example is the observation that heat waves have been accompanied by extremely high levels of O_3 (Vautard et al., 2005). This can be due to a combination of factors such as higher O_3 production with higher temperatures and solar radiation, but also increased emissions of biogenic VOCs from urban vegetation with higher temperatures, enhancing O_3 production in a NO_x-saturated environment (Lee et al., 2006). The latter influence might become particularly relevant with a changing climate, in which more frequent and warmer heat waves are expected (Stocker et al., 2013). Though studies exist that aim at assessing the impact of a warming climate on air quality, there are still large uncertainties. In particular, the relative contribution of biogenic VOC emissions to episodes of high air pollution in mid-latitude cities have not been quantified.

1.3. Modelling air pollution

Increased concerns of adverse impacts of air pollution on human health and ecosystems have driven the development of air quality models at different scales in the last four decades (Rao et al., 2011).

Different model types exist for air quality modelling, which differ in the way in which the dispersion of air pollutants into the atmosphere is formulated mathematically, but also differ in complexity, resolution and consequently spatial scale on which they can be applied. The most widely used type of model in both air quality planning and research in Europe are mesoscale chemistry transport models (Thunis et al., 2016). Mesoscale refers to the spatial extent typically covered by these models, and implies a coverage of some tens to hundreds of kilometers. These models belong to the class of Eulerian models, characterized by mathematically describing the behavior of species relative to a fixed coordinate system (Seinfeld and Pandis, 2016).

A subset of mesoscale chemical transport models used for air quality research explicitly takes into account the tight linkages of air pollutants with meteorology. These so-called

online (integrated) meteorology chemistry transport models (Baklanov et al., 2014) calculate gaseous and particulate pollutant transport and chemistry at the same time and on the same grid as atmospheric dynamics including meteorological parameters such as temperature, wind speed and humidity. As an alternative, offline chemistry transport models continuously read meteorological data calculated with other modelling systems as input and, based on this, calculate pollutant transport and chemistry.

It is argued that online-coupled models represent the atmosphere more realistically (as the different processes are connected also in reality), are numerically more consistent when forecasting air quality and allow for considering feedback mechanisms (Grell and Baklanov, 2011). Offline-coupled models, on the other hand, have a lower computational cost and are thus usually more flexible in specifying a range of different scenarios or ensembles. However, offline approaches require pre-processing of meteorological input data. At high model resolutions, Grell and Baklanov (2011) note that the additional computational cost of running an online-coupled model might be offset, as the additional processing cost of input data in offline models increases with higher (spatial and temporal) resolutions. However, Grell and Baklanov (2011) also note that more research is needed for showing that online-coupled models perform well enough for application in operational air quality forecasting and regulatory emission work.

One very widely used online-coupled model is the chemistry version of the Weather Research and Forecasting Model (WRF-Chem, Fast et al., 2006; Grell et al., 2005; Skamarock et al., 2008), which is the model used for the studies contributing to this thesis and introduced in greater detail in Chapter 2.

1.3.1. Air quality modelling at urban scales

Though chemical transport models were initially developed for regional scales, they are increasingly also used at urban scales and horizontal resolutions of down to ca. 1 km x 1km.

In urban areas, high model resolutions and a representation of the urban structure are needed when studying the impact of local emission sources on urban air quality, as air pollutant dispersion within an urban area depends not only on the mesoscale meteorological situation, but also on the influence of dynamic effects of the urban structure, thermal exchange between the urban environment and surrounding air, or even traffic induced turbulence (Thunis et al., 2016, also see Section 1.2.3). In the WRF model, these effects are taken into account through a sub-grid scale parameterization of the urban processes (e.g. Chen et al., 2011; Loridan et al., 2010). Parameterizations of different complexities are

available, requiring detailed input data about the structure and thermal characteristics of the urban area (also see Section 2.1.2).

From an application perspective, high model resolutions are also needed e.g. when assessing health effects of air pollution and the exposure of the urban population, which depends on the pollution field and the urban population density. Both might vary considerably throughout the city.

However, increasing the model resolution does not necessarily guarantee better model results. It might strongly increase the computational cost and must be done in consistency with available model input data: several studies have assessed the resolution-dependent model performance for simulating different air pollutants and concluded that increasing the model resolution does improve the model performance at urban stations, but requires emission data at similarly high spatial and temporal resolution (e.g. Schaap et al., 2015, and references therein). They emphasize that it is only useful to go to model resolutions finer than 20 km if the model input data are also available at similarly high resolutions. Other studies note that grid sizes down to a few km cannot be applied for operational regional modelling due to high data demands and computational cost (Colette et al., 2014). Performing air quality simulations in Mexico city, Tie et al. (2007, 2010) have explicitly assessed how the model resolution impacts the simulated ozone and ozone precursors in an online-coupled model, and concluded that a resolution of 24 km is not suitable for simulating concentrations of CO, NO_x and O_3 in the city center. They suggest a ratio of city size to model resolution of 6 : 1 for Mexico City, and also recommend this ratio as a test value in other urban areas for setting the model resolution.

Considering these results, a careful model configuration and setup is needed when simulating air quality at high resolution in urban areas. It remains to be assessed in greater detail which model options and input data specifications might lead to promising results, especially at very high horizontal resolutions down to 1km x 1km.

1.3.2. Model evaluation

A model evaluation - the comparison of model results to measured meteorological and chemical species - helps assess how well the model captures observed conditions and can support the decision of whether a model (setup) is suitable for a given application.

Different networks of measurement stations exist that monitor air quality (e.g. O_3, NO_x, PM). These are for example used to validate compliance with air quality limit values, but the use for research, including model evaluations, is also widespread. A commonly used database of air quality measurements in Europe is AirBase (EEA, 2017), where air quality information reported by EU member states and cooperating countries is collected. The

stations included in the database are classified by the type of conditions they represent, e.g. rural or urban background conditions, or conditions directly at the emission source such as along a road or near industrial facilities. For the comparison of model results with measurement data, and particularly for the evaluation of simulated air quality, it is important to compare with station measurements that represent scales which can also be represented by the model. Depending on the model resolution, chemical transport models can typically represent rural and urban background conditions.

The specific purpose of a model evaluation might vary depending on the model application. Commonly, an "operational" model evaluation is done, calculating aggregated model performance statistics. For example, Pernigotti et al. (2013) and Thunis et al. (2012) calculate model performance indicators, which they compare against benchmarks to assess whether a model setup can be used to support policy. However, this kind of operational evaluation merely diagnoses model errors, but does not relate them to specific processes being misrepresented in the model.

Several recent studies (e.g. Solazzo et al., 2017a,b) pursue a "diagnostic" model evaluation aimed at understanding the errors related to different processes as a basis for model improvements. The diagnostic evaluation is based on a spectral decomposition of both modeled and observed time series of air pollutants into components representing variations on different time scales. The spectral decomposition uses a Kolmogorov-Zurbenko filter (Zurbenko, 1986), essentially iteratively applying a moving average to the selected time series. The error of each component can then be assessed individually by "error apportionment" (Solazzo et al., 2017a), breaking down the mean square error into bias, variance error and minimum achievable mean square error. These can then more easily be related to errors of different processes in the model. Further detail on this procedure is given in Article 2 and its supplementary material as well as in Section 2.2.

1.3.3. Modelling NO_x concentrations in Europe

Recent findings on modelling NO_x concentrations in Europe

Recently, several studies have been published comparing the performance of different online- and offline-coupled regional models, including many setups using WRF-Chem (e.g. Badia and Jorba, 2015; Baró et al., 2015; Bessagnet et al., 2016; Brunner et al., 2015; Forkel et al., 2015; Giordano et al., 2015; Im et al., 2015a,b; Knote et al., 2015; Solazzo et al., 2017a,b). In addition to that, many individual studies have published evaluations of WRF-Chem setups (e.g. Mar et al., 2016; Tucella et al., 2012; Žabkar et al., 2015) and other models.

Many of these studies report discrepancies between modelled and observed NO_2 concentrations: During the model intercomparison project AQMEII phase 2, all but one model simulating the European domain underestimate annual mean NO_2 concentrations in the rural background by 9%-45% on average. Some of them overestimate NO_2 concentrations at nighttime (Im et al., 2015a), meaning that daytime concentrations are underestimated even more than the average model bias would indicate. The European models contributing to the more recent AQMEII phase 3 intercomparison also show an underestimation of NO_2 concentrations in the rural background throughout the whole year, with the exception of one model (Solazzo et al., 2017b). In the Eurodelta model intercomparison study (Bessagnet et al., 2016), most participating models underestimate daytime NO_2 on average in the rural background, particularly in summer (Fig. 9 from Bessagnet et al., 2016).

A number of studies focusses on NO_2 in urban areas: Terrenoire et al. (2015) simulated air quality over Europe at a horizontal resolution of $0.125° \times 0.0625°$ with the CHIMERE model for 2009 and found that NO_2 concentrations are underestimated by more than 50% in urban areas. Schaap et al. (2015) show that the bias in modelled NO_2 concentrations in urban areas is reduced with higher model resolutions, but still report negative biases for a model resolution of 7 km x 7 km, between 6 and 10 $\mu g\ m^{-3}$ for different offline-coupled chemistry transport models. Fallmann et al. (2016) report a negative bias in NO_2 concentrations simulated with WRF-Chem at 3km x 3km of ca. 50% on average and up to 60% during daytime. Degraeuwe et al. (2016) report a negative bias in modelled urban background NO_2 concentrations of ca. 20% using LOTOS-EUROS at a horizontal resolution of ca. 7 km x 7 km.

Underestimation of NO_x traffic emissions as a cause of model bias

Many modelling studies attribute model biases of NO_x and O_3 concentrations to problems with emission data (e.g. Degraeuwe et al., 2016; Giordano et al., 2015; Solazzo and Galmarini, 2016). More specifically, Solazzo and Galmarini (2016) apply a a diagnostic model evaluation to O_3 concentrations simulated with models during AQMEII phase 1 and 2, and find that the model bias varies only by small amounts throughout the whole modelled period. One interpretation of a little-varying bias is that it is continuously fed into the model externally, which they link to either (O_3 precursor) emission data or boundary conditions. At the same time, similar spatial structures of the bias across different models might indicate common sources of error such as emission data. Degraeuwe et al. (2016), using LOTOS-EUROS at a horizontal resolution of 7km x 7km and finding underestimations of observed NO_2 concentrations of 20% (see above) assume that one cause of model error might be the emission input data, and subsequently apply a correction factor for further analysis of traffic emission scenarios. Giordano et al. (2015) assess the impact of

boundary conditions on models contributing to AQMEII phase 2. As NO_x concentrations in the planetary boundary layer are relatively short-lived and thus strongly influenced by local emission sources, they relate a consistent negative bias in simulated NO_2 mainly to an underestimation of emissions in the inventories.

Terrenoire et al. (2015) relate a negative bias of simulated NO_x concentrations in urban areas to an underestimation of traffic emissions specifically. As described above, they simulated air quality over Europe at a horizontal resolution of 0.125° x 0.0625° with the CHIMERE model, with a bias in simulated NO_x concentrations of more than 50% in urban areas. As the bias over urban areas is largest during traffic rush hours, they conclude that a "very likely" reason is the underestimation of NO_x traffic emissions.

Several studies suggest different methodologies to assess NO_x emissions from traffic, and come to similar conclusions: recent studies for London show that NO_x emissions from flux measurements are up to 80% (Lee et al., 2015), or a factor of 1.5-2 (Vaughan et al., 2016) higher than NO_x emissions from the UK National Atmospheric Emissions Inventory. Largest discrepancies were found in cases where traffic is the dominant source of NO_x concentrations. Karl et al. (2017) conclude from eddy covariance measurements in Austria that traffic related NO_x emissions in emission inventories frequently used by air quality models can be underestimated by up to a factor of 4 for countries where diesel cars represent a major fraction of the vehicle fleet, and thus have a significant contribution to reported biases in modelled NO_2 concentrations.

Modelling studies also list other potential causes of the negative bias in simulated NO_x concentrations. These may include problems with simulating the correct PBL height and mixing in the model (e.g. Solazzo et al., 2017b), but also an underestimation of the chemical lifetime of NO_x and too high dry deposition (Giordano et al., 2015). Other causes of NO_x model bias are also discussed in depth in Article 2 (Chapter 4).

1.3.4. Berlin-Brandenburg as a case study

The Berlin-Brandenburg area is particularly interesting as a case study, for several reasons.

Geographically, it is suitable for modelling studies as an isolated, big (more than 3.5 million inhabitants and almost 900 km^2), but largely flat city. At the same time, it represents an interesting case through its heterogeneous structure shaped by the former division of the city, with many vegetated green spaces in central parts of the urban area (see Fig. 1.2).

Meteorologically, it is influenced by air masses from both west and east, characterized by very different plume compositions, again influenced by its location at the edge of former western and eastern European states.
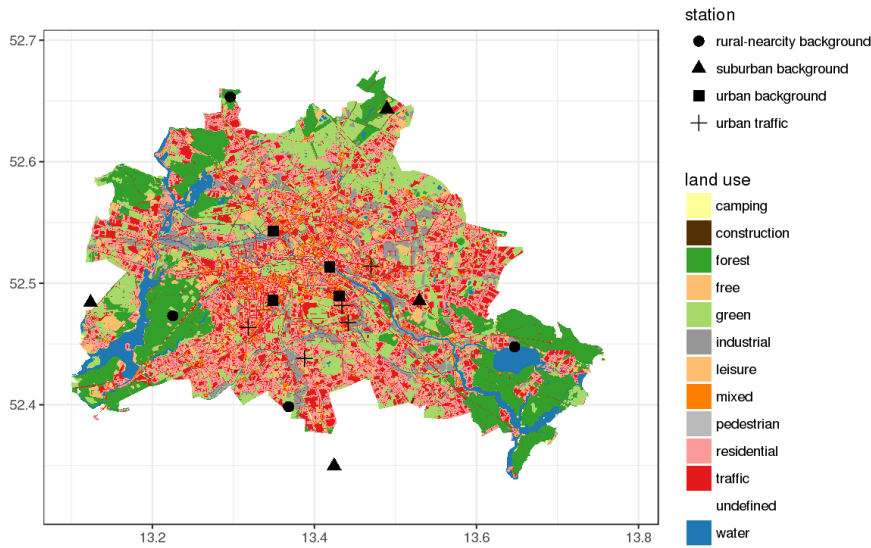
Figure 1.2.: Locations of measurement stations in and close to Berlin, including their AirBase station area
            classification and type and the land use classes in Berlin according to Berlin Senate Department
            for Urban Development and the Environment (2011a).

From an air quality perspective, Berlin struggles with exceedances of the NO_2 annual
limit value at all measurement sites close to traffic (Berlin Senate Department for the En-
vironment and Protection, 2017), with (inner-city) traffic being the main contributor to
high concentrations. For studying air quality, a wide range of official air quality measure-
ment stations (Fig. 1.2), as well data on air quality and meteorology from measurement
campaigns and university networks are available in Berlin and the surrounding areas (e.g.
Bonn et al., 2016, 2018; Fenner et al., 2014; von Schneidemesser et al., 2018).

1.4. Contribution of this thesis

1.4.1. Scope of the thesis and research questions

Summarizing what has been introduced in the previous sections, the exceedance of limit
values and non-compliance with emission thresholds make action on reducing NO_x concen-
trations and emissions necessary. Research and in particular modelling plays an important
role in the integrated assessment of air quality issues and design and evaluation of emission
control measures. In this context, it is not only important to assess how NO_x concentra-
tions can be kept to below limit values, but also to assess the broader consequences of high
urban NO_x concentrations for air quality, and urban environmental measures in their in-

teraction. Furthermore, modelling can only make a reliable contribution if available tools are thoroughly developed and evaluated.

This thesis contributes to the literature on several levels. It contributes to the development of the modelling tools needed for studying air quality at urban scales with very high resolution, and assesses the potential underestimation of traffic NO_x emissions, an often-quoted source of model bias, in a commonly used emission inventory. It applies the developed model setup, analyzing to what extent urban NO_2 concentrations could be reduced if vehicle emission standards were met. It also looks at broader consequences of high urban NO_x concentrations, assessing the contribution of biogenic VOC emissions to O_3 concentrations during a heat wave. The WRF-Chem model is used throughout the thesis, and the Berlin-Brandenburg region is used as a case study. Specifically, the thesis aims at answering the following research questions:

- What model resolution and level of detail in the input data is needed in order to simulate air quality in the Berlin-Brandenburg area?

- If an underestimation of NO_x emissions in commonly used inventories is a major cause of the negative bias in modelled NO_2 concentrations frequently reported for urban areas, how strong is this underestimation?

- By how much would NO_x concentrations in the Berlin-Brandenburg area be reduced if diesel emission standards were met?

- How do heat waves affect emissions of volatile organic compounds from urban/suburban vegetation and corresponding ground-level ozone in the Berlin-Brandenburg area?

In addition, more general conclusions and needs for developments when using WRF-Chem with high resolution for simulating air quality in an urban area are drawn based on the articles contributing to this thesis.

1.4.2. Structure of the thesis and overview of articles

Chapter 2 of this thesis introduces to the main methodological developments undertaken in the context of this thesis. It also briefly describes efforts to include inter- and transdisciplinary elements in the work for this thesis. The following chapters include the articles contributing to this thesis in full length. Four published articles contribute to this thesis. Each article includes an own introduction to the topic, details on the methods used, results and a discussion of the results. All articles are based on WRF-Chem modelling studies, with the model setup introduced in greatest detail in Article 1, building a basis for Articles 2-4. Chapter 7 summarizes, outlines future research needs and reflects on the inter- and

transdisciplinary elements included in the thesis work. The Appendix lists contributions to each of the articles, and includes a list of peer-reviewed publications and conference contributions. In addition, it includes the supplementary material of all articles, and a technical Appendix.

In the following, each article contributing to this thesis is briefly outlined:

1. **Air quality modelling in the Berlin-Brandenburg region using WRF-Chem v3.7.1: sensitivity to resolution of model grid and input data**
   Friderike Kuik, Axel Lauer, Galina Churkina, Hugo A. C. Denier van der Gon, Daniel Fenner, Kathleen A. Mar and Tim M. Butler
   Geosci. Model Dev., 9, 4339-4363, 2016, doi:10.5194/gmd-9-4339-2016, 2016.

   This article presents an evaluation of a WRF-Chem setup for the Berlin-Brandenburg region of Germany against meteorological and air quality observations for the summer of 2014. The objective of the study is to assess which resolution and level of detail in the input data is needed for simulating urban background air pollutant concentrations and their spatial distribution in the Berlin-Brandenburg area. For this, three sensitivity simulations are presented, updating input parameters to the single-layer urban canopy model based on structural data for Berlin, specifying land use classes on a sub-grid scale and downscaling the original emissions to a resolution of ca. 1km x 1km for Berlin based on proxy data including traffic density and population density. The results show that the simulation of urban meteorology can be improved when specifying the input parameters to the urban model, and to a lesser extent when specifying land use classes on a sub-grid scale. NO_x concentrations are simulated reasonably well on average, but nighttime concentrations are overestimated due to the model's underestimation of the mixing layer height, and urban daytime concentrations are underestimated. The daytime underestimation is improved when using downscaled, and thus locally higher emissions, suggesting that part of this bias is due to deficiencies in the emission input data and their resolution. The results further demonstrate that a horizontal resolution of 3km improves the results and spatial representativeness of the model compared to a horizontal resolution of 15km. A horizontal resolution of 1km without a further specification of input data does not improve the results considerably compared to a resolution of 3km, suggesting that a 3km horizontal resolution is a reasonable choice for simulating air quality in the Berlin-Brandenburg area.

2. **Top-down quantification of NO_x emissions from traffic in an urban area using a high resolution regional atmospheric chemistry model**
   Friderike Kuik, Andreas Kerschbaumer, Axel Lauer, Aurelia Lupascu, Erika von

Schneidemesser, Tim Butler

Building on the previously introduced work, this article extends and deepens the model evaluation for NO_x, and assesses the underestimation of traffic emissions, one of the main sources of model error, in greater detail. The WRF-Chem model is used at a 3 km x 3 km horizontal resolution, simulating the whole year 2014, using emission data downscaled to the model resolution. The model evaluation is deepened using spectral decomposition of observed and modelled time series and error apportionment. The results are consistent with an underestimation in traffic emissions being one of the main causes of the bias in modelled NO_2 concentrations in the urban background, where NO_2 concentrations are underestimated by ca. 8 μg m^{-3} (-30%) on average over the whole year. Furthermore, a diurnal cycle of the bias in modelled NO_2 suggests that a more realistic treatment of the diurnal cycle of traffic emissions might be needed. Model problems in simulating the correct mixing in the urban planetary boundary layer probably play a role in contributing to the model bias, particularly in summer. Vertically resolved measurement data, and in particular vertical profiles of NO_2 concentrations, would be needed for a more comprehensive assessment of this potential source of model bias. Taking into account this and other possible sources of model bias, a correction factor for traffic NO_x emissions of ca. 3 is estimated for weekday daytime traffic emissions in the core urban area. This corresponds to an underestimation of weekly mean traffic NO_x emissions in the core urban area of ca. a factor of ca. 2 and an underestimation of total NO_x emissions in the city centre by a factor of ca. 1.5. Sensitivity simulations for the months of January and July using the calculated correction factor show that the model bias on weekdays can be improved from -8.8 μg m^{-3} (-26%) to -5.4 μg m^{-3} (-16%) in January on average in the urban background, and -10.3 μg m^{-3} (-46%) to -7.6 μg m^{-3} (-34%) in July. In addition, the negative bias of weekday NO_2 concentrations downwind of the city in the rural and suburban background can be reduced from -3.4 μg m^{-3} (-12%) to -1.2 μg m^{-3} (-4%) in January and -3.0 μg m^{-3} (-22%) to -1.9 μg m^{-3} (-14%) in July. The results and their consistency with findings from other studies based on different methods (e.g. measurements) suggest that more research is needed in order to more accurately understand the magnitude, but also spatial and temporal variability in real-world NO_x emissions from traffic, and apply this understanding to the inventories used in high resolution chemical transport models.

3. **Potential reduction in ambient NO_2 concentrations from meeting diesel vehicle emission standards**

Erika von Schneidemesser, Friderike Kuik, Kathleen A. Mar and Tim M. Butler

Exceedances of the concentration limit value for ambient NO_2 at roadside measurement sites are linked to the emissions of light duty diesel vehicles, which have on-road emissions that are far greater than the regulatory standards. This article explores the possible gains in ambient air quality if light duty diesel vehicles were able to meet the regulatory standards (including both emissions standards from Europe and the United States). Two independent methods are used: a measurement-based and a model-based method. As in the previous articles, the city of Berlin is used as a case study. The measurement-based method uses data from 16 monitoring stations throughout the city of Berlin to estimate annual average reductions in roadside NO_2 of 9.0 to 23 μg m^{-3} and in urban background NO_2 concentrations of 1.2 to 2.7 μg m^{-3}. For this estimation, the reduction of the roadside increment (the difference between roadside and urban background concentrations) was assumed to be proportional to the reduction in traffic NO_x emissions if emission standards were met, and the reduction in the urban background increment (the difference between urban and rural background concentrations) was assumed to be proportional to the overall reduction in NO_x emissions if standards were met. The model simulations show reductions in urban background NO_2 of 2.0 μg m^{-3}, and at the scale of the greater Berlin area of 1.6 to 2.0 μg m^{-3} depending on the setup of the simulation and resolution of the model. Overall, the results show the significant potential for NO_2 reductions if regulatory standards for light duty diesel vehicles were to be met under real-world operating conditions. The similarities in results using both measurement- and model-based methods support the robustness of these conclusions, which are not dependent on the assumptions behind either methodology. By considering the changes in roadside and urban increments for the measurement-based methodology, the results do not depend on a potential underestimation of total traffic NO_x emissions.

4. **Effect of VOC emissions from vegetation on air quality in Berlin during a heatwave**
Galina Churkina, Friderike Kuik, Boris Bonn, Axel Lauer, R$^{'}$udiger Grote, Karolina Tomiak and Tim M. Butler

Emissions from urban vegetation combined with anthropogenic NO_x emissions can produce ozone and particulate matter. This potential increases with rising temperatures and may lead to severe problems with air quality in densely populated areas during heat waves. This article investigates how heat waves affect emissions

of volatile organic compounds from urban/suburban vegetation and corresponding ground-level ozone using the WRF-Chem model. The heat wave in summer 2006 and Berlin, Germany, are used as a case study. The model simulations indicate that the contribution of biogenic VOC emissions to ozone formation is lower in June (9 - 11%) and August (6 - 9%) than in July (17 - 20%). On particular days within the analyzed heat wave period, this contribution increases up to 60%. The actual contribution is expected to be even higher, as the model underestimates isoprene concentrations over urban forests and parks by 0.6 - 1.4 ppbv. The study demonstrates that biogenic VOCs can considerably enhance air pollution during heat waves. This shows that urban environmental measures need to be assessed comprehensively in order for cities to fully benefit from these measures. For example, urban tree planting campaigns would have to be accompanied by a reduction of anthropogenic sources of O_3 precursors (NO_x, VOCs), e.g. in the area of road transport.

2. Methodological developments

2.1. Air quality modelling with WRF-Chem

The studies contributing to this thesis are based on the chemistry version of the Weather Research and Forecasting Model (WRF-Chem, Fast et al., 2006; Grell et al., 2005; Skamarock et al., 2008). As mentioned in Section 1.3, WRF-Chem is an online-coupled atmosphere chemistry transport model, in which physical and chemical variables are calculated on the same grid and with the same time steps.

Numerically, the model setup used here is based on the *Advanced Research WRF* (ARW), which solves the fully compressible, non-hydrostatic Euler equations on a grid. The vertical coordinate of the model is a terrain-following hydrostatic pressure coordinate, with constant pressure at the model top.

WRF-Chem is mainly developed by NCAR (National Center for Atmospheric Research), NOAA (National Oceanic and Atmospheric Administration) and PNNL (Pacific Northwest National Laboratory) in the US, but is, as a community model, open to contributions from other researchers. This has lead to a vast variety of available parameterizations, submodels describing physical and chemical processes on the sub-grid scale, with the optimal suitability of a parameterization depending on the model application. For this thesis, a number of different model settings and parameterizations have been tested and are listed in Table 2.2, with the final recommended/used schemes in bold[1]. They are described in greater detail in Section 2.1.1. The most recent namelist of the final setup can be found in the Appendix.

Here, WRF-Chem is used as a regional model, set up with two or three nested domains of horizontal resolutions of 15kmx15km, 3kmx3km and 1kmx1km. As such, it requires a number of input datasets, optimally at equally high resolution (see Section 1.3.1). The input data include meteorological and chemical initial and boundary conditions, static data describing for example the land use classes of the chosen model domain as well as anthropogenic and natural emission data of chemical species and particles. The model

---

[1]A research stay with the model developers at NOAA and NCAR in summer 2015 has greatly helped in the identification of suitable schemes.

Table 2.1.: Model input datasets

Data use	Dataset	Remarks
Anthropogenic emissions	**TNO-MACC III**	
Biogenic emissions	**online**	MEGAN
Dust and sea salt emissions	**online**	dust_opt=3, seas_opt=2
Meteorological boundary conditions including sea surface temperature	**ERA-Interim**	sst_update=1
Chemical boundary conditions	**MOZART4-GEOS5**	
Land use data	**CORINE**	mapped to USGS classes

is used for simulating air quality over the Berlin-Brandenburg urban area and includes a parameterization of urban processes on sub-grid scale (urban canopy model), which additionally requires the user to specify parameters describing the urban characteristics. Model input data are listed in Table 2.1. The changes to the standard WRF-Chem configuration, including the calculation of the urban parameters, is described in Section 2.1.2, and the processing of anthropogenic emissions is further described in Section 2.1.3.

2.1.1. Sensitivity tests

For the work presented in this thesis, several schemes of WRF-Chem were tested, most importantly related to the choice in planetary boundary layer, but also concerning the sensitivity of the results to the choice in chemical mechanism. The considerations and results of these tests are briefly described in the following.

Other model options were changed in the course of this work, mainly because they represent the latest developments and were recommended by the developers (Georg Grell, Ravan Ahmadov, personal communication, 2015). This concerns in particular the convection scheme.

Planetary boundary layer

The choice in planetary boundary layer scheme is important for simulating aerosols and chemistry: it parameterizes processes in the boundary layer and calculates exchange coefficients, that are then used in the model to calculate the vertical mixing of air pollutants. Its choice is "the most contested", and the "results can differ significantly depending on its choice" (Peckham et al., 2013). This is why several different planetary boundary layer schemes were tested for Article 2, based on the results described in Article 1. The tested schemes include the Mellow-Yamada-Janjic scheme (MYJ, Janjić, 1990, 1994), the Yonsai

Table 2.2.: Model configuration

Process	Option	Remarks
Land surface model	**Noah LSM**	CORINE land use data
		tested: mosaic option
Urban processes	**single layer UCM**	3 categories: roofs, walls, trees
		parameters calculated for Berlin
Boundary layer	MYJ, YSU, **MYNN**	
Cumulus convection	Grell, **Grell-Freitas**	switched on for both domains
Cloud microphysics	**Morrison double-moment**	
Radiation (sw+lw)	**RRTMG**	
Aerosols	**MADE/SORGAM**	chem_opt=106
Chemistry	**RADM2**	with KPP
Photolysis	**Madronich F-TUV**	

University Scheme (YSU, Hong et al., 2006) and the Mellor-Yamada Nakanishi & Niino scheme (MYNN, Nakanishi and Niino, 2004, 2006).

The results presented in Article 1 suggest that simulated NO_x concentrations are too high during nighttime, and modelled mixing at nighttime might be underestimated. While only minor differences were found between the three different PBL schemes for grid cells outside of the urban area, the MYNN scheme was found to simulate a higher nighttime boundary layer in urban areas and slightly reduce the positive bias in simulated nighttime NO_x concentrations, which is why this scheme was eventually chosen and is at the moment also recommended for future simulations with WRF-Chem over the Berlin-Brandenburg area. However, a lack of measurement data of temperature and wind speed profiles or planetary boundary layer height did not allow for a quantitative evaluation of simulated planetary boundary layer height over the urban area. Thus, additional measurement data would help to inform better the choice of the planetary boundary layer scheme in future studies.

Aerosols and chemistry

For simulating aerosols and chemistry, the Regional Acid Deposition Model chemical mechanism (RADM2, Stockwell et al., 1990) with the Kinetic PreProcessor (KPP) and the MADE/SORGAM aerosol scheme - based on the Modal Aerosol Dynamics Model for Europe (MADE, Ackermann et al., 1998; Binkowski and Shankar, 1995) and the Secondary Organic Aerosol Model (SORGAM, Schell et al., 2001) - were used. The priority was given to the KPP solver instead of the quasi-steady-state approximation (QSSA), because Forkel

et al. (2015) found that the latter underestimates nighttime ozone titration for areas with high NO emissions. However, with this option it is not possible to include the full aqueous-phase chemistry, including aerosol-cloud interactions and wet scavenging. Furthermore, it is known that the MADE/SORGAM aerosol scheme underestimates the secondary organic aerosol contribution to PM (Ahmadov et al., 2012). Thus, this choice in chemistry and aerosol scheme is expected to result in an underestimation of simulated particulate matter. The focus of this thesis is on nitrogen oxides and not on particulate matter, but the results for simulated particulate matter are in line with what is known from the literature (see Article 1). Thus, for simulating particulate matter and fully exploiting the benefits of an online-coupled model such as representing aerosol-cloud interactions, a different choice in aerosol and chemical mechanism would be recommended.

A sensitivity simulation has been done in the context of Article 2, testing the impact of a different choice in chemical mechanism on simulated NO_x and O_3 concentrations. The chemical mechanism tested was the Model for Ozone and Related Chemical Tracers chemical mechanism (MOZART, Emmons et al., 2010; Knote et al., 2014). The simulation was done for the month of July 2014, and used the settings described in Article 2. The results show that the differences in simulated O_3 concentrations are quite substantial, while there is only a very small difference in simulated NO_x concentrations: the difference between monthly mean simulated NO_x is 0.4 μg m^{-3} for rural near-city and suburban stations, and essentially 0 for urban background stations. For O_3, on the other hand, the difference in mean concentrations is of the order of ca. 30-35 μg m^{-3}, with the simulation using the MOZART mechanism indicating the higher values. Looking at the simulated time series, a comparison with measurements shows that the simulation using the RADM2 mechanism generally underestimates observed peak values during episodes with higher O_3 concentrations. However, compared to the simulation using the MOZART mechanism, it better captures the overall diurnal variation and periods with lower observed daily maxima. The simulation using the MOZART mechanism, on the other hand, better captures observed peak values during periods with high O_3 concentrations, but overestimates concentrations overall. Both simulations do not capture the full amplitude of observed diurnal variations of O_3 concentrations and do not seem to capture the (longer-term) variability of observed O_3 concentrations.

These results are consistent with results reported in the literature, e.g. from the AQMEII phase 2 intercomparison study of online-coupled models (Im et al., 2015b). The authors find that, all over Europe, daily maximum 8-h average surface ozone concentrations below 50-60 μg m^{-3} are overestimated by all models in the intercomparison study, and concentrations over 120-140 μg m^{-3} are underestimated. The study also included several model setups of WRF-Chem using the RADM2 mechanism. The model bias of daily maximum 8-h average surface ozone in Europe is even larger for WRF-Chem setups using other

chemical mechanisms such as the CBMZ or RACM mechanisms compared to those using the RADM2 mechanism (Fig. 9 in Im et al., 2015b). Three other online-coupled model setups (NMMB-BSC-CTM, RACMO LOTOS-EUROS and MetUM-UKCA RAQ) also show the same pattern in model bias, but overall smaller biases at higher observed ozone levels. Furthermore, a comparison of the RADM2 and MOZART mechanisms in WRF-Chem for a European domain (Mar et al., 2016) finds similar results as described above: the simulation using the MOZART chemical mechanism predicts O_3 concentrations of up to 20 μg m^{-3} higher than the simulation using the RADM2 mechanism, and measurements are overestimated in the simulation using the MOZART mechanism and underestimated in the simulation using the RADM2 mechanism. At the same time, NO_x concentrations simulated with both mechanisms were found to be relatively similar. In addition, O_3 concentrations simulated with both mechanisms were found to show a similar sensitivity to NO_x.

Based on these results and to maintain an overall consistency among the different articles contributing to this thesis, the studies presented in this thesis are all based on the RADM2 chemical mechanism. However, the results from the literature and the sensitivity test discussed above clearly show that further research is needed to better represent O_3 concentrations at levels that are relevant for air quality management, as this seems to be a problem common to many WRF-Chem setups and, to a lesser extent, also to other online-coupled air quality models.

2.1.2. Changes made to the standard WRF-Chem configuration

Land use data

The default USGS land use data in WRF is replaced with the European CORINE-dataset (EEA, 2014), which provides a more accurate representation of land use in Europe. As physical and chemical parameterizations are partly linked directly to a set of default land use classes (hard-coded in several modules of the model code), the CORINE land use classes are mapped to the USGS classes. Three urban land use categories are used, including the classes low density residential, high density residential, and commercial, industry, transport. The differences between those three categories are characterized via an input table to the urban scheme (see below). Articles 1 and 4 of this thesis as well as their supplementary material explain the choice of land use data and mapping procedure in somewhat greater detail. Article 1 also assesses the impact of a sub-grid-scale parameterization of land use (Li et al., 2013) on model results.

When combining the use of three urban land use categories with the chemistry version of the model, the initialization of dry deposition (module_dep_simple.F) needs to be modified

(Fallmann et al., 2016), as it is hard-coded to the land use classes, but only includes one urban class. Thus, it needs to be extended in order to account for three urban classes. Here, the same parameters are assumed for all urban land use classes, and the modified code can be found in the Appendix of this thesis.

In addition, input data on land use and vegetation classes are needed for the online calculation of biogenic VOC emissions with the Model of Emissions of Gases and Aerosols from Nature (MEGAN, Guenther et al., 2006). As described in Article 4, the default dataset used by MEGAN does not take into account urban areas, which is why the CORINE dataset is used in order to adjust the default data for grid cells identified as "urban" in CORINE.

Urban processes

The urban scheme, in this case the single-layer urban canopy model (UCM, e.g. Chen et al., 2011; Kusaka and Kimura, 2004; Kusaka et al., 2001; Liao et al., 2014; Loridan et al., 2010; Martilli et al., 2002), accounts for modified dynamics by cities. It takes into account energy and momentum exchange between urban areas and the atmosphere. Surface fluxes and temperature are calculated as a combination of fluxes from urban and vegetated surfaces, coupled via the urban fraction assigned to the land use type of each grid cell (Chen et al., 2004).

An input table specifies the characteristics of each of the three urban classes (low intensity residential, high intensity residential, commercial/industry/transport). These include geometric characteristics as for example average building height and width, average road with, share of sealed surface per grid cell, but also thermodynamic parameters such as surface albedo and emissivity. As the default parameters are calculated for Houston, USA, it is advised to calculate the most important parameters from existing data when applied to other cities (Fei Chen, personal communication, 2015). This is particularly important when applying the urban scheme in WRF to European cities, which differ significantly from American cities in structure and building material. Data used for the calculation of the parameters include data on building height and location, the road network and land use classes for Berlin, provided by the Berlin Senate Department for the Urban Development and Housing[2] and largely available online (Berlin Senate Department for Urban Development and Housing, 2018). The process of calculating these parameters is described in further detail in Article 1 of this thesis, and modifications made in the input table (URBPARM.TBL) used are provided in the Appendix.

---

[2]Formerly the Berlin Senate Department for Urban Development and the Environment

The results for modelled temperature and to a lesser extent planetary boundary layer height were found to be particularly sensitive to the urban fraction, or share of sealed surface per grid cell, specified for each of the three urban land use classes. Thus, when aiming at further improving the modelled meteorology in the urban area, more detailed input data, potentially extending beyond specifying only three urban land use classes, could be used. This applies in particular for relatively heterogeneous urban areas such as Berlin.

Nighttime mixing

Mixing in the planetary boundary layer, particularly over urban areas, is an often-highlighted difficulty reported for WRF-Chem (Ravan Ahmadov, personal communication, 2017) and other models (e.g. CHIMERE, Schaap et al., 2015). This might be due to the difficulty of accurately simulating processes in the urban boundary layer, influenced by both the larger-scale synoptic situation and the influence of the urban area on local meteorology, e.g. through anthropogenic heat and momentum fluxes in the city. These processes might be very variable even within one single city. However, difficulties also arise from a lack of measurement data to which the model output (e.g. temperature and wind speed profiles, vertical pollutant distributions) can be compared.

In WRF-Chem, nighttime mixing over urban areas is often reported to be too weak (Ravan Ahmadov, personal communication, 2017). A modification in the model code (dry_dep_driver.F) was introduced to account for increased mixing in case carbon monoxide emissions (as a proxy for anthropogenic emissions in general) exceed a certain threshold in case no urban scheme is used to account for additional mixing due to anthropogenic heat and momentum sources. However, this additional mixing is also switched on in many studies even in case an urban scheme is used (Ravan Ahmadov, personal communication, 2016). Here, these changes in order to take into account increased nighttime mixing in urban areas are introduced in Article 2, with the changes in the code documented in the Appendix of Article 2 and discussed in the conclusions of this thesis.

2.1.3. Emission processing

Adapting and downscaling TNO-MACC III emission data for the Berlin-Brandenburg area

As already outlined in Section 1.3, some studies suggest that air quality modelling at high resolution only improves the model results if input data, most importantly emission input data, is available at a similarly high resolution (e.g. Schaap et al., 2015; Tie et al.,

2010). For this reason, the TNO-MACC III anthropogenic emission inventory (Kuenen et al., 2014) was downscaled from its original horizontal resolution of ca. 7kmx7km to ca. 1kmx1km. The impact of using emissions at different resolutions on simulated air pollutants was tested, and the results are described in detail in Article 1.

The downscaling was done in two steps: first it was done for Berlin only (Article 1 and 3) based on locally available proxy data including population density (Berlin Senate Department for Urban Development and the Environment, 2011a) and traffic densities (Berlin Senate Department for Urban Development and the Environment, 2011b) for Berlin. As it was tested successfully, the downscaling was refined in a second step to include a larger geographical area around the city of Berlin, using in addition data on the location of roads from OpenStreetMap and, in cooperation with TNO, data on population density from LandScan2010. This had the aim of improving the representation of air pollutants also at the edge and just outside of the city. The second downscaling step further limited the emission (SNAP) categories to be downscaled to those for which the available proxy data were assumed to actually improve the distribution, e.g. road transport emissions, residential heating emissions and product use emissions. The second stage of the emission downscaling is described in detail in Article 2 and its Supplementary Material.

Technically, the downscaling redistributes emissions from the TNO-MACC III inventory within one original, coarse grid cell (ca. 7km x 7km) into 7 x 7 sub grid cells, and thus conserves the original emissions within each coarse grid cell. For this, the proxy data was re-gridded to the TNO-MACC III coarse grid as well as the fine sub grid, and factors were calculated indicating the share of population/traffic in each sub grid cell, compared to the "parent" coarse grid cell. These factors were then used to distribute the emissions onto the fine sub grid.

In addition to the downscaling, airport emissions for Berlin were corrected: the original version of the TNO-MACC III emission inventory still includes airport emissions from the Tempelhof airport, which was closed to air traffic in 2008. Thus, airport emissions from all three airports in the original inventory were summed and then distributed on the two still operating airports Schönefeld and Tegel. The distribution is based on their respective passenger and freight transport volumes.

Temporal and vertical distribution of emissions

For modelling air quality with a high temporal resolution, better results are achieved when distributing the annual total anthropogenic emissions temporally. As the distribution is not part of the WRF-Chem model, separate pre-processing routines need to be developed. Like the emission downscaling, the temporal distribution of emissions was refined in two

stages. Initially, the temporal distribution of emissions for model simulations contributing to this thesis was done based on a program developed by the author of Mar et al. (2016) (Articles 1, 3 and 4), but due to higher specification needs a separate program was developed in order to process the emissions for model simulations contributing to Article 2. The latter reads in all necessary specifications (temporal and vertical distribution, NO_x, VOC and PM splitting) from easily modifiable csv-files.

In the first stage, the temporal distribution of emissions was based on profiles calculated by Builtjes et al. (2002), including distribution factors depending on the month of the year (annual cycle), the day of the week (weekly cycle) and the hour of the day (diurnal cycle). In the second stage, the diurnal cycle of traffic emissions was replaced by a diurnal cycle calculated based on traffic counts for Berlin, assuming a linear scaling of traffic emissions with traffic counts as also done by Builtjes et al. (2002). Article 2 describes this procedure.

Distributing anthropogenic emissions vertically instead of releasing them into the first model layer does not change the model results considerably when using a coarse model resolution (Mar et al., 2016). However, the results from Article 1 suggest that a vertical distribution might be more important for higher model resolutions of only a few km. This is why anthropogenic emissions are distributed vertically for the model simulations contributing to Article 2 of this thesis, as described in the article. In brief, emissions from residential heating, energy and non-energy industry as well as airports are distributed into up to seven vertical layers. The vertical distribution is also included in the routines written for the second stage of the emission pre-processing.

In addition to the modification of Berlin airport emissions described above, a further modification to the original data is introduced. Airport emissions are included in the category of non-road transport emissions in the inventory. Emissions for Berlin from the emission category non-road transport emissions are split into airport emissions and non-airport emissions. This is possible, as in the case of Berlin airport emissions are indicated as point sources. Emissions for airports are then distributed vertically considering both emissions of airport ground transportation and the LTO-cycle (landing, take-off), while other non-road transport emissions are only released into the first model layer.

2.2. Model evaluation

Since the WRF-Chem model can be set up with numerous different combinations of parameterizations, domain configurations and settings related to the model dynamics, it is necessary that every new setup is evaluated against measurement data (also see Section 1.3.2). The main focus of Article 1 of this thesis is an operational model evaluation

(though at a high level of spatial and temporal disaggregation). This is extended in Article 2, analyzing the model results additionally with methods of a diagnostic model evaluation.

For the diagnostic model evaluation, a Kolmogorov-Zurbenko filter (Zurbenko, 1986) is used in order to decompose modelled and observed time series. Following Galmarini et al. (2013); Hogrefe et al. (2000); Solazzo et al. (2017b), the time series are decomposed into a long-term (LT, >21 days), synoptic (SY, 2.5-21 days), diurnal (DU, 0.5-2.5 days) and intra-diurnal (ID, < 0.5 day) component, each representing processes characteristic for these time scales. Specifically, the components are defined as follows, with the Kolmogorov-Zurbenko filter $kz_{m,k}$, the time window m and smoothing parameter k, time series x and time t:

$$ID(t) \quad = \quad x(t) - kz_{3,3}(x(t)) \tag{2.1}$$

$$DU(t) \quad = \quad kz_{3,3}(x(t)) - kz_{13,5}(x(t)) \tag{2.2}$$

$$SY(t) \quad = \quad kz_{13,5}(x(t)) - kz_{103,5}(x(t)) \tag{2.3}$$

$$LT(t) \quad = \quad kz_{103,5}(x(t)) \tag{2.4}$$

The mean square error (MSE) of each component is then assessed by breaking it down into bias, variance error (σ) and minimum achievable mean square error (mMSE) as follows (Solazzo and Galmarini, 2016):

$$MSE = (mod - obs)^2 + (\sigma_{mod} - r\sigma_{obs})^2 + mMSE \tag{2.5}$$

Where *mod* and *obs* indicate model results and observations, respectively, and r denotes the correlation coefficient. The decomposition and error apportionment is described in detail in Article 2. For the decomposition, the "kza" library of the R programming language was used. An exemplary R-script for spectrally decomposing a NO_x time series can be found in the Appendix to this thesis.

2.3. Inter- and transdisciplinary work

The work for this thesis was done at the Institute for Advanced Sustainability Studies (IASS). In its mission, the IASS states that "[its] research is transdisciplinary, conducted together with scientific, political and societal partners, in order to develop solutions for urgent sustainability challenges [...]" [3]. In this context and within the limits of what is possible within a single, natural-scientific thesis, this work aimed at integrating elements of transdisciplinary work in the process.

---

[3] http://www.iass-potsdam.de/en/our-approach

There is a range of literature on the definition, principles and criteria of transdisciplinary research. However, it is argued that this literature is "rather fragmented and dispersed, without providing good guidance to interested researchers and practitioners [...]" (Lang et al., 2012), and "a universally accepted definition is not available" (Jahn et al., 2012). In brief, transdisciplinary (or similar) research approaches are often characterized by focusing on collaborations between scientists encompassing different disciplines as well as stakeholders from outside academia, such as from business, governments, civil society or generally those who use the knowledge generated during the process (Kates et al., 2001; Lang et al., 2012). Jahn et al. (2012) find that a combination of *interdisciplinarity* and *participation* of actors from outside of science "seems to be the common recipe for defining transdisciplinarity".

Part of the aim of this work was to address "real-world problem settings" (Jahn et al., 2012), which calls for the integration of scientific knowledge with extra-scientific expert knowledge. Along these lines, the attempt to include transdisciplinary elements in this work included reaching out to and exchanging with relevant, local stakeholders on local air quality and mobility in Berlin and Potsdam. They included representatives of the Berlin, Brandenburg and Potsdam authorities responsible for air quality and/or traffic and representatives of non-governmental organizations. This part of the work was highly experimental with limited incorporation into the articles contributing to this thesis. However, these efforts lead to an intensified exchange with a member of the Berlin Senate Department for the Environment, Transport and Climate Change, who also co-authors Article 2 of this thesis. Some general learnings from these transdisciplinary efforts are sketched in the conclusion of this thesis.

3. Article 1: Air quality modelling in the Berlin-Brandenburg region using WRF-Chem v3.7.1: sensitivity to resolution of model grid and input data

Geoscientific
Model Development

Air quality modelling in the Berlin–Brandenburg region using WRF-Chem v3.7.1: sensitivity to resolution of model grid and input data

Friderike Kuik[1,2]**, Axel Lauer**[3]**, Galina Churkina**[1]**, Hugo A. C. Denier van der Gon**[4]**, Daniel Fenner**[5]**, Kathleen A. Mar**[1]**, and Tim M. Butler**[1]

[1]Institute for Advanced Sustainability Studies, Potsdam, Germany
[2]University of Potsdam, Faculty of Science, Potsdam, Germany
[3]Deutsches Zentrum für Luft- und Raumfahrt (DLR), Institut für Physik der Atmosphäre, Oberpfaffenhofen, Germany
[4]TNO, Netherlands Organization for Applied Scientific Research, Utrecht, the Netherlands
[5]Technische Universität Berlin, Faculty VI – Planning Building Environment, Institute of Ecology, Chair of Climatology, Berlin, Germany

Correspondence to: Friderike Kuik (friderike.kuik@iass-potsdam.de)

Abstract. Air pollution is the number one environmental cause of premature deaths in Europe. Despite extensive regulations, air pollution remains a challenge, especially in urban areas. For studying summertime air quality in the Berlin–Brandenburg region of Germany, the Weather Research and Forecasting Model with Chemistry (WRF-Chem) is set up and evaluated against meteorological and air quality observations from monitoring stations as well as from a field campaign conducted in 2014. The objective is to assess which resolution and level of detail in the input data is needed for simulating urban background air pollutant concentrations and their spatial distribution in the Berlin–Brandenburg area. The model setup includes three nested domains with horizontal resolutions of 15, 3 and 1 km and anthropogenic emissions from the TNO-MACC III inventory. We use RADM2 chemistry and the MADE/SORGAM aerosol scheme. Three sensitivity simulations are conducted updating input parameters to the single-layer urban canopy model based on structural data for Berlin, specifying land use classes on a sub-grid scale (mosaic option) and downscaling the original emissions to a resolution of ca. $1\,\mathrm{km} \times 1\,\mathrm{km}$ for Berlin based on proxy data including traffic density and population density. The results show that the model simulates meteorology well, though urban 2 m temperature and urban wind speeds are biased high and nighttime mixing layer height is biased low in the base run with the settings described above. We show that the simulation of urban meteorology can be improved when specifying the input parameters to the urban model, and to a lesser extent when using the mosaic option. On average, ozone is simulated reasonably well, but maximum daily 8 h mean concentrations are underestimated, which is consistent with the results from previous modelling studies using the RADM2 chemical mechanism. Particulate matter is underestimated, which is partly due to an underestimation of secondary organic aerosols. NO_x ($NO + NO_2$) concentrations are simulated reasonably well on average, but nighttime concentrations are overestimated due to the model's underestimation of the mixing layer height, and urban daytime concentrations are underestimated. The daytime underestimation is improved when using downscaled, and thus locally higher emissions, suggesting that part of this bias is due to deficiencies in the emission input data and their resolution. The results further demonstrate that a horizontal resolution of 3 km improves the results and spatial representativeness of the model compared to a horizontal resolution of 15 km. With the input data (land use classes, emissions) at the level of detail of the base run of this study, we find that a horizontal resolution of 1 km does not improve the results compared to a resolution of 3 km. However, our results suggest that a 1 km horizontal model resolution could enable a detailed simulation of

local pollution patterns in the Berlin–Brandenburg region if the urban land use classes, together with the respective input parameters to the urban canopy model, are specified with a higher level of detail and if urban emissions of higher spatial resolution are used.

1 Introduction

Despite extensive regulations, air pollution in Europe remains a challenging issue: causing up to 400 000 premature deaths per year in Europe (EEA, 2015), air pollution is the number one environmental cause of premature deaths (OECD, 2012). Especially in urban areas, air pollution is a problem, with 97–98 % of the urban European population (EU-28) exposed to ozone levels higher than 8 h average concentrations of $100 \mu g m^{-3}$, which the World Health Organisation (WHO) recommends not to be exceeded for the protection of human health, and ca. 90 % of the urban European population (EU-28) exposed to $PM_{2.5}$ (particulate matter with a diameter smaller than $2.5 \mu m$) levels higher than the WHO-recommended annual mean of $10 \mu g m^{-3}$ in 2011–2013 (EEA, 2016). Similarly, annual and hourly NO_2 limit values are still exceeded, mainly at measurement site close to traffic. In 2013, the European limit value of $40 \mu g m^{-3}$ was exceeded at 13 % of all stations, all of them situated at traffic or urban sites (EEA, 2016). In Berlin, measured NO_2 annual means exceeded the European limit value of the annual mean at all but three measurement sites close to traffic in 2014 (Berlin Senate Department for Urban Development and the Environment, 2015a). In addition, current controversies on NO_2 emissions from cars have triggered additional discussions on NO_2 in urban areas.

Numerical modelling is an important tool for assessing air quality from global to local scales. Over the last decades, air quality models have been used to understand the processes leading to air pollution as well as to build a basis for policies defining measures to improve air quality. With increasing computing capacities, model resolution has been increasing, and different types of 3-D regional chemistry transport models are able to resolve relevant processes down to a horizontal resolution of ca. $1 km \times 1 km$ (Schaap et al., 2015). At these resolutions, the models can be used to study the atmospheric composition in the urban background.

As a basis for modelling work assessing air quality in the Berlin–Brandenburg area, this study evaluates a setup with the online-coupled numerical atmosphere-chemistry model WRF-Chem (chemistry version of the Weather Research and Forecasting model, Skamarock et al., 2008; Fast et al., 2006; Grell et al., 2005). In the setup presented here, WRF-Chem is coupled with a single-layer urban canopy model (Chen et al., 2011; Loridan et al., 2010). We evaluate the model setup with respect to its skill in simulating meteorological conditions and air pollutant concentrations, with a focus on

NO_x ($NO + NO_2$), but also evaluating for particulate matter (PM_{10}, $PM_{2.5}$) and O_3. The skill in simulating air quality in an online-coupled model is, besides the choice of the chemical mechanism, influenced by the prescribed emissions, the model resolution and the skill in reproducing the observed meteorology. The latter depends on the model resolution, on input data, such as land use data, and on parameterisations of the sub-grid-scale processes, such as effects of urban areas on meteorology. The objective of this study is to address which resolution and level of detail in the input data, including land use, emissions and parameters characterising the urban area, is needed for simulating urban background air pollutant concentrations and their spatial distribution in the Berlin–Brandenburg area. This is done by evaluating the model results of three nested model domains at 15, 3 and 1 km horizontal resolutions as well as three sensitivity simulations, including updating the representations of the urban area within the urban canopy model, taking into account a sub-grid-scale parameterisation of the land use classes, and downscaling the original emission input data from a horizontal resolution of ca. 7 to ca. 1 km. In light of the high computational costs of running the model at a 1 km horizontal resolution, it is particularly helpful to find out under which conditions using this model resolution can lead to improved results compared to coarser resolutions. This can directly help the design of future air quality modelling studies over the Berlin–Brandenburg region and other European urban agglomerations of similar extent.

The WRF-Chem model has been applied and evaluated in different modelling studies over Europe. For example, Tuccella et al. (2012) evaluate a European setup at a horizontal resolution of $30 km \times 30 km$. Brunner et al. (2015) and Im et al. (2015b, a) analyse the performance of several online-coupled models set up for the Air Quality Model Evaluation International Initiative (AQMEII) phase 2. Among the simulations for a European domain, there are seven with different setups of WRF-Chem, performed with a horizontal resolution of $23 km \times 23 km$. Commonly reported biases of WRF-Chem in comparison to observations from synoptic surface stations include an underestimation of daily maximum temperatures and an overestimation of wind speed (Tuccella et al., 2012; Brunner et al., 2015). Furthermore, Brunner et al. (2015) conclude that the representation of other meteorological parameters relevant to air quality simulations, such as solar radiation at the surface, precipitation and planetary boundary layer height, is still challenging. WRF-Chem tends to underestimate ozone daily maxima over Europe (Tuccella et al., 2012) with especially pronounced underpredictions of observed ozone values exceeding policy guidelines (Im et al., 2015b). They attribute the deficiencies to the simulated meteorology, the chemical mechanism and the chemical boundary conditions. Mar et al. (2016) evaluated the performance of WRF-Chem for a European domain with respect to ozone, comparing different chemical mechanisms. They concluded that the simulated ozone concentration strongly depends on

the choice of chemical mechanism, and that RADM2 leads to an underestimations of observed ozone concentrations. PM_{10} is underestimated by WRF-Chem as compared to regional background observations (Im et al., 2015a). Tuccella et al. (2012) also report an underestimation of $PM_{2.5}$. Both studies give various reasons for the mismatch in PM model results and observations, including an underestimation of secondary organic species by the aerosol mechanisms applied. Im et al. (2015a) report an overestimation of nighttime NO_x in some models, including WRF-Chem, which they attribute both to a general underestimation of NO_2 during low-NO_x conditions and to problems in simulating nighttime vertical mixing. They report that NO_2 is underestimated by most models.

WRF-Chem has also been applied at high spatial resolutions over urban areas, for example, Mexico City (Tie et al., 2007, 2010), Los Angeles (Chen et al., 2013), Santiago (Mena-Carrasco et al., 2012), the Yangtze River Delta (Liao et al., 2014) and Stuttgart (Fallmann et al., 2016). Tie et al. (2007, 2010) have explicitly assessed how the model resolution impacts the simulated ozone and ozone precursors in Mexico City and concluded that a resolution of 24 km is not suitable for simulating concentrations of CO, NO_x and O_3 in the city centre. They suggest a ratio of city size to model resolution of 6 : 1 and conclude that a horizontal resolution of about 6 km is the best balance between model performance and computational time when simulating ozone and precursors in Mexico City. Furthermore, they conclude that the model results for ozone are more sensitive to the model resolution than to the resolution of the emission input data. Other studies have shown that increasing the model resolution does not necessarily lead to an improvement in model results, but that it can be beneficial for amplifying the urban signal (e.g. Schaap et al., 2015, and references therein). They emphasise that it is only useful to go to model resolutions finer than 20 km if model input data, such as land use data and emission data, are also available at similarly high resolutions. Fallmann et al. (2016) have combined WRF-Chem with RADM2 chemistry and MADE/SORGAM aerosols with a multi-layer urban canopy model for the area of Stuttgart, studying effects of urban heat island mitigation measures on air quality. One of their findings from the model evaluation is an underestimation of daytime NO_2 by up to 60 %, while O_3 is slightly overestimated during the day.

In the Berlin–Brandenburg region, there have been regional model simulations of particulate matter with an offline chemistry transport model (Beekmann et al., 2007), along with a measurement campaign focusing on particulate matter in 2001/02. Other modelling studies in this region focused on meteorology: Schubert and Grossman-Clarke (2013) assessed the impact of different measures on extreme heat events in Berlin. Trusilova et al. (2016) tested different urban parameterisations in the COSMO-CLM model and their impact on air temperature. Jänicke et al. (2016) used the WRF model to dynamically downscale global atmospheric reanalysis data over Berlin to a resolution of 2 km × 2 km,

testing combinations of different planetary boundary layer schemes and urban canopy models. They conclude that simulated urban–rural as well as intra-urban differences in 2 m air temperature are underestimated and that the more complex urban canopy models did not outperform the simple slab/bulk approach.

To our knowledge, there are no published studies for the Berlin–Brandenburg region simulating chemistry and aerosols with an online-coupled regional chemistry transport model. Furthermore, only few of the above-mentioned studies included an assessment of urban NO_x concentrations. In light of the recent exceedances of NO_2 in European urban areas, including Berlin, this study can contribute to filling this gap and serve as a basis for future modelling studies addressing NO_x in European urban areas.

2   Model setup

2.1   Model description, chemistry and physics schemes

For this study, we use the Weather Research and Forecasting model (WRF) version 3.7.1 (Skamarock et al., 2008), with chemistry and aerosols (WRF-Chem, Grell et al., 2005; Fast et al., 2006). We use three one-way nested model domains centred around Berlin, at horizontal resolutions of 15 km × 15 km, 3 km × 3 km and 1 km × 1 km (Fig. 1). The model top is at 50 hPa, using 35 vertical levels. The first model layer is at approximately 30 m above the surface, with 12 levels in the first 3 km. The setup includes the RADM2 chemical mechanism with the Kinetic PreProcessor (KPP) and the MADE/SORGAM aerosol scheme. RADM2 has been used frequently in air quality applications over Europe (e.g. Mar et al., 2016; Im et al., 2015a; Tuccella et al., 2012); the effect of this choice of chemical mechanism on modelled concentrations is further discussed in Sect. 4.2. We give the priority to using the KPP solver instead of the QSSA (quasi-steady-state approximation) solver, because Forkel et al. (2015) found that the latter underestimates nighttime ozone titration for areas with high NO emissions. However, this option does not allow us to include the full aqueous-phase chemistry, including aerosol–cloud interactions and wet scavenging, and might thus reduce the model skill in simulating aerosols formed through aqueous-phase reactions as reported in Tuccella et al. (2012). All settings, including the physics schemes used in this study, are listed in Table 1, and the namelist can be found in the Supplement. We use the European Centre for Medium-Range Forecast (ECMWF) Interim reanalysis (ERA-Interim, Dee et al., 2011) with a horizontal resolution of 0.75° × 0.75°, temporal resolution of 6 h, interpolated to 37 pressure levels (with 29 levels below 50 hPa) as meteorological initial and lateral boundary conditions. This also includes the sea surface temperature, which is updated every 6 h. The data are interpolated to the model grid using the standard WRF preprocessing system (WPS).

Table 1. Physics and chemistry parameterisation.

Process	Scheme	Remarks
Cloud microphysics	Morrison double-moment	
Radiation (short wave)	RRTMG	called every 15 min
Radiation (long wave)	RRTMG	called every 15 min
Boundary layer physics	YSU	
Urban scheme	Single-layer urban canopy model	3 categories: roofs, walls, streets
Land surface processes	Noah LSM	CORINE land use input data
Cumulus convection	Grell–Freitas	switched on for all domains
Chemistry	RADM2	KPP version (chem_opt = 106)
Aerosol particles	MADE/SORGAM	
Photolysis	Madronich F-TUV	
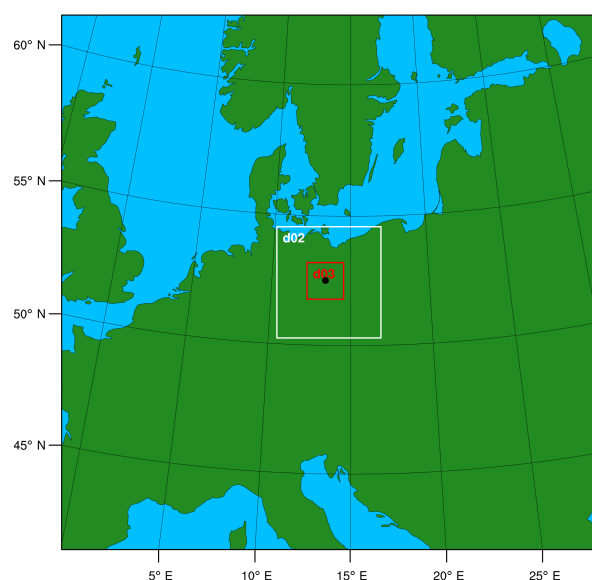
Figure 1. WRF-Chem model domains with horizontal resolutions of 15 km (d01, outer domain), 3 km (d02, middle domain) and 1 km (d03, inner domain), centred around Berlin, Germany, which is marked black in the figure.

Chemical boundary conditions for trace gases and particulate matter are created from simulations with the global chemistry transport Model for OZone and Related chemical Tracers (MOZART-4/GEOS-5, Emmons et al., 2010).

2.2   Land use specification

An analysis of the USGS land use data commonly used in WRF showed that the land cover of the region around Berlin is not represented well. In addition, the MODIS land use dataset as implemented in the WRF model from v3.6 only includes one category classifying urban areas. Therefore, we implemented the CORINE dataset (EEA, 2014) to replace the USGS dataset. The original CORINE dataset includes

50 land use classes. The land use classes at the spatial resolution of 250 m are remapped to 33 USGS land use classes read by WRF, following suggestions of Pineda et al. (2004) (see also Table S1). Additionally, we distinguish between inland water bodies (USGS class 28) and other water bodies (USGS class 16). We map the urban land use classes in CORINE to three urban classes used in WRF-Chem, including "commercial/industry/transport" (USGS class 33), high (USGS class 32) and low (USGS class 31) intensity residential (Tewari et al., 2008), which can be characterised as follows: "low intensity residential" (31) includes areas with a mixture of constructed materials and vegetation. Constructed materials account for 30–80 % of the cover and vegetation may account for 20–70 % of the cover. These areas most commonly include single-family housing units, and population densities are lower than in high intensity residential areas. "High intensity residential" (32) includes highly developed areas with a high population density. Examples include apartment complexes and row houses. Vegetation accounts for less than 20 % of the area and constructed materials account for 80 to 100 %. Commercial/industrial/transportation (33) includes infrastructure (e.g. roads, railroads) and all highly developed areas not classified as high intensity residential.

We implement the new land use categories as described in Tewari et al. (2008) (Fig. 2). In addition, we adjust the initialisation of the dry deposition of gaseous species to account for these new land use categories, as described in Fallmann et al. (2016). For the base run, we use the bulk approach of the land surface scheme, assigning the most abundant land use class within a model grid cell to the whole grid cell. In a sensitivity simulation, we test the mosaic approach (Li et al., 2013), allowing us to account for a heterogeneous land use classification within one model grid cell. Up to eight different land use types within one model grid cell are considered in our setup.

F. Kuik et al.: Evaluation of a WRF-Chem setup for the Berlin–Brandenburg region   **4343**

(a) d01 - 15 km x 15 km   (b) d02 - 3 km x 3 km   (c) d03 - 1 km x 1 km
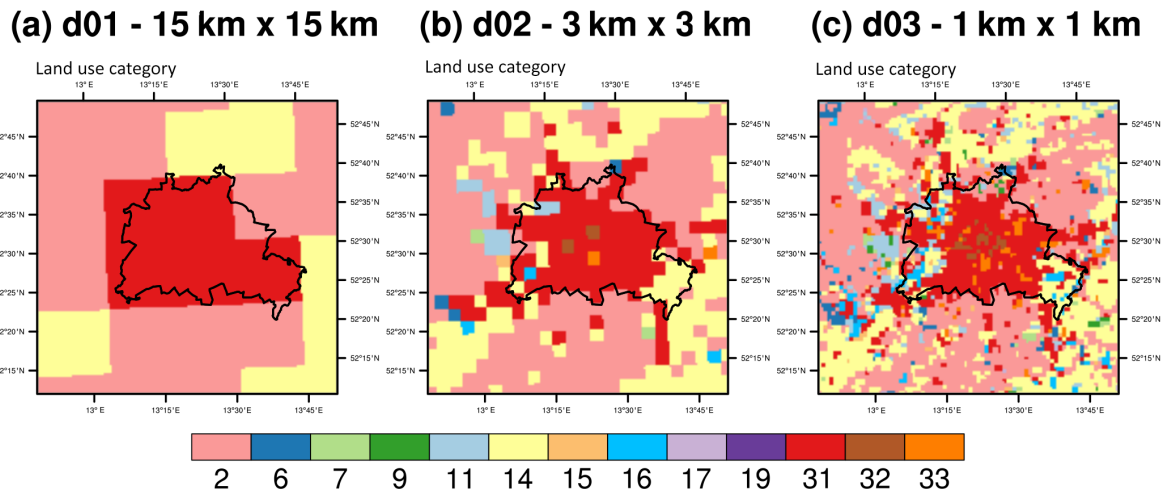
Figure 2. CORINE land use classes over Berlin mapped to USGS classes and interpolated to the WRF-Chem grids of **(a)** 15 km, **(b)** 3 km and **(c)** 1 km horizontal resolutions. The classes are the following: 2 – dryland cropland and pasture, 6 – cropland/woodland mosaic, 7 – grassland, 9 – mixed shrubland/grassland, 11 – deciduous broadleaf forest, 14 – evergreen needle leaf forest, 15 – mixed forest, 16 – water bodies, 17 – herbaceous wetland, 19 – barren or sparsely vegetated, 31 – low intensity residential, 32 – high intensity residential, 33 – commercial/industry/transport.

2.3   Urban parameters

We use the single-layer urban canopy model (Kusaka et al., 2001; Kusaka and Kimura, 2004) to account for the modified dynamics by cities, especially Berlin and Potsdam. The urban model takes into account energy and momentum exchange between urban areas (roofs, walls, streets) and the atmosphere and is coupled to the Noah land surface model. Surface fluxes (heat, moisture) and temperature are calculated as a combination of fluxes from urban and vegetated surfaces, coupled via the urban fraction assigned to the land use type of the grid cell (Chen et al., 2004). We choose to not use a more complex parameterisation of the urban canopy, such as the building effect parameterisation (BEP), because the computational cost is already very high at a horizontal resolution of 1 km × 1 km, and a more complex parameterisation of the urban canopy, along with the required increase of vertical model resolution, would increase the computational cost further and require a more detailed input dataset describing the urban structure. Moreover, the BEP is not applicable with the mosaic option in WRF so far and the only applicable planetary boundary layer (PBL) scheme in combination with the BEP and WRF-Chem is the Mellor–Yamada–Janjić scheme. This scheme often led to stronger biases in simulated 2 m air temperature than other parameterisations such as the YSU scheme (Hu et al., 2010; Loridan et al., 2013; Jänicke et al., 2016), the scheme selected for this study. In addition, Jänicke et al. (2016) could show that the BEP did not outperform simpler approaches such as the bulk scheme or the single-layer urban canopy model with respect to simu-

lating 2 m temperature and that the PBL scheme had stronger influence on simulated 2 m air temperature than the urban canopy parameterisation.

In our base simulation, we use the default input parameters as specified in the look-up table included in the standard distribution of the WRF source code available from UCAR. For a sensitivity simulation (Sect. 2.5), we calculate some of the urban input parameters to the model for Berlin (Table 2), which in previous studies have been found to be important. Geometric parameters include roof-level building height, standard deviation of the roof height, roof width and road width. The calculations are based on detailed maps of Berlin provided by the Senate Department for Urban Development and the Environment of Berlin. From the original data containing information on the location and number of floors of each house, the mean building height and the standard deviation of the building height is calculated assuming an average height of 3 m per floor, and the mean building length is calculated with the software QGIS, by calculating the surface area of each building geometry in the dataset and assuming its square root as each building's mean length. We combine these data with the CORINE land use data for Berlin mapped to the USGS classes (Sect. 2.2), averaging these parameters over the parts of the city characterised by the same urban class. The maps further provide the location of individual road segments, which we use to calculate the total area covered by roads in Berlin. We combine this with the total length of all roads in Berlin (Berlin Senate Department for Urban Development and the Environment, 2011b) to obtain the average road width, which we assign to all

Table 2. Urban parameters for Berlin for the three urban classes low intensity residential (31), high intensity residential (32) and commercial/industry/transport (33).

Parameter	Default (class 31/32/33)	Updated (class 31/32/33)
Roof level (m)	5/7.5/10	3/15/3
Standard deviation of roof height (m)	1/3/4	4.4/6.3/5.2
Roof width (m)	8.3/9.4/10	8.3/16.0/11.8
Road width (m)	8.3/9.4/10	17.5/17.5/17.5
Fraction of urban landscape without natural vegetation	0.5/0.9/0.95	0.4/0.7/0.48

three urban land use categories. We further update the urban fraction using a spatially more detailed classification of the land use types and the fraction of impervious surface of each area, provided by the Senate Department for Urban Development and the Environment of Berlin. Following Schubert and Grossman-Clarke (2013), we assume the urban fraction of a grid cell to be equal to the fraction of impervious surface. We then define the mean of impervious surface area, weighted by the area of the respective surface within each land use class as the updated urban fraction of the respective class. Following Fallmann et al. (2016) we use the values for thermal conductivity, heat capacity, emissivity and albedo of roofs, walls and streets specified in Salamanca et al. (2012).

2.4   Emissions

For the base run, anthropogenic emissions of CO, NO_x, SO_2, non-methane volatile organic compounds (NMVOCs), PM_{10}, $PM_{2.5}$ and NH_3 are taken from the TNO-MACC III inventory, with a horizontal resolution of $0.125° \times 0.0625°$. The inventory is based on nationally reported emissions for specific sectors, distributed spatially based on proxy data. In comparison to version II of the inventory (Kuenen et al., 2014), version III includes, amongst other updates, an improved distribution of emissions especially around cities. The distribution was improved by no longer using population density as a default for diffuse (non-point-source) industrial emissions but using industrial land use as a distribution proxy. Residential solid fuel use (wood, coal) was allocated more to rural areas than to large city centres on a per capita basis. Seasonal, weekly and diurnal emission profiles for Germany are applied to the aggregated emissions. This, as well as the speciation of the different NMVOCs, is described in Mar et al. (2016) and von Schneidemesser et al. (2016a). Mar et al. (2016) found that distributing emissions vertically did not strongly impact the model results near the surface. This, along with the low stack height of point sources within Berlin, is why in this study all emissions are released into the first model layer. As much of the NO_x emitted within Berlin is emitted from diesel vehicles (off-road and on-road), which studies have shown to be composed of high proportions of NO_2 (e.g. Alvarez et al., 2008), NO_x is emitted as 70 % NO and 30 % NO_2 (by mole). The latest available emis-

sion dataset is for 2011, which is used in the 2014 simulations. Dust, sea salt and biogenic emissions are calculated online, the latter using the Model of Emissions of Gases and Aerosols from Nature (MEGAN v2, Guenther et al., 2006).

We perform a sensitivity simulation for testing the model sensitivity to the spatial resolution of the emission input data (Sect. 2.5). As input to this sensitivity simulation, we downscale the anthropogenic emissions within Berlin onto a grid that is one-seventh of the original resolution, based on two proxy datasets, including traffic densities and population (Berlin Senate Department for Urban Development and the Environment, 2011a, b). Traffic densities are used to downscale all emissions from road transport, and population data are used to downscale emissions from industry, residential combustion and product use. Point sources are included in the grid cell within which the point source is located. In the TNO-MACC III inventory, all emissions from the energy industry within Berlin are point sources, and of the point-source emissions from other industry sectors ca. 55 % of the total emissions within Berlin for CO, 9–17 % for particulate matter and up to 1 % for other gases are included as point sources. Agricultural emissions within the city boundaries of Berlin are close to zero, which is why these are used at the original resolution.

2.5   Model simulations

Simulations are done for summer 2014 (31 May–28 August). We chose to simulate the summer of 2014, as this corresponds to the time period of the BAERLIN measurement campaign (e.g. Bonn et al., 2016). While mean observed temperatures in June and August showed little deviations from the observed 30-year mean (1961–1990) with mean temperatures of 17.0 °C (June) and 17.2 °C, the July mean temperature of 21.3 °C was 3.4 °C higher than the 30-year mean. Precipitation was 12 and 13 % lower than the 30-year mean in June (62.5 mm) and July (60.2 mm), respectively, and it was 48 % lower than the 30-year mean in August, with 33.8 mm (Berlin Senate Department for Urban Development and the Environment, 2014a, b, c).

For the analysis, the first day of all simulations is discarded as spinup. A base run with the settings described above is done in order to evaluate the model performance in simulat-

ing observed meteorology and atmospheric composition. In addition, sensitivity simulations done for this study are the following, with the changes applied to all three model domains of horizontal resolutions of 15, 3 and 1 km:

- S1_urb: updated representation of the urban characteristics of Berlin (see Sect. 2.3 and Table 2);

- S2_mos: consideration of the heterogeneity of the land use categories within one model grid cell (mosaic approach; see Sect. 2.2); and

- S3_emi: using emissions downscaled to ca. 1 km × 1 km (see Sect. 2.4).

The purpose of the sensitivity simulations is to assess which resolution and level of detail in the input data, including land use (S2_mos), emissions (S3_emi) and parameters characterising the urban area (S1_urb), are needed for simulating urban background air pollutant concentrations and their spatial distribution in the Berlin–Brandenburg area, particularly focusing on NO_x. We particularly ask whether a horizontal model resolution of 1 km, together with the above-listed specifications of the input data, leads to model results that differ from those obtained with a horizontal resolution of 3 km.

3　Observational data description and model evaluation procedure

3.1　Data description

In the following, we list the data and data sources that we use for evaluating the present WRF-Chem setup for Berlin and its surroundings. Table 3 gives an overview over all observational data and measurement stations in Berlin and its surroundings used in this study.

3.1.1　DWD stations

We use observations from the German Weather Service (DWD) for the variables of 2 m temperature, 10 m wind speed and direction and precipitation from stations within Berlin and Potsdam for 2014. A second-level quality control, as described in Kaspar et al. (2013), has been applied to the data. Additionally, we obtained mixing layer heights calculated from radiosonde observations directly from the DWD at the Lindenberg station south-east of Berlin, as described in Beyrich and Leps (2012). In addition, we use specific humidity data from the Global Weather Observation dataset provided by the British Atmospheric Data Centre (BADC) for the same stations.

3.1.2　TU stations

The Chair of Climatology of Technische Universität Berlin (TU) runs an urban climate observation network (Fenner

et al., 2014), from which we use observations of 2 m air temperature to complement observations from DWD stations. We include this additional data source, as many of the TU stations are situated in urban built-up areas (see Table 3). We use quality-checked data aggregated to hourly mean values.

3.1.3　GRUAN network

The Global Climate Observing System Upper-Air Network (GRUAN) hosts radiosonde observations at high vertical resolution, of which we use observations of temperature in Lindenberg (Sommer et al., 2012) to compare them to the modelled profiles. The data used for this study are quality checked, processed and bias corrected as described in Sommer et al. (2012) and Dirksen et al. (2014).

3.1.4　UBA database and BLUME network

Legally required air quality observations in Germany are reported to the Federal Environment Agency (UBA). We use observations of PM_{10}, $PM_{2.5}$, NO_2, NO and O_3 for 2014 reported to UBA. The data are collected from measurement networks operated by the federal states. In Berlin, the official measurement network is the BLUME network (Berliner Luftgüte-Messnetz), operated by the Senate Department for Urban Development and the Environment of Berlin. In addition to the data reported to the UBA database, we use PM_{10} concentrations measured at three stations in Berlin and the 2 m temperature measured at the urban built-up station Nansenstraße from the BLUME network.

3.1.5　BAERLIN2014

The BAERLIN2014 ("Berlin Air quality and Ecosytem Research: Local and long-range Impact of anthropogenic and Natural hydrocarbons 2014") campaign took place in Berlin in summer 2014 and is described in detail in Bonn et al. (2016) and von Schneidemesser et al. (2016b). For the present study, we use observations of $PM_{2.5}$ calculated from particle number concentrations collected near the Nansenstraße station of the BLUME network and observations of the mixing layer height collected at Nansenstraße with a ceilometer. In addition, filter samples taken at Nansenstraße were analysed for the composition of PM_{10} (von Schneidemesser et al., 2016), which we use to compare to simulated aerosols.

3.2　Model evaluation procedure

In order to assess the model's skill in simulating observed meteorology, we compare the modelled (coarse domain) weather types with weather types calculated from the ERA-Interim reanalysis data for Berlin (Sect. 4.1). The weather types are based on indices calculated to classify circulation patterns and are further described in Otero et al. (2016). We then focus on evaluating the modelled meteorology includ-

Table 3. Observational data in Berlin and Potsdam. If one class is given, it refers to the meteorology class if the network is Deutscher Wetterdienst (DWD), Global Climate Observing System Upper-Air Network (GRUAN) or TU, and to the chemistry class otherwise. The abbreviated name (Abbr.) is referred to in tables summarising statistics for the different stations.

Station	Abbr.	Network	Class (meteorology/chemistry)	Species used
Nansenstraße	nans	BAERLIN	urban built-up/urban background	$PM_{2.5}$, PM comp., MLH
Nansenstraße	nans	BLUME	urban built-up/urban background	NO, NO_2, O_3, PM_{10}, $T2$
Amrumer Straße	amst	BLUME	urban background	PM_{10}, $PM_{2.5}$, NO, NO_2, O_3
Belziger Straße	belz	BLUME	urban background	PM_{10}, NO, NO_2
Brückenstraße	brue	BLUME	urban background	PM_{10}, $PM_{2.5}$, NO, NO_2
J. u. W. Brauer Platz	jwbp	BLUME	urban background	NO, NO_2
Potsdam-Zentrum	pots	UBA	urban background	PM_{10}, $PM_{2.5}$, NO, NO_2, O_3
Blankenfelde-Mahlow	blan	UBA	suburban background	PM_{10}, $PM_{2.5}$, NO, NO_2, O_3
Buch	buch	BLUME	suburban background	PM_{10}, NO, NO_2, O_3
Grunewald	grun	BLUME	suburban background	PM_{10}, NO, NO_2, O_3
Potsdam, Groß Glienicke	glie	UBA	suburban background	PM_{10}, NO, NO_2, O_3
Schichauweg	schw	BLUME	rural industrial	NO, NO_2, O_3
Müggelseedamm	mueg	BLUME	rural background	PM_{10}, NO, NO_2, O_3
Frohnau	froh	BLUME	rural background	NO, NO_2, O_3
Marzahn	marz	DWD	urban built-up	$T2$, prec., $Q2$
Botanischer Garten	botg	DWD/FU	urban green	$T2$, prec., $Q2$
Tegel	tege	DWD	urban green	$T2$, WS10, WD10, prec., $Q2$
Tempelhof	temp	DWD	urban green	$T2$, WS10, WD10, prec., $Q2$
Buch	buch	DWD	urban green	$T2$, prec., $Q2$
Kaniswall	kani	DWD	rural	$T2$, prec., $Q2$
Potsdam	pots	DWD	rural	$T2$, WS10, WD10, prec., $Q2$
Schönefeld	scho	DWD	rural	$T2$, WS10, WD10, prec., $Q2$
Lindenberg	lind	DWD/GRUAN	rural	T, ws, q profiles
Bamberger Straße	bamb	TU	urban built-up	$T2$
Dessauer Straße	dest	TU	urban built-up	$T2$
Rothenburgstraße	roth	TU	urban built-up	$T2$
Albrechtstraße	albr	TU	urban green	$T2$
Tiergarten	tier	TU	urban green	$T2$
Dahlemer Feld	dahf	TU	rural	$T2$

ing the following diagnostic variables: 2 m temperature ($T2$), 10 m wind speed and direction (WS10 and WD10), the atmospheric structure via comparing temperature profiles and mixing layer height (MLH), as well as 2 m specific humidity ($Q2$) and precipitation. While $T2$, WS10, WD10 and atmospheric vertical structure are important parameters for simulating atmospheric chemistry and aerosols, $Q2$ and precipitation will not have an impact on our results, as our setup does not include aqueous-phase chemistry or wet scavenging. However, we include $Q2$ and precipitation to complete the picture of the evaluation of simulated meteorology as well as to give an indication for future studies based on this setup. Finally, we evaluate the model performance for the main air pollutants including surface O_3, NO_x and PM, with a main focus on NO_x. We evaluate the model results from all three domains with horizontal resolutions of 15, 3 and 1 km, which we also refer to as d01, d02 and d03.

3.2.1 Comparison with surface station data

The evaluation of surface parameters is based on statistical metrics including the Pearson correlation coefficient (r), the mean bias (MB) and the normalised mean bias (NMB). The metrics are defined as follows, with n the number of model–observation pairs, M the modelled values, O the observations and σ the standard deviation of modelled or observed values:

$$r = \frac{1}{(n-1)} \sum_{i=1}^{n} \left(\frac{M_i - \overline{M}}{\sigma_M} \right) \left(\frac{O_i - \overline{O}}{\sigma_O} \right)$$

$$MB = \frac{1}{n} \sum_{i=1}^{n} M_i - O_i$$

$$NMB = \frac{\sum_{i=1}^{n} M_i - O_i}{\sum_{i=1}^{N} O_i}.$$

For the meteorological parameters, the metrics are calculated from instantaneous hourly modelled values and hourly averages of the observations. Wind speed is considered as a

F. Kuik et al.: Evaluation of a WRF-Chem setup for the Berlin–Brandenburg region   **4347**

scalar and no metrics are calculated for wind direction. The O_3, NO_x and PM values are calculated from daily averages. The NMB was only calculated for air pollutants and the mixing layer height. For ozone, we also consider the maximum daily 8 h mean (MDA8) concentrations, a metric used in the European Union's Air Quality Directive.

As an additional means of assessing the model performance, we look at conditional quantile plots (Carslaw and Ropkins, 2012) for some species. The conditional quantile plot displays the model results, split into evenly spaced bins, in comparison to observations temporally matching the values in the model result bins. Thus, it gives additional insight into how well the modelled values agree with the observations, e.g. on the range of modelled and observed values.

For the comparison between model and observations, we classify the stations in terms of their surroundings, distinguishing between urban built-up, urban green and rural areas for the meteorology observations, and between urban background, suburban background and rural areas for air quality observations, excluding those from traffic stations.

3.2.2 Evaluation of the atmospheric structure

The mean modelled temperature profiles are compared to observations from radiosondes as follows: as the observed temperatures have a much higher spatial resolution than the model, we select a subset of the observations for comparison with the model. For every modelled temperature profile at 00:00, 06:00, 12:00 and 18:00 UTC, we select the observations closest to the modelled geopotential height of each model level. The time averaging of modelled geopotential heights is done as follows: we divide the values into vertical bins corresponding to the 5th, 10th, 15th percentiles and so on, until the 95th percentile of the modelled geopotential height, and average the temperature as well as the geopotential height over each bin for both model and observations, and over each day of the modelled period. Even though observations of temperature profiles are only available outside of the urban area of Berlin, we include this comparison in order to get a general impression of how the model performs in simulating the vertical atmospheric structure in the lowest 2–3 km.

The modelled MLH is compared to observations in two different ways: firstly, using the planetary boundary layer height directly diagnosed by WRF-Chem, which in the YSU scheme is calculated based on comparing the Richardson number with a critical value of 0 (Hong et al., 2006). Secondly, by calculating the MLH from the simulated profiles of temperature, wind speed and humidity, defining the mixing layer height as the height where the Richardson number is 0.2, following Beyrich and Leps (2012). This corresponds to the method the MLH is derived from using radiosonde observations at Lindenberg.
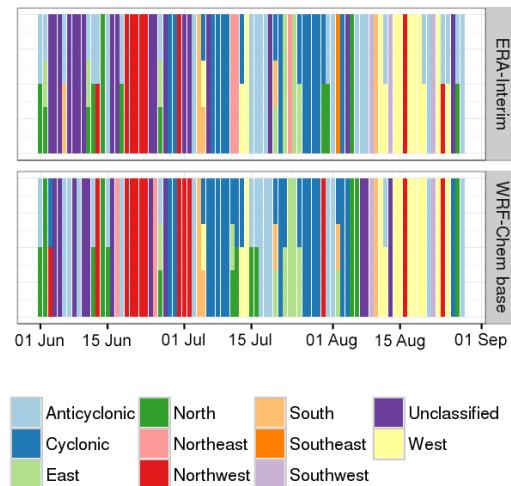
Figure 3. Comparison of weather types for Berlin calculated from ERA-Interim reanalysis data (top panel) and from WRF-Chem output from the domain with 15 km horizontal resolution (bottom panel). Up to three weather types are calculated for each day.
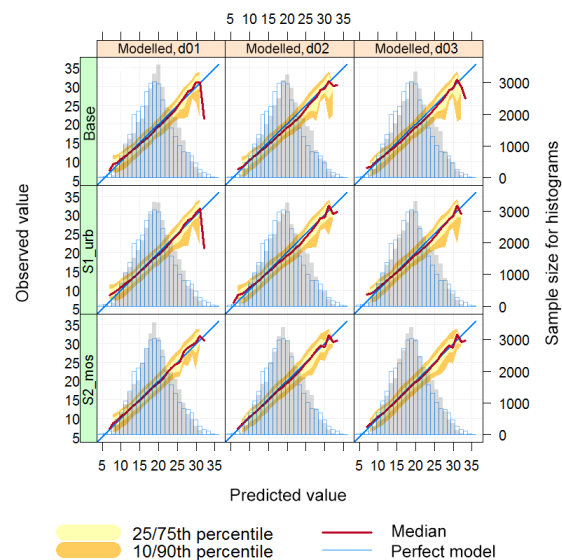
Figure 4. Conditional quantile plot of simulated and observed temperature (°C). The model results are split into evenly spaced bins and compared to observations spatially and temporally matching the values in the model result bins. The red line denotes the median of each of these bins. Grey bars show the distribution of model results, blue outline bars the distribution of observations. The results are shown for the base run and sensitivity simulations S1_urb and S2_mos, each for all three model domains (d01 – 15 km horizontal resolution, d02 – 3 km, d03 – 1 km).

Table 4. Statistics of hourly 2 m temperature for JJA for stations, where the land use class of the respective grid cell changes with resolution. "LU" refers to the WRF land use class of the grid cell in the respective domain, "Obs" refers to the JJA observed mean, "Mod" refers to the JJA modelled mean for the respective grid cell. MB is the mean bias for JJA and *r* is the correlation of hourly values. Obs, Mod and MB are in °C. The statistics are shown for the results from the model domains of 15 km (d01), 3 km (d02) and 1 km (d03) horizontal resolution.

Station				Base			S1_urb			S2_mos		
		LU	Obs	Mod	MB	*r*	Mod	MB	*r*	Mod	MB	*r*
kani	d01	31	18.1	19.6	1.5	0.88	19.3	1.2	0.88	19.2	1	0.89
	d02	2	18.1	19.4	1.3	0.9	19.3	1.2	0.9	19.3	1.1	0.89
	d03	2	18.1	19.4	1.2	0.9	19.2	1.1	0.9	19.2	1.1	0.89
marz	d01	2	19.2	18.8	−0.4	0.91	18.7	−0.6	0.9	18.9	−0.4	0.92
	d02	31	19.2	19.6	0.4	0.91	19.4	0.2	0.9	19.2	0	0.9
	d03	31	19.2	19.7	0.4	0.91	19.3	0.1	0.9	19.2	0	0.9
scho	d01	31	18.8	19.6	0.8	0.92	19.3	0.6	0.91	19.2	0.4	0.92
	d02	31	18.8	19.9	1.1	0.91	19.7	0.9	0.91	19.4	0.6	0.91
	d03	2	18.8	19.3	0.6	0.92	19.2	0.4	0.91	19.3	0.6	0.91
temp	d01	31	19.3	19.6	0.3	0.92	19.3	0	0.91	19.3	−0.1	0.92
	d02	33	19.3	20.3	0.9	0.9	19.7	0.4	0.9	19.6	0.3	0.9
	d03	33	19.3	20.2	0.8	0.9	19.6	0.3	0.9	19.5	0.2	0.9
nans	d01	31	20.8	19.6	−1.1	0.91	19.3	−1.4	0.9	19.3	−1.5	0.91
	d02	31	20.8	19.9	−0.9	0.9	19.6	−1.1	0.89	19.6	−1.2	0.9
	d03	32	20.8	20.2	−0.5	0.9	20	−0.8	0.89	19.6	−1.2	0.9
dahf	d01	31	17.9	19.6	1.6	0.88	19.3	1.4	0.89	19.1	1.1	0.9
	d02	14	17.9	19.3	1.4	0.9	19.1	1.2	0.9	19.3	1.4	0.88
	d03	14	17.9	19.2	1.3	0.9	19	1.1	0.9	19.2	1.3	0.88
bamb	d01	31	19.3	19.6	0.4	0.9	19.3	0.1	0.89	19.3	0	0.91
	d02	31	19.3	19.9	0.6	0.89	19.6	0.4	0.88	19.6	0.3	0.9
	d03	32	19.3	20.2	0.9	0.9	19.9	0.7	0.89	19.5	0.2	0.9

4 Model evaluation results: base run

4.1 Meteorology

Generally, the modelled weather types (see Sect. 3.2) are consistent with those derived from the reanalysis (Fig. 3). Periods in which WRF-Chem weather types disagree with ERA-Interim weather types never exceed two subsequent days and the frequency of WRF-Chem weather types agrees similarly well with ERA-Interim weather types.

The temporal correlation of modelled hourly 2 m temperature with observations is between 0.88 and 0.91 at all stations in and around Berlin and all model domains (Tables 4 and S3 in the Supplement), which shows that the model represents the observed temperature variability well. This is supported by the analysis of the conditional quantiles (Fig. 4), which show that the modelled temperatures match the observations well for a wide range of values. The model is generally biased positively with up to +1.6 °C, though the bias at most stations is smaller than +1 °C (Tables 4 and S3). In absolute terms, this is within the same range, but never larger than the biases that Trusilova et al. (2016) and Schubert and Grossman-Clarke (2013) found using COSMO-CLM in combination with different urban canopy models for Berlin. Besides, the absolute mean biases are comparable to those

reported by Jänicke et al. (2016), who mainly found negative biases in near-surface air temperature applying WRF 3.6.1 for Berlin and its surroundings, testing two planetary boundary layer schemes and three urban canopy models.

The histogram in the conditional quantile plot and the extent of the blue line marking the "perfect model" show that WRF-Chem does not reproduce the highest observed temperatures. This suggests that the model might have difficulties in simulating pronounced heat wave periods. However, comparing the modelled daily maximum temperatures to the observed daily maximum temperatures (Tables 5 and S4) shows that the bias of the daily maximum temperatures is of a similar magnitude as the mean bias, with one difference: while the bias of maximum temperatures modelled with 3 and 1 km resolutions is mainly positive, the bias of the maximum temperatures modelled with a 15 km resolution is negative. In absolute terms, the bias of the daily maximum temperatures is smallest for results obtained with a 1 km resolution, though they only differ very little from the results obtained with a 3 km resolution.

We find two important relationships with respect to model resolution: firstly, the model simulates higher temperatures in the model domain of which the model grid cell land use type is urban (stations Kaniswall, Dahlemer Feld, Marzahn, Schönefeld). Secondly, while the modelled 2 m temperatures

Table 5. Statistics of daily maximum 2 m temperature for JJA for stations, where the land use class of the respective grid cell changes with resolution. "LU" refers to the WRF land use class of the grid cell in the respective domain, "Obs" refers to the JJA observed mean, "Mod" refers to the JJA modelled mean for the respective grid cell. MB is the mean bias for JJA and r is the correlation of hourly values. Obs, Mod and MB are in °C. The statistics are shown for the results from the model domains of 15 km (d01), 3 km (d02) and 1 km (d03) horizontal resolution.

Station		LU	Obs	Base			S1_urb			S2_mos		
				Mod	MB	r	Mod	MB	r	Mod	MB	r
kani	d01	31	24.2	23.8	−0.4	0.88	23.6	−0.6	0.87	23.3	−0.9	0.89
	d02	2	24.2	24.4	0.2	0.9	24.3	0.1	0.87	23.9	−0.3	0.9
	d03	2	24.2	24.3	0.1	0.9	24.2	0	0.87	23.8	−0.4	0.89
marz	d01	2	23.9	23.4	−0.5	0.88	23.2	−0.8	0.86	23	−1	0.9
	d02	31	23.9	24.2	0.2	0.89	24	0	0.87	23.5	−0.4	0.9
	d03	31	23.9	24.1	0.2	0.89	23.9	0	0.87	23.5	−0.5	0.9
scho	d01	31	23.8	23.8	0	0.88	23.6	−0.3	0.87	23.3	−0.5	0.9
	d02	31	23.8	24.4	0.6	0.9	24.3	0.5	0.88	23.8	0	0.91
	d03	2	23.8	24.3	0.5	0.9	24.1	0.3	0.88	23.7	−0.1	0.9
temp	d01	31	24.1	23.8	−0.3	0.88	23.5	−0.6	0.87	23.3	−0.8	0.89
	d02	33	24.1	24.5	0.3	0.9	24.3	0.2	0.87	23.8	−0.3	0.9
	d03	33	24.1	24.4	0.2	0.9	24.2	0	0.87	23.6	−0.5	0.91
nans	d01	31	25.5	23.8	−1.7	0.86	23.5	−1.9	0.85	23.3	−2.2	0.88
	d02	31	25.5	24.4	−1.1	0.87	24.2	−1.3	0.85	23.8	−1.7	0.88
	d03	32	25.5	24.5	−1	0.87	24.2	−1.3	0.85	23.6	−1.8	0.88
dahf	d01	31	23.8	23.7	−0.1	0.89	23.5	−0.3	0.88	23.3	−0.5	0.9
	d02	14	23.8	24.1	0.3	0.9	24	0.2	0.88	23.7	−0.1	0.9
	d03	14	23.8	24	0.2	0.9	23.8	0	0.88	23.5	−0.3	0.9
bamb	d01	31	22.9	23.8	0.9	0.88	23.5	0.7	0.87	23.3	0.4	0.9
	d02	31	22.9	24.4	1.5	0.89	24.2	1.3	0.87	23.8	0.9	0.9
	d03	32	22.9	24.4	1.5	0.9	24.1	1.2	0.87	23.6	0.7	0.9

generally differ between the 15 and 3 km resolution even if the land use type of both grid cells in which the station is located is the same; the June–July–August (JJA) mean modelled temperature only changes by more than 0.1 °C between the 3 and 1 km resolution if the land use type changes (stations Bamberger Straße, Nansenstraße, Schönefeld). This indicates that switching from a horizontal resolution of 15 to 3 km might improve the spatial distribution of modelled temperatures, while switching from a horizontal resolution of 3 to 1 km has only a very little effect on improving the model's skill in simulating the observed temperature, but might be more beneficial if the land use input data are specified with a higher level of accuracy.

The comparison of simulated with observed temperature profiles (Fig. 5) shows that the model reproduces the observed temperature profile well at all times, but that the modelled temperature profile at 12:00 UTC is shifted to higher temperatures by ca. 1 °C. The result is similar for all model resolutions (the profiles for the 15 km and 3 km resolutions can be found in the Supplement in Figs. S1 and S2). In order to further evaluate how the present WRF-Chem setup simulates the observed vertical structure, we compare the simulated mixing layer height derived from simulated profiles of temperature, wind speed and humidity (in the fol-
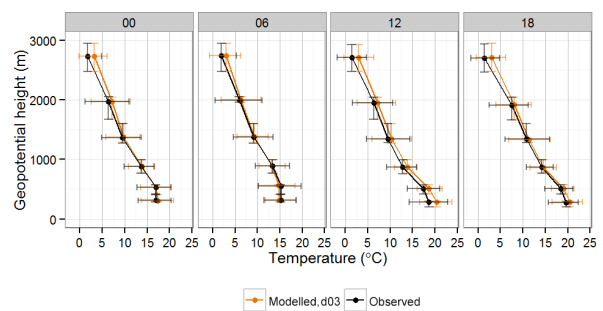
Figure 5. JJA mean profiles of observed and modelled (base run, 1 km × 1 km horizontal resolution) temperature at Lindenberg at 00:00, 06:00, 12:00 and 18:00 UTC. Error bars show the 25th and 75th percentiles of temperature and geopotential height.

lowing also referred to as MLH-calc) to the mixing layer height derived from radiosonde observations at Lindenberg as described in Beyrich and Leps (2012) (Fig. 6). The results show that the model simulates the observed diurnal cycle of the MLH as well as the magnitude of the observed MLH at Lindenberg reasonably well: the bias of the daily mean MLH ranges between +87 m (13 %) and +113 m (16 %),

Table 6. Statistics of daily minimum, mean and maximum mixing layer height for JJA. "Obs" refers to the JJA observed mean, "Mod" refers to the JJA modelled mean for the respective grid cell. MB is the mean bias for JJA, NMB refers to the normalised mean bias and r is the correlation of hourly values. The values given in the column "YSU" refer to the MLH diagnosed directly by WRF-Chem, while "Calc" refers to the MLH calculated from modelled profiles of temperature, wind speed and humidity. Obs, Mod and MB are given in metres and NMB is given in %. The statistics are shown for the results from the model domains of 15 km (d01), 3 km (d02) and 1 km (d03) horizontal resolution.

Station				YSU				Calc			
			Obs	Mod	MB	NMB	r	Mod	MB	NMB	r
Lindenberg	max	d01	1414.1	1657.9	243.8	17.2	0.29	1681.8	267.7	18.9	0.28
		d02	1414.1	1701.5	287.3	20.3	0.22	1761.1	347	24.5	0.2
		d03	1414.1	1635.4	221.3	15.6	0.21	1708.8	294.7	20.8	0.19
	mean	d01	689.8	736.3	46.6	6.8	0.33	777.2	87.4	12.7	0.27
		d02	689.8	718.7	28.9	4.2	0.28	802.8	113	16.4	0.22
		d03	689.8	685.7	−4	−0.6	0.27	783.3	93.5	13.6	0.22
	min	d01	187.5	88.8	−98.7	−52.6	0.09	202.1	14.6	7.8	0.26
		d02	187.5	74.4	−113.1	−60.3	0.07	228.8	41.4	22.1	0.27
		d03	187.5	75	−112.4	−60	0.17	235.8	48.4	25.8	0.31
Nansenstraße	max	d01	2312.8	1672.2				1701.4			
		d02	2312.8	1792.7				1825.8			
		d03	2312.8	1760.6				1787.2			
	mean	d01	906.7	774				825.6			
		d02	906.7	785.2				843.9			
		d03	906.7	741.4				843.7			
	min	d01	175.4	93.7				210.1			
		d02	175.4	76.9				197.2			
		d03	175.4	53.1				212.3			

depending on model resolution, and the biases of the daily maximum and daily minimum are between +268 m (19 %) and +347 m (25 %) and between +26 m (14 %) and +48 m (26 %), respectively (Table 6). There is no consistent trend with increasing model resolution. It is important to note that these results refer to the MLH that we calculated from simulated profiles of temperature, wind speed and humidity. However, the MLH diagnosed by the model, in the following also referred to as MLH-YSU, underestimates the observations especially during nighttime (Fig. 6), with a bias of the daily minimum MLH between −99 m (−53 %) and −113 m (−60 %), or a MLH lower than the calculated one between −128 and −214 %. Differences between the different ways of deriving the MLH for daily maximum values are less pronounced, ranging between 24 m (1 %) and 73 m (4 %). This leads to the conclusion that the model generally simulates the atmospheric structure well, but that the planetary boundary layer scheme underestimates observed MLH during nighttime. Similarly, this indicates that the mixing might also be underestimated by the boundary layer scheme during nighttime conditions.

Comparing the model results to ceilometer observations from Berlin at the Nansenstraße station also indicates that the diurnal variation is reproduced correctly (Fig. S9 in the Supplement). The comparison of daily minimum MLH with ceilometer observations also shows an underestimation of MLH-YSU in the same range as at Lindenberg. However,
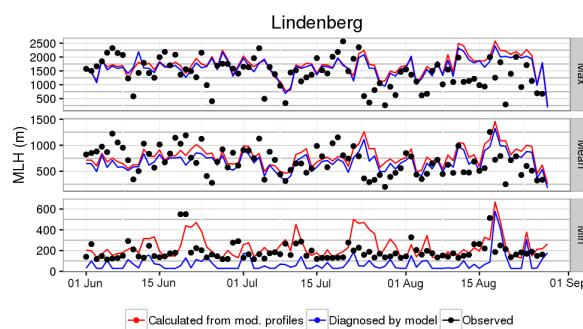
Figure 6. Daily minimum, mean and maximum mixing layer height as observed in Lindenberg, diagnosed by WRF-Chem and calculated from modelled profiles of temperature, wind speed and humidity (base run, 1 km × 1 km horizontal resolution).

we do not know whether the magnitude of the mixing layer height derived from the ceilometer backscatter profile is directly comparable with the mixing layer height calculated from profiles of temperature, wind speed and humidity or with the mixing layer height calculated by the model. This makes it more difficult to evaluate the modelled mixing layer height quantitatively at the urban site Nansenstraße. For this, further studies assessing the comparability of MLH derived from radiosonde and ceilometer observations would be necessary.
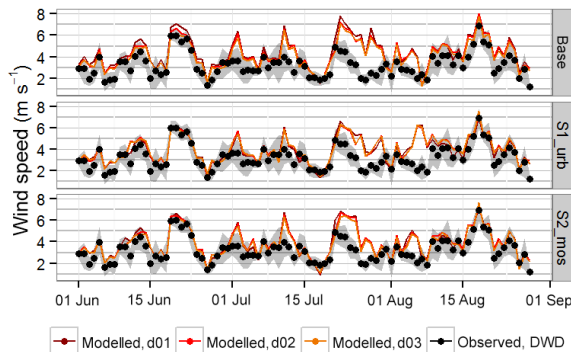
Figure 7. Daily mean observed and modelled wind speed from the base run, S1_urb and S2_mos, for all three model domains (d01 – 15 km horizontal resolution, d02 – 3 km, d03 – 1 km). The figures show means over the daily means of three stations in Berlin (Tegel, Schönefeld and Tempelhof). The grey shades show the variability between the daily means of these stations, corresponding to the 25th and 75th percentiles of the individual stations' daily means. For the model results, the grid cells corresponding to the location of the stations were extracted.

Figure 8. Wind roses over observed and modelled values for JJA, including observations and model results for three stations in Berlin (Tegel, Schönefeld and Tempelhof) and from all three model domains (d01 – 15 km horizontal resolution, d02 – 3 km, d03 – 1 km). The bars refer to the frequency of how often wind was coming from the respective direction and the colours indicate how often the wind speed was observed or modelled in the indicated interval.

Simulated hourly wind speed correlates with observations with a correlation coefficient between 0.5 and 0.6 (Table S5 in the Supplement), which is comparable to simulations for the European domain (Mar et al., 2016). Wind speed is overestimated between $0.4 \, \mathrm{m \, s^{-1}}$ (15 %) and $1.4 \, \mathrm{m \, s^{-1}}$ (50 %), depending on the station. The overestimation is especially strong at stations with mean observed wind speeds below $3 \, \mathrm{m \, s^{-1}}$, as well as for a period of easterly winds in mid-July (Fig. 7). The most frequently observed wind direction at three stations in Berlin and in Potsdam in June, July and August 2014 is westerly. This is reproduced by the model, with better skill with increasing resolution (Fig. 8). Depending on the modelled wind direction, the bias in wind speed differs: while the bias (averaged over all four stations) is lower than $1 \, \mathrm{m \, s^{-1}}$ for modelled wind from north to south-east, the bias is larger for wind simulated from east and north-east. In addition, the conditional quantile plot of wind speed, split by modelled wind direction, also shows that the model's skill in simulating wind speed from west and south-west is higher (see Fig. S3 in the Supplement).
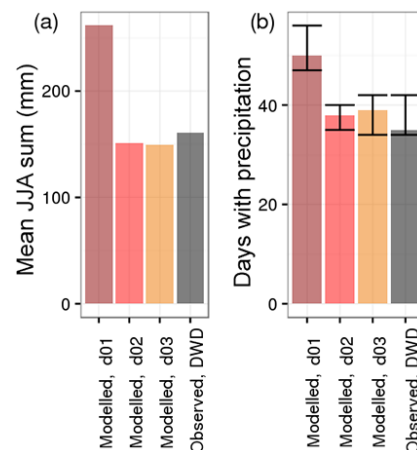
Both the diurnal variability and the magnitude of specific humidity are simulated well by the model, with normalised mean biases between −7 and +7 % and correlation coefficients of 3-hourly values of around 0.8 (not shown). Precipitation is simulated well with the 3 and 1 km horizontal resolution: both the number of days with precipitation rates larger than $0.01 \, \mathrm{mm \, h^{-1}}$ and the total amount of precipitation in the simulated period agree well with the observations (Fig. 9). Model results from the 15 km resolution overestimate the number of days with precipitation larger than $0.01 \, \mathrm{mm \, h^{-1}}$ by ca. 30 % and the amount by ca. 50 %. This shows that the

Figure 9. (a) Station average (mean) precipitation sum of observations and model results (base run), **(b)** median number of days with precipitation observed or modelled. A day is counted if observed or modelled precipitation was more than $1 \, \mathrm{mm \, h^{-1}}$. Ranges indicate the variability between the different stations. Both panels **(a)** and **(b)** show averages over nine stations and the corresponding model grid cells in Berlin and its surroundings. Model results are given for all three model domains (d01 – 15 km horizontal resolution, d02 – 3 km, d03 – 1 km).

higher-resolved domains in the nested setup, using the Grell–Freitas cumulus scheme on all domains, improve the skill in simulating precipitation, which is an important conclusion for future studies with a similar setup aiming at including aqueous-phase chemistry and wet scavenging.

Table 7. Statistics of daily NO_x for JJA. "Obs" refers to the JJA observed mean, "mod" refers to the JJA modelled mean for the respective grid cell. MB is the mean bias for JJA, NMB refers to the normalised mean bias and r is the correlation of hourly values. Obs, Mod and MB are given in $\mu g\,m^{-3}$ and NMB is given in %. The statistics are shown for the results from the model domains of 15 km (d01), 3 km (d02) and 1 km (d03) horizontal resolution.

| Station		Obs	Base				S1_urb				S2_mos				S3_emi			
			Mod	MB	NMB	r	Mod	MB	NMB	r	Mod	MB	NMB	r	Mod	MB	NMB	r
froh	d01	8.3	20.2	11.9	143.7	0.56	22	13.7	164.6	0.43	26	17.7	213.2	0.55	18.4	10.1	121.2	0.45
	d02	8.3	10.3	2	24.6	0.55	10.6	2.3	28.1	0.48	11.4	3.1	37.1	0.55	8.4	0.1	1.6	0.5
	d03	8.3	10.1	1.8	21.4	0.56	10.7	2.4	28.5	0.49	10.7	2.4	29.3	0.56	8.2	−0.1	−0.8	0.49
grun	d01	9.1	12.4	3.3	36.2	0.46	13.1	4	43.7	0.46	16.4	7.3	80	0.49	9.3	0.2	1.7	0.42
	d02	9.1	16.1	7	76.6	0.3	16.7	7.6	83.2	0.38	18.4	9.3	101.7	0.39	12.8	3.7	40.2	0.42
	d03	9.1	15.8	6.7	73.8	0.27	16.5	7.3	80.5	0.37	18.7	9.6	104.9	0.33	11.6	2.5	27.3	0.31
mueg	d01	9.1	14	4.9	53.7	0.42	15.4	6.2	68.1	0.36	17.7	8.6	94.2	0.49	12.1	3	32.9	0.37
	d02	9.1	14.4	5.3	58	0.4	16.2	7.1	77.5	0.36	16.7	7.5	82.6	0.5	13.2	4.1	44.8	0.33
	d03	9.1	13.5	4.3	47.6	0.45	14.7	5.5	60.4	0.38	15.3	6.2	67.6	0.52	12.1	3	32.7	0.37
schw	d01	11.7	21.8	10.1	86	0.41	23.3	11.6	98.7	0.34	27.4	15.7	133.6	0.49	20.5	8.8	74.8	0.31
	d02	11.7	14.2	2.5	20.9	0.36	15.2	3.5	29.7	0.36	16.3	4.6	38.9	0.48	10.5	−1.3	−10.9	0.2
	d03	11.7	14	2.3	19.3	0.39	15.4	3.6	31.1	0.38	16	4.3	36.8	0.47	11.3	−0.4	−3.2	0.18
blan	d01	11.9	10.8	−1.1	−9.2	0.26	10.7	−1.2	−10	0.2	10.8	−1	−8.6	0.24	9.6	−2.2	−18.8	0.17
	d02	11.9	12.8	0.9	7.6	0.22	13.7	1.8	15.5	0.21	14.8	2.9	24.6	0.31	10.4	−1.5	−12.4	0.17
	d03	11.9	11.2	−0.6	−5.4	0.26	11.7	−0.2	−1.8	0.18	12.5	0.7	5.6	0.29	9.1	−2.7	−23.1	0.16
buch	d01	11	20.2	9.3	84.2	0.62	22	11	100	0.54	26	15	136.7	0.57	18.4	7.4	67.2	0.54
	d02	11	11.1	0.1	0.8	0.7	12.4	1.4	12.5	0.65	12.9	2	17.9	0.68	9.6	−1.4	−12.9	0.66
	d03	11	10.3	−0.7	−6.2	0.7	12.2	1.2	11.1	0.62	12.2	1.2	11	0.67	9	−2	−18.2	0.64
glie	d01	8.7	12.4	3.7	42.8	0.44	13	4.4	50.6	0.48	16.3	7.7	88.4	0.38	9.2	0.6	6.7	0.44
	d02	8.7	15.4	6.7	77.3	0.5	15.4	6.7	77.5	0.52	17.8	9.1	105.2	0.43	8.9	0.2	2.4	0.53
	d03	8.7	13.4	4.8	54.9	0.49	13.6	4.9	56.7	0.51	15.7	7	80.9	0.42	8.6	0	−0.4	0.57
amst	d01	26.6	20.2	−6.3	−23.8	0.67	22	−4.6	−17.3	0.62	26	−0.6	−2.1	0.68	18.4	−8.2	−30.9	0.63
	d02	26.6	24.9	−1.7	−6.4	0.64	27.3	0.8	2.8	0.6	29.9	3.3	12.5	0.63	26.9	0.3	1.1	0.6
	d03	26.6	23.5	−3	−11.4	0.61	26.5	−0.1	−0.3	0.59	29.5	3	11.1	0.59	29	2.4	9.2	0.58
belz	d01	23.4	21.8	−1.6	−6.9	0.49	23.3	−0.1	−0.6	0.4	27.4	4	16.9	0.52	20.5	−2.9	−12.5	0.46
	d02	23.4	22.2	−1.2	−5.2	0.45	24	0.5	2.3	0.4	25.9	2.5	10.7	0.48	20.3	−3.1	−13.2	0.3
	d03	23.4	20.9	−2.6	−11	0.45	22.5	−0.9	−4	0.46	24.9	1.5	6.5	0.53	19.7	−3.7	−15.8	0.31
brue	d01	28.5	21.8	−6.7	−23.6	0.44	23.3	−5.2	−18.3	0.35	27.4	−1.1	−4	0.45	20.5	−8	−28.2	0.41
	d02	28.5	26.3	−2.2	−7.7	0.56	29	0.4	1.5	0.49	29.2	0.7	2.3	0.56	30	1.5	5.2	0.49
	d03	28.5	24.4	−4.1	−14.5	0.56	27.1	−1.4	−5	0.52	28.3	−0.3	−0.9	0.56	54.2	25.7	90	0.48
nans	d01	25.3	21.8	−3.5	−13.7	0.46	23.3	−2	−7.9	0.42	27.4	2.1	8.3	0.51	20.5	−4.8	−18.9	0.47
	d02	25.3	26.3	1.1	4.2	0.54	29	3.7	14.5	0.52	29.2	3.9	15.5	0.6	30	4.7	18.7	0.5
	d03	25.3	23.1	−2.2	−8.7	0.51	25.6	0.4	1.4	0.5	26.9	1.6	6.5	0.58	23.2	−2.1	−8.2	0.38
pots	d01	15.7	12.4	−3.4	−21.5	0.44	13	−2.7	−17.1	0.33	16.3	0.6	3.7	0.35	9.2	−6.5	−41.3	0.31
	d02	15.7	10	−5.7	−36.5	0.42	10.1	−5.6	−35.8	0.3	11.3	−4.4	−28.2	0.37	8.6	−7.1	−45.1	0.36
	d03	15.7	9.1	−6.7	−42.5	0.4	9.3	−6.4	−41	0.3	10	−5.7	−36.3	0.35	7.9	−7.9	−49.9	0.36

4.2 Chemistry and aerosols

4.2.1 Nitrogen oxides and ozone

The mean bias of modelled NO_x depends on the type of observations that it is compared with (Table 7): for rural sites close to Berlin and Potsdam, it is biased positively. Modelled NO_x at urban background sites is mainly biased negatively, while the bias is positive or negative at suburban background sites. The maximum bias of all sites (Table 7) is improved with increasing spatial resolution from 15 to 3 km, from +11.9 to +5.3 $\mu g\,m^{-3}$ (rural), +9.3 to +6.7 $\mu g\,m^{-3}$ (suburban background) and −6.7 to −5.7 $\mu g\,m^{-3}$ (urban background). This indicates that generally a horizontal resolution of 3 km is better suited to resolve the spatial NO_x patterns within a city of the size of Berlin even with emission input data coarser than 3 km, which is in line with the results of Tie et al. (2010) for Mexico City. A 15 km resolution is not suffi-

cient to resolve the differences between rural and urban concentrations (Fig. 10). Comparing the mean bias between the 3 and 1 km resolutions further shows that, with an emission inventory of 7 km horizontal resolution, the 1 km resolution does not generally improve the results.

As a first step for model-based assessments of urban NO_x concentrations, it is important to be able to simulate daily maximum urban background NO_x concentrations well. In order to assess the model's skill in reproducing these concentrations, we compare modelled diurnal cycles of NO_x to observed diurnal cycles (Fig. 11). The comparison shows that the WRF-Chem setup presented here is not able to simulate the observed diurnal cycle at any of the three resolutions, overestimating NO_x concentrations during nighttime and underestimating during daytime, not capturing the peak in observed concentrations due to increased traffic densities in the morning and evening hours. The main reason for the night-
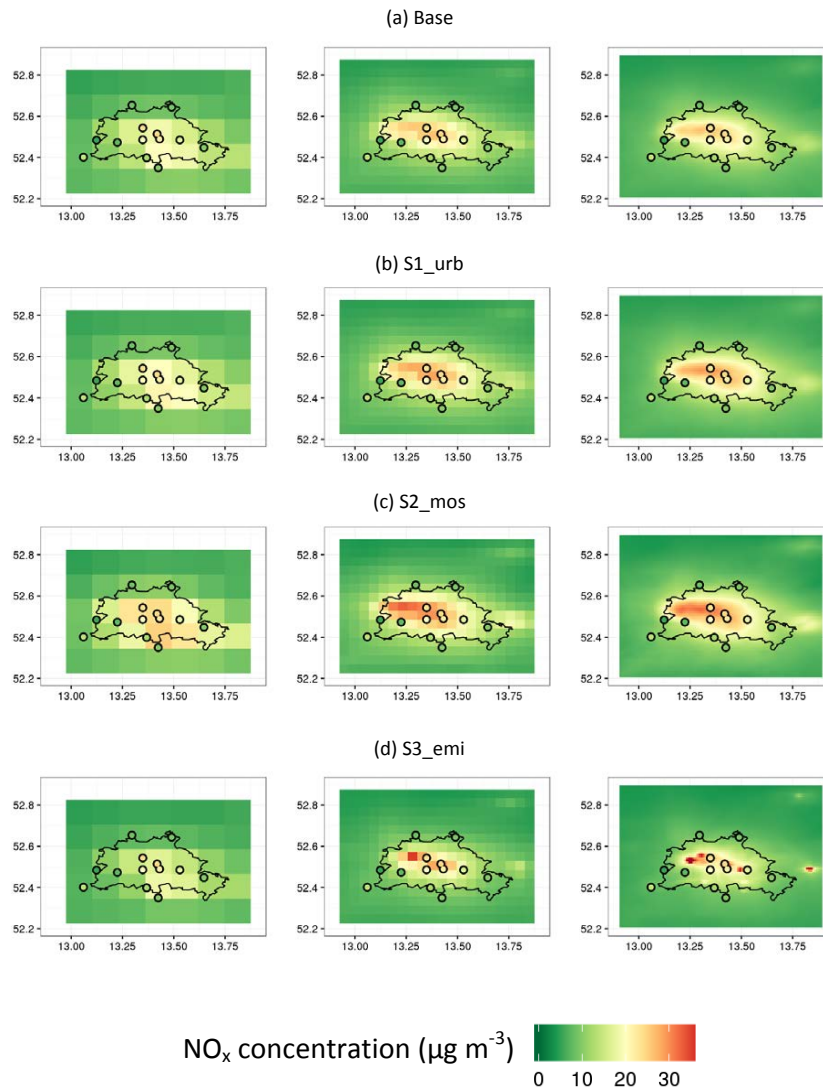
Figure 10. JJA mean modelled (coloured fields) and observed (coloured circles) NO_x concentration in Berlin and its surroundings from **(a)** the base run, **(b)** S1_urb, **(c)** S2_mos and **(d)** S3_emi. The left column shows results obtained with the 15 km horizontal resolution, the middle shows results from a 3 km horizontal resolution and the right column shows results from a 1 km horizontal resolution.

time overestimation is likely the model's underestimation of nighttime mixing as discussed above. This is supported by the vertical distribution of NO_x at several locations in the urban area, which shows a strong gradient between the first and second model layer (e.g. Fig. S10 in the Supplement as an example). A contribution to the daytime underestimation might be uncertainties in the emission inventory: while the share of traffic NO_x emissions to total NO_x emissions within Berlin is just above 35 % in the TNO-MACC III inventory, estimates from the Berlin Senate range around 40–45 % for 2008 and 2009 (Berlin Senate Department for Urban Development and

the Environment, 2015b). Using an up-to-date bottom-up local inventory might contribute to correcting this bias. We can exclude the diurnal cycle applied to the traffic emissions as a reason for the underestimation of the traffic peak in the morning hours – comparing it to diurnal cycles calculated from traffic counts in Berlin shows a good agreement (Fig. S8 in the Supplement). An additional source of bias might be the chemical mechanism itself: in box model studies, Knote et al. (2015) compared different chemical mechanisms and found a difference in simulated summertime NO_x of up to 25 % between the mechanisms. However, the deviation from
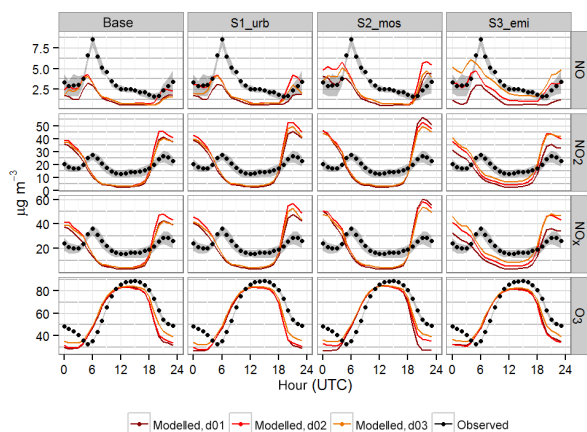
Figure 11. Mean diurnal cycles of NO, NO$_2$, NO$_x$ and O$_3$ for all Berlin and Potsdam urban background stations as observed and modelled by the base run, S1_urb, S2_mos and S3_emi. Model results are given for all three model domains (d01 – 15 km horizontal resolution, d02 – 3 km, d03 – 1 km). The diurnal cycle is averaged over six stations for NO, NO$_2$ and NO$_x$ and three stations of O$_3$. The grey shaded areas represent the variability between the different stations' diurnal cycles, showing the 25th and 75th percentiles.

the multi-mechanism mean was only of the order of a few per cent for summertime conditions simulated with RADM2, which is the mechanism used in this study. A further reason for the model bias might also be the principal challenge of comparing grid cell averages with point observations, particularly in regions with a high variability on small spatial scales, which is quite typical for cities. Regarding the relatively coarse vertical resolution of the model, extrapolation from the first model level to the surface (e.g. Simpson et al., 2012) might allow for a better comparability between model and observation. The spatial representativeness of a measurement site for a larger area such as the 1 km × 1 km grid cells, however, might be somewhat limited particularly for urban background sites, which can be influenced by local sources and sub-grid-scale variations in emissions that cannot be captured with WRF-Chem.

Additionally, we compare the simulated NO and NO$_2$ to observations as described in Sect. 3.1 (Figs. 11, S6, S7 and Tables S6, S7 in the Supplement). As for NO$_x$, the bias of modelled NO depends on the station type. For suburban and urban background stations, NO is on average mainly biased negatively up to −2.5 µg m^{-3} (−60 %), while it shows a positive bias at some of the rural stations. Part of this negative bias is due to a lower detection limit in the observation data ranging between 0.1 and 2 µg m^{-3} depending on the station. While this is not the main contribution to the bias in NO$_x$, it does play a larger role when only looking at NO, as for some of the stations a large share of the observed hourly values lies at or below this threshold both in the observed and modelled data (up to 94 %). The diurnal cycle of NO is modelled in

good agreement with the observations, but the peak values are underestimated (Fig. 11). Especially for urban sites, the bias is larger when simulated with a 15 km resolution than with 3 and 1 km resolutions. Modelled NO$_2$ is on average mostly biased high, with up to 11.1, 5.3 and 4.5 µg m^{-3} for rural sites and up to 10.2, 7.3 and 6.5 µg m^{-3} for suburban sites (15, 3 and 1 km resolution). Urban background sites are both biased high and low. It is important to note that the positive bias always results from overestimations during nighttime, while daytime NO$_2$, as total NO$_x$, is always biased low, though with a smaller daytime bias for suburban and rural sites than for the urban background. These results are in line with what has been discussed for NO$_x$ above and indicate that, in addition to the model resolution, the resolution of emissions might play an important role for simulating daytime NO$_x$ concentrations in cities, as more NO$_x$ is emitted near streets than at the edges of the city, which can hardly be captured with emission input data of a horizontal resolution of 7 km.

O$_3$ daily means and especially MDA8 ozone are underestimated by the model (Fig. 11 and Table S8), with biases of up to ca. −10 µg m^{-3} (mean) and −13 µg m^{-3} (MDA8). This is consistent with what has been reported for a coarse European domain using RADM2 chemistry (Mar et al., 2016) and in line with previous studies showing a deficiency of many online-coupled models, including WRF-Chem with the RADM2 chemical mechanism, in simulating peak ozone concentrations (e.g. Im et al., 2015a). Mar et al. (2016) suggested that the low bias in modelled ozone could be partially explained by the inorganic rate coefficients used in the RADM2 mechanism. Furthermore, it is in line with studies identifying the choice of chemical mechanism as a reason for differences in simulated ozone concentrations (e.g. Coates and Butler, 2015; Knote et al., 2015). The choice of chemical mechanism, but not so much the modelled meteorology being an important cause of this bias is further supported by the fact that maximum temperatures are generally simulated well by the model, and MDA8 ozone is underestimated even when daily maximum temperatures are simulated correctly. The mean O$_3$ is still simulated reasonably well, though the model underestimates at night and overestimates during the morning hours. The bias is consistent with a bias in NO$_x$ diurnal cycles discussed above: in particular, the underestimation of O$_3$ during nighttime is consistent with an overestimation of NO$_x$; the overestimation of O$_3$ in the morning hours might result from too much NO$_2$ accumulating at the surface, which is photolysed when the sun rises.

4.2.2 Particulate matter

The mean bias of the simulated PM$_{10}$ amounts to −50 % (Fig. 12 and Table S9 in the Supplement), which is relatively consistent at all eight stations within and around Berlin as well as at all three model resolutions. Modelled PM$_{2.5}$ concentrations are biased between −20 and −35 % (Fig. 12 and

F. Kuik et al.: Evaluation of a WRF-Chem setup for the Berlin–Brandenburg region   **4355**
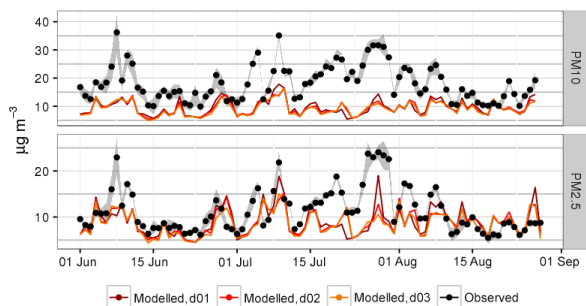
Figure 12. Daily mean PM_{10} and $PM_{2.5}$ concentrations as observed and modelled (base run) at urban background stations in Berlin. Daily means are averaged over five stations for PM_{10} and four stations for $PM_{2.5}$. The grey shaded areas represent the variability between the different stations, showing 25th and 75th percentiles. Model results are given for all three model domains (d01 – 15 km horizontal resolution, d02 – 3 km, d03 – 1 km).

Table S10 in the Supplement). From previous studies with the MADE/SORGAM aerosol scheme it is known that it underestimates the secondary organic aerosol contribution to PM (Ahmadov et al., 2012). Comparing the JJA-averaged model output to components of PM_{10} observed at Nansenstraße during the BAERLIN2014 campaign is in line with these results: while the observations show a mean concentration of organic carbon of $5.6\,\mu g\,m^{-3}$, the modelled particulate organic matter, including organic carbon, is on average $0.8\,\mu g\,m^{-3}$. In addition, the comparison shows that the contribution of black carbon (BC) to PM might be underestimated, with observed elemental carbon (EC) concentrations of $1.4\,\mu g\,m^{-3}$ on average and mean modelled BC concentrations of $0.2\,\mu g\,m^{-3}$, though the modelled value is still within the range of observed values in individual samples. The underestimation of organic carbon (OC) and, to a lesser extent, BC being causes of the underestimation of PM_{10} is supported by the fact that, on average, model results compare reasonably well with the observations of other components of PM_{10}: modelled sulfate, nitrate and ammonium amounts to 1.8, 0.5 and $0.7\,\mu g\,m^{-3}$, while the mean observed concentrations are 1.9, 0.9 and $0.6\,\mu g\,m^{-3}$. Modelled sea salt amounts to $1.0\,\mu g\,m^{-3}$, and observed sodium and chloride are 0.5 and $0.6\,\mu g\,m^{-3}$, respectively. An additional underestimation of mineral dust or re-suspended road dust emissions, such as brake and tyre wear, primarily contributing to PM_{10}, might explain why PM_{10} is underestimated more than $PM_{2.5}$. As for the simulated chemical species, part of the bias might be due to a somewhat limited comparability of grid-cell-averaged particulate matter with observations at a measurement site. It should further be noted that the bias of $PM_{2.5}$ daily means varies throughout the simulated period, with the concentrations being biased more negatively in periods where the wind speed is overestimated more strongly. This underlines that the correct simulation of meteorological parameters in the

online-coupled model WRF-Chem plays an important role in simulating aerosols. The correlation of modelled daily mean PM_{10} concentrations with observations ranges from 0.26 to 0.46 for the 15 km resolution, from 0.31 to 0.51 for the 3 km resolution and from 0.34 to 0.56 for the 1 km resolution. Correlations of simulated $PM_{2.5}$ daily means also fall into this range except at two urban background sites, Brückenstraße and Amrumer Straße, where the correlation coefficient is between 0.17 and 0.26 at all resolutions.

5   Sensitivity studies

In this section, we address whether the skill in simulating meteorology ($T2$, WS10, MLH) is improved when updating the urban parameters and specifying land use classes on a sub-grid scale, as well as whether this has an impact on the skill in simulating NO_x concentrations. Furthermore, we analyse whether using a higher-resolved emission inventory leads to differences in simulated NO_x concentrations with horizontal model resolutions of 3 and 1 km. We focus on NO_x, since as mentioned before, the bias found in the base run mean ozone concentrations and maximum daily 8 h ozone is likely not due to the simulated meteorology or resolution of emissions. Similarly, the bias of model results for PM_{10} and $PM_{2.5}$ is mainly due to an underestimation of secondary organic aerosols by the aerosol mechanism as well as missing emissions and potentially also the vertical resolution as previously discussed.

5.1   Changes in meteorology in S1_urb and S2_mos

The positive bias in $T2$ found in the model results at many sites is decreased for urban areas if the input parameters to the urban scheme are specified based on data describing the city of Berlin (simulation S1_urb, Table 4), which is mainly due to the fact that $T2$ is overall simulated lower for urban areas in this sensitivity simulation. Specifically, there is only one site within the urban area (among all urban built-up and urban green stations) for which the model results with the 1 km horizontal resolution (d03) are biased more than $\pm 1\,^{\circ}C$ (S1_urb, d02: 3 stations; base run, d03: 3 stations; base run, d02: 6 stations). Likewise, the simulation of daily maximum temperatures is improved. The results from this sensitivity simulation, similarly to the results from the base run, show that the differences between the results of the 3 and 1 km resolutions are largest if the urban class of the grid cell changes with changing resolution, though overall the results of the 1 km resolution match the observations slightly better than the results obtained with the 3 km resolution (Table 4). Even though on average the temperature bias is lower in S1_urb than for the base run, the conditional quantile plots show that the highest observed values are still not captured by the model (Fig. 4).

Difference in nighttime boundary layer height
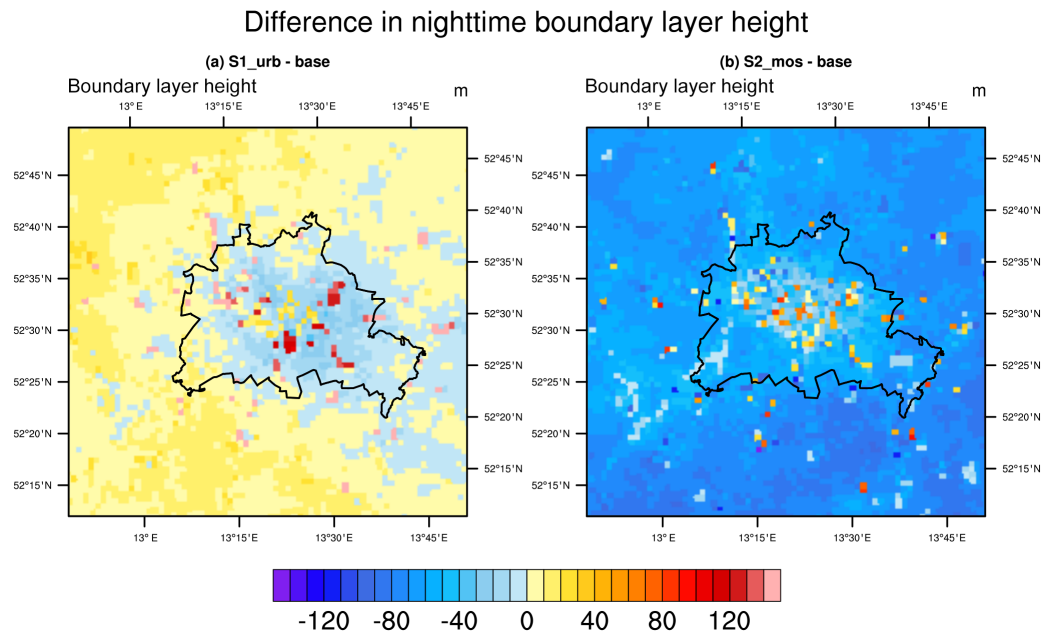
Figure 13. Differences in nighttime (20:00–02:00 UTC) mean JJA planetary boundary layer height as diagnosed from WRF-Chem, **(a)** S1_urb – base run, **(b)** S2_mos – base run (at 1 km horizontal resolution).

Using the mosaic option of the land surface scheme, and thereby taking into account the sub-grid-scale variability of the land use classes within one model grid cell (simulation S2_mos), has a similar effect on simulated $T2$ as in S1_urb: overall, simulated $T2$ is lower than in the base run, which leads to a decrease in $T2$ bias compared to observations. Furthermore, it leads to the results from the 1 and 3 km resolutions being more similar even at sites with different land use categories, which is referred to as grid convergence by Li et al. (2013) and might indicate that a resolution higher than 3 km is not needed in this case. The conditional quantile plots (Fig. 4) underline these results, showing almost identical median values and distributions for the 1 and 3 km resolutions, and furthermore reveal that the temperatures simulated with the 15 km resolution resemble the results with 3 and 1 km resolutions more than in any of the other simulations. At the 15 km model resolution and when applying the mosaic option, gradients at the edges of the city are resolved better than in the other simulations at the 15 km resolution, which is expressed through a lower mean bias at sites at the boundaries of Berlin. An important limitation using this option is the simulated daily maximum $T2$, which is underestimated at most stations (Table 5). This feature was also found by Jänicke et al. (2016) for Berlin and its surroundings when applying the single-layer urban canopy model in combination with the mosaic approach and indicates that $T2$ might be decreased too much when using this option.

There is no observational data from radiosondes available within the city, which is why we cannot draw conclusions on the importance of updating the urban parameters or using the mosaic option for urban areas from comparisons with observed profiles of temperatures or MLH. However, knowing that the MLH diagnosed from WRF-Chem (MLH-YSU) is biased low in the base run during nighttime, we compare JJA mean nighttime (20:00–02:00 UTC) MLH from the base run and S1_urb as well as S2_mos (Fig. 13). The results show that the nighttime MLH-YSU is simulated on average up to ca. 30 m lower in S1_urb than in the base run for most grid cells with the land use type low intensity residential. It is simulated higher than in the base run for grid cells with the land use type high intensity residential and commercial/industry/transport. This shows that the urban parameters can strongly influence the meteorology simulated in urban areas and suggests that they might have to be further refined for simulating the urban atmospheric structure correctly.

The nighttime MLH simulated with S2_mos is up to ca. 70 m lower than in the base run for urban areas, which is an even larger reduction than in S1_urb. As for S1_urb, grid cells with the dominant urban classes being high intensity residential and commercial/industry/transport have a higher MLH-YSU than other urban grid cells, though this effect is smoothed through the use of the mosaic option.

The bias in 10 m wind speed is reduced in S1_urb, ranging from $+0.3\,\mathrm{m\,s^{-1}}$ (10 %) to $+1\,\mathrm{m\,s^{-1}}$ (34 %) depending on the station (Figs. 7, 8 and Table S5). The bias is especially de-

creased for two periods in mid-June and mid-August, where observed daily mean wind speeds are between 5 and 6 m s^{-1}, which is relatively high compared to the rest of the simulated period. In the base run, the model overestimates the observations during these periods, which is not the case in S1_urb. Similarly, the wind speeds during the periods in mid-July with easterly wind, where the base run strongly overestimates wind speeds, are biased by ca. 1–2 m s^{-1} less (Fig. 7). The histograms in the conditional quantile plots further shows that the range of modelled wind speeds from S1_urb matches the range of observed wind speed better than in the base run (Fig. S4 in the Supplement).

Similar to S1_urb, the bias in wind speed is decreased in S2_mos, ranging from below $+0.1$ m s^{-1} (2%) to $+1.2$ m s^{-1} (40%) (Figs. 7, 8, S4 and Table S5 in the Supplement). However, it should be noted that unlike for S1_urb, where the decrease in wind speed is distributed evenly throughout the day, wind speed in S2_mos is especially lower during nighttime, while maximum diurnal wind speeds are similar to those simulated in the base run (not shown).

Overall, the results show that when using a model setup with highly resolved nests, the simulated meteorology seems to be improved both by specifying land use input data and urban parameters for the simulated region and when using the mosaic option, though the biases in the diurnal cycles of $T2$ and wind speed are reduced more in S1_urb. Particularly the differences between S1_urb and the base run for grid cells with land use types high intensity residential and industry/commercial/transport reveal that the specification of urban parameters can contribute to improving the model bias also in MLH. The results from S2_mos show that the mosaic option might be a useful alternative if computational resources are too limited to include higher-resolved nested domains.

5.2 Impact of meteorology changes on simulated NO$_x$ concentrations

Mean NO$_x$ concentrations simulated with S1_urb are generally higher than those simulated with the base run, with the difference between S1_urb and the base run for grid cells of the measurement stations of up to 9% (15 km resolution), up to 13% (3 km resolution) and up to 18% (1 km resolution). Thus, the positive bias which has been found in the base run is increased in S1_urb. For all three domains, the differences are larger for urban grid cells. An analysis of the diurnal cycles reveals that these differences are mainly due to higher nighttime NO$_x$ concentrations in S1_urb (Fig. 11). This is consistent with previous results: an underestimation of MLH by the model (MLH-YSU) during nighttime leads to an overestimation of NO$_x$. An even lower MLH in this sensitivity simulation (Sect. 5.1) explains nighttime NO$_x$ concentrations being higher than in the base run. The overestimation of nighttime NO$_x$ might be further reinforced by lower

simulated wind speeds in S1_urb. Daytime NO$_x$, which we define as NO$_x$ concentrations between 07:00 and 17:00 UTC, changes only little in S1_urb compared with the base run at urban background stations in Berlin: results with a 3 km horizontal resolution show an increase in daytime NO$_x$ in S1_urb between 2 and 5% and an increase between 5 and 7% with a 1 km resolution compared to the base run.

Results for simulated NO$_x$ from S2_mos are consistent with the results from S1_urb: simulated nighttime NO$_x$ is even higher than that simulated in the base run and in S1_urb, which is consistent with the larger difference between MLH-YSU simulated with the base run settings and within S2_mos. Daytime NO$_x$ changes even less in S2_mos compared to the base run, with changes between -1 and $+2\%$ (3 km resolution) or $+3$ to $+5\%$ (1 km resolution).

Overall, the results underline that the underestimation of mixing in the boundary layer is likely to have a strong influence on simulated nighttime NO$_x$ concentrations in urban areas, which is not corrected using the mosaic option or specifying the input parameters to the urban scheme. However, since the simulated MLH is sensitive to the change in urban parameters for high intensity residential and commercial/industry/transport urban areas, it shows that this could potentially have an impact on simulated NO$_x$ concentrations. The results from both S1_urb and S2_mos show that daytime NO$_x$ is influenced little by changes in the modelled meteorology, suggesting that the bias in daytime NO$_x$ is due to emissions that are too low or an incorrect distribution of emissions resulting from a resolution of the emission inventory that is too coarse, as mentioned in Sect. 4.2. As previously mentioned, a further reason for this bias might be limitations in comparability between grid-cell-averaged simulated concentrations and point observations near the surface.

5.3 Resolution of the emission inventory

Evaluating the base run (Sect. 4), we found that the improvement in simulating NO$_x$ concentrations with a 1 km horizontal resolution, as compared to a horizontal resolution of 3 km, is negligible when using emission input data at 7 km horizontal resolution. This result changes when providing emission input data with a horizontal resolution of ca. 1 km as described in Sect. 2.4 (Fig. 10): the model is then able to resolve small-scale air pollution patterns and hotspots, which cannot be resolved at a horizontal resolution of 3 km. A comparison of the results for the urban background stations within Berlin (Amrumer Straße, Belziger Straße, Nansenstraße, Johanna und Willi Brauer Platz, Brückenstraße) helps to illustrate this: in order to minimise the bias by too little nighttime mixing, we only compare daytime (07:00–17:00 UTC) NO$_x$ simulated with 3 and 1 km horizontal resolution and downscaled emissions. Going from a 3 to a 1 km resolution, daytime NO$_x$ changes by $+40$, $+12$, -25, $+16$ and $+161\%$ in S3_emi for the above-mentioned urban background sites, respectively (Fig. 11). As a comparison, the respective changes

55

from the base run are $+3$, $+1$, -8, -3 and -3%. This shows that a 1 km horizontal model resolution only leads to different results from a 3 km horizontal resolution when also using highly resolved emission input data.

Furthermore, the results from the above-mentioned urban background stations show that emissions that are too low within the city (either due to emissions that are too low overall or locally because of a coarse resolution of the emission inventory) can be a cause of the bias in daytime NO_x concentrations. To illustrate that, we compare the daytime NO_x concentrations from the base run and S3_emi. Using the original emissions, the emissions summed up over JJA in the grid cell where the respective station is located are 7.0, 5.4, 6.9, 3.1 and $7.0\,\mathrm{t\,km^{-2}}$ for the above-mentioned urban background stations, respectively, and 22.4, 8.4, 6.2, 2.5 and $79.9\,\mathrm{t\,km^{-2}}$ in the downscaled emission data. It should, however, be noted that, though downscaling of the original emissions can lead to a decrease in emission strength in some of the urban grid cells, it generally results in an increase in the city centre and a decrease in the suburban areas. This is due to the population density and the traffic density, which are used as proxies for the emission downscaling, being higher in the city centre. Using the downscaled emission data leads to an increase in simulated daytime NO_x of 23, 22, 52, 20 and 51% (3 km resolution) or 68, 36, 24, 44 and 308% (1 km resolution) at the above-mentioned urban background stations, as compared to the base run. This shows that, despite small decreases in emissions in some of the grid cells, the generally increased NO_x emissions in the city centre led to increases in simulated NO_x concentration at all five sites. This result indicates that the downscaled emissions might be more suitable to represent gradients in emissions in the urban area, contributing to correcting the bias in simulated daytime urban NO_x in the base run.

A comparison of results from S3_emi with observations at Brückenstraße (Table 7) shows that locally the bias in simulated NO_x concentrations can increase strongly. While for most urban background stations in Berlin using the downscaled emissions improves both the bias of mean NO_x and the bias of daytime NO_x, the example of Brückenstraße shows that further modifications to the emission downscaling and processing might be necessary when simulating local NO_x patterns: at the Brückenstraße site, the mean bias increases from $-4\,\mathrm{\mu g\,m^{-3}}$ (1 km resolution, base run) to $+26\,\mathrm{\mu g\,m^{-3}}$ (1 km resolution, S3_emi). The large overestimation is due to a point source being close to the site and the way point sources have been treated: as mentioned in Sect. 2.4, point-source emissions are all released into the first model layer. Furthermore, the point-source emissions are distributed as area sources at the resolution of the emission inventory. This results in much higher emissions over a much smaller area in the downscaled emission inventory, locally increasing the concentrations in the vicinity of point sources. Likewise, the comparison of simulated and observed concentrations at rural and suburban sites just outside of Berlin

shows that the model skill suffers from the lack of proxy data specifying the spatial distribution of emissions directly outside of Berlin.

Generally, comparing the results from the base run with the results from S3_emi leads to several conclusions: when simulating NO_x concentrations in urban areas, a higher horizontal model resolution can be beneficial if an emission inventory of similarly high resolution is available. However, using a highly resolved emission inventory for a model domain with a similarly high resolution is only beneficial for improving the comparability with observations and the application to local studies if the emission inventory is of sufficient spatial precision. The downscaling approach presented here shows how locally highly resolved emissions can be calculated effectively and consistently by combining a readily available emission inventory with data available for many urban areas, such as population and traffic densities. Our results suggest that a further refinement of the proxy data could be useful, e.g. using proxy datasets covering more than the urban area itself. Further refinements could consist in using the housing type (or high population density as an indication for high-rise buildings) for better distributing residential heating emissions. As for the vertical distribution of emissions, as well as an increased vertical model resolution, Mar et al. (2016) state it has little impact on the model results. While this might hold for simulations of rural background air quality with domain resolutions of the order of 45 km, the present results suggest that it is of higher relevance to distribute point-source emissions into several vertical model levels when decreasing the model resolution and the resolution of the emission input data. Similarly, increasing the vertical model resolution at the same time might both help distribute emissions better and improve the modelled mixing.

6   Summary and conclusions

In this study, we evaluate a WRF-Chem setup for the Berlin–Brandenburg area with three nested model domains of 15, 3 and 1 km horizontal resolutions for 3 months in summer 2014. The results show that the model generally simulates meteorology well, though urban 2 m temperature and urban wind speeds are biased high and nighttime mixing layer height is biased low in the base run. On average, ozone is simulated reasonably well, but maximum daily 8 h mean concentrations are underestimated, which is consistent with the results from previous modelling studies using the RADM2 chemical mechanism. Particulate matter is underestimated, which is at least partly explained by an underestimation of secondary organic aerosols and consistent with previous studies. NO_x concentrations are simulated reasonably well on average, but overestimated during nighttime and underestimated during daytime especially in the urban areas.

We specifically assess how the skill in simulated NO_x is influenced by the model resolution, the prescribed emissions and the simulated meteorology, in turn depending on the model resolution, land use input data to the model and the parameterisation of the urban structure. This is done with three sensitivity simulations, including updating the representations of the urban structure within the urban canopy model (S1_urb), taking into account a sub-grid-scale parameterisation of the land use classes (S2_mos) and downscaling the original emission input data from a horizontal resolution of ca. 7 to ca. 1 km (S3_emi).

For the base model run, a horizontal resolution of 1 km did not generally improve the results compared to a model resolution of 3 km. Furthermore, the mosaic option of the Noah land use model, enabling a sub-grid-scale parameterisation of the land use classes, led to a convergence of the results at the different model resolutions rather than an improvement of the results at the 1 km model resolution. However, this study has shown that a 1 km horizontal model resolution can be very valuable for simulating urban background air quality in the Berlin–Brandenburg region with small modifications, including a better representation of the nighttime mixing layer height in the model, a more detailed specification of urban land use together with the respective input parameters to the urban canopy model and a better spatial representation of urban emissions.

The simulation of the urban boundary layer height is crucial for correctly simulating diurnal cycles of NO_x. In the base run, daily minimum (nighttime) mixing layer height simulated by the model is lower than observations outside of the urban area by more than 50 % on all domains. This is consistent with a strong modelled overestimation of NO_x during nighttime. However, when calculating the mixing layer height from modelled profiles of temperature, wind speed and humidity the nighttime bias decreases from ca. +8 to ca. 26 %. Daily maximum mixing layer height is biased less, and the difference is smaller between the two different approaches of calculating the mixing layer height. This indicates that the calculation of the urban boundary layer height and nighttime mixing in the model might need to be adapted to better represent observed conditions during nighttime.

A more detailed specification of urban land use classes together with the respective input parameters can help better represent the heterogeneity of urban area in a model domain with 1 km horizontal resolution. This is shown by the modelled 2 m temperature only differing by more than 0.1 °C between the model resolutions of 3 and 1 km if the land use class of the respective grid cell changes. It is further shown by the simulation with updated urban parameters decreasing the positive bias in simulated wind speed in the base run by up to 0.5 m s^{-1}, from a mean bias in wind speed up to 1.5 m s^{-1} in the base run to a mean bias in wind speed of maximally 1 m s^{-1} in the sensitivity simulation where urban parameters have been updated. In addition, the nighttime mixing layer height is simulated higher in this sensi-

tivity simulation for grid cells of the urban types high intensity residential and commercial/industry/transport, suggesting that the negative bias in mixing layer height during nighttime can also be corrected by better specifying the input parameters to the urban scheme and the urban land use classes. Further studies could target a comparison between the urban parameterisation used in this study with the more complex – and computationally expensive – approach of representing the urban meteorology with the building effect parameterisation (BEP) urban canopy model combined with a higher vertical resolution of the boundary layer.

When downscaling the emissions from a horizontal resolution of 7 to 1 km based on proxy data for Berlin, including population density and traffic densities, local pollution patterns can be resolved better with a model domain with a horizontal resolution of 1 km, compared to 3 km. A particular strength of this approach is its effective and consistent combination of a readily available emission inventory and locally available data, which can be applied generically to urban areas. In order to further refine this approach, the downscaling of the coarse emission inventory could be extended especially at and beyond the boundaries of the urban area, or the proxy data for industrial and residential heating emissions could be further refined. Alternatively, a highly resolved local bottom-up emission inventory can help increase the model's skill when simulating with a horizontal resolution of 1 km. In addition, the results have shown that a more detailed treatment of point-source emissions including their vertical distribution, as well as the vertical model resolution itself, could become important when going to a horizontal model resolution of 1 km.

Overall, these results can build a basis for the design of future air quality modelling studies over the Berlin–Brandenburg region and other European urban agglomerations of similar extent. The above-mentioned suggested modifications to the setup are based on data which, to a large extent, are available or easily producible for the Berlin–Brandenburg region and other European urban areas. Considering these modifications, we find the presented WRF-Chem configuration at a 1 km horizontal resolution a suitable setup for simulating urban background NO_x concentrations, when used together with the single-layer urban canopy model with input parameters specified for the city of interest and combined with emission input data of a similar resolution as the model domain.

7 Code availability

WRF-Chem is an open-source, publicly available community model. A new, improved version is released approximately twice a year. The WRF-Chem code is available at http://www2.mmm.ucar.edu/wrf/users/download/get_source.html. The corresponding author will provide the modifications introduced and described in Sect. 2 upon request.

8 Data availability

The WRF-Chem source code is publicly available (see Sect. 7 – code availability). The input data used for simulations in this study are either publicly available or available upon request from the data owners. Initial and boundary conditions for meteorological fields were obtained from ECMWF, http://www.ecmwf.int/en/research/climate-reanalysis/era-interim.
Initial and boundary conditions for chemical fields were from MOZART-4/GEOS-5, provided by NCAR at http://www.acom.ucar.edu/wrf-chem/mozart.shtml. Corine land cover data were obtained from EEA (2014), http://www.eea.europa.eu/data-and-maps/data/corine-land-cover-2006-raster-2. TNO-MACC III anthropogenic emissions data were obtained from TNO; others interested in using this data should contact TNO directly (hugo.deniervandergon@tno.nl). Observations of the German Weather Service are available online: ftp://ftp-cdc.dwd.de/pub/CDC/ (Kaspar et al., 2013). The Global Weather Observation dataset was provided by the UK Met Office via the British Atmospheric Data Centre; others interested in using these data should contact the data center directly. The GRUAN dataset is available online upon request at http://www.dwd.de/EN/research/international_programme/gruan/data_products/rs92-gdp_2.html (Sommer et al., 2012). Air quality observations of the federal states were provided directly by the Federal Environment Agency (UBA), but will also be available in AirBase. AirBase is the public air quality database of the EEA; data can be obtained at http://www.eea.europa.eu/data-and-maps/data/airbase-the-european-air-quality-database-7. Data from the BAERLIN2014 campaign were provided by the authors of the study; others interested are referred to Bonn et al. (2016) and von Schneidemesser et al. (2016b). Data from the TU stations are available upon request and scientific users interested in these data should contact the Chair of Climatology at TUB directly (http://www.klima.tu-berlin.de/). WRF-Chem tools for preprocessing boundary conditions as well as anthropogenic emissions were provided by NCAR (http://www.acom.ucar.edu/wrf-chem/download.shtml).
Model output produced in this study can be provided upon request by the corresponding author.

The Supplement related to this article is available online at doi:10.5194/gmd-9-4339-2016-supplement.

References

Ahmadov, R., McKeen, S. A., Robinson, A. L., Bahreini, R., Middlebrook, A. M., de Gouw, J. A., Meagher, J., Hsie, E.-Y., Edgerton, E., Shaw, S., and Trainer, M.: A volatility basis set model for summertime secondary organic aerosols over the eastern United States in 2006, J. Geophys. Res.-Atmos., 117, D06301, doi:10.1029/2011JD016831, 2012.

Alvarez, R., Weilenmann, M., and Favez, J.-Y.: Evidence of increased mass fraction of NO_2 within real-world NO_x emissions of modern light vehicles – derived from a reliable online measuring method, Atmos. Environ., 42, 4699–4707, doi:10.1016/j.atmosenv.2008.01.046, 2008.

Beekmann, M., Kerschbaumer, A., Reimer, E., Stern, R., and Möller, D.: PM measurement campaign HOVERT in the Greater Berlin area: model evaluation with chemically specified particulate matter observations for a one year period, Atmos. Chem. Phys., 7, 55–68, doi:10.5194/acp-7-55-2007, 2007.

Berlin Senate Department for Urban Development and the Environment: Environment Atlas Berlin/Population Density 2014, available at: http://www.stadtentwicklung.berlin.de/umwelt/umweltatlas/edua_index.shtml (last access: December 2015), 2011a.

Berlin Senate Department for Urban Development and the Environment: Environment Atlas Berlin/Traffic Volumes 2009, available at: http://www.stadtentwicklung.berlin.de/umwelt/umweltatlas/edua_index.shtml (last access: December 2015), 2011b.

Berlin Senate Department for Urban Development and the Environment: Luftverunreinigungen in Berlin, Monatsbericht Juni 2014, Berlin, Germany, 2014a.

Berlin Senate Department for Urban Development and the Environment: Luftverunreinigungen in Berlin, Monatsbericht Juli 2014, Berlin, Germany, 2014b.

Berlin Senate Department for Urban Development and the Environment: Luftverunreinigungen in Berlin, Monatsbericht August 2014, Berlin, Germany, 2014c.

Berlin Senate Department for Urban Development and the Environment: Luftgütemessdaten, Jahresbericht 2014, Berlin, Germany, 2015a.

Berlin Senate Department for Urban Development and the Environment: Environment Atlas Berlin, available at: http://www.stadtentwicklung.berlin.de/umwelt/umweltatlas/ed312_01.htm, last access: December 2015b.

Beyrich, F. and Leps, J.-P.: An operational mixing height data set from routine radiosoundings at Lindenberg: Methodology, Meteorol. Z., 21, 337–348, doi:10.1127/0941-2948/2012/0333, 2012.

Bonn, B., von Schneidemesser, E., Andrich, D., Quedenau, J., Gerwig, H., Lüdecke, A., Kura, J., Pietsch, A., Ehlers, C., Klemp, D., Kofahl, C., Nothard, R., Kerschbaumer, A., Junkermann, W., Grote, R., Pohl, T., Weber, K., Lode, B., Schönberger, P., Churkina, G., Butler, T. M., and Lawrence, M. G.: BAERLIN2014 – the influence of land surface types on and the horizontal heterogeneity of air pollutant levels in Berlin, Atmos. Chem. Phys., 16, 7785–7811, doi:10.5194/acp-16-7785-2016, 2016.

Brunner, D., Savage, N., Jorba, O., Eder, B., Giordano, L., Badia, A., Balzarini, A., Baró, R., Bianconi, R., Chemel, C., Curci, G., Forkel, R., Jiménez-Guerrero, P., Hirtl, M., Hodzic, A., Honzak, L., Im, U., Knote, C., Makar, P., Manders-Groot, A., van Meijgaard, E., Neal, L., Pérez, J. L., Pirovano, G., Jose, R. S., Schröder, W., Sokhi, R. S., Syrakov, D., Torian, A., Tuccella, P., Werhahn, J., Wolke, R., Yahya, K., Zabkar, R., Zhang, Y., Hogrefe, C., and Galmarini, S.: Comparative analysis of meteorological performance of coupled chemistry-meteorology models in the context of AQMEII phase 2, Atmos. Environ., 115, 470–498, doi:10.1016/j.atmosenv.2014.12.032, 2015.

Carslaw, D. and Ropkins, K.: openair – An R package for air quality data analysis, Environ. Modell. Softw., 27–28, 52–61, 2012.

Chen, D., Li, Q., Stutz, J., Mao, Y., Zhang, L., Pikelnaya, O., Tsai, J. Y., Haman, C., Lefer, B., Rappenglück, B., Alvarez, S. L., Neuman, J. A., Flynn, J., Roberts, J. M., Nowak, J. B., de Gouw, J., Holloway, J., Wagner, N. L., Veres, P., Brown, S. S., Ryerson, T. B., Warneke, C., and Pollack, I. B.: WRF-Chem simulation of NO_x and O_3 in the L.A. basin during CalNex-2010, Atmos. Environ., 81, 421–432, doi:10.1016/j.atmosenv.2013.08.064, 2013.

Chen, F., Kusaka, H., Tewari, M., Bao, J.-W., and Harakuchi, H.: Utilizing the coupled WRF/LSM/urban modeling system with detailed urban classification to simulate the urban heat island phenomena over the Greater Houston area, Proceedings of the 5th Conference on Urban Environment, 25 August 2004, Vancouver, BC, Canada, 2004.

Chen, F., Kusaka, H., Bornstein, R., Ching, J., Grimmond, C. S. B., Grossman-Clarke, S., Loridan, T., Manning, K. W., Martilli, A., Miao, S., Sailor, D., Salamanca, F. P., Taha, H., Tewari, M., Wang, X., Wyszogrodzki, A. A., and Zhang, C.: The integrated WRF/urban modelling system: development, evaluation, and applications to urban environmental problems, Int. J. Climatol., 31, 273–288, doi:10.1002/joc.2158, 2011.

Coates, J. and Butler, T. M.: A comparison of chemical mechanisms using tagged ozone production potential (TOPP) analysis, Atmos. Chem. Phys., 15, 8795–8808, doi:10.5194/acp-15-8795-2015, 2015.

Dee, D. P., Uppala, S. M., Simmons, A. J., Berrisford, P., Poli, P., Kobayashi, S., Andrae, U., Balmaseda, M. A., Balsamo, G., Bauer, P., Bechtold, P., Beljaars, A. C. M., van de Berg, L., Bidlot, J., Bormann, N., Delsol, C., Dragani, R., Fuentes, M., Geer, A. J., Haimberger, L., Healy, S. B., Hersbach, H., Hólm, E. V., Isaksen, L., Kållberg, P., Köhler, M., Matricardi, M., McNally, A. P., Monge-Sanz, B. M., Morcrette, J.-J., Park, B.-K., Peubey, C., de Rosnay, P., Tavolato, C., Thépaut, J.-N., and Vitart, F.: The ERA-Interim reanalysis: configuration and performance of the data assimilation system, Q. J. Roy. Meteor. Soc., 137, 553–597, doi:10.1002/qj.828, 2011.

Dirksen, R. J., Sommer, M., Immler, F. J., Hurst, D. F., Kivi, R., and Vömel, H.: Reference quality upper-air measurements: GRUAN data processing for the Vaisala RS92 radiosonde, Atmos. Meas. Tech., 7, 4463–4490, doi:10.5194/amt-7-4463-2014, 2014.

EEA: CORINE land cover data 2006, European Environment Agency, Copenhagen, Denmark, updated, available at: http://www.eea.europa.eu/data-and-maps/data/corine-land-cover-2006-raster-3 (last access: 25 January 2016), 2014.

EEA: The European Environment – State and Outlook 2015, European Environment Agency, Copenhagen, Denmark, 2015.

EEA: Air quality in Europe – 2015 report, European Environment Agency, Copenhagen, Denmark, 2016.

Emmons, L. K., Walters, S., Hess, P. G., Lamarque, J.-F., Pfister, G. G., Fillmore, D., Granier, C., Guenther, A., Kinnison, D., Laepple, T., Orlando, J., Tie, X., Tyndall, G., Wiedinmyer, C., Baughcum, S. L., and Kloster, S.: Description and evaluation of the Model for Ozone and Related chemical Tracers, version 4 (MOZART-4), Geosci. Model Dev., 3, 43–67, doi:10.5194/gmd-3-43-2010, 2010.

Fallmann, J., Forkel, R., and Emeis, S.: Secondary effects of urban heat island mitigation measures on air quality, Atmos. Environ., 125, 199–211, doi:10.1016/j.atmosenv.2015.10.094, 2016.

Fast, J. D., Gustafson, W. I., Easter, R. C., Zaveri, R. A., Barnard, J. C., Chapman, E. G., Grell, G. A., and Peckham, S. E.: Evolution of ozone, particulates, and aerosol direct radiative forcing in the vicinity of Houston using a fully coupled meteorology-chemistry-aerosol model, J. Geophys. Res.-Atmos., 111, D21305, doi:10.1029/2005JD006721, 2006.

Fenner, D., Meier, F., Scherer, D., and Polze, A.: Spatial and temporal air temperature variability in Berlin, Germany, during the years 2001–2010, Urban Climate, 10, 308–331, doi:10.1016/j.uclim.2014.02.004, 2014.

Forkel, R., Balzarini, A., Baró, R., Bianconi, R., Curci, G., Jiménez-Guerrero, P., Hirtl, M., Honzak, L., Lorenz, C., Im, U., Pérez, J. L., Pirovano, G., José, R. S., Tuccella, P., Werhahn, J., and Žabkar, R.: Analysis of the WRF-Chem contributions to AQMEII phase 2 with respect to aerosol radiative feedbacks on meteorology and pollutant distributions, Atmos. Environ., 115, 630–645, doi:10.1016/j.atmosenv.2014.10.056, 2015.

Grell, G. A., Peckham, S. E., Schmitz, R., McKeen, S. A., Frost, G., Skamarock, W. C., and Eder, B.: Fully coupled "online" chem-

istry within the WRF model, Atmos. Environ., 39, 6957–6975, doi:10.1016/j.atmosenv.2005.04.027, 2005.

Guenther, A., Karl, T., Harley, P., Wiedinmyer, C., Palmer, P. I., and Geron, C.: Estimates of global terrestrial isoprene emissions using MEGAN (Model of Emissions of Gases and Aerosols from Nature), Atmos. Chem. Phys., 6, 3181–3210, doi:10.5194/acp-6-3181-2006, 2006.

Hong, S.-Y., Noh, Y., and Dudhia, J.: A New Vertical Diffusion Package with an Explicit Treatment of Entrainment Processes, Mon. Weather Rev., 134, 2318–2341, doi:10.1175/MWR3199.1, 2006.

Hu, X.-M., Nielsen-Gammon, J. W., and Zhang, F.: Evaluation of Three Planetary Boundary Layer Schemes in the WRF Model, J. Appl. Meteor. Climatol., 49, 1831–1844, doi:10.1175/2010JAMC2432.1, 2010.

Im, U., Bianconi, R., Solazzo, E., Kioutsioukis, I., Badia, A., Balzarini, A., Baró, R., Bellasio, R., Brunner, D., Chemel, C., Curci, G., Flemming, J., Forkel, R., Giordano, L., Jiménez-Guerrero, P., Hirtl, M., Hodzic, A., Honzak, L., Jorba, O., Knote, C., Kuenen, J. J., Makar, P. A., Manders-Groot, A., Neal, L., Pérez, J. L., Pirovano, G., Pouliot, G., Jose, R. S., Savage, N., Schroder, W., Sokhi, R. S., Syrakov, D., Torian, A., Tuccella, P., Werhahn, J., Wolke, R., Yahya, K., Zabkar, R., Zhang, Y., Zhang, J., Hogrefe, C., and Galmarini, S.: Evaluation of operational on-line-coupled regional air quality models over Europe and North America in the context of AQMEII phase 2. Part I: Ozone, Atmos. Environ., 115, 404–420, doi:10.1016/j.atmosenv.2014.09.042, 2015a.

Im, U., Bianconi, R., Solazzo, E., Kioutsioukis, I., Badia, A., Balzarini, A., Baró, R., Bellasio, R., Brunner, D., Chemel, C., Curci, G., van der Gon, H. D., Flemming, J., Forkel, R., Giordano, L., Jiménez-Guerrero, P., Hirtl, M., Hodzic, A., Honzak, L., Jorba, O., Knote, C., Makar, P. A., Manders-Groot, A., Neal, L., Pérez, J. L., Pirovano, G., Pouliot, G., Jose, R. S., Savage, N., Schroder, W., Sokhi, R. S., Syrakov, D., Torian, A., Tuccella, P., Wang, K., Werhahn, J., Wolke, R., Zabkar, R., Zhang, Y., Zhang, J., Hogrefe, C., and Galmarini, S.: Evaluation of operational online-coupled regional air quality models over Europe and North America in the context of AQMEII phase 2. Part II: Particulate matter, Atmos. Environ., 115, 421–441, doi:10.1016/j.atmosenv.2014.08.072, 2015b.

Jänicke, B., Meier, F., Fenner, D., Fehrenbach, U., Holtmann, A., and Scherer, D.: Urban–rural differences in near-surface air temperature as resolved by the Central Europe Refined analysis (CER): sensitivity to planetary boundary layer schemes and urban canopy models, Int. J. Climatol., doi:10.1002/joc.4835, online first, 2016.

Kaspar, F., Müller-Westermeier, G., Penda, E., Mächel, H., Zimmermann, K., Kaiser-Weiss, A., and Deutschländer, T.: Monitoring of climate change in Germany – data, products and services of Germany's National Climate Data Centre, Adv. Sci. Res., 10, 99–106, doi:10.5194/asr-10-99-2013, 2013.

Knote, C., Tuccella, P., Curci, G., Emmons, L., Orlando, J. J., Madronich, S., Baró, R., Jiménez-Guerrero, P., Luecken, D., Hogrefe, C., Forkel, R., Werhahn, J., Hirtl, M., Pérez, J. L., José, R. S., Giordano, L., Brunner, D., Yahya, K., and Zhang, Y.: Influence of the choice of gas-phase mechanism on predictions of key gaseous pollutants during the

AQMEII phase-2 intercomparison, Atmos. Environ., 115, 553–568, doi:10.1016/j.atmosenv.2014.11.066, 2015.

Kuenen, J. J. P., Visschedijk, A. J. H., Jozwicka, M., and Denier van der Gon, H. A. C.: TNO-MACC_II emission inventory; a multi-year (2003–2009) consistent high-resolution European emission inventory for air quality modelling, Atmos. Chem. Phys., 14, 10963–10976, doi:10.5194/acp-14-10963-2014, 2014.

Kusaka, H. and Kimura, F.: Thermal Effects of Urban Canyon Structure on the Nocturnal Heat Island: Numerical Experiment Using a Mesoscale Model Coupled with an Urban Canopy Model, J. Appl. Meteorol., 43, 1899–1910, doi:10.1175/JAM2169.1, 2004.

Kusaka, H., Kondo, H., Kikegawa, Y., and Kimura, F.: A Simple Single-Layer Urban Canopy Model For Atmospheric Models: Comparison With Multi-Layer And Slab Models, Bound.-Lay. Meteorol., 101, 329–358, doi:10.1023/A:1019207923078, 2001.

Li, D., Bou-Zeid, E., Barlage, M., Chen, F., and Smith, J. A.: Development and evaluation of a mosaic approach in the WRF-Noah framework, J. Geophys. Res.-Atmos., 118, 11918–11935, doi:10.1002/2013JD020657, 2013.

Liao, J., Wang, T., Wang, X., Xie, M., Jiang, Z., Huang, X., and Zhu, J.: Impacts of different urban canopy schemes in WRF/Chem on regional climate and air quality in Yangtze River Delta, China, Atmos. Res., 145–146, 226–243, doi:10.1016/j.atmosres.2014.04.005, 2014.

Loridan, T., Grimmond, C. S. B., Grossman-Clarke, S., Chen, F., Tewari, M., Manning, K., Martilli, A., Kusaka, H., and Best, M.: Trade-offs and responsiveness of the single-layer urban canopy parametrization in WRF: An offline evaluation using the MOSCEM optimization algorithm and field observations, Q. J. Roy. Meteor. Soc., 136, 997–1019, doi:10.1002/qj.614, 2010.

Loridan, T., Lindberg, F., Jorba, O., Kotthaus, S., Grossman-Clarke, S., and Grimmond, C. S. B.: High Resolution Simulation of the Variability of Surface Energy Balance Fluxes Across Central London with Urban Zones for Energy Partitioning, Bound.-Layer. Meteorol., 147, 493–523, doi:10.1007/s10546-013-9797-y, 2013.

Mar, K. A., Ojha, N., Pozzer, A., and Butler, T. M.: Ozone air quality simulations with WRF-Chem (v3.5.1) over Europe: model evaluation and chemical mechanism comparison, Geosci. Model Dev., 9, 3699–3728, doi:10.5194/gmd-9-3699-2016, 2016.

Mena-Carrasco, M., Oliva, E., Saide, P., Spak, S. N., de la Maza, C., Osses, M., Tolvett, S., Campbell, J. E., es Chi-Chung Tsao, T., and Molina, L. T.: Estimating the health benefits from natural gas use in transport and heating in Santiago, Chile, Sci. Total Environ., 429, 257–265, doi:10.1016/j.scitotenv.2012.04.037, 2012.

OECD: OECD Environmental Outlook to 2050, OECD Publishing, doi:10.1787/9789264122246-en, 2012.

Otero, N., Sillmann, J., Schnell, J. L., Rust, H. W., and Butler, T.: Synoptic and meteorological drivers of extreme ozone concentrations over Europe, Environ. Res. Lett., 11, 024005, doi:10.1088/1748-9326/11/2/024005, 2016.

Pineda, N., Jorba, O., Jorge, J., and Baldasano, J. M.: Using NOAA AVHRR and SPOT VGT data to estimate surface parameters: application to a mesoscale meteorological model, Int. J. Remote Sens., 25, 129–143, doi:10.1080/0143116031000115201, 2004.

R Core Team: R: A Language and Environment for Statistical Computing, R Foundation for Statistical Computing, Vienna, Austria,

available at: http://www.R-project.org (last access: 1 July 2016), 2013.

Salamanca, F., Martilli, A., and Yagüe, C.: A numerical study of the Urban Heat Island over Madrid during the DE-SIREX (2008) campaign with WRF and an evaluation of simple mitigation strategies, Int. J. Climatol., 32, 2372–2386, doi:10.1002/joc.3398, 2012.

Schaap, M., Cuvelier, C., Hendriks, C., Bessagnet, B., Baldasano, J., Colette, A., Thunis, P., Karam, D., Fagerli, H., Graff, A., Kranenburg, R., Nyiri, A., Pay, M., Rouïl, L., Schulz, M., Simpson, D., Stern, R., Terrenoire, E., and Wind, P.: Performance of European chemistry transport models as function of horizontal resolution, Atmos. Environ., 112, 90–105, doi:10.1016/j.atmosenv.2015.04.003, 2015.

Schubert, S. and Grossman-Clarke, S.: The Influence of green areas and roof albedos on air temperatures during Extreme Heat Events in Berlin, Germany, Meteorol. Z., 22, 131–143, doi:10.1127/0941-2948/2013/0393, 2013.

Simpson, D., Benedictow, A., Berge, H., Bergström, R., Emberson, L. D., Fagerli, H., Flechard, C. R., Hayman, G. D., Gauss, M., Jonson, J. E., Jenkin, M. E., Nyíri, A., Richter, C., Semeena, V. S., Tsyro, S., Tuovinen, J.-P., Valdebenito, Á., and Wind, P.: The EMEP MSC-W chemical transport model – technical description, Atmos. Chem. Phys., 12, 7825–7865, doi:10.5194/acp-12-7825-2012, 2012.

Skamarock, W., Klemp, J., Dudhia, J., Gill, D., Barker, D., Duda, M., Huang, X.-Y., Wang, W., and Powers, J.: A Description of the Advanced Research WRF Version 3, NCAR Technical Note/TN-475+STR, doi:10.5065/D68S4MVH, 2008.

Sommer, M., Dirksen, R., and Immler, F.: RS92 GRUAN Data Product Version 2 (RS92-GDP.2), doi:10.5676/GRUAN/RS92-GDP.2, 2012.

Tewari, M. F., Chen, F., Kusaka, H., and Miao, S.: Coupled WRF/Unified Noah/urban-canopy modeling system, NCAR WRF Documentation, NCAR, Boulder, USA, 1–20, 2008.

Tie, X., Madronich, S., Li, G., Ying, Z., Zhang, R., Garcia, A. R., Lee-Taylor, J., and Liu, Y.: Characterizations of chemical oxidants in Mexico City: A regional chemical dynamical model (WRF-Chem) study, Atmos. Environ., 41, 1989–2008, doi:10.1016/j.atmosenv.2006.10.053, 2007.

Tie, X., Brasseur, G., and Ying, Z.: Impact of model resolution on chemical ozone formation in Mexico City: application of the WRF-Chem model, Atmos. Chem. Phys., 10, 8983–8995, doi:10.5194/acp-10-8983-2010, 2010.

Trusilova, K., Schubert, S., Wouters, H., Früh, B., Grossman-Clarke, S., Demuzere, M., and Becker, P.: The urban land use in the COSMO-CLM model: a comparison of three parameterizations for Berlin, Meteorol. Z., 25, 231–244, doi:10.1127/metz/2015/0587, 2016.

Tuccella, P., Curci, G., Visconti, G., Bessagnet, B., and Menut, L.: Modeling of gas and aerosol with WRF/Chem over Europe: Evaluation and sensitivity study, J. Geophys. Res., 117, D03303, doi:10.1029/2011JD016302, 2012.

UCAR/NCAR/CISL/TDD: The NCAR Command Language (Version 6.3.0) [Software], Boulder, Colorado, doi:10.5065/D6WD3XH5, 2016.

von Schneidemesser, E., Coates, J., Denier van der Gon, H., Visschedijk, A., and Butler, T.: Variation of the NMVOC speciation in the solvent sector and the sensitivity of modelled tropospheric ozone, Atmos. Environ., 135, 59–72, doi:10.1016/j.atmosenv.2016.03.057, 2016a.

von Schneidemesser, E., Bonn, B., Ehlers, C., Gerwig, H., Hellén, H., Kerschbaumer, A., Klemp, D., Kofahl, C., Kura, J., Lüdecke, A., Nothard, R., Pietsch, A., Pohl, T., Schaefer, K., and Weber, K.: BAERLIN2014 – stationary measurements and source apportionment at an urban background station in Berlin, Germany, in preparation, 2016b.

4. Article 2: Top-down quantification of NO$_x$ emissions from traffic in an urban area using a high resolution regional atmospheric chemistry model

**Atmospheric
Chemistry
and Physics**

Top–down quantification of NO_x emissions from traffic in an urban area using a high-resolution regional atmospheric chemistry model

Friderike Kuik[1,2], **Andreas Kerschbaumer**[3], **Axel Lauer**[4], **Aurelia Lupascu**[1], **Erika von Schneidemesser**[1], and **Tim M. Butler**[1,2]

[1]Institute for Advanced Sustainability Studies, Potsdam, Germany
[2]Freie Universität, Fachbereich Geowissenschaften, Institut für Meteorologie, Berlin, Germany
[3]Senatsverwaltung für Umwelt, Verkehr und Klimaschutz Berlin, Berlin, Germany
[4]Deutsches Zentrum für Luft- und Raumfahrt (DLR), Institut für Physik der Atmosphäre, Oberpfaffenhofen, Germany

Correspondence: Friderike Kuik (friderike.kuik@gmail.com)

Abstract. With NO_2 limit values being frequently exceeded in European cities, complying with the European air quality regulations still poses a problem for many cities. Traffic is typically a major source of NO_x emissions in urban areas. High-resolution chemistry transport modelling can help to assess the impact of high urban NO_x emissions on air quality inside and outside of urban areas. However, many modelling studies report an underestimation of modelled NO_x and NO_2 compared with observations. Part of this model bias has been attributed to an underestimation of NO_x emissions, particularly in urban areas. This is consistent with recent measurement studies quantifying underestimations of urban NO_x emissions by current emission inventories, identifying the largest discrepancies when the contribution of traffic NO_x emissions is high. This study applies a high-resolution chemistry transport model in combination with ambient measurements in order to assess the potential underestimation of traffic NO_x emissions in a frequently used emission inventory. The emission inventory is based on officially reported values and the Berlin–Brandenburg area in Germany is used as a case study. The WRF-Chem model is used at a $3\,km \times 3\,km$ horizontal resolution, simulating the whole year of 2014. The emission data are downscaled from an original resolution of ca. $7\,km \times 7\,km$ to a resolution of $1\,km \times 1\,km$. An in-depth model evaluation including spectral decomposition of observed and modelled time series and error apportionment suggests that an underestimation in traffic emissions is likely one of the main causes of the bias in modelled NO_2 concentrations in the urban background, where NO_2 con-

centrations are underestimated by ca. $8\,\mu g\,m^{-3}$ ($-30\,\%$) on average over the whole year. Furthermore, a diurnal cycle of the bias in modelled NO_2 suggests that a more realistic treatment of the diurnal cycle of traffic emissions might be needed. Model problems in simulating the correct mixing in the urban planetary boundary layer probably play an important role in contributing to the model bias, particularly in summer. Also taking into account this and other possible sources of model bias, a correction factor for traffic NO_x emissions of ca. 3 is estimated for weekday daytime traffic emissions in the core urban area, which corresponds to an overall underestimation of traffic NO_x emissions in the core urban area of ca. $50\,\%$. Sensitivity simulations for the months of January and July using the calculated correction factor show that the weekday model bias can be improved from $-8.8\,\mu g\,m^{-3}$ ($-26\,\%$) to $-5.4\,\mu g\,m^{-3}$ ($-16\,\%$) in January on average in the urban background, and $-10.3\,\mu g\,m^{-3}$ ($-46\,\%$) to $-7.6\,\mu g\,m^{-3}$ ($-34\,\%$) in July. In addition, the negative bias of weekday NO_2 concentrations downwind of the city in the rural and suburban background can be reduced from $-3.4\,\mu g\,m^{-3}$ ($-12\,\%$) to $-1.2\,\mu g\,m^{-3}$ ($-4\,\%$) in January and from $-3.0\,\mu g\,m^{-3}$ ($-22\,\%$) to $-1.9\,\mu g\,m^{-3}$ ($-14\,\%$) in July. The results and their consistency with findings from other studies suggest that more research is needed in order to more accurately understand the spatial and temporal variability in real-world NO_x emissions from traffic, and apply this understanding to the inventories used in high-resolution chemical transport models.

1   Introduction

Limit values for ambient NO_2 concentrations (Ambient Air Quality Directive 2008/50/EC) as well as NO_x exhaust emission standards are set by European legislation, but ambient measurements show that NO_2 concentrations still frequently exceed the European annual mean limit value of $40\,\mu g\,m^{-3}$ (EEA, 2016; Minkos et al., 2017). For example, 12 % of all measurement sites in Europe registered exceedances of the annual mean limit value in 2014, most of them located at the roadside. Within Europe, Germany had the highest median NO_2 concentrations in 2014 (EEA, 2016), where it was estimated that the limit value was exceeded at 57 % of all traffic sites (Minkos et al., 2017). While there is a downward trend in NO_2 concentrations due to decreasing NO_x emissions, extrapolating the current trend to 2020, exceedances are still expected at 7 % of the stations in 2020, requiring additional measures in order for the European air quality goals to be met (EEA, 2016).

In general, traffic is the most important source of NO_x emissions in Europe, contributing 46 % in 2014 in the EU-28, with considerably higher contributions to ambient NO_2 concentrations in urban areas (EEA, 2016). NO_x emissions from diesel vehicles, the main traffic NO_x source, have recently been a strong focus of international media attention: despite increasingly strict emission standards for diesel cars with the introduction of the Euro 5 and Euro 6 norms, under real-world driving conditions, i.e. the pollutants a car produces while being driven on real roads as opposed to being tested in a lab, Euro 5-certified cars exceed the emission limit of $0.18\,g\,km^{-1}$ by an average factor of 4–5 (e.g. EEA, 2016; Hausberger and Matzer, 2017) and the newer Euro 6 cars exceed the emission limit of $0.08\,g\,km^{-1}$ by an average factor of 6–7 (e.g. EEA, 2016; ICCT Briefing, 2016).

NO_x impacts human health, ecosystems and climate directly and indirectly as a precursor of tropospheric ozone (O_3) and particulate matter (PM). Health impacts of NO_2 include adverse respiratory effects (WHO, 2013), and the effect of road traffic NO_2 on premature mortality might be more than 10 times larger than the effect of road traffic $PM_{2.5}$ (Harrison and Beddows, 2017).

In order to support policy makers in identifying suitable measures to reduce roadside and urban background NO_2 concentrations to levels well below the limit value, as well as to assess the health impact of current and future NO_2 concentrations, air pollution modelling is a valuable tool (e.g. von Schneidemesser et al., 2017). Chemistry transport models can be used to assess the impact of local emissions on air chemistry and air quality in the surroundings and downwind of the emission sources. Online-coupled models, such as the chemistry version of the Weather Research and Forecasting model (WRF-Chem, Grell et al., 2005), have several advantages compared with offline approaches. These include, for example, a numerically more consistent treatment and a more

realistic representation of the atmosphere, particularly in case of high model resolution (Grell and Baklanov, 2011).

Due to its short lifetime in the atmosphere, NO_2 is more spatially variable than for example O_3, particularly in urban areas with locally high NO_x emissions. This is one of the reasons why models with higher spatial resolutions of a few kilometres are capable of representing observed NO_2 concentrations better than coarser models, with better performance if emission input and meteorological data are also available at the high resolution (e.g. Schaap et al., 2015). In terms of model evaluation, comparing NO_2 concentrations averaged over a coarse model grid cell with point measurements can lead to mismatches (Solazzo et al., 2017), with a better comparability achieved through high model resolutions of only a few kilometres or less, depending on the size of the city. Simulating air quality in Mexico City, Tie et al. (2010) showed that reasonable model results can be achieved at a ratio of city size to model resolution of ca. $6:1$.

However, many modelling studies report discrepancies between modelled and observed NO_2 concentrations, which are in parts attributed to an underestimation of traffic NO_x emissions. All but one model simulating the European domain during model intercomparison project AQMEII phase 2 underestimate annual mean NO_2 concentrations by 9–45 % on average. Some of them overestimate NO_2 concentrations at nighttime (Im et al., 2015), meaning that daytime concentrations are underestimated even more than the average model bias would indicate. Similarly, the European models contributing to the more recent AQMEII phase 3 intercomparison show an underprediction of NO_2 concentrations throughout the whole year, with the sole exception of one model (Solazzo et al., 2017). In the Eurodelta model intercomparison study (Bessagnet et al., 2016), the participating models simulate NO_2 concentrations reasonably well on average compared with observations in the rural background, but most models show an underestimation of daytime NO_2 on average, particularly in summer (Fig. 9 from Bessagnet et al., 2016). Few studies focus particularly on NO_2 in urban areas: Terrenoire et al. (2015) simulated air quality over Europe at a horizontal resolution of $0.125° \times 0.0625°$ with the CHIMERE model for 2009 and found that NO_2 concentrations are underestimated by more than 50 % in urban areas. Schaap et al. (2015) show that the bias in modelled NO_2 concentrations in urban areas is reduced with increasing model resolutions, but still report negative biases for a model resolution of $7\,km \times 7\,km$, between 6 and $10\,\mu g\,m^{-3}$ for different offline-coupled chemistry transport models. Fallmann et al. (2016) report a negative bias in NO_2 concentrations simulated with WRF-Chem at $3\,km \times 3\,km$ of ca. 50 % on average and up to 60 % during daytime. Degraeuwe et al. (2016) assess the impact of different diesel NO_x emission scenarios on air quality in Antwerp, combining model simulations with LOTOS-EUROS at a horizontal resolution of ca. $7\,km \times 7\,km$ (urban background) with a street canyon model. They report a low bias in modelled urban background NO_2

concentrations of ca. 20 %, requiring bias correction for the further analysis of the emission scenarios. Kuik et al. (2016) evaluated air quality simulated with WRF-Chem over the Berlin–Brandenburg region and found underestimations of NO_2 concentrations at daytime, and overestimations at nighttime.

Many studies attribute an underestimation of observed NO_2 concentrations to an underestimation of emissions (e.g. Solazzo and Galmarini, 2016; Degraeuwe et al., 2016; Giordano et al., 2015) and particularly traffic emissions in urban areas (Terrenoire et al., 2015). Further reported causes of the disagreement include problems with simulating the correct PBL height and mixing in the model (e.g. Solazzo et al., 2017; Kuik et al., 2016).

Modelling studies for North America report lower negative or even positive biases in modelled NO_2 concentrations (e.g. Solazzo et al., 2017). While total NO_x emissions reported for Europe are on average already larger than for North America by a factor of more than 2 (Im et al., 2015), these differences might indicate an even larger contribution of diesel car emissions to measured NO_2 concentrations, as the share of diesel cars is a main difference in emission sources between Europe and North America. Thus, large differences in the model bias between Europe and North America would be consistent with an underestimation of diesel traffic emissions in Europe.

Emissions are typically estimated from a combination of activity data (e.g. fuel burnt) and emission factors. Emission factors for road transport emissions depend on the fuel type and the car type (heavy duty or light duty, exhaust treatment) as well as on the driving conditions, including road type and speed (e.g. Hausberger and Matzer, 2017). While activity data are only assumed to have an uncertainty of ca. 5–10 %, the emission factor is more difficult to quantify in many cases (Kuenen et al., 2014, and references therein). Emission factors for road transport, for example, may have an error range between 50 and 200 %, while emission factors for energy industry emissions, the second largest source of NO_x emissions in Berlin, are much better constrained, with an error range between 20 and 60 % (Kuenen et al., 2014). Emission error ranges for the TNO-MACC III inventory used in this study are determined following the EEA Emission Inventory Guidebook, and depend, for example, on the number of measurements made for deriving the emission factor (EEA, 2013; Kuenen et al., 2014). Recent studies for London show that NO_x emissions from flux measurements are up to 80 % (Lee et al., 2015), or a factor of 1.5–2 (Vaughan et al., 2016) higher than NO_x emissions from the UK National Atmospheric Emissions Inventory, with the largest discrepancies found in cases where traffic is the dominant source of NO_x concentrations. Karl et al. (2017) conclude from eddy covariance measurements in Austria that traffic-related NO_x emissions in emission inventories frequently used by air quality models can be underestimated by up to a factor of 4 for countries where diesel cars represent a major fraction of the vehi-

cle fleet and have a significant contribution to reported biases in modelled NO_2 concentrations.

In this study the aim is to quantify the underestimation of traffic emissions in a widely used state-of-the-art emission inventory based on officially reported emissions, for simulating NO_2 concentrations in an urban area with high resolution. We use the Berlin–Brandenburg area as a case study, and use the WRF-Chem model to simulate NO_2 concentrations. The model set-up, model simulations and input data are described in Sect. 2, and observational data used are described in Sect. 3. The emission inventory used here is the TNO-MACC III inventory (Kuenen et al., 2014), downscaled to ca. 1 km × 1 km for the Berlin–Brandenburg area (Kuik et al., 2016), also described in Sect. 2. The analysis builds on advanced model evaluation techniques, including an operational and a diagnostic evaluation (outlined in Sect. 4) of the modelled NO_2 concentrations (Dennis et al., 2010), with the aim of assessing the contribution of different sources of model error (Sect. 5). Based on this analysis, a correction factor for traffic emissions is calculated, and additional sources of the model bias are discussed (Sect. 6). The factor is then tested in two individual 1-month long simulations for January and July 2014, in the following referred to as sensitivity simulations. In addition, we analyse observational data of NO_2 concentrations and traffic counts, assessing the linear scaling assumed between emissions and traffic counts for the temporal distribution of emissions in chemistry transport models. Section 7 closes with a summary and conclusions from the results.

2 Model simulations

2.1 Model set-up

We use the Weather Research and Forecasting model (WRF) version 3.8.1 (Skamarock et al., 2008), with chemistry and aerosols (WRF-Chem, Grell et al., 2005; Fast et al., 2006). The set-up includes two model domains centred over Berlin, at horizontal resolutions of 15 km × 15 km and 3 km × 3 km, using one-way nesting. The model top is at 50 hPa, using 35 vertical levels with the first model layer top at approximately 30 m above the surface. There are 12 levels in the lowest 3 km. Urban processes (meteorology) are parameterized with the single-layer urban canopy model, with input parameters specified for Berlin as described in Kuik et al. (2016) and three urban land use categories. The setup further includes the RADM2 chemical mechanism with the Kinetic Pre-Processor (KPP) and the MADE/SORGAM aerosol scheme. The MOZART chemical mechanism is used in a sensitivity test. All physics and chemistry schemes used in this study are listed in Table 1.

Small changes in the code have been made. The initialization of the dry deposition (module_dep_simple.F) has been adapted in order to account for three urban land use cat-

Table 1. Model configuration and input data.

Process	Option/dataset	Remarks
Land surface model	Noah LSM	CORINE land use data
Urban processes	single-layer UCM	three categories: roofs, walls, trees
Boundary layer	MYNN	
Cumulus convection	Grell–Freitas	switched on for both domains
Cloud microphysics	Morrison double-moment	
Radiation (sw+lw)	RRTMG	
Aerosols	MADE/SORGAM	chem_opt=106
Chemistry	RADM2	with KPP
Photolysis	Madronich F-TUV	
Anthropogenic emissions	TNO-MACC III	see Sect. 2.4 for details
Biogenic emissions	online	MEGAN
Dust and sea salt emissions	online	dust_opt=3, seas_opt=2
Meteorological boundary conditions	ERA-Interim	sst_update=1
Chemical boundary conditions	MOZART4-GEOS5	

egories as described in Kuik et al. (2016), and references therein. Nighttime mixing over urban areas is not accounted for sufficiently by the urban parameterization and the PBL scheme and is thus adjusted (dry_dep_driver.F) as described in the Supplement. There, we also show illustrative results (Figs. S1–S3 in the Supplement) of two test simulations comparing the impact of changes in this model set-up with respect to Kuik et al. (2016), including the modification of nighttime mixing and the modification of the diurnal distribution of traffic emissions (see Sect. 2.4).

2.2 Model input data

We use the European Centre for Medium-Range Weather Forecasting (ECMWF) Interim reanalysis (ERA-Interim, Dee et al., 2011) with a horizontal resolution of 0.75° × 0.75° and a temporal resolution of 6 h, interpolated to 37 pressure levels (with 29 levels below 50 hPa) as meteorological initial and lateral boundary conditions. The sea surface temperature is updated every 6 h. The data are interpolated to the model grid using the standard WRF pre-processing system (WPS). Chemical boundary conditions for trace gases and particulate matter are created from simulations with global chemistry transport Model for Ozone and Related chemical Tracers (MOZART-4/GEOS-5, Emmons et al., 2010). Instead of the standard USGS land use data we use CORINE data (EEA, 2014), remapped to the USGS classes, using three categories characterizing the urban area. This provides a more realistic characterization of the land use in the Berlin–Brandenburg area (Kuik et al., 2016; Churkina et al., 2017). The emission input data and their pre-processing are described in Sect. 2.4.

2.3 Simulation procedure

Following the workflow used in AQMEII phase 2 (Brunner et al., 2015), we re-initialize the simulation every 2 days, with a 1-day spin-up of the model meteorology. To ensure

consistency in the chemical fields, we start each new 2-day simulation from the chemistry fields of the previous simulation. For the base run using the RADM2 chemistry scheme, we do a full-year (2014) simulation. The results of this simulation are used to derive a correction factor for road traffic emissions, as explained in Sect. 6.1. For computational reasons, the simulation is divided into two parts covering the first 6 and last 6 months of the year. Both simulations are initialized using data from ERA-Interim (meteorology) and MOZART4/GEOS5 (chemistry) and are preceded by a spin-up period of 4 days. We do a 1-month sensitivity simulation with the MOZART chemistry scheme (July 2014), and two sensitivity simulations with increased traffic emissions for January and July 2014, all with the same simulation procedure. All model simulations are listed in Table 2.

2.4 Emissions

2.4.1 General description

The emission data used in this study are from the TNO-MACC III inventory (Kuenen et al., 2014). The latest available year is 2011, which we use for simulating the year 2014. From comparing the TNO-MACC III emissions for Germany in the years available, there was generally only a very small (decreasing) trend in reported emissions up to 2011, expected to continue also after 2011. This allows use of the latest available year of emissions (2011) also for 2014 simulations (Hugo Denier van der Gon, personal communication, 2016). Details on the emission inventory and the way these emissions are used in the present WRF-Chem set-up can be found in Kuik et al. (2016), and references therein, and are briefly summarized here. The data are originally at a horizontal resolution of ca. 7 km × 7 km, which we downscale for the Berlin–Brandenburg region based on proxy data (Fig. 1). As it has been shown that downscaling the emission data to the resolution of the model grid helps to better capture the spatial

Table 2. Model simulations presented in this paper.

Simulation	Chemistry	Period	Emissions
2014_ref	RADM2	1 January 2014–31 December 2014	TNO-MACC III
2014_moz	MOZART	July 2014	TNO-MACC III
2014_emis	RADM2	January 2014 July 2014	TNO-MACC III Traffic NO_x increased (Sect. 6.1)

distribution of air pollutant concentrations, we updated the downscaling procedure (see Supplement). The updates include an extension of the region for which the emissions are downscaled from Berlin to the whole Berlin–Brandenburg region. In addition, we only downscale those emission categories (SNAP categories) which are both of main interest for studying NO_2 in an urban area and also represented well by the proxy data chosen. This ensures that we are not suggesting a higher precision than is achievable with the available proxy data. We thus only downscale emissions from SNAP categories 2 (residential combustion), 6 (product use) and 71–75 (traffic), as these emissions can be represented well by population density (SNAP 2 and 6) and traffic density (SNAP 71–75).

2.4.2 Emission processing

Kuik et al. (2016) concluded that when simulating urban air quality with high resolution and using emission input data at high resolution, a more detailed treatment of the vertical distribution of point source emissions might further improve the model results. For this reason in this study, the emissions are distributed vertically based on profiles adapted from Bieser et al. (2011), i.e. emissions from the energy industry are distributed between the third and seventh model layer, emissions from other industrial sources as well as from the extraction and distribution of fossil fuels are distributed between the first four model layers, waste treatment emissions are distributed in the first five model layers and airport emissions (LTO cycle) are distributed vertically into the first seven layers (see Supplement for further details). For reference, the layer tops are at ca. 30 m (layer 1), 95 m (layer 2), 190 m (layer 3), 310 m (layer 4), 460 m (layer 5), 650 m (layer 6) and 890 m (layer 7).

TNO-MACC III emissions are provided as annual totals. For each emission (SNAP) category separately, we apply factors distributing the emissions for each month, day of the week (weekend vs. weekday), and hour of the day (diurnal cycle) based on Builtjes et al. (2002), with the exception of the diurnal cycle of traffic emissions. Previous studies highlighted the importance of using locally available information when specifying temporal profiles of emissions (e.g. Mues et al., 2014). Here we apply a diurnal cycle of traffic emissions (fraction of total daily emissions per hour of the day) calculated based on traffic counts provided by the Berlin
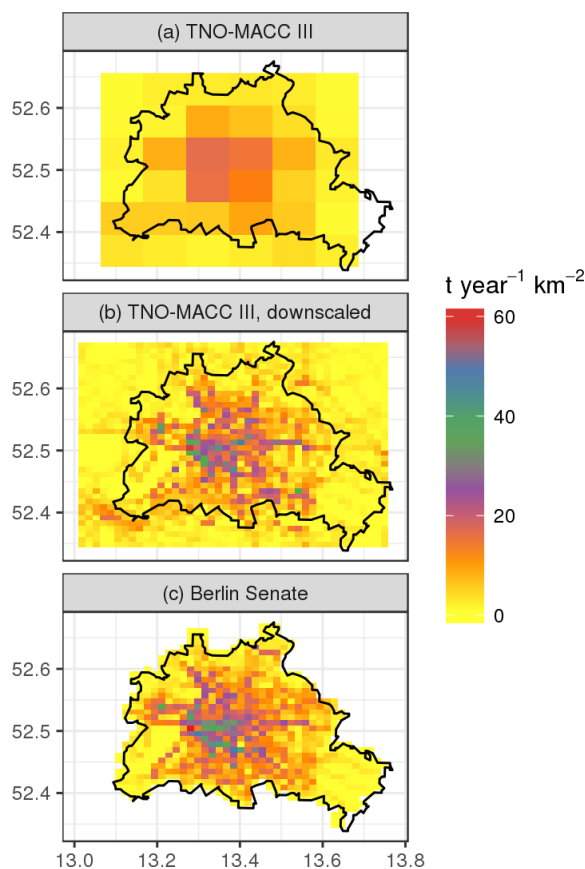
Figure 1. Total NO_x emissions from traffic in Berlin; **(a)** from the TNO-MACC III inventory, 2011; **(b)** from the TNO-MACC III inventory, downscaled to a horizontal resolution of ca. 1 km, 2011; **(c)** from the Berlin Senate Department for Urban Development and Housing for the year 2009.

Senate Department for the Environment, Transport and Climate (data used from 2007 to 2016) and by the German Federal Highway Research Institute – BASt (Bundesanstalt für Straßenwesen, 2017, data used from 2003 to 2016). The diurnal cycle applied here is obtained by calculating the fraction of average daily traffic counts in Berlin at each hour of the day, thus assuming a linear scaling of traffic emissions with

traffic counts as also assumed by Builtjes et al. (2002). Following Builtjes et al. (2002), we apply a uniform diurnal cycle for each day of the week, making no distinction between the diurnal cycle of weekends and weekdays. As mentioned above, we do however also apply a weekly profile; thus, the magnitude of the daily emissions on weekends is different from that on weekdays. The main differences between the profiles calculated based on locally available information and the hourly emission factors from Builtjes et al. (2002) include an earlier increase in traffic emissions in the morning by ca. 1 h and more evenly distributed high traffic emissions during the day with less pronounced morning and afternoon peaks.

NO$_x$ is emitted mainly as NO, but also includes a fraction directly emitted as NO$_2$ (the primary NO$_2$ fraction, f-NO$_2$) by combustion engines. Here, NO$_x$ is emitted as NO for all SNAP categories except "road transport" and "non-road transport". For non-road transport and all road transport emissions except diesel, NO$_x$ is emitted as 10 % NO$_2$ and 90 % NO (by mass). Road transport diesel emissions include both light duty vehicle (LDV) and heavy duty vehicle (HDV) emissions. For the latter, we also assume a f-NO$_2$ of 10 %, while for light duty vehicles we assume a f-NO$_2$ of 26 % (Carslaw, 2005). Combining this with the TNO-MACC share of diesel emissions attributable to LDV (43 %) and HDV (57 %), we obtain a combined f-NO$_2$ for road transport diesel NO$_x$ emissions (SNAP 72) of 17 %. Test simulations varying the f-NO$_2$ for diesel LDV between 10 and 55 % have shown that the simulated NO, NO$_2$ and NO$_x$ concentrations have very little sensitivity towards the f-NO$_2$ of LDV diesel emissions, while small differences in the simulated ozone concentrations were seen. As further sensitivity simulations on this topic are beyond the scope of this study and differences were small, we chose to use a f-NO$_2$ that was around the mid-point of those values documented for LDV diesel NO$_x$ emissions (26 %).

2.4.3 Comparison of the downscaled TNO-MACC III emissions with a local inventory

Local NO$_x$ emissions from road transport are available for 2009 (Berlin Senate Department for Urban Development and Housing). In comparison with the downscaled TNO-MACC III emissions for the Berlin grid cells (2011), traffic NO$_x$ emissions from the local inventory are 6 % higher. The geographical distribution of the emissions in the local inventory is very similar to the downscaled version of TNO-MACC III used in this study (Fig. 1).

3 Observational data

3.1 AirBase observations and NO$_2$ uncertainty

NO$_2$, NO$_x$ and O$_3$ measurements are taken from AirBase (EEA, 2017), a database compiling air quality observations from the EU Member States and associated countries, per-

formed as required by EU clean air legislation. The files can directly be downloaded from the AirBase website. In the case of Germany the measurements are performed by the federal states. For the comparison with model results, observations from stations within Berlin and in the adjacent surroundings in the Federal State of Brandenburg representing "urban background", "suburban background" and "rural near-city" conditions are used (Fig. 2; also see Supplement Fig. S4 and Table S1). For our analysis, we reclassify AirBase station DEBE066 in Berlin–Karlshorst from "urban background" to "suburban background", as the station is not located in the core area of the city and pollutant concentrations measured there are similar to concentrations measured at other suburban background stations. As a result, four stations for each classification type are used in this study: Amrumer Straße (DEBE010), Brückenstraße (DEBE068), Belziger Straße (DEBE018) and Nansenstraße (DEBE034) in the urban background, Blankenfelde-Mahlow (DEBB086), Buch (DEBE051), Groß Glienicke (DEBB075) and Johanna und Willy Brauer Platz (DEBE066) in the suburban background, and Frohnau (DEBE062), Grunewald (DEBE032), Müggelseedamm (DEBE056) and Schichauweg (DEBE027) in the rural near-city background.

In addition, five measurement stations representing "traffic" conditions within Berlin, which are located next to major roads within the core area of the city, and assumed to be primarily influenced by traffic emissions, are used for the observation-based analysis (Sect. 6.3).

NO$_2$ concentrations used for this study were measured using chemiluminescence. With this method, NO$_2$ is converted to NO with a molybdenum converter before being detected using chemiluminescence, as NO reacts with O$_3$ to form NO$_2$ and O$_2$ while emitting light (see e.g. Gerboles et al., 2003; Steinbacher et al., 2007). A limitation of this method is that other nitrogen-containing species (PAN, HNO$_3$) are also converted to NO in this process. In a comparison study, Steinbacher et al. (2007) found that only 73–82 % of the NO$_2$ measured with this method is "real" NO$_2$, at a rural background site in Switzerland. However, they state that reasonable results are obtained with this type of converter at urban background sites. Villena et al. (2012) compared NO$_2$ concentrations in urban smog conditions in Santiago de Chile using chemiluminescence detection with a molybdenum converter and differential optical absorption spectroscopy and found large differences between measured concentrations during daytime. Further sources of uncertainty are introduced in the detection itself, for which NO reacts with O$_3$, producing the luminescence signal to be detected. Gerboles et al. (2003) assess the uncertainty of NO$_2$ measurements, and Pernigotti et al. (2013) derive a simplified procedure in order to calculate the NO$_2$ measurement uncertainty, which we apply in order to obtain a rough estimate of the uncertainty range of NO$_2$. Accordingly, the uncertainty (u) of the observed NO$_2$
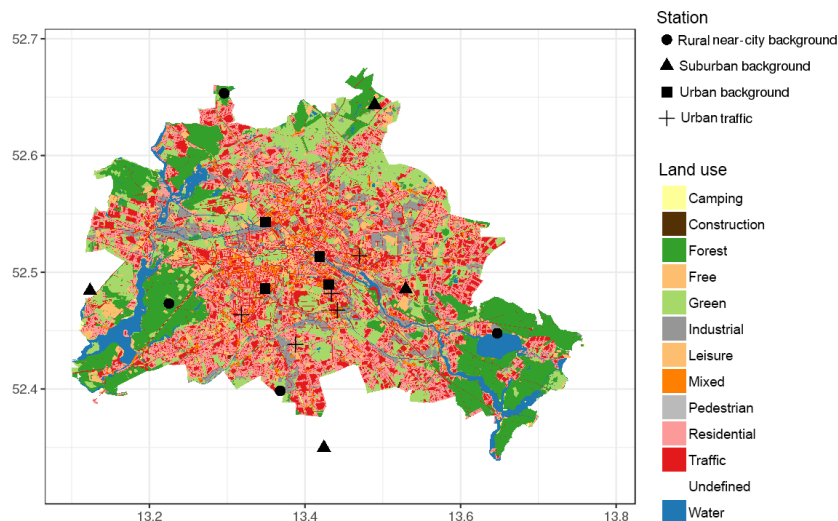
Figure 2. Locations of measurement stations in and close to Berlin, including their AirBase station area classification and type and the land use classes in Berlin according to the Berlin Senate Department for Urban Development and Housing (2015).

concentrations x at time i is quantified as follows:

$$u(x_i) = u_{\text{rRV}} \cdot \sqrt{(1-\alpha)x_i^2 + \alpha \cdot \text{RV}^2}. \tag{1}$$

Here, u_{rRV} is an estimate of the relative uncertainty around a reference value RV, and α is the fraction of uncertainty not proportional to the reference value. We use the coefficients corresponding to the mean uncertainties of the individual parameters, i.e. $u_{\text{rRV}} = 0.09$, $\alpha = 0.06$ and the reference value $\text{RV} = 200\,\mu\text{g m}^{-3}$ (Pernigotti et al., 2013).

3.2   Meteorological data

In order to complement the analysis and to investigate potential influences of the modelled meteorology on modelled NO$_2$ concentrations, we include a comparison of modelled meteorology with observations. This includes observations of 2 m temperature, and 10 m wind speed and direction, all provided by the German Weather Service and available online (Kaspar et al., 2013). In addition, mixing layer height derived from ceilometer measurements at Nansenstraße during the BAERLIN2014 campaign (Geiß et al., 2017) are used for a qualitative comparison with the modelled mixing layer height (see Kuik et al., 2016, for a discussion of this type of comparison). The data are generally available between 20 June and 27 August 2014, but include a number of gaps.

4   Analysis and evaluation metrics

4.1   Analysis of model results

Modelled NO$_2$ concentrations are evaluated with the aim of using the model set-up for policy-relevant analyses of urban

NO$_2$ concentrations and NO$_2$ reduction measures with high temporal and spatial resolution, and in order to identify the main sources of the errors in modelled NO$_2$ concentrations. For this, we use both operational and diagnostic evaluation metrics, which are explained in the following.

Operational evaluation metrics applied here are based on Thunis et al. (2012) and Pernigotti et al. (2013). They include an analysis of the mean bias (MB) and normalized mean bias (NMB), the correlation coefficient (R), and the root mean square error (RMSE, as defined in the Supplement). The model error is compared with the model quality objective (MQO) and performance criteria calculated from NO$_2$ observations and their uncertainty. The MQO is defined as follows:

$$\text{MQO} = \frac{1}{2} \frac{\text{RMSE}}{\text{RMS}_\text{U}}, \tag{2}$$

with RMS_U being the root mean square of the measurement uncertainty. Following Thunis et al. (2012) and Pernigotti et al. (2013), a MQO lower than 0.5 indicates that the model results are on average within the range of the measurement uncertainty, and further efforts to improve model performance are not meaningful. A MQO between 0.5 and 1 indicates that the uncertainties of model and observations overlap, and that the model might still be a better predictor of the true value than the observations. A MQO greater than 1, on the other hand, indicates significant differences between the model and the observations.

The performance criteria for mean bias, normalized mean bias and correlation coefficient as defined in Pernigotti et al. (2013) are listed in the Supplement. As the uncertainty of NO$_2$ measurements is partly concentration-dependent, the

MQO and the other performance criteria differ between station classes and seasons.

The operational evaluation and model quality objectives are intended to support an assessment of the extent to which a model can be used for policy-relevant analyses, but do not point to the underlying processes that might lead to a disagreement between model results and observations. Furthermore, the calculation of the NO$_2$ measurement uncertainty underlying the calculation of the MQO and performance criteria is also based on a number of uncertain parameters.

We thus complement the analysis with a diagnostic evaluation, comparing the individual spectral components of the modelled and observed time series. This is done following Solazzo and Galmarini (2016) and Solazzo et al. (2017): we use a Kolmogorov–Zurbenko filter (Zurbenko, 1986), a widely used filter in the analysis of air quality data based on calculating the iterative moving average of a time series, in order to decompose the modelled and observed time series into contributions from different timescales. The Kolmogorov–Zurbenko filter is a low pass filter, with the length of the moving average window and the number of iterations determining the spectral component to be filtered. Taking the difference between two filtered time series (bandpass filter) makes it possible to decompose the observed and measured time series into an intra-diurnal component (ID, < 0.5 days), a diurnal component (DU, 0.5–2.5 days), a synoptic component (SY, 2.5–21 days) and a long-term component (LT, > 21 days) with the property

$$TS(x) = LT(x) + SY(x) + DU(x) + ID(x). \tag{3}$$

Here, TS describes the full time series of species x. This is described in detail in Solazzo et al. (2017) and Solazzo and Galmarini (2016), and references therein. Further details are also given in the Supplement.

By assessing the error of each component individually it is then easier to relate the error to the model process(es) characteristic at the respective timescale. The error analysis of the different spectral components is done by "error apportionment" (Solazzo et al., 2017), breaking down the mean square error (MSE) into bias, variance (σ) error and minimum achievable mean square error (mMSE) as follows:

$$MSE = (mod - obs)^2 + (\sigma_{mod} - r\sigma_{obs})^2 + mMSE. \tag{4}$$

As described by Solazzo and Galmarini (2016), the minimum achievable mean square error is determined by the observed variability that is not reproduced by the model. While this approach helps in investigating the sources of model errors, it does not allow for clear identification or quantification of them as several processes take place on similar timescales, and because this filtering method does not allow for a complete separation of the different spectral components (see Solazzo et al., 2017, for a discussion of this issue).

In addition to this operational and diagnostic analysis of simulated NO$_2$ concentrations, we include a brief evaluation of selected key meteorological parameters (temperature, wind speed and direction) as well as further chemical species (O$_3$, NO$_x$), the former because WRF-Chem is an online-coupled model, and the latter because NO$_2$ is tightly linked to NO and O$_3$.

4.2 Observation-based analysis

As traffic emissions are the focus of this study, the analysis of the model results is complemented with an analysis based on observations of roadside and urban background NO$_2$ concentrations and traffic counts. Like in many chemistry transport modelling studies, we assume a linear scaling of traffic emissions with traffic counts, which are used as a proxy for calculating time profiles of traffic emissions for each month, day of the week and hour of the day. While it has been shown that model results can be improved by taking into account country-specific driving patterns as well as by applying separate diurnal cycles for heavy and light duty vehicles (Mues et al., 2014), local traffic conditions (e.g. congestion) are currently not taken into account in the calculation of the diurnal cycles.

Using observations of traffic counts and roadside NO$_x$ concentrations in Berlin obtained at the same locations and times (data described in Sects. 2.4.2 and 3.1), we assess how much of the observed variance in NO$_x$ concentrations can be explained with traffic counts in a linear model. In addition to a linear fit, other types of relationships (e.g. quadratic, exponential) are also explored. We neglect other influences on observed NO$_x$ concentrations such as other emission sources and large-scale and local meteorological conditions. In order to account for different conditions at different hours of the day, we fit the data separately for each hour of the day. The intention of this analysis is not to build a statistical model for roadside NO$_x$ concentrations, but rather to give insight into the type of relationship between roadside NO$_x$ concentrations and traffic counts, complementing the model simulations done in this study.

5 Model evaluation

5.1 Meteorology

An in-depth evaluation of modelled meteorology obtained with a similar model set-up is presented in Kuik et al. (2016) for the summer (JJA) of 2014. Here, model results for the whole year of 2014 are presented and discussed. Changes in the model set-up compared with the set-up presented in Kuik et al. (2016) are the planetary boundary layer scheme (MYNN, Nakanishi and Niino, 2006 instead of YSU, Hong et al., 2006) and re-initialization of the model meteorology every 2 days as described in Sect. 2. Tests showed that though the change in the planetary boundary layer scheme did not introduce considerable improvements, it did seem to lead to a slightly better match of model results with observations in the timing of the decrease in the boundary layer in the evening.

Here an additional brief model evaluation is done in order to ensure that the modelled meteorology still reproduces observations reasonably well.

Modelled and observed 2 m temperature and 10 m wind speed are compared at five stations run by the German Weather Service, including Schönefeld, Tegel and Tempelhof in Berlin and Lindenberg and Potsdam outside of Berlin (Table 3). Across the stations, annual mean temperature is simulated well, with mean biases smaller than $-1\,°C$ outside of Berlin and just above $-1\,°C$ within Berlin. Modelled and observed hourly temperatures correlate well with $R = 0.96$ at all five stations. Small seasonal differences exist, with somewhat higher biases in winter (as large as $-1.7\,°C$ in Tegel) and somewhat lower biases in spring (e.g. $-0.1\,°C$ in Schönefeld). Annual mean wind speed is somewhat overestimated within Berlin (between 0.02 and $0.45\,m\,s^{-1}$, or up to 13 %), with correlations of the hourly values between 0.74 and 0.78 within Berlin. In winter, wind speed is slightly underestimated at two out of the three stations within Berlin (-2 and -7 % at Tegel and Schönefeld, respectively), while it is overestimated somewhat more in spring and summer (up to $0.58\,m\,s^{-1}$, or ca. 20 % in Tegel). In spring and summer, the main wind directions are captured relatively well by the model (see Figs. S6 and S7 in the Supplement). In autumn, wind from the east, the main wind direction, is modelled less frequently than observed, but wind from the southeast is modelled too frequently compared with observations. In winter, modelled wind comes from south and south-west too frequently compared with observations, at the expense of south-easterly wind directions, as depicted in Figs. S6 and S7. Compared with Kuik et al. (2016), an improvement in summer mean bias in wind speed is seen; with the JJA mean bias between 0.3 and $0.4\,m\,s^{-1}$ smaller than that of the comparable simulation in Kuik et al. (2016) at all Berlin stations, and JJA correlation coefficients improved by ca. 0.1. This can probably be attributed to the continuous re-initialization of modelled meteorology in this simulation.

In addition, modelled and ceilometer-derived mixing layer heights (MLHs) are compared (Fig. S8 in the Supplement). Even though a quantitative comparison between the modelled MLH and the MLH height derived from optical measurements is difficult to interpret (see Kuik et al., 2016), a qualitative comparison of mean diurnal cycles gives insight into the timing of the deepening of the MLH. The comparison shows that the modelled increase in the summer MLH in the morning is too early, already starting at ca. 04:00 in the model. Though the precise time of the observed MLH increase cannot be determined from the available data, it takes place between 05:00 and 07:00 (Fig. S8 in the Supplement). An early modelled deepening of the mixing layer might lead to overly early and thus overly strong mixing of chemical species in the model.

5.2 Operational evaluation of simulated chemical species

Seasonally and station-class averaged performance metrics are listed in Table 4 for NO_2, NO_x and O_3. NO_2 and total NO_x are biased low throughout the seasons and station classes, with the highest (absolute and relative) mean biases for urban background stations both annually and seasonally. The model bias is relatively low at rural and suburban background stations, with annual mean biases of only up to $-2.8\,µg\,m^{-3}$ (-19 %). Correlation coefficients of modelled with observed hourly concentrations are $R = 0.50$ and $R = 0.55$ in the rural and suburban backgrounds, respectively.

NO_2 at urban background sites is biased by $-7.8\,µg\,m^{-3}$ (-29 %) on average, with a higher negative bias in spring ($-10.2\,µg\,m^{-3}$, -38 %) and summer ($-9.3\,µg\,m^{-3}$, -41 %) and smaller negative biases in autumn ($-4.9\,µg\,m^{-3}$, -17 %) and winter ($-6.8\,µg\,m^{-3}$, -22 %). Modelled hourly concentrations correlate reasonably well with observations in autumn, spring and winter (R between 0.51 and 0.55), but worse in summer (0.36).

Modelled hourly ozone concentrations correlate reasonably well with observations at all station classes throughout the whole year (R between 0.70 and 0.73), but with lower correlations for individual seasons. This shows that intra-seasonal differences are represented well by WRF-Chem, with slightly worse representations of inter-seasonal variations. Modelled ozone concentrations are biased high at most stations and in most seasons, with the exception of a low bias in summer in the urban background.

For NO_2, the MQO (Eq. 2) is greater than 0.5, but smaller than 1, both annually averaged and in all seasons at rural near-city background and suburban background stations. For urban background sites the MQO is larger than 1 both on annual average and in spring and summer, and just below 1 in autumn and winter, emphasizing that the model performs reasonably well in the rural and suburban background, but the disagreement between model results and observations is larger in the urban background. This suggests that processes or emissions typical for urban areas are an important source of model error.

In order to test the sensitivity of the results to the selected chemical mechanism, we compare modelled NO_2 and total NO_x concentrations for July with two different chemical mechanisms: RADM2 (the base configuration in this study) and MOZART. For all station classes in and around Berlin, the modelled NO_x and NO_2 concentrations only show very small mean differences of -0.04 to $-0.4\,µg\,m^{-3}$ (NO_x) and -0.4 to $-0.5\,µg\,m^{-3}$ (NO_2, RADM2 – MOZART). This suggests that the model bias in NO_2 and total NO_x concentrations of the base configuration is not strongly influenced by the choice of chemical mechanism, but rather results from other sources of error.

Table 3. Modelled meteorology compared to observations and annual and seasonal performance indicators. Mean bias (MB) and root mean square error (RMSE) are indicated in K (temperature) and m s^{-1} (wind speed); the normalized mean bias (NMB) and correlation coefficient (R) are unitless. Data are aggregated as follows: MAM – March, April, May, JJA – June, July, August, SON – September, October, November, and DJF – December, January, February.

		Temperature				Wind speed			
		MB	NMB	RMSE	R	MB	NMB	RMSE	R
Lindenberg	2014	−0.66	−0.06	2.17	0.96	0.81	0.25	1.63	0.69
	spring (MAM)	−0.48	−0.04	2.26	0.91	0.87	0.27	1.8	0.68
	summer (JJA)	−0.89	−0.05	2.4	0.89	0.87	0.31	1.68	0.61
	autumn (SON)	−0.55	−0.05	1.99	0.95	0.92	0.32	1.58	0.63
	winter (DJF)	−0.7	−0.3	2	0.93	0.57	0.14	1.43	0.76
Potsdam	2014	−0.71	−0.06	2.25	0.96	−0.47	−0.12	1.4	0.69
	spring (MAM)	−0.49	−0.04	2.16	0.93	−0.34	−0.08	1.42	0.73
	summer (JJA)	−0.45	−0.02	2.1	0.91	−0.14	−0.04	1.41	0.55
	autumn (SON)	−0.76	−0.07	2.34	0.94	−0.46	−0.12	1.27	0.62
	winter (DJF)	−1.15	−0.44	2.42	0.9	−0.99	−0.2	1.47	0.79
Schoenefeld	2014	−0.61	−0.06	2.16	0.96	0.02	0	1.3	0.78
	spring (MAM)	−0.12	−0.01	1.97	0.94	0.07	0.02	1.34	0.81
	summer (JJA)	−0.63	−0.03	2.1	0.92	0.16	0.05	1.39	0.66
	autumn (SON)	−0.73	−0.06	2.27	0.94	0.12	0.04	1.21	0.7
	winter (DJF)	−0.98	−0.39	2.3	0.91	−0.31	−0.07	1.25	0.85
Tegel	2014	−1.25	−0.11	2.48	0.96	0.4	0.12	1.33	0.75
	spring (MAM)	−0.83	−0.07	2.26	0.93	0.58	0.18	1.43	0.77
	summer (JJA)	−1.02	−0.05	2.23	0.92	0.58	0.2	1.44	0.66
	autumn (SON)	−1.44	−0.12	2.65	0.94	0.47	0.16	1.24	0.69
	winter (DJF)	−1.72	−0.54	2.76	0.9	−0.08	−0.02	1.17	0.84
Tempelhof	2014	−1.21	−0.11	2.51	0.96	0.45	0.13	1.32	0.74
	spring (MAM)	−0.67	−0.06	2.22	0.93	0.47	0.13	1.38	0.77
	summer (JJA)	−1.17	−0.06	2.35	0.91	0.5	0.16	1.51	0.63
	autumn (SON)	−1.38	−0.11	2.65	0.93	0.43	0.14	1.25	0.7
	winter (DJF)	−1.63	−0.54	2.76	0.9	0.38	0.1	1.12	0.81

5.3 Diagnostic evaluation of simulated NO$_2$ concentrations

In order to further assess the model performance and identify the main sources of the model bias, a diagnostic evaluation is done, by spectrally decomposing the modelled and observed time series of NO$_2$ and analysing the type of error of each component.

Averaging the decomposed time series over each station class, the modelled long-term (LT) and synoptic (SY) components as defined in Sect. 4.1 correlate well with the observations: the correlation coefficient for the LT component is 0.83, 0.81 and 0.72 for rural near-city, suburban and urban backgrounds, respectively, and 0.60, 0.63 and 0.65 for the SY component (Fig. 3). This suggests that changes on timescales of ca. 2.5 days to a few weeks are captured relatively well by WRF-Chem, which includes for example the modelled synoptic (meteorological) situation and is consistent with the good model performance in simulating observed meteorology. The correlation coefficients for the diurnal (DU) compo-

nent are smaller, with 0.45, 0.52 and 0.48 for rural near-city, suburban and urban backgrounds, respectively. This suggests that the model has more difficulties in capturing variations on timescales of a few hours to 2.5 days than on longer timescales. This might be related to the diurnal variations in modelled mixing, but also to the diurnal cycle of emissions. Particularly the latter is strongly influenced by traffic emissions in the urban area and might also point to deviations of the model-prescribed diurnal cycle in emissions from the real-world diurnal cycle.

With the procedure used for spectrally decomposing the NO$_2$ time series, the LT component is the only systematically biased component, with the other components fluctuating around zero. Decomposing the model error shows that the bias of the LT component has the largest contribution to the error for urban background stations (ca. 30 %, Fig. 4). NO$_2$ has a short lifetime and is mainly influenced by local and regional sources. This means that the boundary conditions are not likely to be a strong source of error. The negative bias in the LT component is consistent with both prob-

Table 4. Modelled chemistry, seasonal performance indicators (averaged for each station class; each class includes four stations) and the model quality objective for NO_2. Mean bias (MB) and root mean square error (RMSE) are indicated in $\mu g \, m^{-3}$; the normalized mean bias (NMB) and correlation coefficient (R) are unitless. Data are aggregated as follows: MAM – March, April, May, JJA – June, July, August, SON – September, October, November, and DJF – December, January, February.

| | | NO_2 | | | | NO_x | | | | O_3 | | | | NO_2 |
		MB	NMB	RMSE	R	MB	NMB	RMSE	R	MB	NMB	RMSE	R	MQO
rural–	2014	−2.12	−0.16	10.2	0.5	−3.77	−0.23	15	0.48	5.02	0.11	22.49	0.7	0.78
near-city	autumn (SON)	−0.97	−0.06	9.97	0.48	−3.9	−0.19	16.2	0.45	11.96	0.41	22.71	0.66	0.76
backgr.	spring (MAM)	−2.91	−0.23	11.69	0.42	−4.26	−0.29	16.39	0.37	3.88	0.07	23.42	0.62	0.89
	summer (JJA)	−2.38	−0.26	8.23	0.37	−2.88	−0.28	9.57	0.32	1.41	0.02	25.49	0.61	0.64
	winter (DJF)	−2.2	−0.12	10.66	0.47	−4.08	−0.18	16.83	0.46	2.85	0.09	17.18	0.55	0.79
suburban	2014	−2.8	−0.19	10.67	0.55	−7.2	−0.35	20.13	0.48	4.88	0.11	22.45	0.7	0.8
backgr.	autumn (SON)	−0.76	−0.05	10.32	0.52	−7.92	−0.32	23.12	0.44	12.22	0.42	22.39	0.67	0.78
	spring (MAM)	−4.41	−0.31	12.2	0.49	−8.25	−0.44	21.71	0.39	4.15	0.07	24.06	0.61	0.92
	summer (JJA)	−2.88	−0.29	9.01	0.44	−5.12	−0.4	13.14	0.34	1.16	0.02	25.49	0.64	0.7
	winter (DJF)	−3.14	−0.16	10.96	0.53	−7.57	−0.28	21.24	0.49	2.02	0.06	16.53	0.57	0.8
urban	2014	−7.83	−0.29	16.69	0.51	−15.84	−0.4	35.57	0.47	3.25	0.08	21.01	0.73	1.13
backgr.	autumn (SON)	−4.89	−0.17	13.9	0.55	−16.9	−0.36	37.3	0.48	9.09	0.37	19.69	0.71	0.95
	spring (MAM)	−10.23	−0.38	19.71	0.51	−17.09	−0.47	40.68	0.4	3.07	0.06	22.62	0.62	1.32
	summer (JJA)	−9.26	−0.41	18.16	0.36	−13.3	−0.47	28.92	0.24	−1.94	−0.03	24.85	0.6	1.28
	winter (DJF)	−6.84	−0.22	14.05	0.53	−16.16	−0.34	34.41	0.5	2.93	0.12	15.35	0.58	0.93
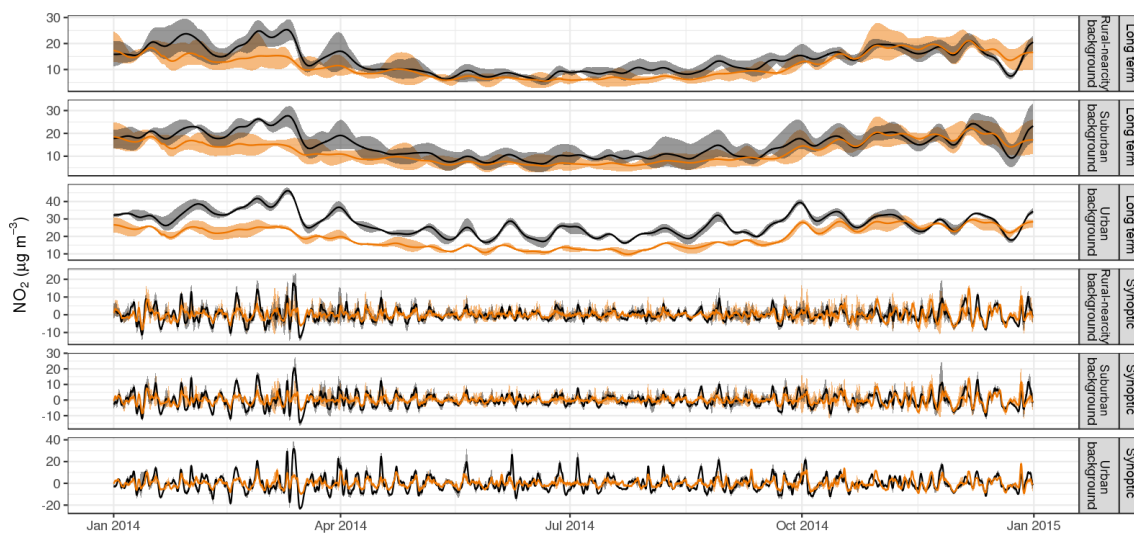
Figure 3. Long-term and synoptic components of modelled (orange) and observed (black) time series, averaged over all stations of each station class. The shaded areas show the variability (25th and 75th percentiles) between the different stations within each class. Note the variable y-axis.

lems in daytime vertical mixing and an underestimation of emissions. As discussed in Sect. 3.1, NO_2 concentrations detected with chemiluminescence using a molybdenum converter might be biased high due to interferences with other nitrogen-containing species (e.g. PAN, HNO_3) and could further contribute to discrepancies between modelled and observed NO_2 concentrations.

The second largest error at urban background stations and the largest error at rural near-city and suburban background

stations is the mMSE of the diurnal component. This means that part of the observed variability is not reproduced by the model and is consistent with the comparably lower correlation coefficients of the diurnal component compared with the synoptic and long-term components. Solazzo et al. (2017) relate this error to problems in comparing single point measurements with model grid cell values (incommensurability) and a disagreement in timing of modelled and observed concentrations, amongst others. The incommensurability can, in
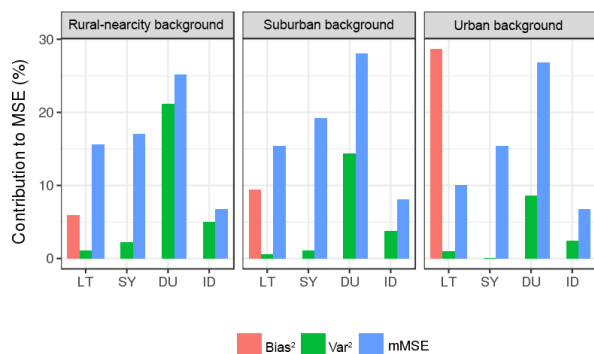
Figure 4. Contribution of different types of error to the mean square error of the model, per station class. The mean square error is divided into squared bias (bias^2), variance error (var^2) and minimum mean square error (mMSE) of the long-term (LT), synoptic (SY), diurnal (DU) and intra-diurnal (ID) components (see Sect. 4.1 for further details).

the case of NO_2, come from NO_2 observations being influenced by local sources that cannot be captured by WRF-Chem run at a horizontal resolution of 3 km × 3 km. The temporal variation of modelled NO_2 concentrations, in the case of the diurnal component, can be influenced by the temporal profiles prescribed to the emission input data. Thus, the error is consistent with problems in the prescribed diurnal cycles of emissions including traffic emissions, but might also be related to a diurnally varying bias in emissions.

At rural near-city background stations, there is a relatively large contribution of the variance error of the diurnal component. This is probably caused by an overestimation of the standard deviation of observed diurnal components in autumn (Fig. S9 in the Supplement), particularly pronounced at the site Frohnau in the north or Berlin, slightly west of the main emission sources. This might be explained by the disagreement in modelled and observed wind direction in autumn, leading to higher than observed NO_2 peaks in the model.

Solazzo et al. (2017) present a diagnostic model evaluation of the AQMEII phase 3 model simulations for the year 2010 and report the largest error of modelled NO_2 in winter, both for the European and North American domains simulated in AQMEII. Our results show the opposite for urban background stations (Fig. S9 in the Supplement): the model error, and particularly the bias, is smallest in autumn and winter. While Solazzo et al. (2017) attribute the winter bias to a potential underestimation in residential combustion emissions, these seem to be captured comparably well by the TNO-MACC III inventory in the case of Berlin. The re-distribution of these emissions based on population density, as described in Sect. 2.4.2, may also have contributed to a better spatial representation in our study.

5.4 Diurnal and weekly variation of the model bias

The results from the operational and diagnostic evaluation of modelled NO_2 concentrations suggest that emissions within the urban area are a main source of model error, both contributing to the model bias and the lower correlation with observations. Traffic emissions have the largest contribution to urban NO_x emissions. As traffic emissions have a distinct weekly and diurnal cycle, we additionally assess mean diurnal cycles of modelled and observed NO_2 concentrations as well as the differences between weekdays and weekends. This also helps to further assess the contribution of problems in modelled mixing to the model error. In addition, we analyse the MQO and performance criteria separately for weekends (Saturday and Sunday) and weekdays (Monday through Friday). Public holidays that fall on a weekday are excluded from this analysis, as they were not treated separately from regular weekdays in the emission processing.

The comparison of mean modelled and observed NO_2 diurnal cycles shows distinct differences between station classes and weekend and weekday diurnal cycles (Fig. 5). The diurnal cycle of observed NO_2 concentrations is modelled reasonably well for rural and suburban background stations. In particular, nighttime concentrations are simulated well for rural and suburban background stations, and mostly underestimated in the urban background. Other WRF-Chem modelling studies often report too little mixing at nighttime over urban areas leading to a strong overestimation of observed concentrations. In this study as in other modelling studies using WRF-Chem (Ravan Ahmadov, personal communication, 2017), a modification of the model code was applied in order to increase nighttime mixing. This, in combination with a more realistic vertical distribution of point source emissions (as described in Sect. 2.4.2), seems to improve model performance for NO_2 during nighttime. In addition, tests revealed that this change to the model code does not impact modelled daytime concentrations.

During weekdays, there is an underestimation of the observed morning peak in all seasons and at all station classes. Weekend diurnal cycles are modelled well at rural and suburban background stations. At urban background stations there is a larger disagreement between modelled and observed concentrations throughout the whole day on both weekends and weekdays. The underestimation of daytime urban background NO_2 concentrations is particularly strong in summer and spring. This might be explained by mixing over urban areas during daytime that is too strong, caused for example by a turbulent diffusion coefficient that is too large during daytime over urban areas in the lowest model layer. Other modelling studies have reported similar problems, reducing the coefficient over urban areas (e.g. of the CHIMERE model set-up used in Schaap et al., 2015). An onset of the deepening of the boundary layer that is too early (Sect. 5.1) might further contribute to the disagreement in the modelled and observed morning peaks. Overall, this discussion shows that the rep-
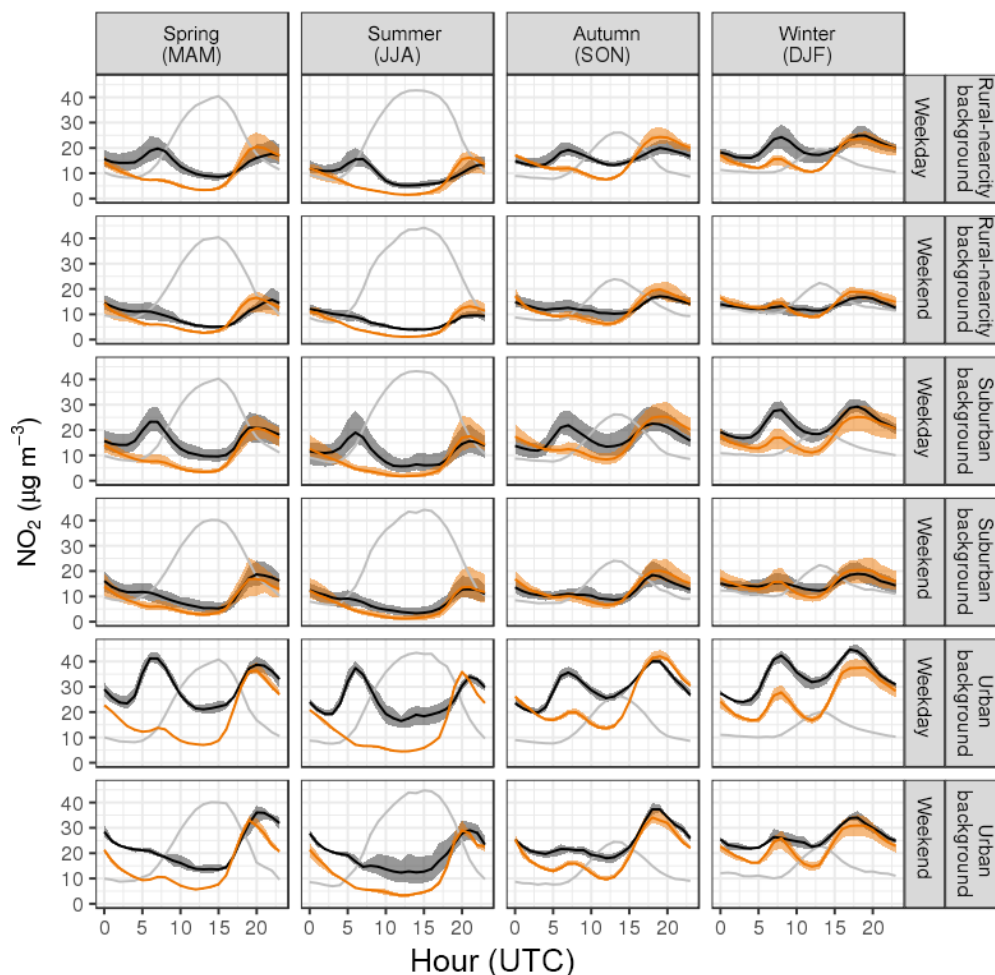
Figure 5. Mean diurnal cycles of modelled (orange) and observed (black) NO_2 concentrations, by station class and weekday/weekend. Shaded areas show the variability between the different stations' mean diurnal cycles (25th and 75th percentiles). Grey lines show the mean modelled planetary boundary layer heights at the respective grid points (scaled, but the relative changes between different hours and seasons are maintained).

resentation of vertical mixing over urban areas might have to be improved to be physically more consistent in regional models, for example by better taking into account urban heat and momentum fluxes and treating the urban parameterization consistently with chemistry. Measurements of vertical profiles of NO_x in cities, particularly in the planetary boundary layer, would be helpful in order to evaluate the models and improve the representation of surface NO_x concentrations, as the NO_x profile in the lowest model layer is not resolved at the model resolution used in this study.

The model underestimation of observed daytime NO_2 concentrations at urban background stations is stronger on weekdays than on weekends, and is particularly noticeable during the morning hours. This is consistent with an overall underestimation of emission sources active in the morning hours

on weekdays and potentially also a misrepresentation of the diurnal cycles of emissions in the model: traffic emissions are distributed in the model throughout the day using a linear scaling with traffic counts (Sect. 2.4.2), which might fall short of accounting for relatively higher emissions during situations with high traffic and associated congestion. This issue is further assessed in Sect. 4.2.

Generally, throughout all seasons, the NO_2 MQO is not met on weekdays for urban background stations, but is smaller than 1 on weekends (Fig. 6). The patterns of the model–observation disagreement, and particularly the weekend–weekday differences, are consistent with traffic emissions as a main source of the bias, with a particularly large contribution to observed urban background concentrations.
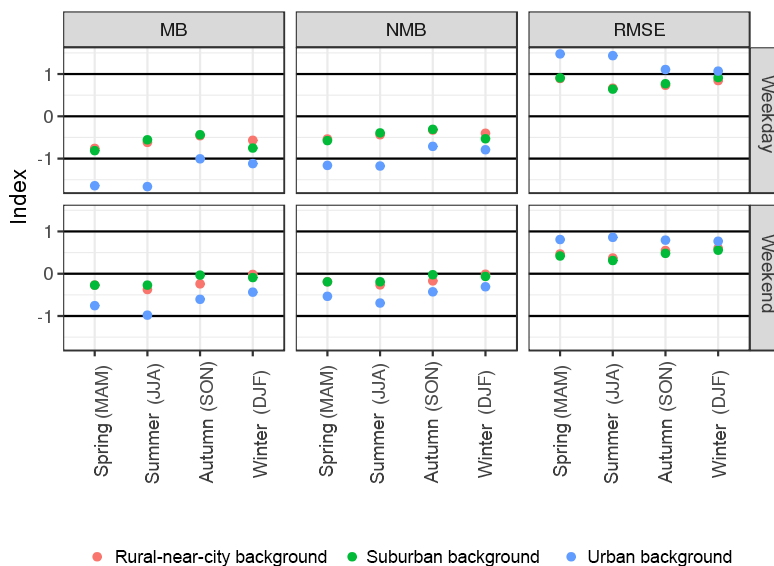
Figure 6. Skill of WRF-Chem in simulating daytime (06:00–17:00 UTC) observed NO$_2$ concentrations. The index represents the the model quality objective for the root mean square error (Sect. 4.1) and the performance criteria for mean and normalized mean bias (described in the Supplement), for weekend and weekday days and each month/season.

6 Top–down quantification of NO$_x$ emissions from traffic

6.1 Calculation of a correction factor

The results from the operational and diagnostic evaluation of modelled NO$_2$ concentrations suggest that traffic emissions are a main source of model error in the urban background: the bias and the mMSE of the diurnal component have the largest contribution to the model error in the urban background throughout all seasons, which is consistent with both an underestimation of the magnitude of traffic emissions, and a problem with their temporal distribution. This is further supported by the smaller (absolute and relative) daytime bias of modelled NO$_2$ concentrations on weekends, where there is less traffic. In the following, we derive a correction factor based on this model bias, which represents the degree to which traffic emissions are underestimated in Berlin, but also takes into account that other sources of model error are likely to also contribute to this bias.

Besides biases in traffic emissions, problems in modelled mixing, which is particularly relevant in summer and spring when the mixed layer is deeper than in other seasons, might contribute to the model bias. Other contributions to the NO$_2$ bias might come from deviations of modelled from observed wind speed in certain periods, and a potential overestimation of NO$_2$ in the observations by detection of other nitrogen-containing compounds as discussed above. These sources of error are likely to impact the model results equally on both weekends and weekdays, whereas an underestimation of traf-

fic emissions will have the largest impact on the results on weekdays. For the quantification of the underestimation of traffic emissions we assume that the weekend bias is entirely caused by non-traffic-emission-related sources of error and thus use the difference between weekday and weekend bias as an estimate for the traffic-related bias. We use the weekday–weekend difference of the relative biases (Fig. 7), thus assuming that the model error due to other sources than traffic emissions roughly scales with the magnitude of modelled concentrations. These are both conservative assumptions, as the correction factor would be much larger if the whole weekday bias was regarded as caused by traffic emissions, and it would also be larger if the absolute weekday–weekend difference was used.

In order to estimate the correction factor for traffic NO$_x$ emissions, we combine the weekday increment of the model bias as defined above with the average fraction of NO$_x$ emissions from traffic to total NO$_x$ emissions in Berlin. The nighttime model bias on weekends and weekdays at urban background stations is of similar magnitude on weekends and weekdays (Fig. 5). A t-test shows that the differences between weekday and weekend bias are not statistically significant at a 95 % confidence interval after ca. 17:00 UTC and before ca. 05:00 UTC (depending on the season). Furthermore, traffic emissions used in the model contribute only little to the total NO$_x$ emissions before 06:00 UTC. This suggests that an underestimation of traffic emissions is only likely to have a significant contribution to the bias in modelled NO$_2$ concentrations between ca. 06:00 and 17:00 UTC. Within the core area of the city where traffic is high (all areas
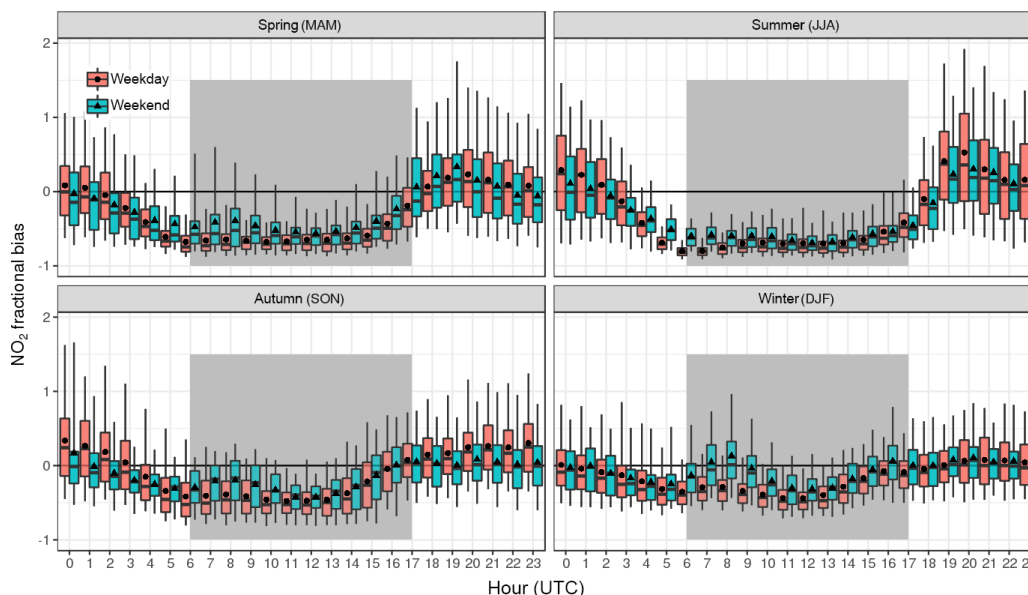
Figure 7. Relative bias in modelled NO_2 concentrations at urban background sites in Berlin, averaged over each season, hour and weekend/weekday. The boxplot shows median (line), 25th and 75th (box), and 5th and 95th (whiskers) percentiles of the hourly bias. Points show the mean. The grey shaded area shows the time period considered for quantifying the underestimation of daytime traffic emissions.

within the "S-Bahn ring"/main core of the city), the average contribution of traffic NO_x to total NO_x between 06:00 and 17:00 UTC is between ca. 30 and 55 %, depending on the month and hour of the day. Seasonal average values over the indicated time period are used for the calculation of the correction factor, with 37 % in winter, 47 % in summer and 42 % in autumn and spring.

With the above assumptions, we quantify the underestimation of traffic NO_x emissions in the core urban area on weekdays between 06:00 and 17:00 UTC as follows, calculating a correction factor f_{NO_x}:

$$f_{NO_x} = \frac{1}{1+\text{NMB}} \cdot \frac{1}{s_t}. \tag{5}$$

With the (negative) $\text{NMB} = \frac{\text{mod}-\text{obs}}{\text{obs}}$, and s_t denoting the traffic share of NO_x emissions. Averaged over all urban background stations, and all seasons, as well as the time period between 06:00 and 17:00 this results in a correction factor of ca. 3. When averaged over all hours of the day, this factor corresponds to an overall underestimation of NO_x traffic emissions in the urban centre by a factor of ca. 2, and an underestimation of all-source NO_x emissions in the urban centre by a factor of ca. 1.5.

In order to gain more insight into the underestimation of the NO_x emissions, we calculate a separate correction factor for each hour and season based on hourly mean seasonal biases and traffic NO_x emission shares (Fig. S10 in the Supplement). The seasonal correction factors show a small increase between 06:00 and 08:00 with a subsequent decrease,

and then remain relatively constant from 11:00 to 17:00. The diurnal variations of the factors for the different seasons are qualitatively similar, and the factors vary in magnitude within a range of ca. 1 between the seasons, with the factors being larger in winter than in summer. The diurnal cycle of the correction factor could be due to a diurnally varying importance of other sources of the modelled NO_2 bias than the traffic emissions, such as mixing, but might also be due to a disagreement in the prescribed diurnal cycle of traffic emissions with the real-world diurnal cycle of traffic emissions. The seasonal differences can at least partly be explained with the seasonally varying relevance of other sources of model error, such as mixing, which has a bigger impact in summer and thus also leads to a bigger bias on the weekends, reducing the weekday increment. The seasonal differences might also be influenced by the temperature dependence of NO_x emissions in newer diesel cars (Hausberger and Matzer, 2017), leading to higher NO_x emissions at colder temperatures, which are not captured by the model.

Overall, the assumptions in these calculations are rather conservative: assuming the weekend bias is not caused by an underestimation of traffic emissions at all is likely to underestimate the effect of any traffic bias. As mentioned above, using the absolute weekday increment of the bias would also lead to higher correction factors. A further discussion of the model bias and correction factor looking into potential reasons contributing to an underestimation of traffic NO_x emissions is presented in Sect. 6.4.

6.2 Sensitivity simulation with increased emissions

The weekday correction factor was applied to NO_x traffic emissions for the core urban area of Berlin (within the "S-Bahn Ring") and tested in two sensitivity simulations for January and July 2014. The results (Table 5 and Fig. 8) show that the bias of modelled NO_2 concentrations at urban background stations decreases on average by $2.6\,\mu g\,m^{-3}$ (NMB decreases from -24 to $-16\,\%$) in January, and by $2.0\,\mu g\,m^{-3}$ (from -43 to $-34\,\%$) in July when applying the correction factors for NO_x emissions from traffic. The decrease is larger when only considering weekdays, with a mean bias lower by $3.4\,\mu g\,m^{-3}$ (from -26 to $-16\,\%$) in January and by $2.7\,\mu g\,m^{-3}$ (from -46 to $-34\,\%$) in July. NO_2 concentrations on weekends are still represented reasonably well by the model in January (Fig. 8). The weekend bias is only changed (decreased) by lower than $0.4\,\mu g\,m^{-3}$ in both cases. Only a minor change would be expected, since emissions on the weekend are not changed in the sensitivity simulations, compared to the base simulation. In January, the correlation of modelled with observed NO_2 concentrations in the urban background is improved by between 0.03 and 0.06 for urban background stations in the sensitivity simulation, but this is not the case in July (Table 5). The lack of improvement in the July correlation coefficient could be related to nighttime concentrations in July that seem to be very sensitive to the increase in emissions during daytime (Fig. 8, lower panel). Despite an improved representation of nighttime concentrations compared to a previous study (Kuik et al., 2016), this sensitivity suggests the need for further attention to mixing processes in urban areas in high-resolution chemistry transport models.

Bigger improvements are seen when comparing total NO_x: the mean bias for urban background stations is reduced from -16.4 to $-10.3\,\mu g\,m^{-3}$ (NMB decreased from -35 to $-22\,\%$) in January and from -11.1 to $-8.1\,\mu g\,m^{-3}$ (from -45 to $-33\,\%$) in July. Only considering weekday concentrations, these are improved by 8.1 and $3.9\,\mu g\,m^{-3}$ (from -37 to -12 and -48 to $-33\,\%$) in January and July, respectively. The differences in NO_2 and NO_x improvements suggest that the impact of the primary NO_2 fraction in emitted NO_x on modelled NO_2 and NO_x concentrations, as well as the influence of chemical processes such as NO titration and other relevant physical and chemical processes, might need to be assessed in greater detail.

While on average the normalized mean bias in a modelled rural and suburban background is only reduced by 1–2 % in both January and July, the simulation of NO_2 and NO_x concentrations downwind of the city centre is improved considerably in the sensitivity simulation. To analyse the change in modelled downwind concentrations, the results are broadly divided based on four main wind directions (N, W, S, E). For each wind direction bin, the results of two stations outside the core urban area are analysed, with Frohnau and Buch in the north, Johanna und Willi Brauer Platz and Mueggelseedamm

in the east, Schichauweg and Blankenfelde-Mahlow in the south and Gross Glienicke and Grunewald in the west. Only situations with wind speeds above $2\,m\,s^{-1}$ are considered. The statistics are calculated for stations where at least 72 hourly model–observation pairs exist in the respective wind direction bin, leaving four stations in January and six stations in July for the analysis, with between 91 and 228 model–observation pairs. With some differences between the stations, the bias of weekday downwind NO_2 concentrations was reduced by between ca. 1.5 and $2.9\,\mu g\,m^{-3}$ January and ca. 0.4 and $1.5\,\mu g\,m^{-3}$ in July. Thus, downwind NO_2 concentrations in the sensitivity simulation are only biased by ca. $-4\,\%$ (January) and $-14\,\%$ (July) on average (as compared to -12 and $-22\,\%$ in the base run). This shows that the increase in traffic emissions also helps improve modelled downwind concentrations.

Overall, in both January and July, the bias in modelled urban background NO_2 and NO_x is improved but still negative. Modelled downwind NO_2 concentrations are improved considerably, but with low negative biases remaining also in this case. The improvements are consistent with an underestimation of traffic emissions being a main source of error. However, the results also suggest that on the one side traffic emissions might still be too low, which is consistent with the correction factor being a rather conservative estimate. On the other side, a still negative bias is also consistent with other sources of error contributing considerably to the model–observation differences as discussed previously. A relatively large bias in July remains, consistent with the mixing being an additional main source of error, particularly in summer.

Modelled O_3 concentrations are not very sensitive to the changes in NO_x concentrations. On average, modelled O_3 is reduced at urban background stations in January by $1.5\,\mu g\,m^{-3}$ (NMB decreases from 29 to 22 %). In July, the increased NO_x leads to a reduction in the already negatively biased O_3 from the model, with the mean bias changing from -7.3 to $-8.6\,\mu g\,m^{-3}$ (-11 to $-13\,\%$). Similarly, simulated O_3 concentrations downwind of the city (in analogue to the downwind NO_2 concentrations described above) are biased negatively in both the base run and sensitivity study in July. The bias of downwind concentrations changes from $-5.4\,\mu g\,m^{-3}$ ($-7\,\%$) in the base run to $-6.8\,\mu g\,m^{-3}$ ($-9\,\%$) in the sensitivity run. The negative bias in both NO_x and O_3 in the base run is consistent with the model simulating insufficient NO_x emissions in a NO_x-limited ozone production regime. The reduction of O_3 concentrations in response to increased NO_x emissions is however consistent with the model actually being in a NO_x-saturated (VOC-limited) ozone production regime. The representation of VOC emissions in the model could play a role in explaining this discrepancy, as for example biogenic VOC emissions in the Berlin–Brandenburg urban area are underestimated when using WRF-Chem and MEGAN (Churkina et al., 2017). A comprehensive analy-
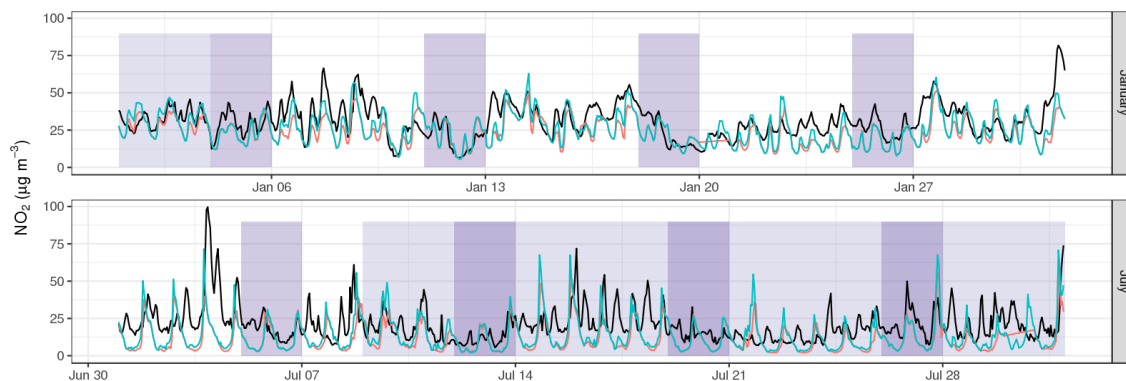
Figure 8. Time series of hourly observed (black line) and modelled NO_2, comparing the base simulation (red) with the sensitivity simulations (blue) using increased traffic emissions by a factor of 3 between 06:00 and 17:00 UTC on weekdays. The time series are averaged over all 4 urban background stations. Weekends are highlighted in dark purple, and holidays are highlighted in light purple.

Table 5. Statistics of modelled NO_2 and NO_x concentrations for January and July, for the base simulation and for the sensitivity simulation with increased traffic emissions, at the urban background stations in Berlin. Mean bias (MB) and root mean square error (RMSE) are indicated in $\mu g\,m^{-3}$, the normalized mean bias (NMB) and correlation coefficient (R) are unitless.

| | | NO_2 | | | | NO_x | | | |
		MB	NMB	RMSE	R	MB	NMB	RMSE	R
Amrumer Str.									
Jan	2014_ref	−6.77	−0.21	11.93	0.65	−14.63	−0.31	28.85	0.65
	2014_emis	−4.16	−0.13	11.09	0.68	−8.01	−0.17	26.18	0.64
July	2014_ref	−10.12	−0.47	17.88	0.34	−12.25	−0.49	22.88	0.27
	2014_emis	−8.9	−0.42	18	0.33	−10.51	−0.42	23.21	0.25
Belziger Str.									
Jan	2014_ref	−10.64	−0.32	15.39	0.51	−20.88	−0.41	34.23	0.51
	2014_emis	−7.97	−0.24	14.04	0.53	−14.57	−0.29	31.6	0.51
July	2014_ref	−7.32	−0.37	15.32	0.31	−8.38	−0.37	17.81	0.23
	2014_emis	−4.02	−0.2	16.73	0.22	−3.67	−0.16	20.43	0.12
Nansenstr.									
Jan	2014_ref	−6.09	−0.21	11.12	0.61	−12.81	−0.3	25.05	0.56
	2014_emis	−3.72	−0.13	10.28	0.64	−7.44	−0.18	23.28	0.55
July	2014_ref	−8.73	−0.43	15.33	0.42	−10.89	−0.45	19.18	0.35
	2014_emis	−6.88	−0.34	15.43	0.36	−8.25	−0.34	19.37	0.28
Brückenstr.									
Jan	2014_ref	−7.1	−0.23	12.51	0.57	−17.27	−0.36	36.4	0.51
	2014_emis	−4.5	−0.15	11.13	0.63	−11.16	−0.24	32.58	0.54
July	2014_ref	−9.92	−0.46	17.24	0.25	−12.85	−0.49	22.7	0.17
	2014_emis	−8.05	−0.37	16.87	0.26	−10.16	−0.39	22.13	0.18

sis of the simulated ozone production regime is beyond the scope of this work.

6.3   Analysis based on traffic counts

The model bias and the calculated correction factors show a diurnal cycle, with a larger model bias/correction factor in the morning hours. As explained in Sect. 5.3 and 5.4, one reason for this might be differences between prescribed and real-world diurnal cycles of the emissions. The diurnal cycle of traffic emissions in the model is calculated based on traffic counts for Berlin, assuming a linear scaling of traffic emissions with traffic counts, as done in many modelling studies.

Here, we use 3 years of hourly observations of roadside NO_x concentrations and traffic counts measured at the same stations in order to get insights into the relationship between NO_x concentrations and traffic counts. A linear regression

model does not explain the variance of observed NO_x concentrations at nighttime, as indicated by the R^2 close to 0 in Fig. 9. However, during daytime, traffic counts alone explain up to ca. 40 % of observed NO_x variance, particularly during the traffic rush hours. The explained variance is smaller during the afternoon peak. In comparison to a linear relationship, a quadratic relationship ($NO_x \propto (\text{traffic\_count})^2$) does not explain more of the observed variance (not shown). An exponential relationship ($NO_x \propto \exp(\text{traffic\_count})$), however, does explain a considerably larger share of the observed variance during daytime and particularly during the traffic rush hours, as depicted in Fig. 9 (up to ca. 60 % depending on the station).

This simple comparison suggests that roadside NO_x concentrations, and thus most likely also road transport NO_x emissions, scale more than linearly with traffic counts at times when the traffic intensity is high and underline that the assumption of a linear scaling of traffic emissions with traffic counts does not reflect the diurnal variation of traffic emissions sufficiently. More highly congested roads are typical in the morning, and emission factors (e.g. from HBEFA) are higher in congested situations compared to free-flowing traffic. Differences in congestion could contribute to explaining the non-linear scaling of NO_x concentrations with traffic intensity. While the impact might not be large when simulating air quality with coarser models, it might play a more important role in high-resolution air quality modelling, and the temporal distribution of emissions could potentially be improved when taking these differences into account.

6.4 Discussion of traffic emissions

Based on a comparison of modelled and observed NO_2 concentrations, we estimate that traffic emissions in the urban core of Berlin are underestimated by a factor of ca. 3 on weekdays between ca. 06:00 and 17:00 UTC. This corresponds to an overall underestimation of NO_x traffic emissions (all-day average) in the urban centre by a factor of ca. 2, and an underestimation of total NO_x emissions (all-day average) in the urban centre by a factor of ca. 1.5. Reasons for the underestimation of emissions used in this study can include limitations in the applicability of the emission inventory used here for high-resolution urban air quality modelling, problems in the temporal distribution of emissions, but also a general underestimation of traffic NO_x emissions in the inventories. These three points are discussed further in the following.

First, while a reasonably good model performance can be achieved using the downscaled version of the TNO-MACC III inventory outside of the urban areas, the deviations of modelled from observed NO_2 in the urban background might point to limitations in the applicability of these types of emission inventories for high-resolution modelling of NO_2 in urban areas. The horizontal resolution of the original TNO-MACC III emission data is ca. 7 km × 7 km and national to-

tals are disaggregated on the grid based on traffic intensities. Spatial differences in congestion, with emissions greatly varying between the different driving conditions and with car speed (e.g. Hausberger and Matzer, 2017), are probably not well resolved. A comparison of the downscaled version of the TNO-MACC III inventory for Berlin with a local inventory has, however, not revealed major differences in road transport emissions (see Sect. 2.4.3), suggesting that a static highly resolved local inventory based on detailed local information is not likely to improve the model results by much.

Second, in addition to spatially unresolved differences in driving conditions and related emission factors locally increasing the underestimation of emissions, the diurnal cycle of the bias in all seasons suggest that the diurnal cycle of traffic emissions also does not sufficiently account for temporal differences in driving conditions. This is consistent with the observation-based analysis, suggesting that observed NO_x concentrations do not scale linearly with traffic counts. While these assumptions might be valid for coarser model resolutions, they may need to be revisited when going to higher resolutions with a focus on urban areas. However, modelled NO_2 concentrations are broadly underestimated throughout the day, which means that deviations of the model diurnal cycle from the real-world diurnal cycle alone cannot explain the underestimation of modelled NO_2 and NO_x concentrations.

Third, traffic NO_x emissions may be underestimated generally by emission inventories. The correction factor calculated here is in line with the results from other studies quantifying traffic emission underestimations in Europe, reporting traffic NO_x underestimations of around 80 % (Lee et al., 2015), a factor of 1.5–2 (Lee et al., 2015) and up to a factor of 4 (Karl et al., 2017). A potential reason for the underestimation in NO_x emissions from traffic can be discrepancies between real-world emission factors and those used in emission inventories. Even though HBEFA emission factors, which are often used for calculating emissions, are based on real-world driving conditions, the latest update of the handbook reports higher emission factors than previously assumed for Euro 6 and Euro 4 diesel cars (Hausberger and Matzer, 2017), e.g. an increase by ca. 50 % in case of Euro 6 vehicles (Fig. 14 in Hausberger and Matzer, 2017). In addition, the update assesses the temperature dependence of emission factors and concludes that it may lead to increases in NO_x emissions of more than 30 %, compared with standard test conditions. NO_x emissions from diesel cars increase with decreasing temperatures (Hausberger and Matzer, 2017). This may also contribute to the larger correction factor calculated for the winter months. Finally, while some amount of congestion is included/assumed in the emission inventories, this might be an aspect that is underestimated in terms of severity and extent.

The first and second points of this discussion suggest that improvements might be achieved by combining high-resolution chemical transport models with more detailed ap-
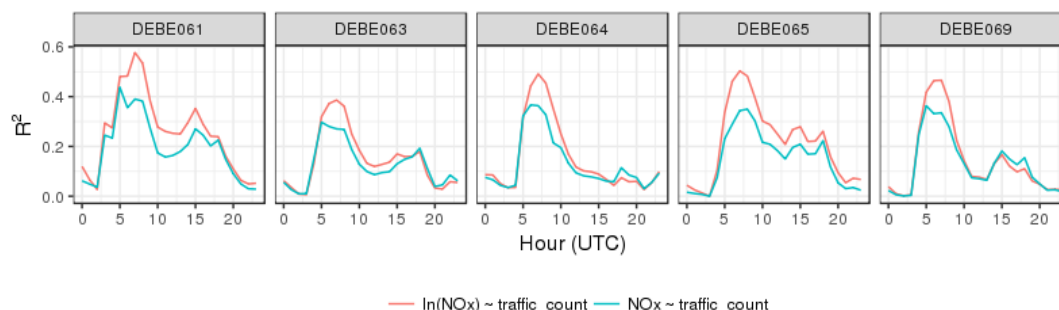
Figure 9. Comparison of R^2 for linear and exponential fits of roadside NO_x concentrations with traffic counts.

proaches of calculating emissions. Coupling with a traffic model, for example, might allow for not only being able to take local differences in traffic conditions into account, but also prescribe a more realistic diurnal cycle of traffic emissions. Dispersion modelling and street canyon modelling (e.g. OSPM, Berkowicz, 2000) often already take a more detailed calculation of traffic emissions into account, and different emission modelling approaches exist (e.g. traffic models such as MATSim, Horni et al., 2016). The benefit of high-resolution chemistry transport modelling, e.g. their ability to assess the impact of different emission sources on air quality on larger scales and downwind of the main emission sources, could be further exploited if coupled with existing, more detailed approaches in calculating traffic emissions or general improvements in the accuracy and resolution of emission inventories.

The consistent findings that inventories of European traffic emissions may be underestimated, coming from studies using very different methodologies, suggest that further research is necessary in order to understand real-world traffic emissions and to represent them in the inventories accordingly. Alternative measurement approaches could help verify the assumptions underlying the calculation of emissions, and help identify potential systematic problems.

7   Summary and conclusions

Several modelling studies, particularly for Europe, have reported an underestimation of modelled NO_2 concentrations compared with observations. Measurement studies also suggest that there might be considerable differences between measured urban NO_x emissions and emissions provided by emission inventories based on official reporting, particularly when the contribution of traffic is large. This study quantifies the underestimation of traffic NO_x emissions using WRF-Chem in a top–down approach, with the Berlin–Brandenburg area in Germany as a case study. The emission inventory used here is TNO-MACC III, downscaled to $1\,km \times 1\,km$ over the Berlin–Brandenburg area based on local proxy data. The

downscaled traffic emissions averaged over Berlin only differ by 6 % from a local bottom–up traffic emission inventory.

A diagnostic evaluation of the model results shows that particularly in the rural and suburban background, the long-term and synoptic components representing processes at timescales of the order of 2.5 to 21 (synoptic) and longer than 21 days (long-term) are simulated well by the model. This suggests that the modelled impact of meteorology on concentrations is represented well overall. The largest contribution to the model error comes from the (negative) bias in the urban background, and from deviations of modelled from observed variability of the diurnal component (0.2–2.5 days). This suggests a possible underestimation of urban emissions, of which traffic is the single most important contributor to NO_x emissions, but is also consistent with deficiencies in other processes varying on the diurnal scale such as the modelled mixing in the planetary boundary layer. The analysis of the model results suggests that the latter is particularly relevant in summer and spring, and that further research is needed in order to better represent urban processes and their coupling with chemistry in WRF-Chem. For example, the changes in the model code applied here to improve nighttime mixing can be critically discussed, and would ideally be replaced by an improved parameterization of urban processes. The latter would need to better account for urban heat and momentum fluxes for a more realistic representation of mixing both at daytime and at nighttime, particularly in summer. An alternative model configuration to be tested could be the recently extended ACM2 planetary boundary parameterization (Pleim, 2007), which now conducts mixing of chemical species within the planetary boundary layer scheme. In addition, measurements of vertical profiles of NO_x in urban areas are needed to evaluate and improve models for applications in urban areas.

The analysis of the diurnal cycle of the model bias as well as a simple observation-based calculation showing that roadside NO_x concentrations scale non-linearly with traffic counts suggest that a further source of error is likely the prescribed diurnal cycle used for traffic emissions. In this study as well as in many other modelling studies, the diurnal cycle

of traffic emissions is calculated assuming a linear scaling of traffic emissions with traffic counts. While this might be sufficient for coarser model resolutions, high-resolution urban air quality modelling with chemistry transport models might benefit from a more detailed temporal distribution, not only taking into account traffic intensity via a scaling with traffic counts, but also diurnal differences in congestion.

We quantify the underestimation of traffic emissions based on the finding that the weekday bias in modelled NO$_2$ is larger than on weekends and that the contribution of traffic NO$_x$ to total NO$_x$ emissions in the urban area is typically higher on weekdays. The results suggest that traffic emissions are underestimated by ca. a factor of 3 in the core urban area on weekdays when traffic is highest (06:00 to 17:00 UTC). The underlying assumption is that other sources of model errors influence the model bias equally on weekdays and weekends, with the underestimation of traffic emissions having the largest effect on modelled NO$_2$ concentrations on weekdays. This underestimation corresponds to an underestimation of weekly mean traffic NO$_x$ emissions in the core urban area of ca. a factor of ca. 2 and an underestimation of total NO$_x$ emissions in the city centre by a factor of ca. 1.5. Two sensitivity simulations for January and July 2014 with NO$_x$ emissions from traffic scaled with the estimated correction factor show that increased traffic emissions improve the model bias in NO$_2$ and NO$_x$ concentrations in both seasons in the urban background, and also improve modelled downwind concentrations. The still negative bias is consistent with the factor being a rather conservative estimate.

The emission inventory used in this study is based on officially reported emissions by the individual countries, and the emissions are spatially distributed by TNO based on proxy data. Assuming the quality and accuracy of the proxy data are similar at least for larger German cities, and considering that modelling studies for other German cities have also shown an underestimation of simulated NO$_2$ concentrations using the same emission inventory, we would assume that the results found in this study for Berlin may generally be transferrable to at least other German metropolitan areas. The underestimation of NO$_2$ concentrations throughout the day, the consistency of the calculated correction factor with findings from other studies and the improvement of model results applying the correction factor suggest that more research is needed in order to more accurately understand the spatial and temporal variability in real-world NO$_x$ emissions from traffic, and apply this understanding to the inventories used in high-resolution chemical transport models. Given the above considerations, this not only holds for the urban area of Berlin, but for German and most likely European metropolitan areas more generally.

The Supplement related to this article is available online at https://doi.org/10.5194/acp-18-8203-2018-supplement.

References

Berkowicz, R.: OSPM – a parameterised street pollution model, in: Urban Air Quality: Measurement, Modelling and Management, Springer, 323–331, https://doi.org/10.1007/978-94-010-0932-4_35, 2000.

Berlin Senate Department for Urban Development and Housing: Environment Atlas Berlin, available at: http://www.stadtentwicklung.berlin.de/umwelt/umweltatlas/ed312_01.htm, last access: December 2015.

Bessagnet, B., Pirovano, G., Mircea, M., Cuvelier, C., Aulinger, A., Calori, G., Ciarelli, G., Manders, A., Stern, R., Tsyro, S., García Vivanco, M., Thunis, P., Pay, M.-T., Colette, A., Couvidat, F., Meleux, F., Rouïl, L., Ung, A., Aksoyoglu, S., Baldasano, J. M., Bieser, J., Briganti, G., Cappelletti, A., D'Isidoro, M., Finardi, S., Kranenburg, R., Silibello, C., Carnevale, C., Aas, W., Dupont, J.-C., Fagerli, H., Gonzalez, L., Menut, L., Prévôt, A. S. H., Roberts, P., and White, L.: Presentation of the EURODELTA III intercomparison exercise – evaluation of the chemistry transport models' performance on criteria pollutants and joint analysis with meteorology, Atmos. Chem. Phys., 16, 12667–12701, https://doi.org/10.5194/acp-16-12667-2016, 2016.

Bieser, J., Aulinger, A., Matthias, V., Quante, M., and Van Der Gon, H. D.: Vertical emission profiles for Europe based on plume rise calculations, Environ. Pollut., 159, 2935–2946, https://doi.org/10.1016/j.envpol.2011.04.030, 2011.

Brunner, D., Savage, N., Jorba, O., Eder, B., Giordano, L., Badia, A., Balzarini, A., Baró, R., Bianconi, R., Chemel, C., Curci, G., Forkel, R., Jiménez-Guerrero, P., Hirtl, M., Hodzic, A., Honzak, L., Im, U., Knote, C., Makar, P., Manders-Groot, A., Meijgaard, E. V., Neal, L., Pérez, J. L., Pirovano, G., Jose, R. S., Schröder, W., Sokhi, R. S., Syrakov, D., Torian, A., Tuccella, P., Werhahn, J., Wolke, R., Yahya, K., Zabkar, R., Zhang, Y., Hogrefe, C., and Galmarini, S.: Comparative analysis of meteorological performance of coupled chemistry-meteorology models in the context of AQMEII phase 2, Atmos. Environ., 115, 470–498, https://doi.org/10.1016/j.atmosenv.2014.12.032, 2015.

Builtjes, P., Loon, M. V., Schaap, M., Teeuwisse, S., Visschedijk, A., and Bloos, J.: The development of an emission data base over Europe and further contributions of TNO-MEP, available at: https://www.umweltbundesamt.de/sites/default/files/medien/publikation/long/3607.pdf (last access: 4 June 2018), 2002.

Bundesanstalt für Straßenwesen: available at: http://www.bast.de/DE/Verkehrstechnik/Fachthemen/v2-verkehrszaehlung/Stundenwerte.html?nn=626916 (last access: 4 June 2018), 2017.

Carslaw, D. C.: Evidence of an increasing NO_2/NOX emissions ratio from road traffic emissions, Atmos. Environ., 39, 4793–4802, https://doi.org/10.1016/j.atmosenv.2005.06.023, 2005.

Churkina, G., Kuik, F., Bonn, B., Lauer, A., Grote, R., Tomiak, K., and Butler, T. M.: Effect of VOC Emissions from Vegetation on Air Quality in Berlin during a Heatwave, Environ. Sci. Technol., 51, 6120–6130, https://doi.org/10.1021/acs.est.6b06514, 2017.

Dee, D. P., Uppala, S. M., Simmons, A. J., Berrisford, P., Poli, P., Kobayashi, S., Andrae, U., Balmaseda, M. A., Balsamo, G., Bauer, P., Bechtold, P., Beljaars, A. C. M., Van De Berg, L., Bidlot, J., Bormann, N., Delsol, C., Dragani, R., Fuentes, M., Geer, A. J., Haimberger, L., Healy, S. B., Hersbach, H., Hólm, E. V., Isaksen, L., Kållberg, P., Köhler, M., Matricardi, M., Mcnally, A. P., Monge-Sanz, B. M., Morcrette, J.-J., Park, B.-K., Peubey, C., De Rosnay, P., Tavolato, C., Thépaut, J.-N., and Vitart, F.: The ERA-Interim reanalysis: configuration and performance of the data assimilation system, Q. J. Roy. Meteor. Soc., 137, 553–597, https://doi.org/10.1002/qj.828, 2011.

Degraeuwe, B., Thunis, P., Clappier, A., Weiss, M., Lefebvre, W., Janssen, S., and Vranckx, S.: Impact of passenger car NOx emissions and NO_2 fractions on urban NO_2 pollution – Scenario analysis for the city of Antwerp, Belgium, Atmos. Environ., 126, 218–224, https://doi.org/10.1016/j.atmosenv.2015.11.042, 2016.

Dennis, R., Fox, T., Fuentes, M., Gilliland, A., Hanna, S., Hogrefe, C., Irwin, J., Rao, S. T., Scheffe, R., Schere, K., Steyn, D., and Venkatram, A.: A framework for evaluating regional-scale numerical photochemical modeling systems, Environ. Fluid Mech., 10, 471–489, https://doi.org/10.1007/s10652-009-9163-2, 2010.

EEA: EMEP/EEA air pollutant emission inventory guidebook 2013 – Technical guidance to prepare national emission inventories, available at: https://www.eea.europa.eu/publications/emep-eea-guidebook-2013 (last access: 4 June 2018), European Environment Agency, Copenhagen, Denmark, 2013.

EEA: CORINE land cover data 2006, updated, available at: http://www.eea.europa.eu/data-and-maps/data/corine-land-cover-2006-raster-3 (last access: 4 June 2018), European Environment Agency, Copenhagen, Denmark, 2014.

EEA: Air quality in Europe – 2016 report, https://doi.org/10.2800/80982, available at: https://www.eea.europa.eu/publications/air-quality-in-europe-2016 (last access: 4 June 2018), 2016.

EEA: AirBase – The European air quality database, available at: https://www.eea.europa.eu/data-and-maps/data/airbase-the-european-air-quality-database-8 (last access: 4 June 2018), 2017.

Emmons, L. K., Walters, S., Hess, P. G., Lamarque, J.-F., Pfister, G. G., Fillmore, D., Granier, C., Guenther, A., Kinnison, D., Laepple, T., Orlando, J., Tie, X., Tyndall, G., Wiedinmyer, C., Baughcum, S. L., and Kloster, S.: Description and evaluation of the Model for Ozone and Related chemical Tracers, version 4 (MOZART-4), Geosci. Model Dev., 3, 43–67, https://doi.org/10.5194/gmd-3-43-2010, 2010.

Fallmann, J., Forkel, R., and Emeis, S.: Secondary effects of urban heat island mitigation measures on air quality, Atmos. Environ., 125, 199–211, https://doi.org/10.1016/j.atmosenv.2015.10.094, 2016.

Fast, J. D., Gustafson, W. I., Easter, R. C., Zaveri, R. A., Barnard, J. C., Chapman, E. G., Grell, G. A., and Peckham, S. E.: Evolution of ozone, particulates, and aerosol direct radiative forcing in the vicinity of Houston using a fully coupled meteorology-chemistry-aerosol model, J. Geophys. Res.-Atmos., 111, d21305, https://doi.org/10.1029/2005JD006721, 2006.

Geiß, A., Wiegner, M., Bonn, B., Schäfer, K., Forkel, R., von Schneidemesser, E., Münkel, C., Chan, K. L., and Nothard, R.: Mixing layer height as an indicator for urban air quality?, Atmos. Meas. Tech., 10, 2969–2988, https://doi.org/10.5194/amt-10-2969-2017, 2017.

Gerboles, M., Lagler, F., Rembges, D., and Brun, C.: Assessment of uncertainty of NO_2 measurements by the chemiluminescence method and discussion of the quality objective of the NO_2 European Directive, J. Environ. Monitor., 5, 529–540, https://doi.org/10.1039/b302358c, 2003.

Giordano, L., Brunner, D., Flemming, J., Hogrefe, C., Im, U., Bianconi, R., Badia, A., Balzarini, A., Baró, R., Chemel, C., Curci, G., Forkel, R., Jiménez-Guerrero, P., Hirtl, M., Hodzic, A., Honzak, L., Jorba, O., Knote, C., Kuenen, J., Makar, P., Manders-Groot, A., Neal, L., Pérez, J., Pirovano, G., Pouliot, G., José, R. S., Savage, N., Schröder, W., Sokhi, R., Syrakov, D., Torian, A., Tuccella, P., Werhahn, J., Wolke, R., Yahya, K., Žabkar, R., Zhang, Y., and Galmarini, S.: Assessment of the MACC reanalysis and its influence as chemical boundary conditions for regional air quality modeling in AQMEII-2, Atmos. Environ., 115, 371–388, https://doi.org/10.1016/j.atmosenv.2015.02.034, 2015.

Grell, G. and Baklanov, A.: Integrated modeling for forecasting weather and air quality: A call for fully coupled approaches, Atmos. Environ., 45, 6845–6851, https://doi.org/10.1016/j.atmosenv.2011.01.017, 2011.

Grell, G. A., Peckham, S. E., Schmitz, R., Mckeen, S. A., Frost, G., Skamarock, W. C., and Eder, B.: Fully coupled "online" chemistry within the WRF model, Atmos. Environ., 39, 6957–6975, https://doi.org/10.1016/j.atmosenv.2005.04.027, 2005.

Harrison, R. M. and Beddows, D. C.: Efficacy of Recent Emissions Controls on Road Vehicles in Europe and Implications for Public

Health, Sci. Rep.-UK, 7, 1152, https://doi.org/10.1038/s41598-017-01135-2, 2017.

Hausberger, S. and Matzer, C.: Update of Emission Factors for EURO 4, EURO 5 and EURO 6 Diesel Passenger Cars for the HBEFA Version 3.3, available at: http://www.hbefa.net/e/documents/HBEFA3-3_TUG_finalreport_01062016.pdf (last access: 4 June 2018), 2017.

Hong, S.-Y., Noh, Y., and Dudhia, J.: A new vertical diffusion package with an explicit treatment of entrainment processes, Mon. Weather Rev., 134, 2318–2341, 2006.

Horni, A., Nagel, K., and Axhausen, K. W. (Eds.): The Multi-Agent Transport Simulation MATSim, London, Ubiquity Press, 618 pp., https://doi.org/10.5334/baw, 2016.

ICCT Briefing: NO$_x$ emissions from heavy-duty and light-duty diesel vehicles in the EU: Comparison of real-world performance and current type-approval requirements, available at: http://www.theicct.org/sites/default/files/publications/Euro-VI-versus-6_ICCT_briefing_06012017.pdf (last access: 4 June 2018), 2016.

Im, U., Bianconi, R., Solazzo, E., Kioutsioukis, I., Badia, A., Balzarini, A., Baró, R., Bellasio, R., Brunner, D., Chemel, C., Curci, G., Flemming, J., Forkel, R., Giordano, L., Jiménez-Guerrero, P., Hirtl, M., Hodzic, A., Honzak, L., Jorba, O., Knote, C., Kuenen, J. J., Makar, P. A., Manders-Groot, A., Neal, L., Pérez, J. L., Pirovano, G., Pouliot, G., Jose, R. S., Savage, N., Schroder, W., Sokhi, R. S., Syrakov, D., Torian, A., Tuccella, P., Werhahn, J., Wolke, R., Yahya, K., Zabkar, R., Zhang, Y., Zhang, J., Hogrefe, C., and Galmarini, S.: Evaluation of operational on-line-coupled regional air quality models over Europe and North America in the context of AQMEII phase 2. Part I: Ozone, Atmos. Environ., 115, 404–420, https://doi.org/10.1016/j.atmosenv.2014.09.042, 2015.

Karl, T., Graus, M., Striednig, M., Lamprecht, C., Hammerle, A., Wohlfahrt, G., Held, A., Heyden, L. V. D., Deventer, M. J., Krismer, A., Haun, C., Feichter, R., and Lee, J.: Urban eddy covariance measurements reveal significant missing NOx emissions in Central Europe, Sci. Rep.-UK, 1–9, Scientific Reports 7 (2536), https://doi.org/10.1038/s41598-017-02699-9, 2017.

Kaspar, F., Müller-Westermeier, G., Penda, E., Mächel, H., Zimmermann, K., Kaiser-Weiss, A., and Deutschländer, T.: Monitoring of climate change in Germany – data, products and services of Germany's National Climate Data Centre, Adv. Sci. Res., 10, 99–106, https://doi.org/10.5194/asr-10-99-2013, 2013.

Kuenen, J. J. P., Visschedijk, A. J. H., Jozwicka, M., and Denier van der Gon, H. A. C.: TNO-MACC_II emission inventory; a multi-year (2003–2009) consistent high-resolution European emission inventory for air quality modelling, Atmos. Chem. Phys., 14, 10963–10976, https://doi.org/10.5194/acp-14-10963-2014, 2014.

Kuik, F., Lauer, A., Churkina, G., Denier van der Gon, H. A. C., Fenner, D., Mar, K. A., and Butler, T. M.: Air quality modelling in the Berlin–Brandenburg region using WRF-Chem v3.7.1: sensitivity to resolution of model grid and input data, Geosci. Model Dev., 9, 4339–4363, https://doi.org/10.5194/gmd-9-4339-2016, 2016.

Lee, J. D., Helfter, C., Purvis, R. M., Beevers, S. D., Carslaw, D. C., Lewis, A. C., Müller, S. J., Tremper, A., Vaughan, A., and Nemitz, E. G.: Measurement of NOx Fluxes from a Tall Tower in Central London, UK and Comparison with Emissions Inventories, Environ. Sci. Technol., 49, 1025–1034, https://doi.org/10.1021/es5049072, 2015.

Minkos, A., Dauert, U., Feigenspan, S., and Kessinger, S.: Luftqualität 2016, available at: https://www.umweltbundesamt.de/publikationen/luftqualitaet-2016 (last access: 4 June 2018), 2017.

Mues, A., Kuenen, J., Hendriks, C., Manders, A., Segers, A., Scholz, Y., Hueglin, C., Builtjes, P., and Schaap, M.: Sensitivity of air pollution simulations with LOTOS-EUROS to the temporal distribution of anthropogenic emissions, Atmos. Chem. Phys., 14, 939–955, https://doi.org/10.5194/acp-14-939-2014, 2014.

Nakanishi, M. and Niino, H.: An improved Mellor–Yamada level-3 model: Its numerical stability and application to a regional prediction of advection fog, Bound.-Lay. Meteorol., 119, 397–407, 2006.

Pernigotti, D., Gerboles, M., Belis, C., and Thunis, P.: Model quality objectives based on measurement uncertainty. Part II: NO$_2$ and PM$_{10}$, Atmos. Environ., 79, 869–878, https://doi.org/10.1016/j.atmosenv.2013.07.045, 2013.

Pleim, J. E.: A Combined Local and Nonlocal Closure Model for the Atmospheric Boundary Layer. Part I: Model Description and Testing, J. Appl. Meteorol. Clim., 46, 1383–1395, https://doi.org/10.1175/JAM2539.1, 2007.

Schaap, M., Cuvelier, C., Hendriks, C., Bessagnet, B., Baldasano, J., Colette, A., Thunis, P., Karam, D., Fagerli, H., Graff, A., Kranenburg, R., Nyiri, A., Pay, M., Rouïl, L., Schulz, M., Simpson, D., Stern, R., Terrenoire, E., and Wind, P.: Performance of European chemistry transport models as function of horizontal resolution, Atmos. Environ., 112, 90–105, https://doi.org/10.1016/j.atmosenv.2015.04.003, 2015.

Skamarock, W., Klemp, J., Dudhia, J., Gill, D., Barker, D., Duda, M., Huang, X.-Y., Wang, W., and Powers, J.: A Description of the Advanced Research WRF Version 3, NCAR Technical Note/TN-475+STR, https://doi.org/10.5065/D68S4MVH, 2008.

Solazzo, E. and Galmarini, S.: Error apportionment for atmospheric chemistry-transport models – a new approach to model evaluation, Atmos. Chem. Phys., 16, 6263–6283, https://doi.org/10.5194/acp-16-6263-2016, 2016.

Solazzo, E., Bianconi, R., Hogrefe, C., Curci, G., Tuccella, P., Alyuz, U., Balzarini, A., Baró, R., Bellasio, R., Bieser, J., Brandt, J., Christensen, J. H., Colette, A., Francis, X., Fraser, A., Vivanco, M. G., Jiménez-Guerrero, P., Im, U., Manders, A., Nopmongcol, U., Kitwiroon, N., Pirovano, G., Pozzoli, L., Prank, M., Sokhi, R. S., Unal, A., Yarwood, G., and Galmarini, S.: Evaluation and error apportionment of an ensemble of atmospheric chemistry transport modeling systems: multivariable temporal and spatial breakdown, Atmos. Chem. Phys., 17, 3001–3054, https://doi.org/10.5194/acp-17-3001-2017, 2017.

Steinbacher, M., Zellweger, C., Schwarzenbach, B., Bugmann, S., Buchmann, B., Ordonez, C., Prevot, A., and Hueglin, C.: Nitrogen oxide measurements at rural sites in Switzerland: Bias of conventional measurement techniques, J. Geophys. Res.-Atmos., 112, D11307, https://doi.org/10.1029/2006jd007971, 2007.

Terrenoire, E., Bessagnet, B., Rouïl, L., Tognet, F., Pirovano, G., Létinois, L., Beauchamp, M., Colette, A., Thunis, P., Amann, M., and Menut, L.: High-resolution air quality simulation over Europe with the chemistry transport model CHIMERE, Geosci. Model Dev., 8, 21–42, https://doi.org/10.5194/gmd-8-21-2015, 2015.

Thunis, P., Pederzoli, A., and Pernigotti, D.: Performance criteria to evaluate air quality modeling applications, Atmos. Environ., 59, 476–482, https://doi.org/10.1016/j.atmosenv.2012.05.043, 2012.

Tie, X., Brasseur, G., and Ying, Z.: Impact of model resolution on chemical ozone formation in Mexico City: application of the WRF-Chem model, Atmos. Chem. Phys., 10, 8983–8995, https://doi.org/10.5194/acp-10-8983-2010, 2010.

Vaughan, A. R., Lee, J. D., Misztal, P. K., Metzger, S., Shaw, M. D., Lewis, A. C., Purvis, R. M., Carslaw, D. C., Goldstein, A. H., Hewitt, C. N., Davison, B., Beeversh, S. D., and Karl, T. G.: Spatially resolved flux measurements of NOx from London suggest significantly higher emissions than predicted by inventories, Faraday Discuss., 189, 455–472, https://doi.org/10.1039/c5fd00170f, 2016.

Villena, G., Bejan, I., Kurtenbach, R., Wiesen, P., and Kleffmann, J.: Interferences of commercial NO_2 instruments in the urban atmosphere and in a smog chamber, Atmos. Meas. Tech., 5, 149–159, https://doi.org/10.5194/amt-5-149-2012, 2012.

von Schneidemesser, E., Kuik, F., Mar, K. A., and Butler, T.: Potential reductions in ambient NO_2 concentrations from meeting diesel vehicle emissions standards, Environ. Res. Lett., 12, 114025, https://doi.org/10.1088/1748-9326/aa8c84, 2017.

WHO: Review of evidence on health aspects of air pollution – REVIHAAP, available at: http://www.euro.who.int/__data/assets/pdf_file/0020/182432/e96762-final.pdf (last access: 4 june 2018), 2013.

Zurbenko, I.: The spectral analysis of time series, Elsevier North-Holland, Inc., https://doi.org/10.2307/2348176, 1986.

5. Article 3: Potential reductions in ambient NO$_2$ concentrations from meeting diesel vehicle emissions standards

Environmental Research Letters

CrossMark

OPEN ACCESS

LETTER

Potential reductions in ambient NO$_2$ concentrations from meeting diesel vehicle emissions standards

Erika von Schneidemesser[1,2], Friderike Kuik[1], Kathleen A Mar[1] and Tim Butler[1]

[1]   Institute for Advanced Sustainability Studies, Berliner Straße 130, 14467 Potsdam, Germany
[2]   Author to whom any correspondence should be addressed.

E-mail: erika.vons@iass-potsdam.de

Abstract

Exceedances of the concentration limit value for ambient nitrogen dioxide (NO$_2$) at roadside sites are an issue in many cities throughout Europe. This is linked to the emissions of light duty diesel vehicles which have on-road emissions that are far greater than the regulatory standards. These exceedances have substantial implications for human health and economic loss. This study explores the possible gains in ambient air quality if light duty diesel vehicles were able to meet the regulatory standards (including both emissions standards from Europe and the United States). We use two independent methods: a measurement-based and a model-based method. The city of Berlin is used as a case study. The measurement-based method used data from 16 monitoring stations throughout the city of Berlin to estimate annual average reductions in roadside NO$_2$ of 9.0 to 23 μg m^{-3} and in urban background NO$_2$ concentrations of 1.2 to 2.7 μg m^{-3}. These ranges account for differences in fleet composition assumptions, and the stringency of the regulatory standard. The model simulations showed reductions in urban background NO$_2$ of 2.0 μg m^{-3}, and at the scale of the greater Berlin area of 1.6 to 2.0 μg m^{-3} depending on the setup of the simulation and resolution of the model. Similar results were found for other European cities. The similarities in results using the measurement- and model-based methods support our ability to draw robust conclusions that are not dependent on the assumptions behind either methodology. The results show the significant potential for NO$_2$ reductions if regulatory standards for light duty diesel vehicles were to be met under real-world operating conditions. Such reductions could help improve air quality by reducing NO$_2$ exceedances in urban areas, but also have broader implications for improvements in human health and other benefits.

1. Introduction

Air pollution is a pressing environmental issue, and not just in developing countries. More than 85% of the urban population in Europe lives in areas where the World Health Organization (WHO) guidelines are exceeded for air pollutants such as particulate matter (PM$_{2.5}$) or ozone (O$_3$) (EEA 2016). Nitrogen oxides (NO$_x$ = NO + NO$_2$) are important contributors to secondary formation of air pollutants, including to concentrations of PM and O$_3$. In addition, adverse human health effects such as increases in all-cause mortality, and respiratory and cardiovascular effects have been associated with both short-term and long-term exposure to nitrogen dioxide (NO$_2$)

(Faustini *et al* 2014, Mills *et al* 2015). A large number of cities in Europe struggle to meet their NO$_2$ targets, among those many cities in Germany, including Berlin (BSV 2017). More specifically, more than half of all roadside measurement stations in Germany have not met the annual limit value of 40 μg m^{-3} for the past decade (Minkos *et al* 2017). These exceedances are generally attributed to vehicle emissions, still one of the largest sources of air pollutant emissions, and in this case specifically diesel vehicles (EEA 2016). While the implementation of a defeat device by Volkswagen (VW) during emissions testing was recently discovered by the research of West Virginia University (Thompson *et al* 2014), the inability of diesel vehicles to meet the emission standards in Europe under on-road

conditions is acknowledged (EEA 2016, Fontaras *et al* 2014, Hagman *et al* 2015, ICCT 2014, Rexeis *et al* 2013). The Euro 5 and Euro 6 diesel passenger vehicles have been documented to have real-world NO_x emissions up to 5x and 4–20x higher, respectively, than the allowed emission levels (EEA/EMEP 2013, Fontaras *et al* 2014, Hagman *et al* 2015). Additionally, current national reported emissions (which are also used as the basis for emission inventories that are implemented in air quality models) are typically calculated using emission factors (EF) from the Handbook Emission Factors for Road Transport (HBEFA) (Rexeis *et al* 2013), as in Germany, or the COmputer Programme to calculate Emissions from Road Transport (COPERT) (Gkatzoflias *et al* 2012). The EFs in the HBEFA report are more reflective of true on-road emissions than the regulatory targets, and were found to capture the higher emissions from diesel vehicles better than COPERT (Fontaras *et al* 2014). For example, the EF for NO_x emissions from Euro 5 light duty diesel vehicles from HBEFA for urban driving conditions is $0.97\,\mathrm{g\,km^{-1}}$ (Rexeis *et al* 2013). Reported real-world driving EFs for Euro 5 diesel vehicles from a number of studies ranged from $0.35\,\mathrm{g\,km^{-1}}$ to $1.12\,\mathrm{g\,km^{-1}}$ under different driving conditions (e.g. urban, motorway, or averages) (Carslaw *et al* 2011, Fontaras *et al* 2014, Weiss *et al* 2012). The EU Euro 5 regulatory standard for NO_x from diesel vehicles is $0.18\,\mathrm{g\,km^{-1}}$ (EC 2007). The United States standard set by the Environmental Protection Agency (EPA) for light duty diesel vehicles is $0.043\,\mathrm{g\,km^{-1}}$.

Several studies have been published recently investigating the effect of NO_x emissions from diesel vehicles, in some cases due to the VW emissions control defeat device, on air pollution and the implications for human health and social cost in the United States (Barrett *et al* 2015, Holland *et al* 2016, Wang *et al* 2016) and Europe (Brand 2016, Chossiere *et al* 2017), as well as addressing the issues more generally (Rojas-Rueda and Turner 2016). The studies focused on the US estimate that 46 and 59 excess deaths and ca. $430 or 450 million excess damages result from the excess NO_x emissions from the affected diesel vehicles between 2008 or 2009 and 2015, respectively (Barrett *et al* 2015, Holland *et al* 2016). Additionally, one study evaluated the effects for California and found that the additional 'hidden' NO_x emissions (difference between the actual on-road NO_x emission factor and the testing emission factor) would result in 12 excess deaths during the same 2009–2015 time period as the US studies, with the majority of the increase in mortality in metropolitan areas (Wang *et al* 2016). In work that parallels the US study by Barrett *et al* (2015), Chossiere *et al* (2017) estimated the cost of excess NO_x emissions from VW vehicles in Germany to be 1200 premature deaths (1.9 billion EUR) in Europe. The study by Brand (2016) highlights the potential trade-offs between human health and climate change mitigation in policies related to diesel vehicles in the

UK (not just those affected by the defeat device), showing that the excess NO_x emissions from diesel vehicles are significant and that the benefit to air quality in reducing these emissions would be much larger and outweigh any of the few potential carbon disbenefits, based on a comparison of damage costs. Holland *et al* (2016) reached a similar conclusion, finding that the estimated damages (in this case limited to those VW vehicles with defeat devices) greatly outweigh any possible benefits from reduced CO_2 emissions resulting from increased fuel economy.

This study explores a broader perspective beyond that of the cars affected by the defeat devices and investigates the potential benefits to air quality based on scenarios in which the light duty diesel vehicle fleet meets the regulatory standards under real-world driving conditions. Two independent approaches are used: (1) an estimation based on ambient NO_2 concentrations from monitoring stations, and (2) a sensitivity study using a chemical transport model. The regional focus is on Berlin, Germany, but includes comparisons to other urban areas in Europe that indicate the potential of such regulation and broader applicability of the results.

2. Methods

2.1. Emissions

The emission inventory used for both the observation-based calculations and the chemical transport modeling scenarios was the TNO-MACCIII inventory, an update to the previous version II (Kuenen *et al* 2014). To estimate the total amount of NO_x emissions originating from diesel vehicles in Berlin, the following calculations were carried out.

This study specifically focuses on the impact of diesel light-duty vehicles (LDV) on air quality. Therefore, we estimate the total NO_x emissions from diesel LDV exhaust in the greater Berlin area based on the TNO-MACCIII inventory, for which the grid cells over Berlin were extracted. The total amount of NO_x emissions for Berlin was 24 598 kT annually, of which 8944 kT are from road transport. 8094 kT are attributed to NO_x emissions from diesel vehicle exhaust. The heavy-duty vehicle (HDV) versus light-duty vehicle (LDV) split provided by TNO attributed 43% of diesel vehicles to the LDV category which is based on the national average for Germany (Kuenen 2015). Information from the city of Berlin indicates that 80% of diesel vehicles in the city of Berlin are LDV (BSV 2013). Using these two percentages we estimated that of the 8094 kT NO_x emissions attributed to diesel vehicle exhaust (LDV + HDV together), either 3464 kT (national average) or 6446 kT (Berlin urban area average) originate from LDV. Using both estimates of the percent of LDV diesel provides upper and lower estimates to explore the sensitivity of our calculations to such numbers.

▶▶ Letters

Table 1. HBEFA emission factors (EF) compared to the regulatory standards for European and US diesel passenger vehicles, shown for the three driving conditions and an overall average. Also presented is the ratio of regulatory standard EF to current HBEFA EF.

	HBEFA EF (g km^{-1})		Regulatory Standards (g km^{-1})			Ratio (reg. Std/HBEFA)	
	Euro 5	Euro 6	Euro 5	Euro 6	US EPA Tier 2 Bin 5	Euro 5	US EPA Std[a]
Urban	0.97	0.26				0.19	0.044
Rural	0.63	0.14				0.28	0.068
Motorway	0.79	0.28				0.23	0.054
Average	**0.80**	**0.23**	0.18	0.08	0.043	**0.23**	**0.055**

[a] The US EPA Std is implemented as the 'best-available technology' scenario.

2.2. Emission factors

To evaluate how air quality would be improved if current emission standards for diesel LDV were met under real-world driving conditions, we compare emission factors used for nationally-reported emissions (a proxy for on-road emissions under real-world conditions) and the emission factors dictated by regulations. The emission factors (EFs) currently used for national reporting of emissions in Europe come from the HBEFA report, which includes g km^{-1} estimates of NO$_x$ emissions for Euro 5 and Euro 6 vehicles (Rexeis *et al* 2013). EF values are provided for urban, rural, and motorway driving conditions. As an example, the HBEFA EF for Euro 5 diesel LDV is 0.9719 g km^{-1} for urban driving. The Euro 5 standard is 0.18 g km^{-1}. The US EPA Tier 2 Bin 5 standard[3] (hereafter US EPA standard) for diesel LDV is 0.043 g km^{-1}. The Euro 6 standard is 0.08 g km^{-1}. These emission factors are summarized in table 1. In our calculations we considered cases where diesel LDV emissions under real-world conditions meet the Euro 5, representative of a less ambitious modern standard, and US EPA standard, which is currently the most stringent for diesel LDV emissions, referred to here as the 'best-available technology' scenario. Note that the Euro 6 standard is not explicitly considered here, as it represents an intermediate point between the two.

To calculate a simple factor of possible improvement in terms of EFs, we first assume that all diesel LDV are emitting as Euro 5 vehicles at the level reported by the HBEFA EF for the 2011 and 2014 time frames considered in this study. While this assumption does not capture all of the emissions from those vehicles that are Euro 4 or lower, according to data from Berlin, over 70% of all diesel LDV are Euro 4 or better (the reported values unfortunately do not include a category for Euro 5 or better) (BSV 2013), and is therefore not unreasonable. Furthermore, by assuming that the existing fleet is lower-emitting than in reality, we ensure that our results will represent a conservative estimate of the potential benefits of further reductions in the emissions due to meeting the stricter standards. Finally, a calculation was carried out, applying higher EFs for the ca. 27% of the fleet that were Euro 3 or

[3] Tier 2 refers to cars and light-duty trucks; Bin 5 refers to the certification bins of different stringency, of which Bin 5 represents the fleet average for NO$_x$ that has to be met.

lower, to assess the sensitivity of this assumption, and the results showed negligible differences.

To then calculate the change in EFs if the regulatory standards were met, we compared the HBEFA EFs for each of the driving conditions (urban, rural, and motorway) to both the Euro 5 and US EPA standard, and calculated a simple average over the three driving conditions to come up with a coarse reduction factor that would be expected. (The amount of vehicle kilometers traveled by passenger cars in Germany are roughly equal among the three driving conditions (Ehlers *et al* 2016).) If current Euro 5-certified diesel LDVs achieved Euro-5 level NO$_x$ emissions (on a per km basis, expressed as an EF) under real-world driving conditions, the reduction in emissions would be 77% (calculated as the ratio Euro 5 to HBEFA emission factors). Similarly, for the best-available technology case (i.e. if the US EPA standard were met), the EF would be 95% lower (table 1). The expected reduction in emissions from the fleet meeting the Euro 5 or US EPA standards would be larger still if Euro 4 and higher-emitting vehicles were included in our emissions estimate for the current fleet composition.

2.3. Potential change evaluated based on ambient monitoring data

The factors from table 1 were used to calculate expected total annual NO$_x$ emission reductions using Berlin as a case study, as shown in table 2. The reduction in road transport emissions attributed to diesel LDV was calculated by multiplying by the emissions with the reduction factor ('Ratio' column in table 1) for both the Euro 5 and the best-available technology case. This calculation was done using the two different estimates of the percent of diesel LDV emissions for Berlin (table 2 and section 2.1). The expected reductions in traffic NO$_x$ emissions are shown in table 2, as absolute kT of emissions and as percent reductions. Similarly, a reduction in total urban NO$_x$ emissions was calculated. This used the same (absolute) estimated road transport emissions reductions, but compared it to all NO$_x$ emission sources in the urban area, rather than just the total road transport NO$_x$, in Berlin. This results in a reduction of 11%–25% in the total NO$_x$ emissions for the city (table 2). All of the values and changes are discussed in more detail in the results and discussion section.

Finally, to estimate how the calculated reductions in emissions would affect ambient concentrations, the

Table 2. Estimated annual NO_x emissions for Berlin from diesel LDVs under two different assumptions for the diesel fleet composition (national vs. city) for the current fleet, and for scenarios in which diesel LDVs meet the Euro 5 standard or best-available technology (US EPA standard) during real-world driving. The percent emission reductions relative to the current emissions situation is also shown for both cases. The total road transport NO_x emissions in Berlin are 8944 kT.

	National fleet (43% LDV)			City fleet (80% LDV)		
	Total NO_x emissions (kT)[a]	Reduction in traffic emissions (%)	Reduction in total urban emissions (%)	Total NO_x emissions (kT)[a]	Reduction in traffic emissions (%)	Reduction in total urban emissions (%)
Current road transport from LDV diesel[b]	3464	—	—	6446	—	—
Euro 5	797	30	11	1483	55	20
Best-available technology	190	40	13	355	75	25

[a] Expressed as kT NO_2.

[b] Based on the TNO-MACCIII inventory for 2011 (the most recent year available at the time of writing).

percent reductions in road transport and total city NO_x emissions were used in combination with monitoring data for NO_x and NO_2 to calculate possible reductions in ambient concentrations at the roadside and for the Berlin urban area more generally. We calculated the expected reduction in NO_x concentration at the roadside based on the 'roadside increment', and the reductions in background NO_x concentration over the entire urban area based on the 'urban background increment'. The roadside increment was defined as the roadside concentration minus the urban background concentration. Similarly, the urban background increment was defined as the urban background concentration minus the rural background concentration, using averages of those monitoring stations from the Berlin area. We assume that reductions in traffic emissions lead to proportional reductions in the roadside increment, and that reductions in total urban emissions similarly lead to proportional reductions in the urban background increment. Specifically, for the urban background, we assume in addition that we can estimate the NO_x attributed to traffic using the traffic NO_x emissions share of total NO_x emissions in the urban background. Note that although the emission standards are for NO_x, the limit values on ambient concentration for Europe are for NO_2, so we estimate the changes in NO_2 concentrations here.

Given that we consider fractional reductions, the relative amount of change is applied to NO_x. NO_2/NO_x ratios have been show to depend on a number of factors, including background NO_x, background O_3, local emissions, as well as vehicle fleet composition and vehicle speeds (that influence the amount of NO_x emitted as primary NO_2), as well as meteorology (Carslaw and Beevers 2005, Carslaw and Carslaw 2007, Clapp and Jenkin 2001). In order to account for this, we calculate the change in NO_2 using the relationship between NO_2 and NO_x, which for the data used in this study was determined to be linear. For urban background sites, the NO_2/NO_x slope is 0.82 ($r^2 = 0.98$), while for roadside stations the slope is 0.48 ($r^2 = 0.94$). The values mentioned here are for July; for a complete list of slopes, for January, July, and the annual

average, see table S4 and figure S1. An analysis of the NO_2/NO_x ratios at the urban background sites as well as the roadside monitoring sites, show consistently similar values at each site type across the city, despite differences in traffic intensities at each of these sites. For the chemical transport model simulations, NO_x chemical cycles are included in the calculations (see section 2.4), meaning that their effects are included in our results at the urban background scale. The data used was hourly NO_x and NO_2 from 16 monitoring stations in Berlin: 6 roadside, 5 urban background, and 5 rural stations for the year 2014 (Stülpnagel *et al* 2015). The rural stations used here are located on the periphery of Berlin[4]. The increments were calculated based on daily mean values averaged over a year, as well as over two individual months (January and July). The July calculation allowed for a comparison with the chemical transport model results which simulated July only. For the calculations for the individual months, sector-specific time factors were applied to the annual emissions before calculating the difference in total urban emissions. Both annual average and July values are presented in the results section; January values are only included in the SI. Standard deviation was propagated to provide an estimate of temporal and spatial variability within the observation-based estimates.

Additional calculations were carried out for the Euro 6 standard (EF: $0.08\,\mathrm{g\,km^{-1}}$) and the Euro 6 conformity factor[5] for September 2017 (EF: $0.168\,\mathrm{g\,km^{-1}}$) (EC 2015) and are included in supplemental information (table S3) available at stacks.iop.org/ERL/12/114025/mmedia. These results are not detailed in the text as they fall between the Euro 5 and best-available technology results. The relationship is roughly linear between the EFs and the reductions expected. The current Euro 5 standard and the Euro 6 conformity factor results show minimal differences, given the similarities in their EFs.

---

[4] For more information see www.stadtentwicklung.berlin.de/umwelt/luftqualitaet/luftdaten/index.shtml.

[5] The conformity factor is the first step in stricter standards, where car manufacturers will need to bring down the discrepancy between 'real driving emissions' and the Euro 6 standard.

▶▶ Letters

Table 3. Estimated reduction in ambient concentrations of daily mean NO$_2$ at the roadside and for the urban background of Berlin from the observation-based calculations. Estimates for both the national and city level fraction of LDV diesel are included. Values are monthly average (July) daily mean values and standard deviation, and for comparison, in parentheses annual average daily mean values and standard deviation. Also shown are estimated reductions in monthly average (July) daily mean NO$_2$ compared to the base case scenario for the European and Berlin simulations. In both model simulations the national (43%) LDV fraction was used for Germany. For the model simulations the 25th and 75th percentiles are indicated by the square brackets. For the European simulations reductions are shown for two chemical mechanisms, RADM2 (MOZART). All units in μg m^{-3}.

	Observation-based calculations				Berlin simulation		European simulation		
	National fleet (43% LDV)		City fleet (80% LDV)		National fleet (43% LDV)		National fleet (varies by country)		
Scenario	Roadside	Urban back-ground	Roadside	Urban back-ground	Greater Berlin area	Berlin city[a]	Greater Berlin area	Benelux	Paris
Euro 5	10 ± 2.5 (9.0 ± 2.8)	1.3 ± 0.43 (1.2 ± 0.65)	19 ± 4.6 (17 ± 5.2)	2.3 ± 0.80 (2.2 ± 1.2)	—	—	—	—	—
Best-available technology	14 ± 3.3 (12 ± 3.8)	1.6 ± 0.53 (1.5 ± 0.80)	26 ± 6.2 (23 ± 7.0)	2.9 ± 0.99 (2.7 ± 1.5)	1.6 [0.8, 2.1]	2.0 [1.1, 2.8]	1.7 [1.2, 2.0] (2.0 [1.4, 2.4])	2.1 [1.5, 2.5] (2.7 [1.7, 3.3])	4.7 [3.6, 5.2] (5.9 [4.3, 6.7])

[a] The values reported for the Berlin city (model simulation) are most comparable to the urban background estimates (observation-based calculations).

2.4. Potential change evaluated based on chemical transport model simulations

In addition to estimating the effect of emission reductions on NO$_2$ concentrations using ambient monitoring data (section 2.3), we also implemented emission reduction scenarios in a chemical transport model, the chemistry version of the Weather Research and Forecasting Model (WRF-Chem) (Fast *et al* 2006, Grell *et al* 2005, Skamarock *et al* 2008).

Two setups of the WRF-Chem model have been used, one setup covering Europe (European simulations) and one setup focusing on Berlin (Berlin simulations). Both setups are included in order to assess the changes at a regional level over Europe and for the urban area of Berlin. With each setup, two model simulations using the chemical mechanism RADM2 were done for July 2011, a base case using emissions for 2011 and a simulation assuming the best-available technology. In addition, the European simulations were repeated with a different chemical mechanism (MOZART-4) (see supplementary material). The US EPA emission standard was chosen for our best-available technology emission reduction scenario since it is the most stringent of the emission standards. Thus, the scenarios illustrate the potential for improvements in air quality achievable (at the regional to urban background scale) based on standards that should, in principle, be achievable today.

The emission reductions for the model simulations were calculated analogously to those for Berlin, using the factors in table 1. To calculate the appropriate reduction factor in diesel road transport emissions (the level at which emissions in TNO-MACCIII are reported) for each country, we use the fraction of diesel LDV vehicles (i.e. as a fraction of total diesel vehicles, LDV+HDV) based on each country's fraction of diesel LDV (national country estimates) (Kuenen 2015).

Both model setups are described in more detail in the supplemental information as well as in Mar *et al* (2016) (European simulations) and Kuik *et al* (2016) (Berlin simulations), and the main features are summarized in table S1 in the supplementary material.

2.4.1. Modeled reductions in ambient concentrations
From the model results, daily mean concentrations of chemical species were calculated. In order to estimate the reductions in ambient NO$_2$ concentrations under the best-available technology scenario, the difference between the base case and the EPA case was calculated. From this, the July 2011 monthly mean differences are evaluated. Spatially averaged reductions were then calculated for the greater Berlin area (larger dashed rectangle in figure 2) and Berlin city (inner dashed rectangle in figure 2). In addition, 25th and 75th percentiles of the differences in daily means were calculated for each grid cell. Their averages over the greater Berlin area as well as the Berlin city center are given as an indication for the average temporal variability within the respective region.

3. Results and discussion

3.1. Potential concentration changes based on ambient monitoring data
The change in ambient NO$_2$ concentrations based on calculations using the monitoring station data and the two different assumptions for how much diesel LDV emissions contribute to the total diesel vehicle fleet (national vs. city fleet composition) are shown in table 3. The reduction in the annual average of daily mean NO$_2$ concentration at the roadside in the best-available technology scenario was estimated to be 12 ± 3.8 μg m^{-3} or 23 ± 7.0 μg m^{-3} (mean ± standard

deviation) assuming the national and city fleet LDV percentages, respectively. For context these reductions would be largely affecting the average difference between the observed roadside and urban background concentrations of NO_2 which was 26 $\mu g\,m^{-3}$ and the annual mean roadside NO_2 concentration of 51 $\mu g\,m^{-3}$.[6] The reduction in the annual average of daily mean urban background NO_2 concentration was 1.5 ± 0.80 $\mu g\,m^{-3}$ and 2.7 ± 1.5 $\mu g\,m^{-3}$ using the national and city LDV percentages, respectively. Similarly, for context, the average difference between the observed urban background and rural NO_2 concentrations was 12 $\mu g\,m^{-3}$ with an annual mean urban background NO_2 concentration of 26 $\mu g\,m^{-3}$.

The monthly reductions were similar to the annual values. Specifically, the reductions calculated for July (table 3) were generally somewhat higher than those for the year, while the January values (table S3) were somewhat lower reductions. The differences were largest for roadside concentrations. For example, the monthly average of daily mean NO_2 concentration if Euro 5 standards were met (national LDV percentage), showed estimated reductions of 8.3 ± 2.3 $\mu g\,m^{-3}$ for January, compared to 10 ± 2.5 $\mu g\,m^{-3}$ for July, and 9.0 ± 2.8 $\mu g\,m^{-3}$ annually. The lesser reductions in January are linked to higher urban background concentrations, corresponding to a reduced roadside increment, as well as larger emissions from energy and non-industrial combustion. Overall, the reductions in January are about 20%–30% lower than in July, or ca. 10%–25% (5%–15%) lower (higher) than the annual reductions for January (July). The reductions calculated for July for the Euro 5 standard scenario were ca. 72% of the reductions calculated for the best-available technology scenario at the roadside, and ca. 80% for the urban background, for both the national fleet and city fleet estimates. In all cases, the standard deviation of the calculated values overlapped between the two scenarios.

Of the six roadside monitoring stations in Berlin providing hourly values, all six exceeded the annual NO_2 limit value of 40 $\mu g\,m^{-3}$ in 2014, with annual average concentrations between 42 and 61 $\mu g\,m^{-3}$ (Stülpnagel *et al* 2015). The potential reduction in the annual average NO_2 roadside increment calculated in this study for the Euro 5 standard was 9.0 ± 2.8 $\mu g\,m^{-3}$ (national LDV percentage) and 17 ± 5.2 $\mu g\,m^{-3}$ (city LDV percentage), with even higher reductions possible with stricter standards such as Euro 6 or US EPA standards. Such reductions have significant potential to help achieve the ambient air quality limit values, especially considering the values in this study are likely conservative estimates.

---

[6] The sum of the difference between the roadside and urban background concentrations (26 $\mu g\,m^{-3}$) and the annual mean urban background (26 $\mu g\,m^{-3}$) should equal the stated annual mean roadside NO_2 concentration (51 $\mu g\,m^{-3}$). For consistency with significant figures, this is not the case owing to rounding.

3.2. Model simulations using WRF-Chem

The model results showing the change in NO_2 concentrations from the European simulation and the Berlin simulation are shown in figures 1 and 2, respectively. Both model setups calculated the change in NO_2 over the greater Berlin area (larger dashed rectangle in figure 2), for which the daily mean NO_2 averaged over the month of July showed reductions of 1.7 $\mu g\,m^{-3}$ and 1.6 $\mu g\,m^{-3}$, respectively. The modeled reductions over the greater Berlin area agreed well between the European and Berlin simulations. Furthermore, a slightly larger reduction of 2.0 $\mu g\,m^{-3}$ was found for the city of Berlin in the high resolution simulation (inner dashed rectangle in figure 2). The European simulation was also carried out with the MOZART-4 chemical mechanism, in addition to the RADM2 mechanism and found to produce similar results (table 3).

As a further comparison, the modeled change in average NO_2 concentrations for the BeNeLux region and Paris, both urban centers with significant vehicular emissions, were also calculated from the regional model results. These urban agglomerations showed larger reductions of 2.1 $\mu g\,m^{-3}$ and 4.7 $\mu g\,m^{-3}$, respectively, relative to the change observed over the greater Berlin area. This is reasonable as the populations of these regions are much higher than those for Berlin.

The modeled results for the daily mean NO_2 concentrations from five urban and four suburban/rural sites in Berlin are shown in figure 3 for the base case and the best-available technology case, with a comparison to observations. The difference between the base case and best-available technology case shows substantial reductions in the daily mean values, with the largest differences often occurring when NO_2 concentrations peak. This further indicates the potential of such improvements to reduce NO_2 exceedances.

The comparison between modeled and observed NO_2 concentrations further shows that the model underestimates observed NO_2 concentrations (figure 3 and table S2 in the SI). While the model bias at suburban and rural background stations ranges between −5% and +6% (July 2011 average), the model consistently underestimates NO_2 concentrations in the urban background between −25% and −31% (−3.4 to −6.5 $\mu g\,m^{-3}$). The difference in model performance for suburban and urban areas shows that the negative bias for urban background sites might be related to a general underestimation of traffic emissions in the emission inventory, which might for example be due to an underestimation of emission factors or the amount of congestion within the city, but might also be due to model limitations in representing the chemistry or boundary layer height (e.g. Giordano *et al* 2015, Karl *et al* 2017, Knote *et al* 2015). As the difference between base run and best-available technology case is generally largest when (modeled) concentrations are higher, the underestimation in simulated concentrations might lead to an underestimation of the effect of emission reductions.

▶▶ Letters

Figure 1. Reduction in daily average modeled NO_2 concentrations in μg m^{-3} averaged over the month of July (2011) owing to the change in emissions in the best-available technology scenario relative to the base case. Shown are the results from the WRF-Chem regional model European simulation using the RADM2 chemical mechanism.

Figure 2. Reduction in daily mean NO_2 concentrations in μg m^{-3} averaged over July (2011) for the best-available technology scenario relative to the base case, 1 km model resolution, from the Berlin simulation (using the RADM2 chemical mechanism). The dashed rectangles show areas for which average reductions have been calculated—inner: Berlin city, outer: greater Berlin area (same as the one used in the European simulation).

Figure 3. Daily mean NO$_2$ concentrations at nine sites in Berlin, black dots: observations (airbase v08), lines: Berlin simulation model results (1 km × 1 km resolution).

3.3. Comparison between model simulations and observation-based estimates

Overall, the NO$_2$ reductions observed in both the European simulation and the Berlin simulation paint a consistent picture of the expected changes in NO$_2$ concentrations were emission standards to be achieved under real-world driving conditions. The reductions estimated for Berlin city in the Berlin simulation (2.0 [1.1, 2.8] μg m^{-3}) are also in line with the urban background increment from the observation-based calculations (1.6 ± 0.53 μg m^{-3}) (table 3). A comparison to the roadside reductions calculated from the monitoring data cannot be made to the models, as the resolutions are too coarse to capture street-level phenomena. However, the consistency of the results obtained with the different methods for different scales suggests that these estimates can give a good indication of the possible decrease of regional background, urban background and roadside NO$_2$ concentrations if the Euro 5 emission standard or best-available technology case (reflecting the US EPA emission standard) were met by diesel LDVs in Europe.

3.4. Implications for ozone concentrations

Finally, the change in ozone concentrations in response to the reduction of NO$_x$ emissions in the best-available technology scenario was also examined in the European

and Berlin simulations. The areas of Europe showing NO$_x$-sensitive and NO$_x$-saturated regimes are consistent for both the RADM2 and MOZART chemical mechanisms and with the findings of Mar *et al* 2016 (where a 30% increase in emissions was applied to NO$_x$ for all sectors). Comparing the best-available technology and base case scenarios, most of the European domain is observed to be NO$_x$-sensitive, with a decrease in traffic NO$_x$ in the best-available technology scenario leading to reductions in daily average O$_3$ concentrations, with decreases in up to a few μg m^{-3} seen in southern Europe and the Mediterranean. When the maximum daily 8 hr mean ozone (MDA8, the metric corresponding to regulatory targets) is considered, a similar pattern is seen, with reductions in MDA8 0.5–1.0 μg m^{-3} greater than reductions in daily average O$_3$. The UK, Benelux, northern France, and northwest Germany, as well as some more isolated urban centers, show NO$_x$-saturated behavior, in which the decreased NO$_x$ emissions led to increases in daily mean O$_3$ with a magnitude up to about 2 μg m^{-3} (1 μg m^{-3} for MDA8), due to a reduced daytime sink of O$_3$ via reaction with NO. For Berlin, the change in O$_3$ concentrations was smaller than for other major European urban areas. The European model simulations showed NO$_x$-saturated behavior for the Berlin center area. However, the results from the high-resolution

model simulation for Berlin show a decrease in O$_3$ with decreasing NO$_x$ concentrations in most of the Berlin urban areas. NO$_x$ titration, wherein the loss reaction of O$_3$ with NO dominates in areas of high NO emissions, tends to reduce high O$_3$ concentrations in urban centers (Sillman 1999). Because reductions in NO$_x$ emissions can then lead to higher O$_3$ concentrations, we see in our simulations that it will take greater reductions in NO$_x$ emissions than in our best-available technology scenario (and/or reductions in NMVOC emissions) to significantly reduce urban ozone concentrations.

4. Conclusions

The expected reductions in NO$_2$ concentrations in a scenario where all diesel LDVs were assumed to meet the Euro 5 and US EPA Tier 2 Bin 5 (best-available technology) standards under real-world driving conditions was evaluated using monitoring data and in two chemical transport model simulations (which considered the best-available technology only). The reductions in NO$_2$ for the Euro 5 standard were smaller than those for the best-available technology scenario (reductions in the annual average roadside increment: 9.0 ± 2.8 μg m^{-3} (national LDV) and 17 ± 5.2 μg m^{-3} (city LDV)), but still substantial. Greater reductions from on the observation-based calculations were estimated for July than for January. Furthermore, while the Euro 6 standard (0.08 g km^{-1}) is not as strict as the US EPA standard (0.043 g km^{-1}), substantial reductions would still be expected. Additional analysis (see SI) indicated that meeting the Euro 6 conformity factor for September 2017, would yield estimated reductions similar to all diesel LDVs meeting the Euro 5 standard. Model simulations yield reductions in urban background NO$_2$ concentration similar to the observation-based approach, indicating robustness of the findings. These results indicate that stricter NO$_x$ emissions standards—if implemented, appropriately controlled, and met—could have a significant impact on the NO$_2$ concentrations in cities and especially at roadside locations. Owing to the NO$_x$-saturated environment in many of the urban areas of Europe, it will take even greater reductions in NO$_x$ (and/or NMVOC reductions) to significantly reduce urban ozone concentrations. These results are however an idealized scenario in that they assume that the standards will be strictly enforced and that under real-world driving conditions the emission factors would still be met, and not allowed to exceed the standard as is currently the case. Based on the assumptions made in this study, the reductions calculated here are likely conservative estimates of what would be possible. Furthermore, any changes in technology that may influence the amount of NO$_x$ emitted as primary NO$_2$ were not considered. Further studies would be needed to investigate the role of potential technologies in NO$_x$ reductions and the implications for primary NO$_2$ emissions and subsequent chemistry effects.

It has become clear that emissions testing procedures are no longer adequate and that the promised improvements in air quality expected from the increasingly stringent standards are not being realized. This study and others, such as Brand (2016), Holland *et al* (2016), and Wang *et al* (2016), are an indication of the scope of the issue and potential benefits that could be realized were policies enacted that would effectively address diesel vehicle emissions standards. Furthermore, if policies addressed urban transport systems in a more comprehensive way, considering the bigger picture and the myriad linkages rather than individual elements in isolation, significant benefits could result, not only for air quality and/or climate change, but also for e.g. safety, noise pollution, levels of physical activity—even reducing social and health inequalities in the population (Rojas-Rueda and Turner 2016).

ORCID iDs

Erika von Schneidemesser ⓘ https://orcid.org/0000-0003-1386-285X

References

Barrett S R H, Speth R L, Eastham S D, Dedoussi I C, Ashok A, Malina R and Keith D W 2015 Impact of the Volkswagen emissions control defeat device on US public health *Environ. Res. Lett.* **10** 114005

Brand C 2016 Beyond dieselgate: implications of unaccounted and future air pollutant emissions and energy use for cars in the United Kingdom *Energy Policy* **97** 1–12

BSV 2013 Berliner Verkehr in Zahlen, Mobilität der Stadt (Berlin: Senatsverwaltung für Stadtentwicklung und Umwelt)

BSV 2017 Luftqualität in Berlin 2016: Feinstaubgrenzwert eingehalten, hoher Handlungsbedarf bei Stickstoffdioxid (Berlin: Senatsverwaltung für Umwelt, V.u.K.) (www.berlin.de/sen/uvk/presse/pressemitteilungen/2017/pressemitteilung.551237.php)

Carslaw D C and Beevers S D 2005 Development of an urban inventory for road transport emissions of NO$_2$ and comparison with estimates derived from ambient measurements *Atmos. Environ.* **39** 2049–59

Carslaw D C, Beevers S D, Tate J E, Westmoreland E J and Williams M L 2011 Recent evidence concerning higher NO$_x$ emissions from passenger cars and light duty vehicles *Atmos. Environ.* **45** 7053–63

95

IOP Publishing   *Environ. Res. Lett.* **12** (2017) 114025   ▶▶ Letters

Carslaw D C and Carslaw N 2007 Detecting and characterising small changes in urban nitrogen dioxide concentrations *Atmos. Environ.* **41** 4723–33

Chossiere G P, Malina R, Ashok A, Dedoussi I C, Eastham S D, Speth R L and Barrett S R H 2017 Public health impacts of excess NO$_x$ emissions from Volkswagen diesel passenger vehicles in Germany *Environ. Res. Lett.* **12** 034014

Clapp L J and Jenkin M E 2001 Analysis of the relationship between ambient levels of O$_3$, NO$_2$ and NO as a function of NO$_x$ in the UK *Atmos. Environ.* **35** 6391–405

EC 2007 Regulation (EC) No 715/2007 of the European Parliament and of the Council of 20 June 2007 on type approval of motor vehicles with respect to emissions from light passenger and commercial vehicles (Euro 5 and Euro 6) and on access to vehicle repair and maintenance information, 715/2007/EC

EC 2015 *Commission welcomes Member States' Agreement on Robust Testing of Air Pollution Emissions by Cars* (Brussels: European Commission)

EEA 2016 *Air Quality in Europe–2016 Report* (Luxembourg: European Environment Agency)

EEA/EMEP 2013 1.A.3. b.i, 1.A.3. b.ii, 1.A.3. b.iii, 1.A.3. b.iv Passenger cars, light commercial trucks, heavy-duty vehicles including buses and motor cycles

Ehlers C, Klemp D, Rohrer F, Mihelcic D, Wegener R, Kiendler-Scharr A and Wahner A 2016 Twenty years of ambient observations of nitrogen oxides and specified hydrocarbons in air masses dominated by traffic emissions in Germany *Faraday Discuss.* **189** 407–37

Fast J D, Gustafson W I, Easter R C, Zaveri R A, Barnard J C, Chapman E G, Grell G and Peckham S E 2006 Evolution of ozone, particulates, and aerosol direct radiative forcing in the vicinity of houston using a fully coupled meteorology-chemistry-aerosol model *J. Geophys. Res. Atmos.* **111** D21305

Faustini A, Rapp R and Forastiere F 2014 Nitrogen dioxide and mortality: review and meta-analysis of long-term studies *Eur. Respir. J.* **44** 744

Fontaras G, Franco V, Dilara P, Martini G and Manfredi U 2014 Development and review of Euro 5 passenger car emission factors based on experimental results over various driving cycles *Sci. Total Environ.* **468–469** 1034–42

Giordano L *et al* 2015 Assessment of the MACC reanalysis and its influence as chemical boundary conditions for regional air quality modeling in AQMEII-2 *Atmos. Environ.* **115** 371–88

Gkatzoflias D, Kouridis C, Ntziachristos L and Samaras Z 2012 COPERT 4: Computer programme to calculate emissions from road transport, user manual EMISIA/EEA

Grell G A, Peckham S E, Schmitz R, McKeen S A, Frost G, Skamarock W C and Eder B 2005 Fully coupled online chemistry within the WRF model *Atmos. Environ.* **39** 6957–75

Hagman R, Weber C and Amundsen A H 2015 *Emissions from New Vehicles–Trustworthy? Institute of Transport Economics* (Oslo: Norwegian Centre for Transport Research)

Holland S P, Mansur E T, Muller N Z and Yates A J 2016 Damages and expected deaths due to excess NOX emissions from 2009 to 2015 volkswagen diesel vehicles *Environ. Sci. Technol.* **50** 1111–7

ICCT 2014 *European Vehicle Market Statistics: Pocketbook 2014* ed P Mock (Berlin: International Council on Clean Transportation Europe)

Karl T *et al* 2017 Urban eddy covariance measurements reveal significant missing NO$_x$ emissions in Central Europe *Sci. Rep.* **7** 2536

Knote C *et al* 2015 Influence of the choice of gas-phase mechanism on predictions of key gaseous pollutants during the AQMEII phase-2 intercomparison *Atmos. Environ.* **115** 553–68

Kuenen J J P 2015 personal communication

Kuenen J J P, Visschedijk A J H, Jozwicka M and Denier van der Gon H A C 2014 TNO MACC_II emission inventory; a multi year 2003–2009 consistent high resolution European emission inventory for air quality modelling *Atmos. Chem. Phys.* **14** 10963–76

Kuik F, Lauer A, Churkina G, Denier van der Gon H A C, Fenner D, Mar K A and Butler T M 2016 Air quality modelling in the Berlin–Brandenburg region using WRF-Chem v3.7.1: sensitivity to resolution of model grid and input data *Geosci. Model Dev.* **9** 4339–63

Mar K A, Ojha N, Pozzer A and Butler T M 2016 Ozone air quality simulations with WRF-Chem (v3.5.1) over Europe: model evaluation and chemical mechanism comparison *Geosci. Model Dev.* **9** 3699–728

Mills I C, Atkinson R W, Kang S, Walton H and Anderson H R 2015 Quantitative systematic review of the associations between short-term exposure to nitrogen dioxide and mortality and hospital admissions *BMJ Open* **5** e006946

Minkos A, Dauert U, Feigenspan S and Kessinger S 2017 *Luftqualität 2016: Vorläufige Auswertung. Umweltbundesamt* (Dessau-Roßlau: English: German Environment Ministry)

Rexeis M, Hausberger S, Kühlwein J, Luz R, Ligterink N E and Kadijk G 2013 *Update of Emission Factors for EURO 5 and EURO 6 vehicles for the HBEFA* (Graz: Institute for Internal Combustion Engines and Thermodynamics, Graz University of Technology)

Rojas-Rueda D and Turner M C 2016 Commentary: diesel, cars, and public health *Epidemiology* **27** 159–62

Sillman S 1999 The relation between ozone, NO$_x$ and hydrocarbons in urban and polluted rural environments *Atmos. Environ.* **33** 1821–45

Skamarock W C, Klemp J B, Dudhia J, Gill D O, Barker M, Duda K G, Huang Y, Wang W and Powers J G 2008 *A Description of the Advanced Research WRF* 1–113

Stülpnagel A v, Kaupp H, Nothard R, Preuß J, Preuß M, Clemen S and Grunow K 2015 *Luftgütemessdaten 2014* (Berlin: Senatsverwaltung für Stadtentwicklung und Umwelt)

Thompson G J, Carder D K, Besch M C, Thiruvengadam A and Kappanna H K 2014 In-use emissions testing of light-duty diesel vehicles in the United States *Center for Alternative Fuels, Engines and Emissions* (Morgantown, WV and Washington, DC: West Virginia University)

Wang T, Jerrett M, Sinsheimer P and Zhu Y 2016 Estimating PM$_{2.5}$-associated mortality increase in California due to the Volkswagen emission control defeat device *Atmos. Environ.* **144** 168–74

Weiss M *et al* 2012 Will Euro 6 reduce the NO$_x$ emissions of new diesel cars?–insights from on-road tests with portable emissions measurement systems (PEMS) *Atmos. Environ.* **62** 657–65

6. Article 4: Effect of VOC emissions from vegetation on air quality in Berlin during a heatwave

7. Conclusions

7.1. Summary of the main findings

In view of the detrimental impacts of air pollution, research and in particular modelling play an important role for assessing air quality issues and emission control strategies. This thesis contributes to the assessment of air quality in urban areas on several levels. Specifically, following research questions were outlined in the introduction and are answered in the following, based on model simulations with the WRF-Chem model and the Berlin-Brandenburg area as a case study:

- What model resolution and level of detail in the input data is needed in order to simulate air quality in the Berlin-Brandenburg area?

- If an underestimation of NO_x emissions in commonly used inventories is a major cause of the negative bias in modelled NO_2 concentrations frequently reported for urban areas, how strong is this underestimation?

- By how much would NO_x concentrations in the Berlin-Brandenburg area be reduced if diesel emission standards were met?

- How do heat waves affect emissions of volatile organic compounds from urban/suburban vegetation and corresponding ground-level ozone in the Berlin-Brandenburg area?

What model resolution and level of detail in the input data is needed in order to simulate air quality in the Berlin-Brandenburg area?

Article 1 serves as an in-depth documentation of different aspects of the high-resolution model setup used as a basis for the studies contributing to this thesis, and contributes to the growing literature on the evaluation of model setups. Its results suggest that a horizontal resolution of 3km improves modelled urban meteorology and air quality compared to a resolution of 15km, but a horizontal resolution of 1km does not generally improve the results compared to a model resolution of 3km. The improvements are largest if the input

parameters to the urban scheme are specified based on locally available data, and when downscaling the emissions to the model resolution.

The model evaluation presented in the article shows that the presented WRF-Chem setup generally simulates meteorology well. 2m temperature and 10m wind speed in the urban area are biased high using the default settings in parameterizing urban processes, but the bias is decreased when specifying the input parameters to the urban scheme based on locally available data. The nighttime mixing layer height is biased low, and changes with specifying input parameters to the urban scheme depend on the land use class. This low bias in nighttime planetary boundary layer height is consistent with a modeled overestimation of NO_x at nighttime. This result indicates that the calculation of the urban boundary layer height and nighttime mixing in the model might need to be adapted to better represent observed conditions at nighttime. NO_x concentrations at daytime, on the other hand, are underestimated by the model. Ozone is on average simulated reasonably well, but maximum daily eight hour mean concentrations are underestimated, which is consistent with the results from previous modelling studies using the RADM2 chemical mechanism in WRF-Chem.

When downscaling the emissions from a horizontal resolution of 7km to 1km based on proxy data for Berlin, local pollution patterns can be resolved better, especially at model resolutions of 3km and 1km. A particular strength of the emission downscaling approach is its effective and consistent combination of a readily available emission inventory and locally available data, which can be applied generically to urban areas. The approach can facilitate air quality modelling at high resolution, which has in previous studies been identified as difficult at resolutions down to 1km, in particular for operational purposes (see Section 1.3.1). Though the approach helps to meet high demands on the resolution of input data, a remaining challenge is the misrepresentation of observed NO_x concentrations by the model.

If an underestimation of NO_x emissions in commonly used inventories is a major cause of the negative bias in modelled NO_2 concentrations frequently reported for urban areas, how strong is this underestimation?

The results of the second study suggest that a possible underestimation of urban NO_x emissions, to which traffic is the single most important contributor, might indeed be a major cause for a negative bias in modelled NO_2 concentrations at daytime. Specifically, the study implements changes to the model setup based on the findings of the first article, and extends the simulation at a horizontal resolution of 3km to simulate air quality for the whole year of 2014. It also extends the evaluation of modelled NO_2, complementing an operational model evaluation with a diagnostic evaluation of the results. It finds that

the largest contribution to the model error comes from the (negative) bias in modelled NO_x concentrations at urban background measurement stations, and from deviations of modelled from observed variability on diurnal time scales. Beyond an underestimation of traffic emissions, the model errors are also consistent with deficiencies in processes varying on the diurnal scale such as the modelled mixing in the planetary boundary layer.

The underestimation of traffic emissions is then quantified based on the finding that the weekday bias in modelled NO_2 is larger than on weekends and that the contribution of traffic NO_x to total NO_x emissions in the urban area is typically higher on weekdays. The underlying assumption is that other sources of model error influence the model bias equally on weekdays and weekends, while the underestimation of traffic emissions has the largest effect on modelled NO_2 concentrations on weekdays. The results suggest that traffic emissions are underestimated by ca. a factor of 3 in the core urban area on weekdays when traffic is highest. This underestimation corresponds to an underestimation of weekly mean traffic NO_x emissions in the core urban area of ca. a factor of 2 and an underestimation of total NO_x emissions in the city centre by a factor of ca. 1.5. Two sensitivity simulations for January and July 2014 with NO_x emissions from traffic scaled with the estimated correction factor show that increased traffic emissions improve the model bias in NO_2 and NO_x concentrations in both seasons in the urban background, and also improve modelled downwind concentrations. The still negative bias is consistent with the factor being a rather conservative estimate, and other sources of model error contributing to the underestimation.

Overall, the results of this study are consistent with findings from other studies, frequently reporting an underestimation of modelled NO_2 concentrations compared with observations in Europe, and with results from measurement studies suggesting that there might be considerable differences between measured urban NO_x emissions and emissions provided by emission inventories based on official reporting. The article thus adds to the literature - using a different methodology from previous assessments - emphasizing that a better assessment of traffic NO_x emissions under real-world driving conditions, and in particular the corresponding emission factors, is needed. Given the consistency with results from other studies, this conclusion is expected to hold not only for the Berlin-Brandenburg area, but for European metropolitan areas more generally.

By how much would NO_x concentrations in the Berlin-Brandenburg area be reduced if diesel emission standards were met?

The third article assesses potential air quality improvements if light duty diesel vehicles were able to meet the regulatory standards. Two independent methods are used, including a measurement-based and a model-based method, including a model setup of WRF-Chem

with high resolution for the Berlin-Brandenburg area. Depending on the assumptions on fleet composition and stringency of the regulatory standard, the estimate for annual average roadside NO_2 reductions based on measurements is 9 to 23 μg m^{-3}, and 1.2 to 2.7 μg m^{-3} in the urban background. Model-based estimates for the urban background show reductions in NO_2 of 2.0 μg m^{-3}.

Compared to observations, the high resolution WRF-Chem simulation underestimates NO_2 concentrations. However, the results show larger reductions when modelled NO_2 concentrations are higher. Thus, the model underestimation of NO_2 concentrations is likely to be one of the reasons for the results to be a rather conservative estimate. Furthermore, the approach used for the measurement-based assessment only depends on the relative change, and not the total amount of NO_x emissions and is thus independent of a potential underestimation of total traffic NO_x emissions.

The similarities in results using the measurement- and model-based methods support the ability to draw robust conclusions that are not dependent on the assumptions behind either methodology. The results of this article show that substantial reductions in NO_x concentrations would be expected with fulfilling the emission limits of the Euro 6 standard, and that stricter NO_x emissions standards - given their correct implementation - could have a significant impact on NO_2 concentrations in cities and especially at roadside locations.

How do heat waves affect emissions of volatile organic compounds from urban/suburban vegetation and corresponding ground-level ozone in the Berlin-Brandenburg area?

The fourth article investigates how heat waves affect emissions of volatile organic compounds from urban/suburban vegetation and corresponding ground-level ozone. The model simulation results indicate that the contribution of biogenic VOC emissions to ozone formation on particular days within the analyzed heat wave period in the Berlin-Brandenburg region is up to 60%. Overall, it is lower in June (9 - 11%) and August (6 - 9%) than in July (17 - 20%). However, the actual contribution is expected to be even higher as the model underestimates isoprene concentrations over urban forests and parks.

The study demonstrates that biogenic VOCs can considerably enhance air pollution during heat waves, emphasizing the broader consequences of high urban NO_x concentrations and the dual role of vegetation for air quality and human health in cities during warm seasons. The results suggest that a reduction of anthropogenic emissions of both NO_x and VOCs, as for example through a reduction of the motorized vehicle fleet, would have to be implemented to minimise the adverse effects of air pollution. In particular, other urban environmental measures such as urban tree planting campaigns would need to be

accompanied by reductions in anthropogenic NO_x emissions for benefiting from the full potential of such measures.

7.2. Discussion and further research needs

The results from all four articles give rise to a range of issues for discussion, model development needs and new/not fully answered research questions:

- Further development of urban processes in WRF-Chem used at high resolution. This includes in particular (vertical) mixing, the anthropogenic impact (heat and momentum fluxes) on small-scale urban meteorology and chemistry, and coupling of sub-grid-scale urban meteorology with chemistry.

- Better understanding anthropogenic emissions, and better representing emissions in high-resolution models. This includes in particular emissions from traffic in both their magnitude and emission patterns, but also the representation of biogenic emissions in WRF-Chem in urban areas.

- Further assessment of the ability to simulate, and improvement of the representation, of tropospheric O_3 concentrations at policy-relevant levels in WRF-Chem.

- Bridging the scales for assessing air quality in urban areas, including the treatment of emissions and coupling of modelling systems.

- Better understanding the interplay of climate change and air quality, especially when it comes to the impact of climate change on (urban) emissions, and the combined effect of heat and air pollution on health.

- Assessing changes in (urban) mobility in a more holistic way, in particular with respect to the current transportation system and potential alternatives.

The remainder of this section elaborates on these points in more detail, and concludes with reflections on transdisciplinary research.

Representation of urban processes and their influence on air pollutants

Article 1 has shown that a specification of the input parameters to the single-layer urban canopy model in WRF-Chem, using city-specific input data, improves the simulated meteorology in Berlin compared to the default settings. It has also shown that a sub-grid scale parameterization of urban land use may improve modelled meteorology if, e.g. for computational reasons, only a relatively coarse model resolution can be used. The results

also suggest that further improvements could be expected when using a model resolution of 1kmx1km combined with an accurate specification of urban land use.

In the specific case of Berlin, a comparison of the CORINE land use data used here with a locally available land use dataset shows that large green areas and public parks such as the "Tiergarten" or "Tempelhofer Feld" are not represented correctly in CORINE. Thus, further improvements of the model results might be expected if the land use input for the area of Berlin would be replaced with locally available data. This could benefit both modelled meteorology and chemistry, the latter through improvements in modelled meteorology, but also through a potentially more realistic representation of urban green areas and thus biogenic VOC emissions. More generally, this example illustrates that local data available in many metropolitan areas might be helpful for improving model results in urban areas.

Overall, the results of Article 1 also show that the changes in urban parameters as implemented at this point only lead to very limited improvements in modelled chemistry, and that the presented WRF-Chem setup still has problems in simulating vertical mixing and related diurnal cycles of air pollutants in the urban planetary boundary layer. This seems particularly relevant in summer and spring. In addition, the changes in the model code applied to improve nighttime mixing might be seen with some criticism, as nighttime mixing is increased based on fixed parameters in the code, rather than on an updated parameterization of physical processes leading to increased mixing.

As a consequence, the parameterization of urban processes would need to better account for urban heat and momentum fluxes for a more realistic representation of mixing both at daytime and at nighttime, particularly in summer. As a first step, the capability of the single layer urban canopy model to specify a diurnal profile of anthropogenic heat fluxes in the urban canopy could be tested, but would require city-specific input data. Moreover, the results suggest that the processes within the urban boundary layer would benefit from directly coupling the sub-grid scale parameterization of urban processes with chemistry. Here, the recently extended ACM2 planetary boundary layer scheme, now conducting mixing of chemical species within the planetary boundary layer scheme, could be tested as a first step.

In addition, measurements of the vertical structure of the atmosphere as well as vertical profiles of NO_x and other chemical species in urban areas are needed to better evaluate and improve models for applications in urban areas. In the specific case of Berlin, ceilometer measurements initiated in recent years by different university departments in several locations of Berlin could already support improving the representation of the urban planetary boundary layer.

A difficulty when simulating meteorological and chemical processes in the urban planetary boundary layer is the need for detailed, city-specific input data (e.g. land use data, data describing the urban structure and thermodynamic characteristics). This need increases even more when using more complex parameterizations of urban processes. However, this and other studies have shown that sing these relatively complex parameterizations and a high model resolution, often coming with a high computational cost, is only beneficial if input data specifically describing the area of interest is used. This leads to the conclusion that the effort of compiling these data is probably often worth it. Furthermore, these data are often publicly available for large European cities, and are also a good opportunity for collaborating with local city administrations and other research groups requiring/processing similar data.

Understanding emissions and their dynamics

European air quality modellers consider air pollutant emissions the most uncertain input to air quality modelling (Thunis et al., 2016).

This thesis has shown that the simulation of NO_x concentrations in Berlin can be improved when downscaling a commonly used emission inventory to a higher resolution. Though a vertical distribution of emissions does not seem to improve model results at coarse resolutions (e.g. Mar et al., 2016), the results from the studies presented here are consistent with suggestions from other studies, indicating that a vertical distribution of emissions is important when simulating air quality at high resolution.

However, results from this thesis also suggest that anthropogenic emissions of NO_x are underestimated, and that the spatial and temporal variability in real-world NO_x emissions from traffic does not seem to be captured well enough in the model setup used here.

Consequently, a more consistent treatment and processing of the spatial, temporal and vertical distributions of emissions is needed in order to fully benefit from a high model resolution over heterogeneous urban areas. Three approaches could lead to improvements: extending the approach presented here by better specifying the spatial and temporal distribution of emissions using local proxy data, dynamically calculating emissions online in chemistry transport models or coupling with emission models, and using real-time data (e.g. GPS data from navigation systems) to realistically distribute/calculate emissions (see, e.g. Chen et al., 2016, for an example estimating traffic emissions based on GPS data used in a dispersion model). Though all of these approaches are already used in existing studies or models, the very widely used WRF-Chem model requires the user to manually pre-process emissions, which might often lead to duplicated efforts and is also

error-prone. Thus, the modelling community could greatly benefit from a more harmonized approach to emission processing in WRF-Chem.

Beyond that, this and other studies suggest that it is not only necessary to improve the representation of emissions in chemistry transport models, but also to develop a better understanding of traffic emissions under real-world driving conditions in general. Here, a better understanding of emission factors is needed both with respect to recent technological developments, and the impact of different driving conditions on emissions.

As for the first aspect, technological developments might be related to the large-scale use of defeat devices, which are increasingly discovered in diesel cars across different brands and models[1]. Beyond that, technological features not fully covered by current emission inventories might also concern a recently documented temperature dependence of NO_x emissions from EURO 4, EURO 5 and EURO 6 diesel cars, with increases of NO_x emissions with decreasing temperature of more than 30%, compared to standard test conditions (e.g. Hausberger and Matzer, 2017). Technological developments, e.g. the use of exhaust after-treatment technologies, may also alter the fraction of primarily emitted NO_2 (Carslaw, 2005), with implications for atmospheric chemistry and air quality.

As for the second aspect, the results from Article 2 suggest that a better understanding of real-world driving condition emission factors under a variety of different driving conditions, including congested situations, is needed. This conclusion is consistent with the assessment included in the official guidance for the compilation of national emissions (Ntziachristos and Samaras, 2017), indicating that the estimation of traffic emissions might require frequent updating, as these technologies and related emissions change rapidly. This concerns emission factors, but the guidebook also refers to a frequent re-assessment of activity data and the methodology used to assess both.

Consequently, alternative road transport emission measurement approaches or more widespread measurement campaigns, e.g. directly measuring exhaust emissions under real-world driving conditions, could help verify the assumptions underlying the calculation of publicly reported emissions including emission factors, and help identify potential systematic problems. A better and more differentiated understanding of the respective emission factors can then help improve the representation of traffic emissions in inventories - regarding their magnitude, but also concerning their spatial representation and temporal distribution. This can in turn contribute to improving the simulation of NO_x concentrations in air quality models.

On biogenic VOC emissions, the results presented here suggest that WRF-Chem has a limited ability to simulate isoprene emissions and mixing ratios over urban forests because

---

[1]As for example documented in this chronology: `https://www.mdr.de/nachrichten/wirtschaft/vw-diesel-skandal-chronik-100.html` (in German, last acess: 13.7.2018)

of a rather poor representation of urban vegetation in the biogenic emission model MEGAN as implemented in WRF-Chem. The simulation of isoprene emissions could be improved by further specifying the location and leaf area index of vegetated areas, but also by revising the VOC emission factors including their temperature sensitivity. An accurate representation of the temperature-dependence is of particular importance when assessing the impact of a warming climate on air quality. A first step could consist in making the use of land use input data more consistent, using the same land use input data for MEGAN as for the WRF model itself.

Representation of O_3 concentrations in WRF-Chem

As stated in the introduction, one important reason for accurately capturing NO_x and VOC emissions are its characteristics as O_3 precursors. However, for accurately simulating O_3 concentrations, the suitability of the chemical mechanism itself plays an important role.

In this thesis, the RADM2 chemical mechanism has been used, and it has been shown that O_3 daily means and especially maximum daily 8 hour O_3 concentrations in summertime are underestimated by the model. However, a sensitivity test has also shown that the MOZART chemical mechanism with the model settings otherwise equal to those described in Article 2 does not necessarily lead to a better agreement with observations. Though the simulated O_3 concentrations using the MOZART mechanism better captured observed maximum peak values, observed concentrations were otherwise overestimated. In addition, there were no substantial differences in simulated NO_x concentrations between both mechanisms. These findings are in line with other results from the literature using WRF-Chem with the RADM2 mechanism (Im et al., 2015b) and comparing it with the MOZART mechanism (Mar et al., 2016). Beyond that, the literature reports similar difficulties in simulating O_3 concentrations in Europe with WRF-Chem using other chemical mechanisms, but also other online-coupled chemistry transport models (Im et al., 2015b).

This shows that a substantial research effort is needed in order to represent O_3 concentrations well over the Berlin-Brandenburg area and other European areas. This includes first of all the choice and potential modification of the chemical mechanism and an assessment of its representativeness for European O_3 levels, in particular concerning the representation of policy-relevant metrics such as maximum daily 8-hour O_3 concentrations. In addition, the assessment should include the representation of biogenic VOCs and anthropogenic NO_x emissions as discussed above. A holistic assessment of air quality and potential measures for its improvement with WRF-Chem is then possible if the model setup is able to accurately capture both O_3 concentrations and its precursors, as well as the chemical regime of the area of interest.

Bridging the scales for assessing air quality in urban areas

As mentioned in the introduction, the largest number of exceedances of NO_x limit values takes place at the roadside. Thus, it is important to be able to draw conclusions on roadside concentrations. However, at the horizontal model resolutions used for the simulations contributing to this thesis (3km or 1km), the model can only represent concentrations measured in the urban background. Article 3 combines a model-based assessment with a measurement-based assessment in order to bridge this gap.

Alternative approaches for bridging the scales, in particular from urban background to street-level, could include coupling the chemistry transport model with a street canyon or computational fluid dynamic model, or using a statistical approach. Examples for these types of downscaling exist (e.g. Degraeuwe et al., 2016, 2017; Kiesewetter et al., 2014; Mueller et al., 2015), but combining different methods often includes many steps. These approaches pose several challenges, as they may require high computational resources, might be relatively complex, bear quite substantial uncertainties e.g. concerning the validity for specific locations, or still lead to biased model results requiring the use of correction factors, in turn limiting the applicability to future scenarios (e.g. Degraeuwe et al., 2016; Kiesewetter et al., 2014). Thus, the development of more consistent, efficient approaches is still necessary.

Assessing the interplay of a changing climate and air quality

There are still large uncertainties around the impacts of a warming climate on air quality, as mentioned in the introduction. This not only concerns the physical impacts of a warmer climate on air quality, but in particular also the emission scenarios themselves, which may both depend on socio-economic developments, and a changing climate.

As an example, Article 4 shows that biogenic VOCs can considerably enhance air pollution during heat waves. At the same time, studies have shown that the heat wave in 2006 resulted in an increased premature mortality in Berlin, which was primarily attributed to high air temperatures. However, the increased air pollution during that heat wave may have contributed to the amplified premature mortality as well, and implications of high temperature combined with high air pollution concentrations for human mortality are still not that clear. Thus, in order to obtain a better picture of the broader impact of high urban NO_x concentrations, more research efforts are needed in order to further enhance understanding of confounding and/or synergistic effects of air pollution, particularly considering the chemical regime in urban areas.

In addition, further research should consider the impacts of a changing climate on other types of emissions, in particular anthropogenic emissions. In urban areas, this might be

related to the temperature-dependence of NO_x emissions from traffic mentioned above, but also to temperature-dependent changes in the timing and intensity of heating and air conditioning systems and their respective emissions. For example, climate change is likely to be linked to more extreme weather including more frequent and warmer heat waves as discussed in the introduction and in Article 4 (Stocker et al., 2013). On the other side, more extreme winter weather due to Arctic warming and changes in atmospheric circulation is also discussed as a possible consequence of a changing climate (e.g. Horton et al., 2015; Shepherd, 2016). Thus, it would be of particular importance to assess the impact of these types of episodes on air quality, particularly considering resulting changes in (anthropogenic) emissions. In addition, extreme dry conditions might increase the occurrence and severity of forest fires, also in mid-latitude locations that are not typically threatened by these types of events such as the Berlin-Brandenburg area. This, in turn, has consequences for air quality which might counteract efforts to reduce air pollution, and thus need to be taken into account when assessing potential air quality improvement measures.

Holistic assessment of changes in urban mobility systems

The continuing exceedance of NO_2 limit values at European and particularly German measurement stations, as discussed in the introduction, shows that no adequate measures have yet been found to guarantee that the population is not exposed to detrimental levels of air pollution.

Article 3 indicates that stricter NO_x emissions standards - if implemented, controlled, and met - could have a significant impact on the NO_2 concentrations in cities and especially at roadside locations. Other measures, such as banning diesel vehicles from polluted areas or an electrification of the vehicle fleet, have been widely discussed in the media.

However, none of these measures have yet been implemented successfully. Moreover, many measures are contested both on the grounds of social inequality - diesel car drivers are not willing to pay the (additional) price that car manufacturers have burdened the environment with - and effectiveness. For example, electric vehicles would emit no pollutants on the road, but still consume energy that might in turn be related to pollutant and greenhouse gas emissions elsewhere, and take up (often scarce) space in cities. As another example, banning diesel cars from selected streets would likely lead to an improvement in NO_x concentrations at these roads, but would otherwise not lead to a reduction in total emissions as car drivers are likely to simply take a different route.

This illustrates the complexity of measures to tackle traffic-related air pollution and shows that a more holistic assessment is needed for a transformation to a truly sustainable

transport system. Furthermore, science and policy need to address the urban transport systems in a comprehensive way, considering the bigger picture and the myriad linkages rather than individual elements in isolation. That way, significant benefits could result, not only for air quality and/or climate change, but also for e.g. safety, noise pollution, levels of physical activity and even reducing social and health inequalities in the population.

Inter- and transdisciplinary air quality research

It is evident that the research needs outlined above could greatly benefit from drawing on knowledge from different disciplines and non-scientific stakeholders - and thus from transdisciplinary work as outlined in Section 2.3.

To some extent, this has already taken place for this thesis, as continuous discussions with a member of the Berlin Senate Department for the Environment, Transport and Climate protection have helped shape the articles contributing to this thesis, and in particular Article 2.

However, the attempts of incorporating input from relevant policy-stakeholders in this work have also shown that a gap between science and policy practice in the field of air quality exists, with differing timelines of policy makers and scientists (relatively immediate vs. longer-term), different intermediate goals (implementation of measures vs. publication), different applicabilities (case-specific analyses vs. broadly valid results), and different requirements for the output (practicability vs. peer-review).

Though this might pose challenges for incorporating elements of transdisciplinary research in a single PhD thesis, the common ultimate goal of mitigating the impact of anthropogenic emissions on human health, ecosystems and climate can still be a motivation for transdisciplinary cooperation in the framework of (larger) projects. Furthermore, the recent public discourse on the "diesel scandal" in Germany suggests that collaboration needs to go beyond the science-policy interface, as science and policy as stakeholders seem insufficient to address the urgent challenges of reducing air pollutant emissions and improving air quality. Further relevant stakeholders would for example include car manufacturers, but also people affected by air pollution or measures against air pollution, such as the population that lives in highly polluted areas but also (diesel) car drivers. Beyond that, policy makers from other areas might need to be involved when it comes to environmental measures impacting jobs, e.g. in the car industry. Engaging in a continuous dialog with relevant stakeholders could thus enable a more direct applicability of the results for policy and society, e.g. through the joint development of more realistic (emission) scenarios, and thus facilitate a more direct translation into (policy) action, while at the same time further increasing the scientific relevance of the results.

Bibliography

Ackermann, I. J., Hass, H., Memmesheimer, M., Ebel, A., Binkowski, F. S., and Shankar, U.: Modal Aerosol Dynamics model for Europe: Development and first applications, Atmos. Environ., 32, 2981–2999, doi:10.1016/S1352-2310(98)00006-5, 1998.

Ahmadov, R., Mckeen, S. A., Robinson, A. L., Bahreini, R., Middlebrook, A. M., De Gouw, J. A., Meagher, J., Hsie, E.-y., Edgerton, E., Shaw, S., and Trainer, M.: A volatility basis set model for summertime secondary organic aerosols over the eastern United States in 2006, J Geophys Res - Atmos, 117, doi:10.1029/2011JD016831, d06301, 2012.

Alvarez, R., Weilenmann, M., and Favez, J.-Y.: Evidence of increased mass fraction of NO_2 within real-world NO_x emissions of modern light vehicles - derived from a reliable online measuring method, Atmos. Environ., 42, 4699–4707, doi:10.1016/j.atmosenv.2008.01.046, 2008.

Anenberg, S. C., Miller, J., Minjares, R., Du, L., Henze, D. K., Lacey, F., Malley, C. S., Emberson, L., Franco, V., Klimont, Z., and Others: Impacts and mitigation of excess diesel-related NO_x emissions in 11 major vehicle markets, Nature, 545, 467, doi:10.1038/nature22086, 2017.

Badia, A. and Jorba, O.: Gas-phase evaluation of the online NMMB/BSC-CTM model over Europe for 2010 in the framework of the AQMEII-Phase2 project, Atmos. Environ., 115, 657–669, doi:10.1016/j.atmosenv.2014.05.055, 2015.

Baklanov, A., Schlünzen, K., Suppan, P., Baldasano, J., Brunner, D., Aksoyoglu, S., Carmichael, G., Douros, J., Flemming, J., Forkel, R., Galmarini, S., Gauss, M., Grell, G., Hirtl, M., Joffre, S., Jorba, O., Kaas, E., Kaasik, M., Kallos, G., Kong, X., Korsholm, U., Kurganskiy, A., Kushta, J., Lohmann, U., Mahura, A., Manders-groot, A., Maurizi, A., Moussiopoulos, N., Rao, S. T., Savage, N., Seigneur, C., Sokhi, R. S., Solazzo, E., Solomos, S., Sørensen, B., Tsegas, G., Vignati, E., Vogel, B., and Zhang, Y.: Online coupled regional meteorology chemistry models in Europe: current status and prospects, Atmos. Chem. Phys., 14, 317–398, doi:10.5194/acp-14-317-2014, 2014.

Baró, R., Jiménez-Guerrero, P., Balzarini, A., Curci, G., Forkel, R., Grell, G., Hirtl, M., Honzak, L., Langer, M., Pérez, J. L., Pirovano, G., San José, R., Tuccella, P.,

Werhahn, J., and Zabkar, R.: Sensitivity analysis of the microphysics scheme in WRF-Chem contributions to AQMEII phase 2, Atmos. Environ., 115, 620–629, doi:10.1016/j.atmosenv.2015.01.047, 2015.

Barrett, S. R., Speth, R. L., Eastham, S. D., Dedoussi, I. C., Ashok, A., Malina, R., and Keith, D. W.: Impact of the Volkswagen emissions control defeat device on US public health, Environ. Res. Lett., 10, 114 005, doi:10.1088/1748-9326/10/11/114005, 2015.

Basu, R. and Samet, J. M.: Relation between elevated ambient temperature and mortality: A review of the epidemiologic evidence, Epidemiol. Rev., 24, 190–202, doi:10.1093/epirev/mxf007, 2002.

Beekmann, M., Kerschbaumer, A., Reimer, E., Stern, R., and Möller, D.: PM measurement campaign HOVERT in the Greater Berlin area: model evaluation with chemically specified particulate matter observations for a one year period, Atmos. Chem. Phys., 7, 55–68, doi:10.5194/acp-7-55-2007, 2007.

Berkowicz, R.: OSPM - a parameterised street pollution model, in: Urban Air Quality: Measurement, Modelling and Management, pp. 323–331, Springer, doi:10.1007/978-94-010-0932-4_35, 2000.

Berlin Senate Department for the Environment, T. and Protection, C.: Berliner Emissionskataster, URL `https://www.berlin.de/senuvk/umwelt/luftqualitaet/de/emissionen/`, last access: 17.7.2018.

Berlin Senate Department for the Environment, T. and Protection, C.: Luftqualität in Berlin 2016: Feinstaubgrenzwert eingehalten, hoher Handlungsbedarf bei Stickstoffdioxid, URL `https://www.berlin.de/sen/uvk/presse/pressemitteilungen/2017/pressemitteilung.551237.php`, last access: 17.7.2018, 2017.

Berlin Senate Department for Urban Development and Housing: Environment Atlas Berlin, URL `http://www.stadtentwicklung.berlin.de/umwelt/umweltatlas/edua_index.shtml`, last access: 17.7.2018, 2018.

Berlin Senate Department for Urban Development and the Environment: Environment Atlas Berlin/Population Density 2014, URL `http://www.stadtentwicklung.berlin.de/umwelt/umweltatlas/edua_index.shtml`, last access: December 2015, 2011a.

Berlin Senate Department for Urban Development and the Environment: Environment Atlas Berlin/Traffic Volumes 2009, URL `http://www.stadtentwicklung.berlin.de/umwelt/umweltatlas/edua_index.shtml`, last access: December 2015, 2011b.

Berlin Senate Department for Urban Development and the Environment: Berliner Verkehr in Zahlen, Mobilität der Stadt, URL `https://www.berlin.de/senuvk/verkehr/`

`politik_planung/zahlen_fakten/download/Mobilitaet_dt_komplett.pdf`, last access: 17.7.2018, 2013.

Berlin Senate Department for Urban Development and the Environment: Luftverunreinigungen in Berlin, Monatsbericht Juni 2014, Berlin, Germany, 2014a.

Berlin Senate Department for Urban Development and the Environment: Luftverunreinigungen in Berlin, Monatsbericht Juli 2014, Berlin, Germany, 2014b.

Berlin Senate Department for Urban Development and the Environment: Luftverunreinigungen in Berlin, Monatsbericht August 2014, Berlin, Germany, 2014c.

Berlin Senate Department for Urban Development and the Environment: Luftgütemessdaten, Jahresbericht 2014, 2015.

Bessagnet, B., Pirovano, G., Mircea, M., Cuvelier, C., Aulinger, A., Calori, G., Ciarelli, G., Manders, A., Stern, R., Tsyro, S., García Vivanco, M., Thunis, P., Pay, M.-t., Colette, A., Couvidat, F., Meleux, F., Rouïl, L., Ung, A., Aksoyoglu, S., Baldasano, J. M., Bieser, J., Briganti, G., Cappelletti, A., D'isidoro, M., Finardi, S., Kranenburg, R., Silibello, C., Carnevale, C., Aas, W., Dupont, J.-c., Fagerli, H., Gonzalez, L., Menut, L., Prévôt, A. S. H., Roberts, P., and White, L.: Presentation of the EURODELTA III intercomparison exercise – evaluation of the chemistry transport models' performance on criteria pollutants and joint analysis with meteorology, Atmos. Chem. Phys., 16, 12 667–12 701, doi:10.5194/acp-16-12667-2016, 2016.

Beyrich, F. and Leps, J.-p.: An operational mixing height data set from routine radiosoundings at Lindenberg: Methodology, Meteorol. Z., 21, 337–348, doi:10.1127/0941-2948/2012/0333, 2012.

Bieser, J., Aulinger, A., Matthias, V., Quante, M., and Van Der Gon, H. D.: Vertical emission profiles for Europe based on plume rise calculations, Environ. Pollut., 159, 2935–2946, doi:10.1016/j.envpol.2011.04.030, 2011.

Binkowski, F. S. and Shankar, U.: The Regional Particulate Matter Model. 1. Model description and preliminary results, J. Geophys. Res., 100, 26,191–26,209, doi:10.1029/95JD02093, 1995.

Bishop, G. A. and Stedman, D. H.: Reactive nitrogen species emission trends in three light-/medium-duty United States fleets, Environ. Sci. Technol., 49, 11 234–11 240, doi:10.1021/acs.est.5b02392, 2015.

Bonn, B., von Schneidemesser, E., Andrich, D., Quedenau, J., Gerwig, H., Lüdecke, A., Kura, J., Pietsch, A., Ehlers, C., Klemp, D., Kofahl, C., Nothard, R., Kerschbaumer, A., Junkermann, W., Grote, R., Pohl, T., Weber, K., Lode, B., Schönberger, P., Churkina,

G., Butler, T. M., and Lawrence, M. G.: BAERLIN2014 -The influence of land surface types on and the horizontal heterogeneity of air pollutant levels in Berlin, Atmos. Chem. Phys., 16, 7785–7811, doi:10.5194/acp-16-7785-2016, 2016.

Bonn, B., von Schneidemesser, E., Butler, T., Churkina, G., Ehlers, C., Grote, R., Klemp, D., Nothard, R., Schäfer, K., Von Stülpnagel, A., Kerschbaumer, A., Yousefpour, R., Fountoukis, C., and Lawrence, M. G.: Impact of vegetative emissions on urban ozone and biogenic secondary organic aerosol: Box model study for Berlin, Germany, J. Cleaner Prod., 176, 827–841, doi:10.1016/j.jclepro.2017.12.164, 2018.

Bowler, D. E., Buyung-Ali, L., Knight, T. M., and Pullin, A. S.: Urban greening to cool towns and cities: A systematic review of the empirical evidence, Landscape Urban Plann., 97, 147–155, doi:10.1016/j.landurbplan.2010.05.006, 2010.

Brand, C.: Beyond dieselgate: implications of unaccounted and future air pollutant emissions and energy use for cars in the United Kingdom, Energy Policy, 97, 1, doi:10.1016/j.enpol.2016.06.036, 2016.

Brilli, F., Hörtnagl, L., Bamberger, I., Schnitzhofer, R., Ruuskanen, T. M., Hansel, A., Loreto, F., and Wohlfahrt, G.: Qualitative and quantitative characterization of volatile organic compound emissions from cut grass, Environ. Sci. Technol., 46, 3859–3865, doi:10.1021/es204025y, 2012.

Brunner, D., Savage, N., Jorba, O., Eder, B., Giordano, L., Badia, A., Balzarini, A., Baró, R., Bianconi, R., Chemel, C., Curci, G., Forkel, R., Jiménez-guerrero, P., Hirtl, M., Hodzic, A., Honzak, L., Im, U., Knote, C., Makar, P., Manders-groot, A., Meijgaard, E. V., Neal, L., Pérez, J. L., Pirovano, G., Jose, R. S., Schröder, W., Sokhi, R. S., Syrakov, D., Torian, A., Tuccella, P., Werhahn, J., Wolke, R., Yahya, K., Zabkar, R., Zhang, Y., Hogrefe, C., and Galmarini, S.: Comparative analysis of meteorological performance of coupled chemistry-meteorology models in the context of AQMEII phase 2, Atmos. Environ., 115, 470–498, doi:10.1016/j.atmosenv.2014.12.032, 2015.

Builtjes, P., Loon, M. V., Schaap, M., Teeuwisse, S., Visschedijk, A., and Bloos, J.: The development of an emission data base over Europe and further contributions of TNO-MEP, URL `https://www.umweltbundesamt.de/en/publikationen/development-of-an-emission-data-over-europe-further`, last access: 17.7.2018, 2002.

Bundesanstalt für Straßenwesen: Stundenwerte der Zählstellen auf Bundesfernstraßen, URL `http://www.bast.de/DE/Verkehrstechnik/Fachthemen/v2-verkehrszaehlung/Stundenwerte.html?nn=626916`, last access: 17.7.2018, 2017.

Calfapietra, C., Fares, S., Manes, F., Morani, A., Sgrigna, G., and Loreto, F.: Role of Biogenic Volatile Organic Compounds (BVOC) emitted by urban trees on ozone concentration in cities: A review, Environ. Pollut., 183, 71–80, doi:10.1016/j.envpol. 2013.03.012, 2013.

Calfapietra, C., Penuelas, J., and Niinemets, T.: Urban plant physiology: Adaptation-mitigation strategies under permanent stress, Trends Plant Sci., 20, 72–75, doi:10.1016/ j.tplants.2014.11.001, 2015.

Carslaw, D. and Ropkins, K.: openair - An R package for air quality data analysis, Environ Modell Softw, 27-28, 52–61, doi:10.1016/j.envsoft.2011.09.008, 2012.

Carslaw, D. C.: Evidence of an increasing NO_2/NO_x emissions ratio from road traffic emissions, Atmos. Environ., 39, 4793–4802, doi:10.1016/j.atmosenv.2005.06.023, 2005.

Carslaw, D. C. and Carslaw, N.: Detecting and characterising small changes in urban nitrogen dioxide concentrations, Atmos. Environ., 41, 4723–4733, doi:10.1016/j.atmosenv. 2007.03.034, 2007.

Carslaw, D. C., Beevers, S. D., Tate, J. E., Westmoreland, E. J., and Williams, M. L.: Recent evidence concerning higher NOx emissions from passenger cars and light duty vehicles, Atmos. Environ., 45, 7053–7063, doi:10.1016/j.atmosenv.2011.09.063, 2011.

Carslaw, N., Ashmore, M., Terry, A. C., and Carslaw, D. C.: Crucial Role for Outdoor Chemistry in Ultrafine Particle Formation in Modern Office Buildings, Environ. Sci. Technol., 49, 11 011–11 018, doi:10.1021/acs.est.5b02241, 2015.

Chameides, W. L., Lindsay, R. W., Richardson, J., and Kiang, C. S.: The role of biogenic hydrocarbons in urban photochemical smog: Atlanta as a case study, Science, 241, 1473–1475, doi:10.1126/science.3420404, 1988.

Chen, D., Li, Q., Stutz, J., Mao, Y., Zhang, L., Pikelnaya, O., Tsai, J. Y., Haman, C., Lefer, B., Rappenglück, B., Alvarez, S. L., Neuman, J. A., Flynn, J., Roberts, J. M., Nowak, J. B., Gouw, J. D., Holloway, J., Wagner, N. L., Veres, P., Brown, S. S., Ryerson, T. B., Warneke, C., and Pollack, I. B.: WRF-Chem simulation of NO_x and O_3 in the L.A. basin during CalNex-2010, Atmos. Environ., 81, 421–432, doi:10.1016/j.atmosenv. 2013.08.064, 2013.

Chen, F., Kusaka, H., Tewari, M., Bao, J.-w., and Harakuchi, H.: Utilizing the coupled WRF/LSM/urban modeling system with detailed urban classification to simulate the urban heat island phenomena over the Greater Houston area, Proceedings of the 5th Conference on Urban Environment, Vancouver, BC, Canada, 2004.

Chen, F., Kusaka, H., Bornstein, R., Ching, J., Grimmond, C. S. B., Grossman-clarke, S., Loridan, T., Manning, K. W., Martilli, A., Miao, S., Sailor, D., Salamanca, F. P., Taha, H., Tewari, M., Wang, X., Wyszogrodzki, A. A., and Zhang, C.: The integrated WRF/urban modelling system: development, evaluation, and applications to urban environmental problems, Int. J. Climatol., 31, 273–288, doi:10.1002/joc.2158, 2011.

Chen, S., Bekhor, S., Broday, D. M., and Others: Aggregated GPS tracking of vehicles and its use as a proxy of traffic-related air pollution emissions, Atmos. Environ., 142, 351–359, doi:10.1016/j.atmosenv.2016.08.015, 2016.

Chossière, G. P., Malina, R., Ashok, A., Dedoussi, I. C., Eastham, S. D., Speth, R. L., and Barrett, S. R.: Public health impacts of excess NO_x emissions from Volkswagen diesel passenger vehicles in Germany, Environ. Res. Lett., 12, 034 014, doi:10.1088/1748-9326/aa5987, 2017.

Churkina, G., Grote, R., Butler, T. M., and Lawrence, M.: Natural selection? Picking the right trees for urban greening, Environ. Sci. Policy, 47, 12–17, doi:10.1016/j.envsci.2014.10.014, 2015.

Clapp, L.: Analysis of the relationship between ambient levels of O_3, NO_2 and NO as a function of NO_x in the UK, Atmos. Environ., 35, 6391–6405, doi:10.1016/s1352-2310(01)00378-8, 2001.

Coates, J. and Butler, T. M.: A comparison of chemical mechanisms using tagged ozone production potential (TOPP) analysis, Atmos. Chem. Phys., 15, 8795–8808, doi:10.5194/acp-15-8795-2015, 2015.

Coates, J., Mar, K. A., Ojha, N., and Butler, T. M.: The influence of temperature on ozone production under varying NO_x conditions–a modelling study, Atmos. Chem. Phys., 16, 11 601–11 615, 2016.

Colette, A., Bessagnet, B., Meleux, F., Terrenoire, E., and Rouïl, L.: Frontiers in air quality modelling, Geosci. Model Dev., 7, 203–210, doi: 10.5194, 2014.

Crutzen, P.: Geology of mankind, Nature, 415, 23, doi:10.1038/415023a, 2002.

Dee, D. P., Uppala, S. M., Simmons, A. J., Berrisford, P., Poli, P., Kobayashi, S., Andrae, U., Balmaseda, M. A., Balsamo, G., Bauer, P., Bechtold, P., Beljaars, A. C. M., Van De Berg, L., Bidlot, J., Bormann, N., Delsol, C., Dragani, R., Fuentes, M., Geer, A. J., Haimberger, L., Healy, S. B., Hersbach, H., H'olm, E. V., Isaksen, L., Kallberg, P., Köhler, M., Matricardi, M., Mcnally, A. P., Monge-sanz, B. M., Morcrette, J.-j., Park, B.-k., Peubey, C., De Rosnay, P., Tavolato, C., Th'epaut, J.-n., and Vitart, F.: The

ERA-Interim reanalysis: configuration and performance of the data assimilation system, Q J Roy Meteor Soc, 137, 553–597, doi:10.1002/qj.828, 2011.

Degraeuwe, B., Thunis, P., Clappier, A., Weiss, M., Lefebvre, W., Janssen, S., and Vranckx, S.: Impact of passenger car NO_x emissions and NO_2 fractions on urban NO_2 pollution–Scenario analysis for the city of Antwerp, Belgium, Atmos. Environ., 126, 218–224, doi:10.1016/j.atmosenv.2015.11.042, 2016.

Degraeuwe, B., Thunis, P., Clappier, A., Weiss, M., Lefebvre, W., Janssen, S., and Vranckx, S.: Impact of passenger car NO_x emissions on urban NO_2 pollution - Scenario analysis for 8 European cities, Atmos. Environ., 171, 330 – 337, doi:https://doi.org/10.1016/j.atmosenv.2017.10.040, 2017.

Dennis, R., Fox, T., Fuentes, M., Gilliland, A., Hanna, S., Hogrefe, C., Irwin, J., Rao, S. T., Scheffe, R., Schere, K., and Others: A framework for evaluating regional-scale numerical photochemical modeling systems, Environ. Fluid Mech., 10, 471–489, doi: 10.1007/s10652-009-9163-2, 2010.

Diem, J. E.: Comparisons of weekday-weekend ozone: Importance of biogenic volatile organic compound emissions in the semi-arid southwest USA, Atmos. Environ., 34, 3445–3451, doi:10.1016/S1352-2310(99)00511-7, 2000.

Dirksen, R. J., Sommer, M., Immler, F. J., Hurst, D. F., Kivi, R., and Vömel, H.: Reference quality upper-air measurements: GRUAN data processing for the Vaisala RS92 radiosonde, Atmos. Meas. Tech., 7, 4463–4490, doi:10.5194/amt-7-4463-2014, 2014.

Duane, M., Poma, B., Rembges, D., Astorga, C., and Larsen, B. R.: Isoprene and its degradation products as strong ozone precursors in Insubria, Northern Italy, Atmos. Environ., 36, 3867–3879, doi:10.1016/S1352-2310(02)00359-X, 2002.

EEA: CORINE land cover data 2006, updated, URL `http://www.eea.europa.eu/data-and-maps/data/corine-land-cover-2006-raster-3`, last access: 17.7.2018, 2014.

EEA: The European Environment - State and Outlook 2015, URL `https://www.eea.europa.eu/soer-2015/synthesis/report`, last access: 17.7.2018, 2015.

EEA: Air quality in Europe - 2016 report, doi:10.2800/80982, URL `https://www.eea.europa.eu/publications/air-quality-in-europe-2016`, last access: 17.7.2018, 2016.

EEA: AirBase -The European air quality database, URL `https://www.eea.europa.eu/data-and-maps/data/airbase-the-european-air-quality-database-8`, last access: 17.7.2018, 2017.

EEA: Air quality in Europe - 2017 report, doi:10.2800/850018, URL `https://www.eea.europa.eu/publications/air-quality-in-europe-2017`, last access: 17.7.2018, 2017.

Ehlers, C., Klemp, D., Rohrer, F., Mihelcic, D., Wegener, R., Kiendler-Scharr, A., and Wahner, A.: Twenty years of ambient observations of nitrogen oxides and specified hydrocarbons in air masses dominated by traffic emissions in Germany, Faraday Discuss., 189, 407, doi:10.1039/c5fd00180c, 2016.

EMEP/EEA: EMEP/EEA emission inventory guidebook 2013 update Sept 2014: 1.A.3.b.i, 1.A.3.b.ii, 1.A.3.b.iii, 1.A.3.b.iv Passenger cars, light commercial trucks, heavy-duty vehicles including buses and motor cycles, URL `https://www.eea.europa.eu/publications/emep-eea-guidebook-2013`, last access: 17.7.2018, 2014.

Emmons, L. K., Walters, S., Hess, P. G., Lamarque, J.-f., Pfister, G. G., Fillmore, D., Granier, C., Guenther, A., Kinnison, D., Laepple, T., Orlando, J., Tie, X., Tyndall, G., Wiedinmyer, C., Baughcum, S. L., and Kloster, S.: Description and evaluation of the Model for Ozone and Related chemical Tracers, version 4 (MOZART-4), Geosci. Model Dev., 3, 43–67, doi:10.5194/gmd-3-43-2010, 2010.

European Commission: Regulation (EC) No 715/2007 of the European Parliament and of the Council of 20 June 2007 on type approval of motor vehicles with respect to emissions from light passenger and commercial vehicles (Euro 5 and Euro 6) and on access to vehicle repair and maintenance information, 715/2007/EC, 2007.

European Commission: Commission welcomes Member States Agreement on Robust Testing of Air Pollution Emissions by Cars, URL `http://europa.eu/rapid/press-release_IP-15-5945_en.htm`, last access: 17.7.2018, 2015.

Fallmann, J., Forkel, R., and Emeis, S.: Secondary effects of urban heat island mitigation measures on air quality, Atmos. Environ., 125, Part A, 199–211, doi:10.1016/j.atmosenv.2015.10.094, 2016.

Fares, S., McKay, M., Holzinger, R., and Goldstein, A. H.: Ozone fluxes in a Pinus ponderosa ecosystem are dominated by non-stomatal processes: Evidence from long-term continuous measurements, Agric. For. Meteorol., 150, 420–431, doi:10.1016/j.agrformet.2010.01.007, 2010.

Fares, S., Weber, R., Park, J. ., Gentner, D., Karlik, J., and Goldstein, A. H.: Ozone deposition to an orange orchard: Partitioning between stomatal and non-stomatal sinks, Environ. Pollut., 169, 258–266, doi:10.1016/j.envpol.2012.01.030, 2012.

Fast, J. D., Gustafson, W. I., Easter, R. C., Zaveri, R. A., Barnard, J. C., Chapman, E. G., Grell, G. A., and Peckham, S. E.: Evolution of ozone, particulates, and aerosol direct radiative forcing in the vicinity of Houston using a fully coupled meteorology-chemistry-aerosol model, J Geophys Res - Atmos, 111, doi:10.1029/2005JD006721, d21305, 2006.

Faustini, A., Rapp, R., and Forastiere, F.: Nitrogen dioxide and mortality: review and meta-analysis of long-term studies, Eur. Respir. J., 44, 744–753, doi:10.1183/09031936.00114713, 2014.

Fenner, D., Meier, F., Scherer, D., and Polze, A.: Spatial and temporal air temperature variability in Berlin, Germany, during the years 2001 - 2010, Urban Clim., 10, Part 2, 308–331, doi:10.1016/j.uclim.2014.02.004, 2014.

Fontaras, G., Franco, V., Dilara, P., Martini, G., and Manfredi, U.: Development and review of Euro 5 passenger car emission factors based on experimental results over various driving cycles, Sci. Total Environ., 468, 1034–1042, doi:10.1016/j.scitotenv.2013.09.043, 2014.

Forkel, R., Balzarini, A., Baró, R., Bianconi, R., Curci, G., Jiménez-guerrero, P., Hirtl, M., Honzak, L., Lorenz, C., Im, U., Pérez, J. L., Pirovano, G., José, R. S., Tuccella, P., Werhahn, J., and Žabkar, R.: Analysis of the WRF-Chem contributions to AQMEII phase2 with respect to aerosol radiative feedbacks on meteorology and pollutant distributions, Atmos. Environ., 115, 630–645, doi:10.1016/j.atmosenv.2014.10.056, 2015.

Fuzzi, S., Baltensperger, U., Carslaw, K., Decesari, S., Denier Van Der Gon, H., Facchini, M. C., Fowler, D., Koren, I., Langford, B., Lohmann, U., Nemitz, E., Pandis, S., Riipinen, I., Rudich, Y., Schaap, M., Slowik, J. G., Spracklen, D. V., Vignati, E., Wild, M., Williams, M., and Gilardoni, S.: Particulate matter, air quality and climate: Lessons learned and future needs, Atmos. Chem. Phys., 15, 8217–8299, doi:10.5194/acp-15-8217-2015, 2015.

Gabriel, K. M. A. and Endlicher, W. R.: Urban and rural mortality rates during heat waves in Berlin and Brandenburg, Germany, Environ. Pollut., 159, 2044–2050, doi:10.1016/j.envpol.2011.01.016, 2011.

Galmarini, S., Kioutsioukis, I., and Solazzo, E.: E pluribus unum*: ensemble air quality predictions., Atmos. Chem. Phys., 13, doi:10.5194/acp-13-7153-2013, 2013.

Geiß, A., Wiegner, M., Bonn, B., Schäfer, K., Forkel, R., von Schneidemesser, E., Münkel, C., Chan, K. L., and Nothard, R.: Mixing layer height as an indicator for urban air quality?, Atmos. Meas. Tech., 10, 2969–2988, doi:10.5194/amt-10-2969-2017, 2017.

Gerboles, M., Lagler, F., Rembges, D., and Brun, C.: Assessment of uncertainty of NO_2 measurements by the chemiluminescence method and discussion of the quality objective of the NO_2 European Directive, J. Environ. Monit., 5, 529–540, doi:10.1039/b302358c, 2003.

Gerosa, G., Vitale, M., Finco, A., Manes, F., Denti, A. B., and Cieslik, S.: Ozone uptake by an evergreen Mediterranean Forest (Quercus ilex) in Italy. Part I: Micrometeorological flux measurements and flux partitioning, Atmos. Environ., 39, 3255–3266, doi:10.1016/j.atmosenv.2005.01.056, 2005.

Ghirardo, A., Xie, J., Zheng, X., Wang, Y., Grote, R., Block, K., Wildt, J., Mentel, T., Kiendler-Scharr, A., Hallquist, M., Butterbach-Bahl, K., and Schnitzler, J. .: Urban stress-induced biogenic VOC emissions and SOA-forming potentials in Beijing, Atmos. Chem. Phys., 16, 2901–2920, doi:10.5194/acp-16-2901-2016, 2016.

Giordano, L., Brunner, D., Flemming, J., Hogrefe, C., Im, U., Bianconi, R., Badia, A., Balzarini, A., Bar'o, R., Chemel, C., Curci, G., Forkel, R., Jiménez-Guerrero, P., Hirtl, M., Hodzic, A., Honzak, L., Jorba, O., Knote, C., Kuenen, J., Makar, P., Manders-Groot, A., Neal, L., Pérez, J., Pirovano, G., Pouliot, G., José, R. S., Savage, N., Schröder, W., Sokhi, R., Syrakov, D., Torian, A., Tuccella, P., Werhahn, J., Wolke, R., Yahya, K., Žabkar, R., Zhang, Y., and Galmarini, S.: Assessment of the MACC reanalysis and its influence as chemical boundary conditions for regional air quality modeling in AQMEII-2, Atmos. Environ., 115, 371–388, doi:10.1016/j.atmosenv.2015.02.034, 2015.

Gkatzoflas, D., Kouridis, C., Ntziachristos, L., and Samaras, Z.: COPERT 4: Computer programme to calculate emissions from road transport, user manual EMISIA/EEA, 2012.

Goldstein, A. H. and Galbally, I. E.: Known and unexplored organic constituents in the earth's atmosphere, Environ. Sci. Technol., 41, 1514–1521, doi:10.1021/es072476p, 2007.

Grell, G. and Baklanov, A.: Integrated modeling for forecasting weather and air quality: A call for fully coupled approaches, Atmos. Environ., 45, 6845–6851, doi:10.1016/j.atmosenv.2011.01.017, 2011.

Grell, G. A., Peckham, S. E., Schmitz, R., Mckeen, S. A., Frost, G., Skamarock, W. C., and Eder, B.: Fully coupled "online" chemistry within the WRF model, Atmos. Environ., 39, 6957–6975, doi:10.1016/j.atmosenv.2005.04.027, 2005.

Grice, S., Stedman, J., Kent, A., Hobson, M., Norris, J., Abbott, J., and Cooke, S.: Recent trends and projections of primary NO_2 emissions in Europe, Atmos. Environ., 43, 2154–2167, doi:10.1016/j.atmosenv.2009.01.019, 2009.

Grimmond, S. U. E.: Urbanization and global environmental change: local effects of urban warming, The Geographical Journal, 173, 83–88, doi:10.1111/j.1475-4959.2007.232_3.x, 2007.

Guenther, A.: A global model of natural volatile organic compound emissions, J. Geophys. Res., 100, 8873–8892, doi:10.1029/94JD02950, 1995.

Guenther, A., Karl, T., Harley, P., Wiedinmyer, C., Palmer, P. I., and Geron, C.: Estimates of global terrestrial isoprene emissions using MEGAN (Model of Emissions of Gases and Aerosols from Nature), Atmos. Chem. Phys., 6, 3181–3210, doi:10.5194/acp-6-3181-2006, 2006.

Guenther, A. B., Zimmerman, P. R., Harley, P. C., Monson, R. K., and Fall, R.: Isoprene and monoterpene emission rate variability: model evaluations and sensitivity analyses, J. Geophys. Res., 98, 12,609–12,617, doi:10.1029/93JD00527, 1993.

Hagman, R., Weber, C., and Amundsen, A. H.: Emissions from new vehicles - trustworthy?, URL `https://www.toi.no/getfile.php/1340128/Publikasjoner/T%C3%98I%20rapporter/2015/1407-2015/1407-2015-sum.pdf`, Institute of Transport Economics, Norwegian Centre for Transport Research, last access: 17.7.2018, 2015.

Harrison, R. M. and Beddows, D. C.: Efficacy of Recent Emissions Controls on Road Vehicles in Europe and Implications for Public Health, Sci. Rep., 7, 1152, doi:10.1038/s41598-017-01135-2, 2017.

Hausberger, S. and Matzer, C.: Update of Emission Factors for EURO 4, EURO 5 and EURO 6 Diesel Passenger Cars for the HBEFA Version 3.3, URL `http://www.hbefa.net/e/documents/HBEFA3-3_TUG_finalreport_01062016.pdf`, last access: 17.7.2018, 2017.

Hellén, H., Tykkä, T., and Hakola, H.: Importance of monoterpenes and isoprene in urban air in northern Europe, Atmos. Environ., 59, 59–66, doi:10.1016/j.atmosenv.2012.04.049, 2012.

Hoffmann, T., Odum, J. R., Bowman, F., Collins, D., Klockow, D., Flagan, R. C., and Seinfeld, J. H.: Formation of organic aerosols from the oxidation of biogenic hydrocarbons, J. Atmos. Chem., 26, 189–222, doi:10.1023/A:1005734301837, 1997.

Hogrefe, C., Rao, S. T., Zurbenko, I. G., and Porter, P. S.: Interpreting the information in ozone observations and model predictions relevant to regulatory policies in the eastern United States, Bull. Amer. Meteor. Soc., 81, 2083–2106, doi:10.1175/1520-0477(2000)081⟨2083:ITIIOO⟩2.3.CO;2, 2000.

Holland, S. P., Mansur, E. T., Muller, N. Z., and Yates, A. J.: Damages and expected deaths due to excess NOX emissions from 2009 to 2015 volkswagen diesel vehicles, Environ. Sci. Technol., 50, 1111, doi:10.1021/acs.est.5b05190, 2016.

Hong, S.-Y., Noh, Y., and Dudhia, J.: A new vertical diffusion package with an explicit treatment of entrainment processes, Mon. Weather Rev., 134, 2318–2341, doi:10.1175/MWR3199.1, 2006.

Horni, A., Nagel, K., and Axhausen, K. W.: The Multi-Agent Transport Simulation MATSim, doi:10.5334/baw, 2016.

Horton, D. E., Johnson, N. C., Singh, D., Swain, D. L., Rajaratnam, B., and Diffenbaugh, N. S.: Contribution of changes in atmospheric circulation patterns to extreme temperature trends, Nature, 522, 465–469, doi:10.1038/nature1455, 2015.

Hu, X.-M., Nielsen-Gammon, J. W., and Zhang, F.: Evaluation of three planetary boundary layer schemes in the WRF model, Journal of Applied Meteorology and Climatology, 49, 1831–1844, doi:10.1175/2010JAMC2432.1, 2010.

ICCT: European Vehicle Market Statistics: Pocketbook 2014, The International Council on Clean Transportation, URL `https://www.theicct.org/sites/default/files/publications/EU_pocketbook_2014.pdf`, last access: 17.7.2018, 2014.

ICCT: NO_x emissions from heavy-duty and light-duty diesel vehicles in the EU: Comparison of real-world performance and current type-approval requirements, URL `http://www.theicct.org/sites/default/files/publications/Euro-VI-versus-6_ICCT_briefing_06012017.pdf`, last access: 17.7.2018, 2016.

Im, U., Bianconi, R., Solazzo, E., Kioutsioukis, I., Badia, A., Balzarini, A., Baró, R., Bellasio, R., Brunner, D., Chemel, C., Curci, G., Flemming, J., Forkel, R., Giordano, L., Jiménez-guerrero, P., Hirtl, M., Hodzic, A., Honzak, L., Jorba, O., Knote, C., Kuenen, J. J., Makar, P. A., Manders-groot, A., Neal, L., Pérez, J. L., Pirovano, G., Pouliot, G., Jose, R. S., Savage, N., Schroder, W., Sokhi, R. S., Syrakov, D., Torian, A., Tuccella, P., Werhahn, J., Wolke, R., Yahya, K., Zabkar, R., Zhang, Y., Zhang, J., Hogrefe, C., and Galmarini, S.: Evaluation of operational on-line-coupled regional air quality models over Europe and North America in the context of AQMEII phase 2. Part I: Ozone, Atmos. Environ., 115, 404–420, doi:10.1016/j.atmosenv.2014.09.042, 2015a.

Im, U., Bianconi, R., Solazzo, E., Kioutsioukis, I., Badia, A., Balzarini, A., Baró, R., Bellasio, R., Brunner, D., Chemel, C., Curci, G., Gon, H. D. V. D., Flemming, J., Forkel, R., Giordano, L., Jiménez-guerrero, P., Hirtl, M., Hodzic, A., Honzak, L., Jorba, O., Knote, C., Makar, P. A., Manders-groot, A., Neal, L., Pérez, J. L., Pirovano, G., Pouliot, G., Jose, R. S., Savage, N., Schroder, W., Sokhi, R. S., Syrakov, D., Torian, A., Tuccella,

P., Wang, K., Werhahn, J., Wolke, R., Zabkar, R., Zhang, Y., Zhang, J., Hogrefe, C., and Galmarini, S.: Evaluation of operational online-coupled regional air quality models over Europe and North America in the context of AQMEII phase 2. Part II: Particulate matter, Atmos. Environ., 115, 421–441, doi:10.1016/j.atmosenv.2014.08.072, 2015b.

Jacob, D.: Introduction to Atmospheric Chemistry, Princeton University Press, URL `https://books.google.de/books?id=FcqHAQAACAAJ`, 1999.

Jahn, T., Bergmann, M., and Keil, F.: Transdisciplinarity: Between mainstreaming and marginalization, Ecol. Econ., 79, 1–10, doi:10.1016/j.ecolecon.2012.04.017, 2012.

Jänicke, B., Meier, F., Fenner, D., Fehrenbach, U., Holtmann, A., and Scherer, D.: Urban-rural differences in near-surface air temperature as resolved by the Central European Refined analysis (CER): sensitivity to planetary boundary layer schemes and urban canopy models, Int. J. Climatol., 37, doi:10.1002/joc.4835, 2016.

Janjić, Z. I.: The step-mountain coordinate: Physical package, Mon. Weather Rev., 118, 1429–1443, doi:10.1175/1520-0493(1990)118⟨1429:TSMCPP⟩2.0.CO;2, 1990.

Janjić, Z. I.: The step-mountain eta coordinate model: Further developments of the convection, viscous sublayer, and turbulence closure schemes, Mon. Weather Rev., 122, 927–945, doi:10.1175/1520-0493(1994)122⟨0927:TSMECM⟩2.0.CO;2, 1994.

Karl, T., Graus, M., Striednig, M., Lamprecht, C., Hammerle, A., Wohlfahrt, G., Held, A., Heyden, L. V. D., Deventer, M. J., Krismer, A., Haun, C., Feichter, R., and Lee, J.: Urban eddy covariance measurements reveal significant missing NO_x emissions in Central Europe, Sci. Rep., pp. 1–9, doi:10.1038/s41598-017-02699-9, 2017.

Kaspar, F., Müller-westermeier, G., Penda, E., Mächel, H., Zimmermann, K., Kaiser-weiss, A., and Deutschländer, T.: Monitoring of climate change in Germany - data, products and services of Germany's National Climate Data Centre, Adv. Sci. Res., 10, 99–106, doi:10.5194/asr-10-99-2013, 2013.

Kates, R. W., Clark, W. C., Corell, R., Hall, J. M., Jaeger, C. C., Lowe, I., Mccarthy, J. J., Schellnhuber, H. J., Bolin, B., Dickson, N. M., Faucheux, S., Gallopin, G. C., Grübler, A., Huntley, B., Jäger, J., Jodha, N. S., Kasperson, R. E., Mabogunje, A., Matson, P., Mooney, H., Moore, B., O'riordan, T., and Svedin, U.: Sustainability Science, Science, 292, 641–642, doi:10.1126/science.1059386, 2001.

Kiesewetter, G., Borken-Kleefeld, J., Schöpp, W., Heyes, C., Thunis, P., Bessagnet, B., Terrenoire, E., Gsella, A., and Amann, M.: Modelling NO_2 concentrations at the street level in the GAINS integrated assessment model: projections under current legislation, Atmos. Chem. Phys., 14, 813–829, doi:10.5194/acp-14-813-2014, 2014.

Kim, S. ., Jiang, X., Lee, M., Turnipseed, A., Guenther, A., Kim, J. ., Lee, S. ., and Kim, S.: Impact of biogenic volatile organic compounds on ozone production at the Taehwa Research Forest near Seoul, South Korea, Atmos. Environ., 70, 447–453, doi: 10.1016/j.atmosenv.2012.11.005, 2013.

Knote, C., Hodzic, A., Jimenez, J., Volkamer, R., Orlando, J., Baidar, S., Brioude, J., Fast, J., Gentner, D., Goldstein, A., Hayes, O., Knighton, W. B., Oetjen, H., Setyan, A., Stark, H., Thalman, R., Tyndall, G., Washenfelder, R., Waxman, E., and Zhang, Q.: Simulation of semi-explicit mechanisms of SOA formation from glyoxal in aerosol in a 3-D model, Atmos. Chem. Phys., 14, 6213–6239, doi:10.5194/acp-14-6213-2014, 2014.

Knote, C., Tuccella, P., Curci, G., Emmons, L., Orlando, J. J., Madronich, S., Baró, R., Jiménez-guerrero, P., Luecken, D., Hogrefe, C., Forkel, R., Werhahn, J., Hirtl, M., Pérez, J. L., José, R. S., Giordano, L., Brunner, D., Yahya, K., and Zhang, Y.: Influence of the choice of gas-phase mechanism on predictions of key gaseous pollutants during the AQMEII phase-2 intercomparison, Atmos. Environ., 115, 553–568, doi:10.1016/j.atmosenv.2014.11.066, 2015.

Knuth, L.: Greening Cities for Improving Urban Livelihood: Legal, Policy and Institutional Aspects of Urban and Peri-urban Forestry in West and Central Asia (with a Case Study of Armenia)., Forestry Outlook Study for West and Central Asia (FOWECA), URL http://www.fao.org/forestry/15803-084381c53bd202e5c270652af25bbe368.pdf, fOA, last access: 17.7.2018, 2006.

Kofahl, C.: Hochempfindliche Bestimmung der organischen und anorganischen Kohlenstoff-Fraktion in Feinstaubproben mittels CRD-Spektroskopie, university of Applied Sciences Aachen, Jülich, 2012.

Kuenen, J. J. P., Visschedijk, A. J. H., Jozwicka, M., and Denier Van Der Gon, H. A. C.: TNO-MACC‿ II emission inventory; a multi-year (2003-2009) consistent high-resolution European emission inventory for air quality modelling, Atmos. Chem. Phys., 14, 10 963–10 976, doi:10.5194/acp-14-10963-2014, 2014.

Kusaka, H. and Kimura, F.: Thermal Effects of Urban Canyon Structure on the Nocturnal Heat Island: Numerical Experiment Using a Mesoscale Model Coupled with an Urban Canopy Model, J. Appl. Meteorol., 43, 1899–1910, doi:10.1175/JAM2169.1, 2004.

Kusaka, H., Kondo, H., Kikegawa, Y., and Kimura, F.: A Simple Single-Layer Urban Canopy Model For Atmospheric Models: Comparison With Multi-Layer And Slab Models, Bound-Lay Meteorol, 101, 329–358, doi:10.1023/A:1019207923078, 2001.

Landrigan, P. J., Fuller, R., Acosta, N. J., Adeyi, O., Arnold, R., Baldé, A. B., Bertollini, R., Bose-O'Reilly, S., Boufford, J. I., Breysse, P. N., et al.: The Lancet Commission on pollution and health, The Lancet, doi:10.1016/S0140-6736(17)32345-0, 2017.

Lang, D., Wiek, A., Bergmann, M., Stauffacher, M., Martens, P., Moll, P., Swilling, M., and Thomas, C.: Transdisciplinary research in sustainability science: Practice, principles, and challenges, Sustainability Sci., 7, 25–43, doi:10.1007/s11625-011-0149-x, 2012.

Lee, J. D., Lewis, A. C., Monks, P. S., Jacob, M., Hamilton, J. F., Hopkins, J. R., Watson, N. M., Saxton, J. E., Ennis, C., Carpenter, L. J., Carslaw, N., Fleming, Z., Bandy, B. J., Oram, D. E., Penkett, S. A., Slemr, J., Norton, E., Rickard, A. R., K Whalley, L., Heard, D. E., Bloss, W. J., Gravestock, T., Smith, S. C., Stanton, J., Pilling, M. J., and Jenkin, M. E.: Ozone photochemistry and elevated isoprene during the UK heatwave of August 2003, Atmos. Environ., 40, 7598–7613, doi:10.1016/j.atmosenv.2006.06.057, 2006.

Lee, J. D., Helfter, C., Purvis, R. M., Beevers, S. D., Carslaw, D. C., Lewis, A. C., Møller, S. J., Tremper, A., Vaughan, A., and Nemitz, E. G.: Measurement of NO_x Fluxes from a Tall Tower in Central London, UK and Comparison with Emissions Inventories, Environ. Sci. Technol., 49, 1025–1034, doi:10.1021/es5049072, 2015.

Li, D., Bou-Zeid, E., Barlage, M., Chen, F., and Smith, J. A.: Development and evaluation of a mosaic approach in the WRF-Noah framework, J Geophys Res - Atmos, 118, 11,918–11,935, doi:10.1002/2013JD020657, 2013.

Li, Z., Liang, Y., Zhou, J., and Sun, X.: Impacts of de-icing salt pollution on urban road greenspace: A case study of Beijing, Frontiers of Environmental Science and Engineering, 8, 747–756, doi:10.1007/s11783-014-0644-2, 2014.

Liao, J., Wang, T., Wang, X., Xie, M., Jiang, Z., Huang, X., and Zhu, J.: Impacts of different urban canopy schemes in WRF/Chem on regional climate and air quality in Yangtze River Delta, China, Atmos. Res., 145-146, 226–243, doi:10.1016/j.atmosres.2014.04.005, 2014.

Loridan, T., Grimmond, C. S. B., Grossman-clarke, S., Chen, F., Tewari, M., Manning, K., Martilli, A., Kusaka, H., and Best, M.: Trade-offs and responsiveness of the single-layer urban canopy parametrization in WRF: An offline evaluation using the MOSCEM optimization algorithm and field observations, Q J Roy Meteor Soc, 136, 997–1019, doi:10.1002/qj.614, 2010.

Loridan, T., Lindberg, F., Jorba, O., Kotthaus, S., Grossman-Clarke, S., and Grimmond, C.: High resolution simulation of the variability of surface energy balance fluxes across

central London with urban zones for energy partitioning, Boundary Layer Meteorol., 147, 493–523, doi:10.1007/s10546-013-9797-y, 2013.

Mar, K. A., Ojha, N., Pozzer, A., and Butler, T. M.: Ozone air quality simulations with WRF-Chem (v3.5.1) over Europe: Model evaluation and chemical mechanism comparison, Geosci. Model Dev., 9, 3699–3728, doi:10.5194/gmd-2016-131, 2016.

Martilli, A., Clappier, A., and Rotach, M. W.: An Urban Surface Exchange Parameterisation for Mesoscale Models, Boundary Layer Meteorol., 104, 261–304, doi:10.1023/A:1016099921195, 2002.

McKeen, S. A., Chung, S. H., Wilczak, J., Grell, G., Djalalova, I., Peckham, S., Gong, W., Bouchet, V., Moffet, R., Tang, Y., Carmichael, G. R., Mathur, R., and Yu, S.: Evaluation of several PM2.5 forecast models using data collected during the ICARTT/NEAQS 2004 field study, J. Geophys. Res. Atmos., 112, 2007.

Megaritis, A. G., Fountoukis, C., Charalampidis, P. E., Pilinis, C., and Pandis, S. N.: Response of fine particulate matter concentrations to changes of emissions and temperature in Europe, Atmos. Chem. Phys., 13, 3423–3443, doi:10.5194/acp-13-3423-2013, 2013.

Melamed, M. L., Schmale, J., and von Schneidemesser, E.: Sustainable policy - key considerations for air quality and climate change, Current opinion in environmental sustainability, 23, 85–91, doi:10.1016/j.cosust.2016.12.003, 2016.

Mena-Carrasco, M., Oliva, E., Saide, P., Spak, S. N., Maza, C. D. L., Osses, M., Tolvett, S., Campbell, J. E., chung Tsao, T. E. C., and Molina, L. T.: Estimating the health benefits from natural gas use in transport and heating in Santiago, Chile, Sci. Total Environ., 429, 257–265, doi:10.1016/j.scitotenv.2012.04.037, 2012.

Mills, I. C., Atkinson, R. W., Kang, S., Walton, H., and Anderson, H.: Quantitative systematic review of the associations between short-term exposure to nitrogen dioxide and mortality and hospital admissions, BMJ open, 5, doi:10.1136/bmjopen-2014-006946, 2015.

Minkos, A., Dauert, U., Feigenspan, S., and Kessinger, S.: Luftqualität 2016, URL `https://www.umweltbundesamt.de/publikationen/luftqualitaet-2016`, umweltbundesamt, last access: 17.7.2018, 2017.

Mueller, M., Wagner, M., Barmpadimos, I., and Hueglin, C.: Two-week NO_2 maps for the City of Zurich, Switzerland, derived by statistical modelling utilizing data from a routine passive diffusion sampler network, Atmos. Environ., 106, 1 – 10, doi:10.1016/j.atmosenv.2015.01.049, 2015.

Mues, A., Kuenen, J., Hendriks, C., Manders, A., Segers, A., Scholz, Y., Hueglin, C., Builtjes, P., and Schaap, M.: Sensitivity of air pollution simulations with LOTOS-EUROS to the temporal distribution of anthropogenic emissions, Atmos. Chem. Phys., 14, 939–955, doi:10.5194/acp-14-939-2014, 2014.

Nakanishi, M. and Niino, H.: An improved Mellor–Yamada level-3 model with condensation physics: Its design and verification, Boundary Layer Meteorol., 112, 1–31, doi:10.1023/B:BOUN.0000020164.04146.98, 2004.

Nakanishi, M. and Niino, H.: An improved Mellor–Yamada level-3 model: Its numerical stability and application to a regional prediction of advection fog, Boundary Layer Meteorol., 119, 397–407, doi:10.1007/s10546-005-9030-8, 2006.

Niinemets, Ü., Kännaste, A., and Copolovici, L.: Quantitative patterns between plant volatile emissions induced by biotic stresses and the degree of damage, Front. Plant Sci., 4, doi:10.3389/fpls.2013.00262, 2013.

Ntziachristos, L. and Samaras, Z.: 1.A.3. b.i, 1.A.3. b.ii, 1.A.3. b.iii, 1.A.3. b.iv Passenger cars, light commercial trucks, heavy-duty vehicles including buses and motor cycles, EMEP/EEA air pollutant emission inventory guidebook 2016, URL https://www.eea.europa.eu/publications/emep-eea-guidebook-2016/part-b-sectoral-guidance-chapters/1-energy/1-a-combustion/1-a-3-b-i/view, last access: 13.7.2018, 2017.

OECD: OECD Environmental Outlook to 2050, doi:10.1787/9789264122246-en, OECD Publishing, 2012.

Otero, N., Sillmann, J., Schnell, J. L., Rust, H. W., and Butler, T.: Synoptic and meteorological drivers of extreme ozone concentrations over Europe, Environ. Res. Lett., 11, 024 005, doi:10.1088/1748-9326/11/2/024005, 2016.

Paasonen, P., Asmi, A., Petäjä, T., Kajos, M. K., Äijälä, M., Junninen, H., Holst, T., Abbatt, J. P. D., Arneth, A., Birmili, W., Van Der Gon, H. D., Hamed, A., Hoffer, A., Laakso, L., Laaksonen, A., Richard Leaitch, W., Plass-Dülmer, C., Pryor, S. C., Räisänen, P., Swietlicki, E., Wiedensohler, A., Worsnop, D. R., Kerminen, V.-M., and Kulmala, M.: Warming-induced increase in aerosol number concentration likely to moderate climate change, Nat. Geosci., 6, 438–442, doi:10.1038/ngeo1800, 2013.

Paoletti, E., De Marco, A., Beddows, D. C. S., Harrison, R. M., and Manning, W. J.: Ozone levels in European and USA cities are increasing more than at rural sites, while peak values are decreasing, Environ. Pollut., 192, 295–299, doi:10.1016/j.envpol.2014.04.040, 2014.

Papiez, M. R., Potosnak, M. J., Goliff, W. S., Guenther, A. B., Matsunaga, S. N., and Stockwell, W. R.: The impacts of reactive terpene emissions from plants on air quality in Las Vegas, Nevada, Atmos. Environ., 43, 4109–4123, doi:10.1016/j.atmosenv.2009.05.048, 2009.

Park, J. ., Goldstein, A. H., Timkovsky, J., Fares, S., Weber, R., Karlik, J., and Holzinger, R.: Active atmosphere-ecosystem exchange of the vast majority of detected volatile organic compounds, Science, 341, 643–647, doi:10.1126/science.1235053, 2013.

Peckham, S. E., Grell, G. A., Mckeen, S. A., Ahmadov, R., Barth, M., Pfister, G., Wiedinmeyer, C., Fast, J. D., Gustafson, W. I., Ghan, S. J., Zaveri, R., Easter, R. C., Barnhard, J., Chapman, E., Hewson, M., Schmitz, R., Salzmann, M., Beck, V., and Freitas, S. R.: WRF/Chem Version 3.5 User's Guide, 2013.

Pernigotti, D., Gerboles, M., Belis, C., and Thunis, P.: Model quality objectives based on measurement uncertainty. Part II: NO_2 and PM_{10}, Atmos. Environ., 79, 869–878, doi:10.1016/j.atmosenv.2013.07.045, 2013.

Pineda, N., Jorba, O., Jorge, J., and Baldasano, J.: Using NOAA AVHRR and SPOT VGT data to estimate surface parameters: application to a mesoscale meteorological model, Int. J. Remote Sens., 25, 129–143, doi:10.1080/0143116031000115201, 2004.

Possell, M. and Hewitt, C. N.: Isoprene emissions from plants are mediated by atmospheric CO_2 concentrations, Global Change Biol., 17, 1595–1610, doi:10.1111/j.1365-2486.2010.02306.x, 2011.

R Core Team: R: A Language and Environment for Statistical Computing, R Foundation for Statistical Computing, Vienna, Austria, URL `http://www.R-project.org`, 2013.

Ramanathan, V. and Feng, Y.: Air pollution, greenhouse gases and climate change: Global and regional perspectives, Atmos. Environ., 43, 37–50, doi:10.1016/j.atmosenv.2008.09.063, 2009.

Rao, S. T., Galmarini, S., and Puckett, K.: Air Quality Model Evaluation International Initiative (AQMEII): Advancing the State of the Science in Regional Photochemical Modeling and Its Applications, Bull. Amer. Meteor. Soc., 92, 23–30, doi:10.1175/2010BAMS3069.1, 2011.

Rexeis, M., Hausberger, S., Kuehlwein, J., Luz, R., Ligterink, N. E., and Kadijk, G.: Update of Emission Factors for EURO 5 and EURO 6 vehicles for the HBEFA, URL `http://www.hbefa.net/e/documents/HBEFA32_EF_Euro_5_6_TUG.pdf`, last access: 17.7.2018, 2013.

Rodes, C. E. and Holland, D. M.: Variations of NO, NO$_2$ and O$_3$ concentrations downwind of a Los Angeles freeway, Atmospheric Environment (1967), 15, 243–250, doi:10.1016/0004-6981(81)90024-X, 1981.

Rößler, M., Koch, T., Janzer, C., and Olzmann, M.: Mechanisms of the NO$_2$ Formation in Diesel Engines, MTZ worldwide, URL `https://www.fvv-net.de/fileadmin/user_upload/medien/fachzeitschriften/2017-07_08_MTZ_1173_NO2_Formation_Mechanisms_EN.pdf`, last access: 17.7.2018, 2017.

Salamanca, F., Martilli, A., and Yagüe, C.: A numerical study of the Urban Heat Island over Madrid during the DESIREX (2008) campaign with WRF and an evaluation of simple mitigation strategies, Int. J. Climatol., 32, 2372–2386, doi:10.1002/joc.3398, 2012.

Schaap, M., Cuvelier, C., Hendriks, C., Bessagnet, B., Baldasano, J., Colette, A., Thunis, P., Karam, D., Fagerli, H., Graff, A., Kranenburg, R., Nyiri, A., Pay, M., Rouïl, L., Schulz, M., Simpson, D., Stern, R., Terrenoire, E., and Wind, P.: Performance of European chemistry transport models as function of horizontal resolution, Atmos. Environ., 112, 90–105, doi:10.1016/j.atmosenv.2015.04.003, 2015.

Schell, B., Ackermann, I. J., Hass, H., Binkowski, F. S., and Ebel, A.: Modeling the formation of secondary organic aerosol within a comprehensive air quality model system, J. Geophys. Res. Atmos., 106, doi:10.1029/2001JD000384, 2001.

Schmale, J., Shindell, D., Von Schneidemesser, E., Chabay, I., and Lawrence, M.: Air pollution: Clean up our skies, Nature, 515, 335–7, doi:10.1038/515335a, 2014.

Schmale, J., Von Schneidemesser, E., and Dörrie, A.: An integrated assessment method for sustainable transport system planning in a middle sized German city, Sustainability, 7, 1329–1354, 2015.

Schubert, S. and Grossman-Clarke, S.: The Influence of green areas and roof albedos on air temperatures during Extreme Heat Events in Berlin, Germany, Meteorol. Z., 22, 131–143, doi:10.1127/0941-2948/2013/0393, 2013.

Seinfeld, J. H. and Pandis, S. N.: Atmospheric chemistry and physics: from air pollution to climate change, John Wiley & Sons, 2016.

Shepherd, T. G.: Effects of a warming Arctic, Science, 353, 989–990, doi:10.1126/science.aag2349, 2016.

Shindell, D., Kuylenstierna, J. C. I., Vignati, E., Van Dingenen, R., Amann, M., Klimont, Z., Anenberg, S. C., Muller, N., Janssens-maenhout, G., Raes, F., Schwartz, J., Faluvegi, G., Pozzoli, L., Kupiainen, K., Höglund-isaksson, L., Emberson, L., Streets, D.,

Ramanathan, V., Hicks, K., Oanh, N. T. K., Milly, G., Williams, M., Demkine, V., and Fowler, D.: Simultaneously Mitigating Near-Term Climate Change and Improving Human Health and Food Security, Science, 335, 183–189, doi:10.1126/science.1210026, 2012.

Sillman, S.: The relation between ozone, NO_x and hydrocarbons in urban and polluted rural environments, Atmos. Environ., 33, 1821–1845, doi:10.1016/s1352-2310(98)00345-8, 1999.

Sillman, S. and He, D.: Some theoretical results concerning O_3-NO_x-VOC chemistry and NO_x-VOC indicators, J. Geophys. Res. Atmos., 107, doi:10.1029/2001JD001123, 2002.

Simpson, D., Benedictow, A., Berge, H., Bergström, R., Emberson, L. D., Fagerli, H., Flechard, C. R., Hayman, G. D., Gauss, M., Jonson, J. E., Jenkin, M. E., Nyíri, A., Richter, C., Semeena, V. S., Tsyro, S., Tuovinen, J.-P., Valdebenito, Á., and Wind, P.: The EMEP MSC-W chemical transport model - technical description, Atmos. Chem. Phys., 12, 7825–7865, doi:10.5194/acp-12-7825-2012, 2012.

Situ, S., Guenther, A., Wang, X., Jiang, X., Turnipseed, A., Wu, Z., Bai, J., and Wang, X.: Impacts of seasonal and regional variability in biogenic VOC emissions on surface ozone in the Pearl river delta region, China, Atmos. Chem. Phys., 13, 11 803–11 817, doi:10.5194/acp-13-11803-2013, 2013.

Skamarock, W., Klemp, J., Dudhia, J., Gill, D., Barker, D., Duda, M., Huang, X.-y., Wang, W., and Powers, J.: A Description of the Advanced Research WRF Version 3, NCAR Technical Note, doi:10.5065/D68S4MVH, 2008.

Solazzo, E. and Galmarini, S.: Error apportionment for atmospheric chemistry-transport models–a new approach to model evaluation, Atmos. Chem. Phys., 16, 6263–6283, doi:10.5194/acp-16-6263-2016, 2016.

Solazzo, E., Bianconi, R., Hogrefe, C., Curci, G., Tuccella, P., Alyuz, U., Balzarini, A., Baró, R., Bellasio, R., Bieser, J., and Others: Evaluation and error apportionment of an ensemble of atmospheric chemistry transport modeling systems: multivariable temporal and spatial breakdown, Atmos. Chem. Phys., 17, 3001–3054, doi:10.5194/acp-17-3001-2017, 2017a.

Solazzo, E., Hogrefe, C., Colette, A., Vivanco, M., and Galmarini, S.: Advanced error diagnostics of the CMAQ and Chimere modelling systems within the AQMEII3 model evaluation framework, Atmos. Chem. Phys., doi:10.5194/acp-17-10435-2017, 2017b.

Sommer, M., Dirksen, R., and Immler, F.: RS92 GRUAN Data Product Version 2 (RS92-GDP.2), doi:10.5676/GRUAN/RS92-GDP.2, 2012.

Stedman, J. R.: The predicted number of air pollution related deaths in the UK during the August 2003 heatwave, Atmos. Environ., 38, 1087–1090, doi:10.1016/j.atmosenv. 2003.11.011, 2004.

Steinbacher, M., Zellweger, C., Schwarzenbach, B., Bugmann, S., Buchmann, B., Ordonez, C., Prevot, A., and Hueglin, C.: Nitrogen oxide measurements at rural sites in Switzerland: Bias of conventional measurement techniques, J. Geophys. Res. Atmos., 112, doi:10.1029/2006jd007971, 2007.

Stocker, T., Qin, D., Plattner, G.-k., Tignor, M., Allen, S., Boschung, J., Nauels, A., Xia, Y., Bex, V., and Midgley, P.: Climate Change 2013: The Physical Science Basis. Working Group I Contribution to the Fifth Assessment Report of the Intergovernmental Panel on Climate Change, 2013.

Stockwell, W. R., Middleton, P., Chang, J. S., and Tang, X.: The second generation regional acid deposition model chemical mechanism for regional air quality modeling, J. Geophys. Res., 95, 16,343–16,367, doi:10.1029/JD095iD10p16343, 1990.

Terrenoire, E., Bessagnet, B., Rouïl, L., Tognet, F., Pirovano, G., Létinois, L., Beauchamp, M., Colette, A., Thunis, P., Amann, M., and Menut, L.: High-resolution air quality simulation over Europe with the chemistry transport model CHIMERE, Geosci. Model Dev., 8, 21–42, doi:10.5194/gmd-8-21-2015, 2015.

Tewari, M., Chen, F., Kusaka, H., and Miao, S.: Coupled WRF/Unified Noah/Urban-Canopy Modeling System, pp. 1–20, URL `https://ral.ucar.edu/sites/default/files/public/product-tool/WRF-LSM-Urban.pdf`, last access: 17.7.2018, 2007.

Thompson, G., Carder, D., Besch, M., Thiruvengadam, A., and Kappanna, H.: In-use emissions testing of light-duty diesel vehicles in the United States, URL `https://www.theicct.org/sites/default/files/publications/WVU_LDDV_in-use_ICCT_Report_Final_may2014.pdf`, center for Alternative Fuels, Engines and Emissions, West Virginia University, last access: 17.7.2018, 2014.

Thunis, P., Pederzoli, A., and Pernigotti, D.: Performance criteria to evaluate air quality modeling applications, Atmos. Environ., 59, 476–482, doi:10.1016/j.atmosenv.2012.05. 043, 2012.

Thunis, P., Miranda, A., Baldasano, J., Blond, N., Douros, J., Graff, A., Janssen, S., Juda-rezler, K., Karvosenoja, N., Maffeis, G., Martilli, A., Rasoloharimahefa, M., Real, E., Viaene, P., Volta, M., and White, L.: Overview of current regional and local scale air quality modelling practices: Assessment and planning tools in the EU, Environ. Sci. Policy, 65, 13–21, doi:10.1016/j.envsci.2016.03.013, 2016.

Tie, X., Madronich, S., Li, G., Ying, Z., Zhang, R., Garcia, A. R., Lee-taylor, J., and Liu, Y.: Characterizations of chemical oxidants in Mexico City: A regional chemical dynamical model (WRF-Chem) study, Atmos. Environ., 41, 1989–2008, doi:10.1016/j. atmosenv.2006.10.053, 2007.

Tie, X., Brasseur, G., and Ying, Z.: Impact of model resolution on chemical ozone formation in Mexico City: application of the WRF-Chem model, Atmos. Chem. Phys., 10, 8983–8995, doi:10.5194/acp-10-8983-2010, 2010.

Trusilova, K., Schubert, S., Wouters, H., Früh, B., Grossman-Clarke, S., Demuzere, M., and Becker, P.: The urban land use in the COSMO-CLM model: a comparison of three parameterizations for Berlin, Meteorol. Z., 25, 231–244, doi:10.1127/metz/2015/0587, 2016.

Tucella, P., Curci, G., Visconti, G., Bessagnet, B., and Menut, L.: Modeling of gas and aerosol with WRF/Chem over Europe: Evaluation and sensitivity study, J. Geophys. Res., 117, doi:10.1029/2011JD016302, d03303, 2012.

Tunved, P., Hansson, H. ., Kerminen, V. ., Ström, J., Dal Maso, M., Lihavainen, H., Viisanen, Y., Aalto, P. P., Komppula, M., and Kulmala, M.: High natural aerosol loading over boreal forests, Science, 312, 261–263, doi:10.1126/science.1123052, 2006.

Tunved, P., Ström, J., Kulmala, M., Kerminen, V. ., Dal Maso, M., Svenningson, B., Lunder, C., and Hansson, H. .: The natural aerosol over Northern Europe and its relation to anthropogenic emissions - Implications of important climate feedbacks, Tellus, Series B: Chemical and Physical Meteorology, 60, 473–484, 2008.

UCAR/NCAR/CISL/TDD: The NCAR Command Language (Version 6.3.0) [Software], Boulder, Colorado, doi:10.5065/D6WD3XH5, 2016.

Vaughan, A. R., Lee, J. D., Misztal, P. K., Metzger, S., Shaw, M. D., Lewis, A. C., Purvis, R. M., Carslaw, D. C., Goldstein, A. H., Hewitt, C. N., and Others: Spatially resolved flux measurements of NO_x from London suggest significantly higher emissions than predicted by inventories, Faraday Discuss., 189, 455–472, doi:10.1039/c5fd00170f, 2016.

Vautard, R., Honore, C., Beekmann, M., and Rouil, L.: Simulation of ozone during the August 2003 heat wave and emission control scenarios, Atmos. Environ., 39, 2957–2967, doi:10.1016/j.atmosenv.2005.01.039, 2005.

Villena, G., Bejan, I., Kurtenbach, R., Wiesen, P., and Kleffmann, J.: Interferences of commercial NO_2 instruments in the urban atmosphere and in a smog chamber, Atmos. Meas. Tech., 5, 149, doi:10.5194/amt-5-149-2012, 2012.

von Schneidemesser, E., Monks, P. S., Allan, J. D., Bruhwiler, L., Forster, P., Fowler, D., Lauer, A., Morgan, W. T., Paasonen, P., Righi, M., and Others: Chemistry and the linkages between air quality and climate change, Chem. Rev., 115, 3856–3897, doi: 10.1021/acs.chemrev.5b00089, 2015.

von Schneidemesser, E., Bonn, B., Butler, T. M., Ehlers, C., Gerwig, H., Hakola, H., Hellén, H., Kerschbaumer, A., Klemp, D., Kofahl, C., and Others: BAERLIN2014– stationary measurements and source apportionment at an urban background station in Berlin, Germany, Atmos. Chem. Phys., 18, 8621–8645, doi:10.5194/acp-18-8621-2018, 2018.

Wang, J. ., Chew, C., Chang, C., Liao, W., Lung, S. C. C., Chen, W., Lee, P., Lin, P., and Chang, C.: Biogenic isoprene in subtropical urban settings and implications forair quality, Atmos. Environ., 79, 369–379, doi:10.1016/j.atmosenv.2013.06.055, 2013.

Wang, T., Jerrett, M., Sinsheimer, P., and Zhu, Y.: Estimating $PM_{2.5}$-associated mortality increase in California due to the Volkswagen emission control defeat device, Atmos. Environ., 144, 168, doi:10.1016/j.atmosenv.2016.08.074, 2016.

Wang, X., Shen, Z., Cao, J., Zhang, L., Liu, L., Li, J., Liu, S., and Sun, Y.: Characteristics of surface ozone at an urban site of Xi'an in Northwest China, J. Environ. Monit., 14, 116–126, doi:10.1039/c1em10541h, 2012.

Weiß, M., Bonnel, P., Kühlwein, J., Provenza, A., Lambrecht, U., Alessandrini, S., Carriero, M., Colombo, R., Forni, F., Lanappe, G., Lijour, P. L., Manfredi, U., Montigny, F., and Sculati, M.: Will Euro 6 reduce the NO_x emissions of new diesel cars - insights from on-road tests with portable emissions measurement systems (PEMS), Atmos. Environ., 62, 657–665, doi:10.1016/j.atmosenv.2012.08.056, 2012.

WHO: Review of evidence on health aspects of air pollution - REVIHAAP, URL `http://www.euro.who.int/__data/assets/pdf_file/0020/182432/e96762-final.pdf`, last access: 17.7.2018, 2013.

Xu, S., Chen, W., Huang, Y., and He, X.: Responses of growth, photosynthesis and VOC emissions of pinus tabulaeformis carr. exposure to elevated CO_2 and/or elevated O_3 in an urban area, Bull. Environ. Contam. Toxicol., 88, 443–448, doi: 10.1007/s00128-011-0462-1, 2012.

Young, R. F.: Planting the living city: Best practices in planning green infrastructure - Results from major U.S. cities, J. Am. Plann. Assoc., 77, 368–381, doi: 10.1080/01944363.2011.616996, 2011.

Žabkar, R., Honzak, L., Skok, G., Forkel, R., Rakovec, J., Ceglar, A., and Žagar, N.: Evaluation of the high resolution WRF-Chem air quality forecast and its comparison with statistical ozone predictions., Geosci. Model Dev. Discuss., 8, doi:10.5194/gmd-8-2119-2015, 2015.

Zhang, Q., Jimenez, J. L., Canagaratna, M. R., Allan, J. D., Coe, H., Ulbrich, I., Alfarra, M. R., Takami, A., Middlebrook, A. M., Sun, Y. L., Dzepina, K., Dunlea, E., Docherty, K., DeCarlo, P. F., Salcedo, D., Onasch, T., Jayne, J. T., Miyoshi, T., Shimono, A., Hatakeyama, S., Takegawa, N., Kondo, Y., Schneider, J., Drewnick, F., Borrmann, S., Weimer, S., Demerjian, K., Williams, P., Bower, K., Bahreini, R., Cottrell, L., Griffin, R. J., Rautiainen, J., Sun, J. Y., Zhang, Y. M., and Worsnop, D. R.: Ubiquity and dominance of oxygenated species in organic aerosols in anthropogenically-influenced Northern Hemisphere midlatitudes, Geophys. Res. Lett., 34, doi:10.1029/2007GL029979, 2007.

Zhao, H., Chen, X., Hao, S., Jiang, Y., Zhao, J., Zou, C., and Xie, W.: Is the wash-off process of road-deposited sediment source limited or transport limited?, Sci. Total Environ., 563-564, 62–70, doi:10.1016/j.scitotenv.2016.04.123, 2016.

Zhao, L., Lee, X., Smith, R. B., and Oleson, K.: Strong contributions of local background climate to urban heat islands, Nature, 511, 216–219, doi:10.1038/nature13462, 2014.

Zurbenko, I.: The spectral analysis of time series, Elsevier North-Holland, Inc., doi:10.2307/2348176, 1986.

Appendices

A. Contributions to articles

1. **Air quality modelling in the Berlin-Brandenburg region using WRF-Chem v3.7.1: sensitivity to resolution of model grid and input data**
   Friderike Kuik, Axel Lauer, Galina Churkina, Hugo A. C. Denier van der Gon, Daniel Fenner, Kathleen A. Mar and Tim M. Butler
   Geosci. Model Dev., 9, 4339-4363, 2016, doi:10.5194/gmd-9-4339-2016, 2016.

   The topic and focus of the article was formulated in cooperation with Tim Butler and Axel Lauer. Preparation of input data, model simulations and evaluation of model results was done by myself. Hugo Denier van der Gon and Daniel Fenner provided emission input data/observational data. The model results and their interpretation were mainly discussed with Tim Butler and Axel Lauer. The article was written by myself and commented by all co-authors.

2. **Top-down quantification of NO_x emissions from traffic in an urban area using a high resolution regional atmospheric chemistry model**
   Friderike Kuik, Andreas Kerschbaumer, Axel Lauer, Aurelia Lupascu, Erika von Schneidemesser, Tim Butler
   Atmos. Chem. Phys., 18, 8203-8225, doi: 10.5194/acp-18-8203-2018, 2018.

   The topic and focus of the article was formulated in cooperation with Tim Butler, and based on discussions with Andreas Kerschbaumer. Preparation of input data, model simulations and evaluation of model results as well as the observation-based assessment of traffic diurnal cycles was done by myself, the latter in close discussions with Erika von Schneidemesser. An additional sensitivity simulation was done by Aurelia Lupascu. The model results and their interpretation were mainly discussed with Tim Butler. The article was written by myself and commented by all co-authors.

3. **Potential reduction in ambient NO_2 concentrations from meeting diesel vehicle emission standards**
   Erika von Schneidemesser, Friderike Kuik, Kathleen A. Mar and Tim M. Butler
   Environ. Res. Lett. 12, 114025, doi: 10.1088/1748-9326/aa8c84, 2017.

   The topic and focus of the article was formulated by Erika von Schneidemesser, Kathleen Mar and Tim Butler. Preparation of input data, model simulations and evaluation of model results of the high-resolution model setup was done by myself. Simulations for the European model setup were done by Kathleen Mar, and the assessment based on measurements was done by Erika von Schneidemesser. The evaluation and comparison of all results was jointly discussed by all co-authors. The article was mainly written by Erika von Schneidmesser, with contributions from

myself to the parts referring to the high-resolution model setup and comments from all co-authors concerning the whole manuscript.

4. **Effect of VOC Emissions from Vegetation on Air Quality in Berlin during a Heatwave**
   Galina Churkina, Friderike Kuik, Boris Bonn, Axel Lauer, Rüdiger Grote, Karolina Tomiak and Tim M. Butler
   Environ. Sci. Technol., 51, 6120-6130, doi: 10.1021/acs.est.6b06514, 2017.

   The topic and focus of the article was formulated by Galina Churkina. Model simulations for were done by Galina Churkina and myself, and I also supported with the preparation of input data and in-depth discussion of the model setup prior to the simulations. In addition, I contributed with an evaluation of simulated meteorology and chemistry. The article was written by Galina Churkina, with input from myself on the parts describing the model setup. The manuscript was commented by all co-authors.

B. Publication list

B.1. Peer-reviewed publications

1. **Friderike Kuik**, Andreas Kerschbaumer, Axel Lauer, Aurelia Lupascu, Erika von Schneidemesser, Tim M. Butler: *Top-down quantification of NO_x emissions from traffic in an urban area using a high resolution regional atmospheric chemistry model*, Atmos. Chem. Phys., 18, 8203-8225, `https://doi.org/10.5194/acp-18-8203-2018`, 2018.

2. Andrea Mues, Axel Lauer, Aurelia Lupascu, Maheshwar Rupakheti, **Friderike Kuik** and Mark G. Lawrence: *WRF and WRF-Chem v3.5.1 simulations of meteorology and black carbon concentrations in the Kathmandu Valley*, Geosci. Model Dev., 11, 2067-2091, `https://doi.org/10.5194/gmd-11-2067-2018`, 2018.

3. Rebecca D. Kutzner, Erika von Schneidemesser, **Friderike Kuik**, Jörn Quedenau, Elizabeth C. Weatherhead and Julia Schmale: *Long-term monitoring of black carbon across Germany*, Atmos. Environ., 185, 41-52, `https://doi.org/10.1016/j.atmosenv.2018.04.039`, 2018.

4. Erika von Schneidemesser, **Friderike Kuik**, Kathleen A. Mar and Tim M. Butler: *Potential reduction in ambient NO_2 concentrations from meeting diesel vehicle emission standards*, Environ. Res. Lett., 12, 114025, `https://doi.org/10.1088/1748-9326/aa8c84`, 2017.

5. Galina Churkina, **Friderike Kuik**, Boris Bonn, Axel Lauer, Rüdiger Grote, Karolina Tomiak and Tim M. Butler: *Effect of VOC Emissions from Vegetation on Air Quality in Berlin during a Heatwave*, Environ. Sci. Technol., 51, 6120-6130, `https://doi.org/10.1021/acs.est.6b06514`, 2017.

6. **Friderike Kuik**, Axel Lauer, Galina Churkina, Hugo A. C. Denier van der Gon, Daniel Fenner, Kathleen A. Mar and Tim M. Butler: *Air quality modelling in the Berlin-Brandenburg region using WRF-Chem v3.7.1: sensitivity to resolution of model grid and input data*, Geosci. Model Dev., 9, 4339-4363, `https://doi.org/10.5194/gmd-9-4339-2016`, 2016.

7. **Friderike Kuik**, Axel Lauer, J.P. Beukes, P.G. van Zyl, M. Josipovic, V. Vakkari, L. Laakso and G.T. Feig: *The anthropogenic contribution to atmospheric black carbon concentrations in southern Africa: a WRF-Chem modeling study*, Atmos. Chem. Phys., 15, 8809-8830, `https://doi.org/10.5194/acp-15-8809-2015`, 2015.

B.2. Conference and workshop contributions

Oral presentations

- **F. Kuik**, A. Lauer, A. Lupascu, T. M. Butler: *Modelling NO₂ concentrations in the urban area of Berlin/Brandenburg with WRF-Chem: model evaluation and sensitivity to traffic emissions*, oral presentation, 18th WRF Users' Workshop (Boulder, USA, 2017)

- **F. Kuik**, A. Lauer, E. von Schneidemesser, T. M. Butler: *A statistical downscaling approach for roadside NO₂ concentrations: Application to a WRF-Chem study for Berlin*, oral presentation, Geophysical Research Abstracts Vol. 19, EGU2017-11911, EGU General Assembly (Vienna, Austria, 2017)

- **F. Kuik**: *Application of WRF-Chem for simulating urban air quality in the Berlin-Brandenburg region*, invited speaker, WRF-Chem workshop and tutorial (Wageningen, the Netherlands, 2016)

- **F. Kuik**: *Doing disciplinary work in a PhD in an inter- and transdisciplinary environment*, joint IGAC-IASS mini-workshop on "Doing good atmospheric chemistry research in an inter- and transdisciplinary environment" (Potsdam, 2015)

Poster presentations

- **F. Kuik**, A. Lauer, E. von Schneidemesser, T. M. Butler: *The impact of traffic emissions on air quality in the Berlin-Brandenburg region - a case study on cycling scenarios*, poster presentation, Abstract B33H-0723, AGU 2016 Fall Meeting (San Francisco, USA, 2016)

- T. M. Butler, **F. Kuik** (presenter), G. Churkina, H. Denier Van der Gon, D. Fenner, K. A. Mar, A. Lauer: *Air Quality Modeling in the Urban Area of Berlin-Brandenburg with WRF-Chem: Sensitivity to Resolution of Model Grid and Emissions*, poster presentation, Abstract A21C-0039, AGU 2016 Fall Meeting (San Francisco, USA, 2016)

- **F. Kuik**, N. Otero, T. M. Butler: *High resolution simulations of air quality in the Berlin/Brandenburg area: model evaluation, potential applications and need for bias correction*, poster presentation, Berlin-Workshop on Bias Correction in Climate Studies (Berlin, 2016)

- **F. Kuik**, G. Churkina, A. Lauer, K. Mar, T. M. Butler: *High-resolution modeling of urban air quality in the Berlin-Brandenburg region with WRF-Chem: a model eval-*

uation, poster presentation, 10th International Conference on Air Quality - Science and Application (Milan, Italy, 2016)

- **F. Kuik**, G. Churkina, T. M. Butler, A. Lauer, K. A. Mar: *Modeling Urban Air Quality in the Berlin-Brandenburg Region: Evaluation of a WRF-Chem Setup*, poster presentation, Abstract B33E-0776, AGU 2015 Fall Meeting (San Francisco, USA, 2015)

Contributions

- R.D. Kutzner, J. Quedenau, **F. Kuik**, E. von Schneidemesser, J. Schmale: *Analyzing 20 years of Black Carbon measurements in Germany*, oral presentation, Abstract A14A-05, AGU 2016 Fall Meeting (San Francisco, USA, 2016)

- G. Churkina, **F. Kuik**, B. Bonn, A. Lauer, R. Grote, T. M. Butler: *Effect of VOC emissions from vegetation on urban air quality during hot periods*, poster presentation, Geophysical Research Abstracts Vol. 18, EGU2016-7220, EGU General Assembly (Vienna, Austria, 2016)

- R. Kutzner, J. Quedenau, **F. Kuik**, E. von Schneidemesser, J. Schmale: *20 years of Black Carbon measurements in Germany*, poster presentation, Geophysical Research Abstracts Vol. 18, EGU2016-4589, EGU General Assembly 2016 (Vienna, Austria, 2016)

- G. Churkina, **F. Kuik**, A. Lauer, B. Bonn, T. M. Butler: *Effect of heat waves on VOC emissions from vegetation and urban air quality*, poster presentation, Abstract B33E-0777, AGU 2015 Fall Meeting (San Francisco, USA, 2015)

C. Supplementary material of published articles

C.1. Air quality modelling in the Berlin-Brandenburg region using WRF-Chem v3.7.1: sensitivity to resolution of model grid and input data

Geoscientific
Model Development

Supplement of

Air quality modelling in the Berlin–Brandenburg region using WRF-Chem v3.7.1: sensitivity to resolution of model grid and input data

Friderike Kuik et al.

Correspondence to: Friderike Kuik (friderike.kuik@iass-potsdam.de)

S1 Mapping of CORINE land use to USGS land use classes

Table S1. Mapping of CORINE land use to USGS land use classes

CORINE land use type	CORINE id	USGS land use type	USGS id
Continuous urban fabric	1	high intensity residential	32
Discontinuous urban fabric	2	low intensity residential	31
Industry, airports, dump sites, constructions, etc.	3-9	commercial, industry, transport	33
Green urban areas, sport and leisure facilities	10-11	low intensity residential	31
Non-irrigated arable land	12	dryland cropland and pasture	2
Permanently irrigated land, rice fields	13-14	irrigated cropland and pasture	3
Vineyards, fruit/berry/olive plantations	15-17	cropland/woodland mosaic	6
Pastures	18	Dryland cropland and pasture	2
Annual crops, complex cultivation, etc.	19-22	Cropland/woodland mosaic	6
Broad-leaf forest	23	Deciduous broadleaf forest	11
Coniferous forest	24	Evergreen needle leaf forest	14
Mixed forest	25	Mixed forest	15
Natural grasslands	26	Grassland	7
Moors and heathland, sclerophyllos vegetation, etc.	27-29	Mixed shrubland/grassland	9
Beaches, bare rocks, sparse vegetation, burns	30-33	Barren or sparsely vegetated	19
Glaciers and perpetual snow	24	snow or ice	24
Marshes, peat bogs, salines, intertidal flats	35-39	herbaceous wetland	17
Water	40-43	inland water bodies	28
Sea and ocean	44	water bodies	16
Unclassified	48-50	unclassified	0

S2 Supplementary figures and tables
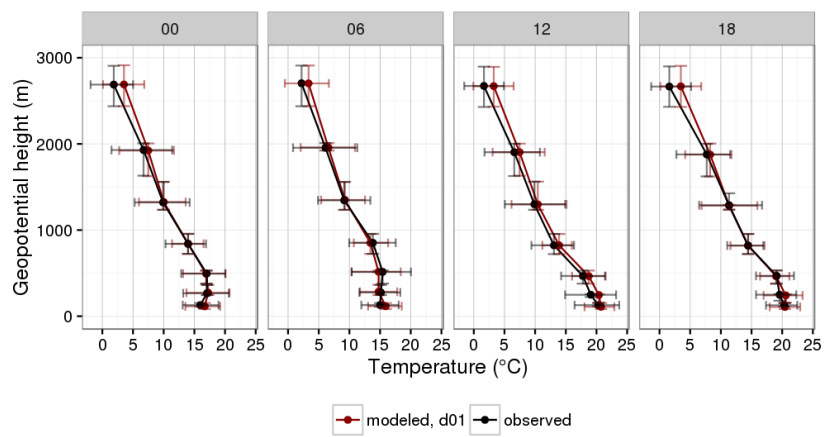
Figure S1. JJA mean profiles of observed and modeled (base run, 15kmx15km horizontal resolution) temperature at Lindenberg at 00:00, 06:00, 12:00 and 18:00 UTC. Error bars show the 25th and 75th percentiles of temperature and geopotential height.
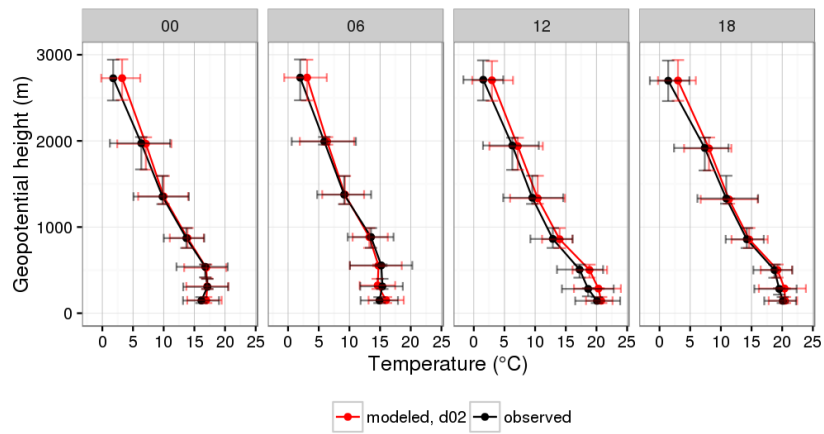
Figure S2. JJA mean profiles of observed and modeled (base run, 3kmx3km horizontal resolution) temperature at Lindenberg at 00:00, 06:00, 12:00 and 18:00 UTC. Error bars show the 25th and 75th percentiles of temperature and geopotential height.
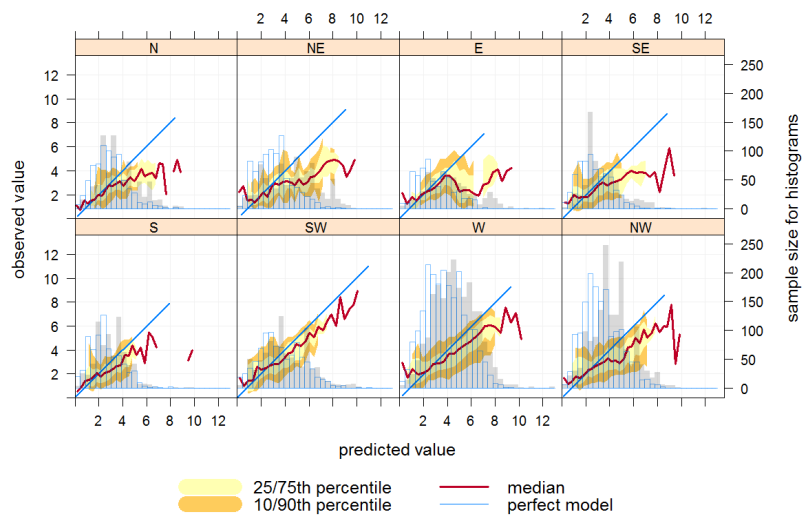
Figure S3. Conditional quantile plot of wind speed, split by modeled wind direction. Observations at Tempelhof, Schöneberg and Tegel are compared to model results extracted for the respective grid cells, 1km horizontal resolution, base run.
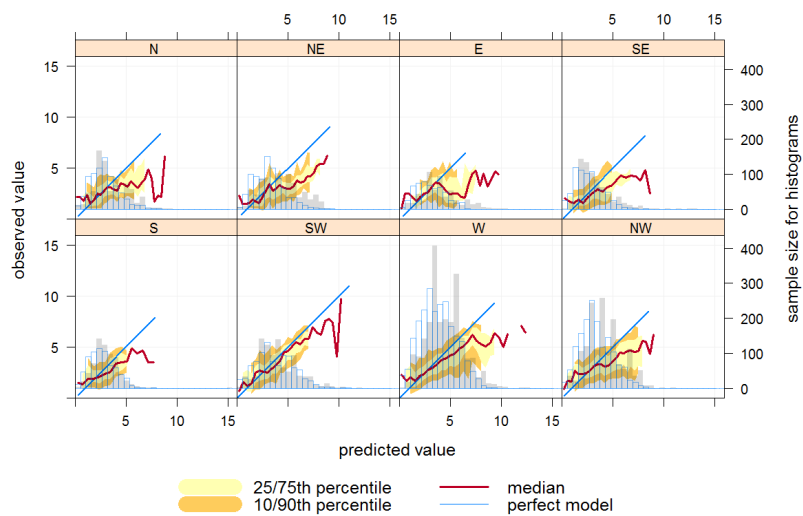
Figure S4. Conditional quantile plot of wind speed, split by modeled wind direction. Observations at Tempelhof, Schöneberg and Tegel are compared to model results extracted for the respective grid cells,1km horizontal resolution, S1_urb.
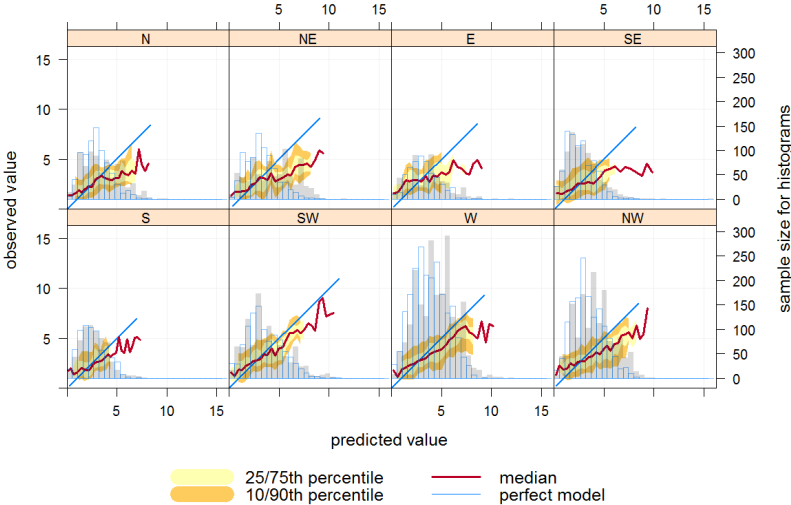
Figure S5. Conditional quantile plot of wind speed, split by modeled wind direction. Observations at Tempelhof, Schöneberg and Tegel are compared to model results extracted for the respective grid cells, 1km horizontal resolution, S2_mos.
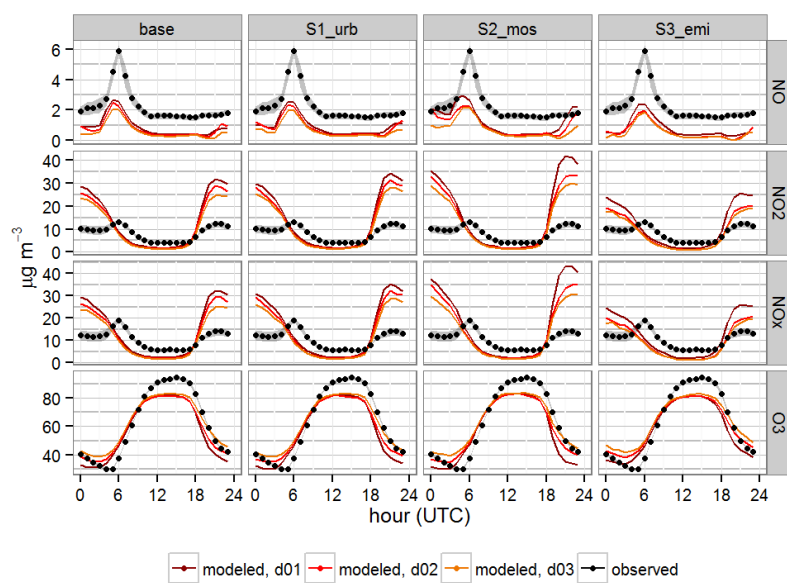
Figure S6. Mean diurnal cycles of NO, NO_2, NO_x and O_3 for all Berlin and Potsdam urban background stations as observed and modeled by the base run, S1_urb, S2_mos and S3_emi. The diurnal cycle is averaged over three stations for NO, NO_2 and NO_x and three stations of O_3. The grey shaded areas represent the variability between the different stations' diurnal cycles, showing 25th and 75th percentiles.
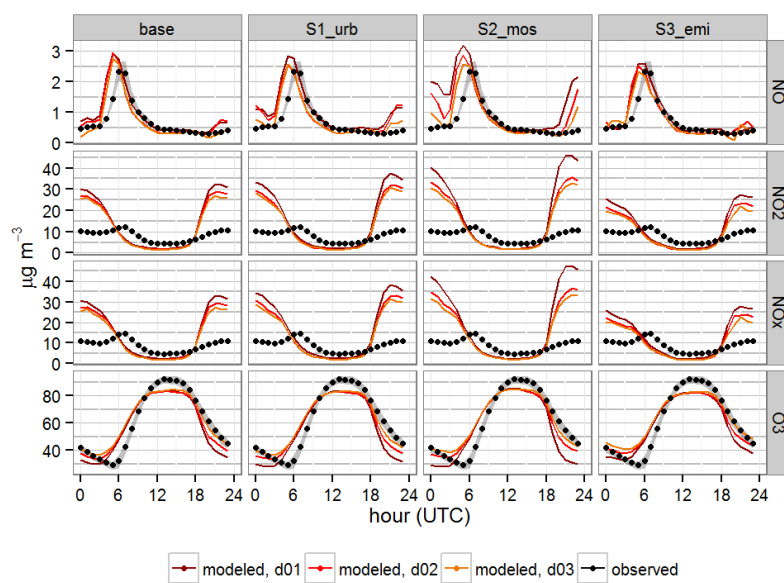
Figure S7. Mean diurnal cycles of NO, NO$_2$, NO$_x$ and O$_3$ for all Berlin and Potsdam urban background stations as observed and modeled by the base run, S1_urb, S2_mos and S3_emi. The diurnal cycle is averaged over four stations for NO, NO$_2$ and NO$_x$ and four stations of O$_3$. The grey shaded areas represent the variability between the different stations' diurnal cycles, showing 25th and 75th percentiles.
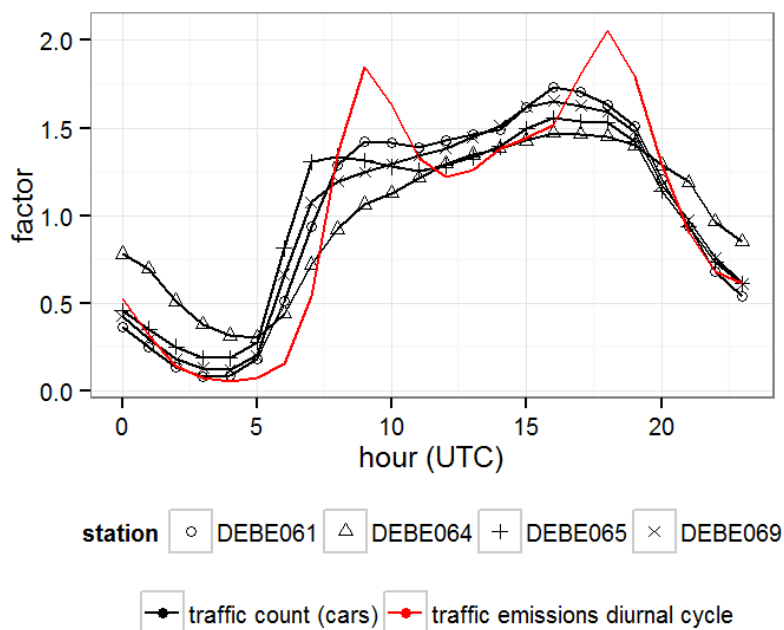
Figure S8. Prescribed diurnal traffic emission factors and factors calculated from JJA 2014 traffic counts at five stations in Berlin, taking into account weekday car traffic in both directions. A factor of one corresponds to the mean over the whole day, a larger factor points to higher emissions/number of cars counted than on average during one day.
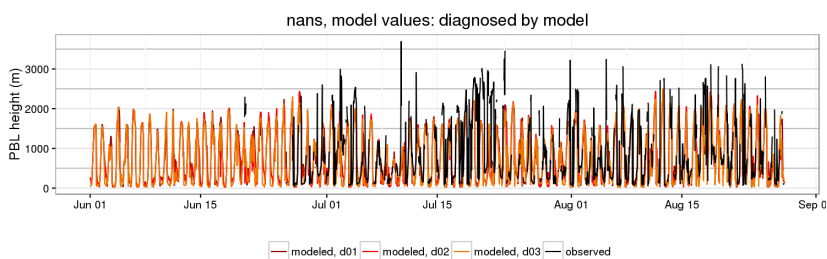
Figure S9. Comparison of modeled PBL height (diagnosed by WRF-Chem) at the Nansenstraße location with the mixing layer height derived from ceilometer observations at Nansenstraße. The results are shown for all three model resolutions (d01 – 15km, d02 – 3km, d03 – 1km).
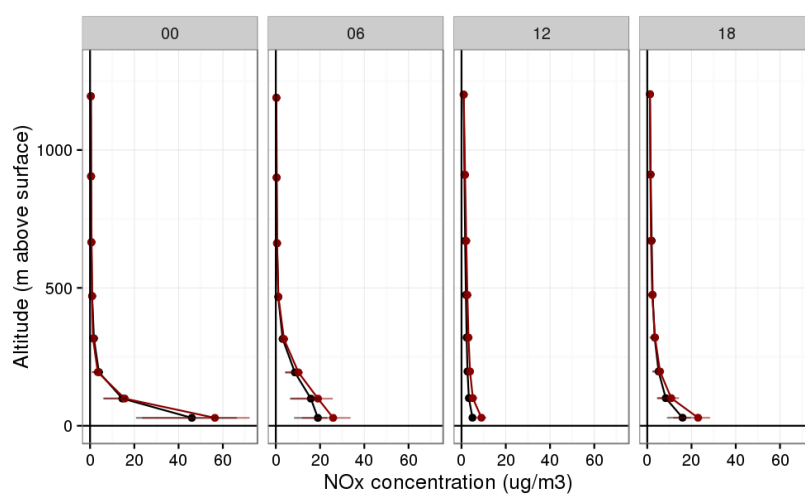
Figure S10. The figure shows mean NO_x profiles in the lower troposphere simulated with a 1kmx1km model resolution at 00:00, 06:00, 12:00 and 18:00 UTC, for the base run (black) and S3 (downscaled emissions, red), for Amrumer Straße. Error bars give the 25th and 75th percentiles.

Table S2. Statistics of hourly 2m temperature for JJA for all stations (top: land use class of the respective grid cell changes with resolution, bottom: same land use class for all three domains). „LU" refers the WRF land use class of the grid cell in the respective domain, „Obs" refers to the JJA observed mean, „Mod" refers to the JJA modeled mean for the respective grid cell. MB is the mean bias for JJA and r is the correlation of hourly values. Obs, Mod and MB are in °C.

Station		LU	Obs	base Mod	MB	r	S1_urb Mod	MB	r	S2_mos Mod	MB	r
kani	d01	31	18.1	19.6	1.5	0.88	19.3	1.2	0.88	19.2	1	0.89
	d02	2	18.1	19.4	1.3	0.9	19.3	1.2	0.9	19.3	1.1	0.89
	d03	2	18.1	19.4	1.2	0.9	19.2	1.1	0.9	19.2	1.1	0.89
marz	d01	2	19.2	18.8	-0.4	0.91	18.7	-0.6	0.9	18.9	-0.4	0.92
	d02	31	19.2	19.6	0.4	0.91	19.4	0.2	0.9	19.2	0	0.9
	d03	31	19.2	19.7	0.4	0.91	19.3	0.1	0.9	19.2	0	0.9
scho	d01	31	18.8	19.6	0.8	0.92	19.3	0.6	0.91	19.2	0.4	0.92
	d02	31	18.8	19.9	1.1	0.91	19.7	0.9	0.91	19.4	0.6	0.91
	d03	2	18.8	19.3	0.6	0.92	19.2	0.4	0.91	19.3	0.6	0.91
temp	d01	31	19.3	19.6	0.3	0.92	19.3	0	0.91	19.3	-0.1	0.92
	d02	33	19.3	20.3	0.9	0.9	19.7	0.4	0.9	19.6	0.3	0.9
	d03	33	19.3	20.2	0.8	0.9	19.6	0.3	0.9	19.5	0.2	0.9
nans	d01	31	20.8	19.6	-1.1	0.91	19.3	-1.4	0.9	19.3	-1.5	0.91
	d02	31	20.8	19.9	-0.9	0.9	19.6	-1.1	0.89	19.6	-1.2	0.9
	d03	32	20.8	20.2	-0.5	0.9	20	-0.8	0.89	19.6	-1.2	0.9
dahf	d01	31	17.9	19.6	1.6	0.88	19.3	1.4	0.89	19.1	1.1	0.9
	d02	14	17.9	19.3	1.4	0.9	19.1	1.2	0.9	19.3	1.4	0.88
	d03	14	17.9	19.2	1.3	0.9	19	1.1	0.9	19.2	1.3	0.88
bamb	d01	31	19.3	19.6	0.4	0.9	19.3	0.1	0.89	19.3	0	0.91
	d02	31	19.3	19.9	0.6	0.89	19.6	0.4	0.88	19.6	0.3	0.9
	d03	32	19.3	20.2	0.9	0.9	19.9	0.7	0.89	19.5	0.2	0.9
botg	d01	31	18.6	19.6	1	0.91	19.3	0.7	0.91	19.3	0.7	0.91
	d02	31	18.6	19.9	1.3	0.91	19.6	1	0.91	19.4	0.8	0.9
	d03	31	18.6	19.8	1.2	0.91	19.5	0.9	0.91	19.3	0.7	0.9
buch	d01	31	18.5	19.5	1	0.9	19.2	0.7	0.9	19.1	0.6	0.9
	d02	31	18.5	19.6	1.1	0.9	19.3	0.8	0.9	19.1	0.6	0.9
	d03	31	18.5	19.5	1	0.9	19.2	0.7	0.9	18.9	0.4	0.9
pots	d01	31	18.5	19.6	1.1	0.91	19.3	0.8	0.91	19.1	0.6	0.92
	d02	31	18.5	19.8	1.3	0.9	19.6	1.1	0.9	19.2	0.7	0.91
	d03	31	18.5	19.7	1.2	0.91	19.5	1	0.9	19.2	0.6	0.9
tege	d01	31	19.1	19.5	0.3	0.92	19.2	0.1	0.91	19.1	0	0.92
	d02	31	19.1	19.9	0.7	0.91	19.6	0.5	0.91	19.5	0.4	0.91
	d03	31	19.1	19.8	0.7	0.91	19.5	0.4	0.91	19.4	0.3	0.91
dest	d01	31	20.1	19.6	-0.4	0.91	19.3	-0.7	0.9	19.3	-0.8	0.91
	d02	31	20.1	20	-0.1	0.9	19.7	-0.4	0.89	19.6	-0.4	0.9
	d03	31	20.1	20	-0.1	0.9	19.6	-0.5	0.89	19.5	-0.5	0.9
roth	d01	31	18.8	19.6	0.8	0.91	19.3	0.5	0.91	19.3	0.4	0.91
	d02	31	18.8	19.9	1	0.91	19.6	0.8	0.9	19.4	0.6	0.9
	d03	31	18.8	19.8	1	0.91	19.5	0.7	0.9	19.3	0.5	0.9
albr	d01	31	18.3	19.6	1.3	0.91	19.3	1	0.91	19.3	0.9	0.91
	d02	31	18.3	19.9	1.5	0.9	19.6	1.3	0.9	19.5	1.1	0.9
	d03	31	18.3	19.9	1.5	0.9	19.5	1.2	0.91	19.3	1	0.9
tier	d01	31	19.1	19.6	0.5	0.91	19.3	0.2	0.9	19.3	0.1	0.91
	d02	31	19.1	19.9	0.8	0.9	19.6	0.5	0.9	19.6	0.4	0.89
	d03	31	19.1	19.9	0.8	0.9	19.6	0.4	0.9	19.5	0.4	0.89

Table S3. Statistics of daily maximum 2m temperature for JJA for all stations (top: land use class of the respective grid cell changes with resolution, bottom: same land use class for all three domains). „LU" refers the WRF land use class of the grid cell in the respective domain, „Obs" refers to the JJA observed mean, „Mod" refers to the JJA modeled mean for the respective grid cell. MB is the mean bias for JJA and r is the correlation of hourly values. Obs, Mod and MB are in °C.

Station		LU	Obs	base Mod	MB	r	S1_urb Mod	MB	r	S2_mos Mod	MB	r
kani	d01	31	24.2	23.8	-0.4	0.88	23.6	-0.6	0.87	23.3	-0.9	0.89
	d02	2	24.2	24.4	0.2	0.9	24.3	0.1	0.87	23.9	-0.3	0.9
	d03	2	24.2	24.3	0.1	0.9	24.2	0	0.87	23.8	-0.4	0.89
marz	d01	2	23.9	23.4	-0.5	0.88	23.2	-0.8	0.86	23	-1	0.9
	d02	31	23.9	24.2	0.2	0.89	24	0	0.87	23.5	-0.4	0.9
	d03	31	23.9	24.1	0.2	0.89	23.9	0	0.87	23.5	-0.5	0.9
scho	d01	31	23.8	23.8	0	0.88	23.6	-0.3	0.87	23.3	-0.5	0.9
	d02	31	23.8	24.4	0.6	0.9	24.3	0.5	0.88	23.8	0	0.91
	d03	2	23.8	24.3	0.5	0.9	24.1	0.3	0.88	23.7	-0.1	0.9
temp	d01	31	24.1	23.8	-0.3	0.88	23.5	-0.6	0.87	23.3	-0.8	0.89
	d02	33	24.1	24.5	0.3	0.9	24.3	0.2	0.87	23.8	-0.3	0.9
	d03	33	24.1	24.4	0.2	0.9	24.2	0	0.87	23.6	-0.5	0.91
nans	d01	31	25.5	23.8	-1.7	0.86	23.5	-1.9	0.85	23.3	-2.2	0.88
	d02	31	25.5	24.4	-1.1	0.87	24.2	-1.3	0.85	23.8	-1.7	0.88
	d03	32	25.5	24.5	-1	0.87	24.2	-1.3	0.85	23.6	-1.8	0.88
dahf	d01	31	23.8	23.7	-0.1	0.89	23.5	-0.3	0.88	23.3	-0.5	0.9
	d02	14	23.8	24.1	0.3	0.9	24	0.2	0.88	23.7	-0.1	0.9
	d03	14	23.8	24	0.2	0.9	23.8	0	0.88	23.5	-0.3	0.9
bamb	d01	31	22.9	23.8	0.9	0.88	23.5	0.7	0.87	23.3	0.4	0.9
	d02	31	22.9	24.4	1.5	0.89	24.2	1.3	0.87	23.8	0.9	0.9
	d03	32	22.9	24.4	1.5	0.9	24.1	1.2	0.87	23.6	0.7	0.9
botg	d01	31	23.6	23.8	0.1	0.89	23.5	-0.1	0.88	23.3	-0.3	0.9
	d02	31	23.6	24.4	0.8	0.9	24.2	0.5	0.88	23.7	0.1	0.9
	d03	31	23.6	24.3	0.6	0.9	24.1	0.4	0.88	23.6	-0.1	0.9
buch	d01	31	23.9	23.6	-0.3	0.89	23.4	-0.6	0.88	23.1	-0.8	0.9
	d02	31	23.9	24.1	0.1	0.9	23.8	-0.1	0.88	23.5	-0.5	0.9
	d03	31	23.9	24	0	0.9	23.7	-0.2	0.87	23.3	-0.6	0.9
pots	d01	31	23.6	23.7	0.2	0.89	23.5	-0.1	0.87	23.3	-0.3	0.89
	d02	31	23.6	24.5	0.9	0.89	24.2	0.7	0.88	23.8	0.2	0.89
	d03	31	23.6	24.3	0.7	0.89	24	0.4	0.87	23.5	0	0.9
tege	d01	31	23.7	23.6	-0.1	0.89	23.4	-0.3	0.87	23.1	-0.6	0.9
	d02	31	23.7	24.4	0.6	0.9	24.2	0.5	0.88	23.7	0	0.9
	d03	31	23.7	24.3	0.6	0.9	24	0.3	0.88	23.5	-0.2	0.9
dest	d01	31	24.2	23.8	-0.4	0.88	23.5	-0.7	0.87	23.3	-0.9	0.9
	d02	31	24.2	24.4	0.2	0.9	24.2	0	0.87	23.8	-0.4	0.9
	d03	31	24.2	24.4	0.2	0.9	24.1	-0.1	0.87	23.7	-0.5	0.9
roth	d01	31	23.5	23.8	0.3	0.89	23.5	0	0.87	23.3	-0.2	0.89
	d02	31	23.5	24.4	0.9	0.89	24.2	0.7	0.88	23.7	0.2	0.9
	d03	31	23.5	24.3	0.8	0.9	24.1	0.6	0.87	23.6	0.1	0.9
albr	d01	31	23.6	23.8	0.8	0.89	23.5	0	0.87	23.3	-0.3	0.89
	d02	31	23.6	24.4	0.8	0.9	24.2	0.6	0.88	23.8	0.2	0.89
	d03	31	23.6	24.3	0.7	0.9	24.1	0.5	0.87	23.6	0.1	0.9
tier	d01	31	24.6	23.8	-0.8	0.88	23.5	-1.1	0.87	23.3	-1.3	0.89
	d02	31	24.6	24.4	-0.2	0.89	24.2	-0.4	0.87	23.8	-0.9	0.89
	d03	31	24.6	24.4	-0.2	0.89	24.1	-0.5	0.86	23.7	-0.9	0.89

Table S4. Statistics of hourly wind speed for JJA. „Obs" refers to the JJA observed mean, „mod" refers to the JJA modeled mean for the respective grid cell. MB is the mean bias for JJA, and r is the correlation of hourly values. Obs, Mod and MB are in ms^{-1}. The statistics are shown for the results from the model domains of 15km (d01), 3km (d02) and 1km (d03) horizontal resolution.

Station		Obs	base Mod	MB	r	S1_urb Mod	MB	r	S2_mos Mod	MB	r
pots	d01	3.6	4.4	0.8	0.51	4	0.4	0.5	3.8	0.2	0.52
	d02	3.6	4.3	0.7	0.5	3.9	0.3	0.48	3.9	0.3	0.51
	d03	3.6	4.3	0.7	0.51	4	0.4	0.48	4	0.4	0.52
scho	d01	3.5	4.4	0.9	0.64	4	0.5	0.59	3.8	0.4	0.67
	d02	3.5	4.3	0.9	0.6	4	0.5	0.57	3.8	0.4	0.65
	d03	3.5	4	0.5	0.62	3.9	0.5	0.58	3.5	0.1	0.65
tege	d01	2.9	4.4	1.5	0.62	3.9	1	0.56	4	1	0.66
	d02	2.9	4.3	1.4	0.6	3.8	0.9	0.58	4.1	1.2	0.65
	d03	2.9	4.2	1.3	0.56	3.9	1	0.56	4.1	1.1	0.66
temp	d01	3.2	4.4	1.1	0.62	3.9	0.6	0.56	3.9	0.6	0.66
	d02	3.2	4.1	0.8	0.57	4.1	0.9	0.54	3.8	0.6	0.63
	d03	3.2	4.1	0.8	0.56	4.2	0.9	0.53	3.8	0.6	0.62

Table S5. Statistics of daily NO$_2$ for JJA. „Obs" refers to the JJA observed mean, „mod" refers to the JJA modeled mean for the respective grid cell. MB is the mean bias for JJA, NMB refers to the normalized mean bias and r is the correlation of hourly values. Obs, Mod and MB are given in µg m^{-3} and NMB is given in %.

St.		Obs	base Mod	MB	NMB	r	S1_urb Mod	MB	NMB	r	S2_mos Mod	MB	NMB	r	S3_emi Mod	MB	NMB	r
froh	d01	7.6	18.6	11.1	146.8	0.56	20.3	12.8	168.8	0.43	23.6	16.1	212.8	0.56	17	9.5	125.3	0.45
	d02	7.6	9.7	2.1	27.8	0.55	10	2.5	32.7	0.49	10.7	3.1	41.1	0.55	7.8	0.3	3.8	0.5
	d03	7.6	9.5	1.9	25.4	0.55	10.1	2.5	33.7	0.5	10.1	2.5	33.7	0.56	7.7	0.1	1.8	0.5
grun	d01	8.6	11.8	3.2	37.6	0.45	12.4	3.9	45.1	0.48	15.5	7	81.4	0.49	8.8	0.2	2.9	0.42
	d02	8.6	15.1	6.6	76.9	0.29	15.8	7.2	84.2	0.4	17.2	8.6	100.6	0.38	11.9	3.3	39.1	0.44
	d03	8.6	15	6.5	75.6	0.26	15.6	7.1	82.7	0.38	17.6	9	105.6	0.33	10.8	2.2	26	0.35
mueg	d01	8.3	13.3	5	60.6	0.41	14.6	6.3	75.5	0.35	16.8	8.5	102.1	0.47	11.5	3.2	38.3	0.37
	d02	8.3	13.6	5.3	63.9	0.4	15.1	6.8	81.3	0.36	15.7	7.4	88.6	0.46	12.4	4.1	49.3	0.33
	d03	8.3	12.8	4.5	53.7	0.45	13.7	5.4	65	0.38	14.5	6.2	74.2	0.49	11.3	3	36.1	0.37
schw	d01	10.8	20.1	9.4	86.9	0.39	21.6	10.8	100.3	0.32	24.6	13.8	128.3	0.46	18.9	8.2	75.7	0.28
	d02	10.8	13.4	2.7	24.7	0.35	14.4	3.6	33.2	0.34	15.3	4.5	42.2	0.45	9.9	-0.9	-8.3	0.19
	d03	10.8	13.3	2.5	23.5	0.36	14.6	3.8	35.5	0.36	15.2	4.4	40.6	0.44	10.7	0	-0.4	0.16
blan	d01	9.5	10.3	0.8	8.7	0.24	10.1	0.7	7.2	0.2	10.3	0.8	8.6	0.23	9.1	-0.3	-3.5	0.16
	d02	9.5	12.2	2.7	28.5	0.19	13	3.5	37.1	0.17	13.9	4.5	47.3	0.27	9.9	0.4	4.4	0.15
	d03	9.5	10.7	1.3	13.5	0.23	11.2	1.7	18	0.16	11.9	2.5	25.9	0.26	8.7	-0.8	-8.1	0.14
buch	d01	8.4	18.6	10.2	121.6	0.59	20.3	11.9	141.4	0.52	23.6	15.2	180.9	0.55	17	8.6	102.3	0.52
	d02	8.4	10.4	2	24.1	0.67	11.7	3.2	38.5	0.63	12.1	3.7	44.2	0.63	9	0.5	6.5	0.64
	d03	8.4	9.8	1.4	16.3	0.67	11.5	3.1	37.2	0.59	11.5	3.1	37.1	0.62	8.5	0.1	0.9	0.63
glie	d01	6.9	11.7	4.8	69.8	0.39	12.4	5.5	79.2	0.46	15.4	8.5	123.6	0.34	8.8	1.9	27.1	0.41
	d02	6.9	14.2	7.3	105.7	0.48	14.2	7.3	106.3	0.53	16.4	9.5	137.3	0.42	8.2	1.3	19.1	0.55
	d03	6.9	12.6	5.7	82.2	0.45	12.7	5.8	84.4	0.5	14.6	7.7	112.1	0.41	8.1	1.2	16.9	0.57
amst	d01	22.6	18.6	-3.9	-17.4	0.68	20.3	-2.3	-10	0.59	23.6	1.1	4.7	0.66	17	-5.5	-24.6	0.6
	d02	22.6	22.2	-0.4	-1.8	0.64	24.4	1.8	8	0.57	25.7	3.1	13.7	0.64	23.2	0.7	3	0.55
	d03	22.6	21.2	-1.4	-6.3	0.64	23.9	1.3	5.8	0.58	25.5	3	13.1	0.62	25	2.4	10.7	0.57
belz	d01	20	20.1	0.2	0.9	0.5	21.6	1.6	8.1	0.41	24.6	4.6	23.2	0.5	18.9	-1	-5.2	0.47
	d02	20	20.5	0.6	2.8	0.46	22.1	2.1	10.7	0.38	23.2	3.2	16.1	0.47	18.8	-1.2	-6.1	0.33
	d03	20	19.3	-0.6	-3.1	0.47	20.9	1	4.8	0.45	22.6	2.6	13.1	0.5	18.2	-1.8	-9	0.33
brue	d01	23.5	20.1	-3.3	-14.2	0.49	21.6	-1.9	-8	0.37	24.6	1.1	4.8	0.47	18.9	-4.5	-19.3	0.44
	d02	23.5	23.9	0.4	1.6	0.59	26	2.5	10.9	0.5	25.4	1.9	8.1	0.57	26.5	3	12.9	0.51
	d03	23.5	22.2	-1.3	-5.5	0.6	24.6	1.1	4.8	0.55	25.1	1.6	6.7	0.59	43.4	19.9	84.9	0.52
nans	d01	21.7	20.1	-1.6	-7.3	0.49	21.6	-0.1	-0.7	0.44	24.6	2.9	13.2	0.53	18.9	-2.8	-12.9	0.5
	d02	21.7	23.9	2.1	9.7	0.57	26	4.3	19.7	0.54	25.4	3.6	16.8	0.62	26.5	4.8	21.9	0.53
	d03	21.7	21.1	-0.6	-2.8	0.54	23.4	1.7	7.8	0.52	24	2.2	10.3	0.61	21	-0.8	-3.6	0.42
pots	d01	13.2	11.7	-1.5	-11.2	0.44	12.4	-0.8	-6.3	0.33	15.4	2.2	17	0.35	8.8	-4.4	-33.5	0.31
	d02	13.2	9.5	-3.7	-27.8	0.41	9.6	-3.5	-26.9	0.29	10.8	-2.4	-18.3	0.36	8.1	-5	-38.2	0.32
	d03	13.2	8.7	-4.5	-34.4	0.4	8.9	-4.3	-32.7	0.29	9.6	-3.6	-27.2	0.34	7.5	-5.7	-43.5	0.33

Table S6. Statistics of daily NO for JJA. „Obs" refers to the JJA observed mean, „mod" refers to the JJA modeled mean for the respective grid cell. MB is the mean bias for JJA, NMB refers to the normalized mean bias and r is the correlation of hourly values. Obs, Mod and MB are given in µg m^{-3} and NMB is given in %.

St.		Obs	base Mod	MB	NMB	r	S1_urb Mod	MB	NMB	r	S2_mos Mod	MB	NMB	r	S3_emi Mod	MB	NMB	r
froh	d01	0.8	1.6	0.8	112.6	0.46	1.7	0.9	122.5	0.35	2.4	1.6	217.5	0.44	1.4	0.6	80.1	0.38
	d02	0.8	0.7	-0.1	-7.5	0.51	0.6	-0.1	-18.7	0.35	0.7	0	-4.1	0.34	0.6	-0.2	-21	0.38
	d03	0.8	0.6	-0.1	-19.5	0.49	0.6	-0.2	-23.5	0.32	0.6	-0.1	-14.8	0.29	0.5	-0.2	-27.2	0.28
grun	d01	0.6	0.7	0.1	16.3	0.22	0.7	0.1	23	0.2	0.9	0.3	59.6	0.29	0.5	-0.1	-12.1	0.28
	d02	0.6	1	0.4	73.3	0.29	1	0.4	70	0.22	1.2	0.7	120.5	0.31	0.9	0.3	61.6	0.32
	d03	0.6	0.8	0.3	46.9	0.27	0.8	0.3	48.3	0.25	1.1	0.5	96	0.25	0.9	0.3	52.6	-0.02
mueg	d01	0.8	0.7	-0.1	-14.2	0.18	0.8	-0.1	-6.3	0.17	0.9	0.1	14.8	0.38	0.7	-0.2	-19.7	0.13
	d02	0.8	0.8	0	0.3	0.06	1.2	0.3	40.8	0.2	1	0.2	23.6	0.47	0.8	0	0.6	0.06
	d03	0.8	0.7	-0.1	-12.7	0.1	1	0.1	15.6	0.21	0.8	0	2.7	0.48	0.8	0	-0.9	0.1
schw	d01	0.9	1.7	0.7	76.1	0.36	1.7	0.8	80	0.33	2.8	1.8	194	0.46	1.6	0.6	64.6	0.3
	d02	0.9	0.7	-0.2	-21.7	0.25	0.9	-0.1	-9.1	0.38	1	0	1.7	0.32	0.6	-0.4	-39.7	0.22
	d03	0.9	0.7	-0.3	-28.1	0.38	0.8	-0.2	-19.3	0.35	0.9	-0.1	-7	0.39	0.6	-0.3	-34.7	0.27
blan	d01	2.4	1.4	-1	-42.2	0.23	1.4	-1	-41.1	0.21	1.5	-0.9	-38.7	0.17	1.4	-1	-42.1	0.17
	d02	2.4	1.4	-1	-40.3	0.14	1.5	-0.9	-36.1	0.38	1.7	-0.7	-30.5	0.23	1.4	-1	-41.5	0.1
	d03	2.4	1.4	-1	-42.9	0.1	1.4	-1	-43.1	0.22	1.5	-0.9	-37.4	0.18	1.4	-1	-43	0.1
buch	d01	2.6	2.7	0.2	6.1	0.4	2.7	0.2	6	0.37	3.4	0.8	32.6	0.4	2.5	-0.1	-3.1	0.34
	d02	2.6	2.3	-0.3	-12.6	0.43	2.3	-0.3	-10.8	0.4	2.4	-0.2	-6.4	0.47	2.3	-0.3	-12.1	0.41
	d03	2.6	2.2	-0.4	-15.7	0.42	2.3	-0.3	-11.7	0.44	2.3	-0.3	-11.9	0.4	2.2	-0.4	-16.1	0.2
glie	d01	1.8	1.5	-0.3	-16.9	0.34	1.5	-0.3	-15.6	0.33	1.7	-0.1	-5.2	0.47	1.4	-0.4	-21.7	0.32
	d02	1.8	1.8	0.1	5.2	0.47	1.8	0.1	3.6	0.37	2.1	0.3	18.3	0.32	1.6	-0.1	-8.4	0.31
	d03	1.8	1.6	-0.1	-7.7	0.5	1.6	-0.1	-7.9	0.38	1.8	0	2.5	0.28	1.5	-0.2	-13.4	0.34
amst	d01	4	1.6	-2.4	-60.1	0.5	1.7	-2.3	-58.2	0.56	2.4	-1.6	-40.4	0.59	1.4	-2.6	-66.2	0.57
	d02	4	2.7	-1.3	-32.4	0.47	2.9	-1	-26.2	0.55	4.2	0.2	5.9	0.45	3.6	-0.4	-9.2	0.61
	d03	4	2.4	-1.6	-40.3	0.39	2.6	-1.4	-34.6	0.4	4	0	-0.3	0.38	4	0	0.5	0.4
belz	d01	3.5	2.7	-0.8	-22.3	0.36	2.7	-0.8	-23.1	0.2	3.7	0.3	8.1	0.48	2.5	-0.9	-26.8	0.21
	d02	3.5	2.7	-0.8	-22.2	0.36	2.8	-0.6	-18.4	0.42	3.8	0.3	8.5	0.39	2.6	-0.9	-24.8	0.06
	d03	3.5	2.6	-0.9	-26	0.3	2.6	-0.9	-25.9	0.4	3.4	-0.1	-2.6	0.43	2.5	-0.9	-26.4	0.11
brue	d01	5.1	2.7	-2.4	-46.9	0.24	2.7	-2.4	-47.5	0.14	3.7	-1.3	-26.1	0.34	2.5	-2.5	-49.9	0.16
	d02	5.1	3.3	-1.8	-35.6	0.35	3.6	-1.4	-27.9	0.31	4.6	-0.4	-8.6	0.45	4	-1.1	-21.8	0.26
	d03	5.1	3.1	-2	-39.4	0.25	3.3	-1.8	-34.6	0.24	4.1	-1	-19.9	0.37	10.8	5.8	113.8	0.32
nans	d01	3.5	1.7	-1.9	-53	0.31	1.7	-1.8	-51.9	0.21	2.8	-0.8	-21.4	0.4	1.6	-2	-56	0.22
	d02	3.5	2.5	-1.1	-29.6	0.39	2.9	-0.6	-17	0.38	3.8	0.3	7.4	0.51	3.5	0	-0.7	0.28
	d03	3.5	2	-1.6	-44.7	0.26	2.2	-1.4	-38.1	0.32	3	-0.6	-16.7	0.42	2.3	-1.3	-36.6	0.11
pots	d01	2.5	1.5	-1.1	-42.6	0.43	1.5	-1.1	-41.7	0.44	1.7	-0.9	-34.5	0.41	1.4	-1.2	-45.9	0.39
	d02	2.5	1.4	-1.2	-45.3	0.4	1.4	-1.2	-45.9	0.32	1.4	-1.1	-43.4	0.4	1.4	-1.1	-45.1	0.34
	d03	2.5	1.3	-1.2	-47.5	0.17	1.3	-1.2	-47.4	0.21	1.4	-1.2	-46.5	0.33	1.4	-1.2	-46.8	0.21

Table S7. Statistics of daily O_3 for JJA. „Obs" refers to the JJA observed mean, „mod" refers to the JJA modeled mean for the respective grid cell. MB is the mean bias for JJA, NMB refers to the normalized mean bias and r is the correlation of hourly values. Obs, Mod and MB are given in $\mu g\,m^{-3}$ and NMB is given in %.

St.		Obs	base Mod	MB	NMB	r	S1_urb Mod	MB	NMB	r	S2_mos Mod	MB	NMB	r	S3_emi Mod	MB	NMB	r
froh	d01	59	54.9	-4	-6.8	0.42	53.6	-5.4	-9.1	0.44	53.6	-5.3	-9	0.42	55.4	-3.5	-6	0.42
	d02	59	61.2	2.3	3.9	0.36	61	2	3.4	0.35	62.2	3.2	5.4	0.39	62.1	3.1	5.3	0.41
	d03	59	62.7	3.8	6.4	0.25	62.2	3.2	5.5	0.29	63.6	4.6	7.9	0.34	63.5	4.6	7.7	0.29
grun	d01	55.4	58.7	3.3	5.9	0.38	58.1	2.7	4.9	0.38	57.6	2.2	4	0.37	60.3	4.8	8.7	0.37
	d02	55.4	58.1	2.6	4.8	0.37	57.6	2.2	4	0.37	58.5	3.1	5.6	0.34	60	4.6	8.2	0.28
	d03	55.4	60.2	4.8	8.7	0.34	59.6	4.2	7.6	0.33	59.9	4.5	8.1	0.26	62.7	7.3	13.2	0.24
mueg	d01	69.2	58.6	-10.5	-15.2	0.53	57.5	-11.7	-16.9	0.56	57.7	-11.4	-16.5	0.59	59.2	-10	-14.4	0.52
	d02	69.2	60.1	-9	-13	0.5	58.9	-10.3	-14.9	0.57	60.2	-9	-13	0.5	60.3	-8.8	-12.8	0.49
	d03	69.2	62.7	-6.4	-9.3	0.45	61.6	-7.5	-10.9	0.5	62.6	-6.5	-9.4	0.44	63	-6.1	-8.8	0.47
schw	d01	65	54.5	-10.5	-16.1	0.5	53.2	-11.8	-18.2	0.52	53.7	-11.3	-17.3	0.48	54.7	-10.3	-15.9	0.48
	d02	65	58.9	-6.1	-9.4	0.53	58.2	-6.8	-10.4	0.59	59	-6	-9.2	0.53	60.8	-4.2	-6.4	0.51
	d03	65	61.9	-3.1	-4.8	0.46	60.8	-4.2	-6.5	0.53	62.1	-2.9	-4.5	0.42	63.1	-1.9	-2.9	0.46
blan	d01	61.9	57.4	-4.6	-7.4	0.56	57.4	-4.5	-7.3	0.61	58.4	-3.5	-5.7	0.57	57.6	-4.3	-7	0.54
	d02	61.9	59.4	-2.5	-4.1	0.55	58.6	-3.3	-5.3	0.62	59.2	-2.7	-4.3	0.53	60.4	-1.5	-2.4	0.52
	d03	61.9	62.5	0.6	1	0.52	62	0	0.1	0.58	62.5	0.6	1	0.47	63.4	1.5	2.3	0.49
buch	d01	64.1	54.9	-9.2	-14.3	0.52	53.6	-10.5	-16.4	0.53	53.6	-10.5	-16.3	0.51	55.4	-8.7	-13.6	0.53
	d02	64.1	60.8	-3.3	-5.2	0.52	60	-4.1	-6.4	0.53	61.2	-2.9	-4.5	0.55	61.4	-2.7	-4.3	0.54
	d03	64.1	63.1	-1	-1.6	0.45	62	-2.1	-3.3	0.47	63.3	-0.9	-1.3	0.52	63.6	-0.5	-0.8	0.49
glie	d01	60.9	58.6	-2.3	-3.8	0.53	58	-2.9	-4.7	0.52	57.5	-3.4	-5.5	0.49	60.1	-0.7	-1.2	0.52
	d02	60.9	57.2	-3.6	-6	0.54	57.3	-3.5	-5.8	0.5	57.4	-3.5	-5.7	0.43	60.8	-0.1	-0.1	0.54
	d03	60.9	60.6	-0.3	-0.4	0.48	60.4	-0.4	-0.7	0.48	60.5	-0.4	-0.7	0.38	63.1	2.2	3.6	0.49
amst	d01	61.7	54.9	-6.8	-11	0.52	53.6	-8.1	-13.2	0.55	53.6	-8.1	-13.1	0.52	55.4	-6.3	-10.2	0.55
	d02	61.7	54.7	-6.9	-11.3	0.48	53.1	-8.6	-14	0.44	55.4	-6.3	-10.3	0.42	54	-7.7	-12.5	0.46
	d03	61.7	57.6	-4.1	-6.6	0.43	55.5	-6.2	-10.1	0.43	57	-4.7	-7.5	0.38	55	-6.7	-10.8	0.43
nans	d01	61.1	54.5	-6.5	-10.7	0.55	53.2	-7.9	-12.9	0.57	53.7	-7.3	-12	0.51	54.7	-6.4	-10.5	0.54
	d02	61.1	54	-7.1	-11.6	0.53	52.5	-8.6	-14.1	0.52	55.9	-5.2	-8.4	0.46	52.1	-8.9	-14.6	0.46
	d03	61.1	58	-3.1	-5.1	0.45	56.1	-5	-8.2	0.47	58.1	-3	-4.9	0.39	57.6	-3.5	-5.7	0.41
pots	d01	64.1	58.6	-5.6	-8.7	0.51	58	-6.1	-9.6	0.52	57.5	-6.6	-10.3	0.45	60.1	-4	-6.2	0.52
	d02	64.1	61.3	-2.8	-4.4	0.5	61.3	-2.9	-4.5	0.48	62.1	-2.1	-3.2	0.46	62.2	-1.9	-3	0.5
	d03	64.1	64.1	0	0	0.46	63.8	-0.4	-0.6	0.45	64.8	0.7	1	0.38	64.6	0.5	0.8	0.45

Table S8. Statistics of daily PM_{10} for JJA. „Obs" refers to the JJA observed mean, „mod" refers to the JJA modeled mean for the respective grid cell. MB is the mean bias for JJA, NMB refers to the normalized mean bias and r is the correlation of hourly values. Obs, Mod and MB are given in $\mu g\,m^{-3}$ and NMB is given in %.

St.		Obs	base Mod	MB	NMB	r	S1_urb Mod	MB	NMB	r	S2_mos Mod	MB	NMB	r	S3_emi Mod	MB	NMB	r
mueg	d01	17.1	8.7	-8.4	-49.1	0.26	8.7	-8.4	-49.3	0.22	8.9	-8.2	-48.1	0.26	7.6	-9.4	-55.3	0.18
	d02	17.1	8.5	-8.6	-50.5	0.31	8.6	-8.5	-49.9	0.26	8.8	-8.3	-48.7	0.26	8.3	-8.7	-51.2	0.28
	d03	17.1	8.2	-8.9	-52.1	0.34	8.3	-8.7	-51.2	0.31	8.5	-8.6	-50.2	0.29	8.2	-8.9	-52.2	0.31
blan	d01	17.1	8.6	-8.5	-49.7	0.38	8.4	-8.7	-50.8	0.33	8.6	-8.5	-49.7	0.41	7.5	-9.6	-55.9	0.24
	d02	17.1	8.6	-8.5	-49.5	0.4	8.7	-8.4	-48.9	0.4	9.1	-8	-46.8	0.4	8.2	-9	-52.3	0.37
	d03	17.1	8.3	-8.8	-51.2	0.43	8.4	-8.7	-50.8	0.45	8.8	-8.3	-48.3	0.42	8	-9.2	-53.5	0.41
buch	d01	18.2	9.1	-9	-49.8	0.36	9.1	-9.1	-49.9	0.33	9.4	-8.8	-48.4	0.36	7.9	-10.3	-56.7	0.3
	d02	18.2	8.2	-10	-54.9	0.4	8.2	-9.9	-54.6	0.36	8.5	-9.6	-53.1	0.33	7.9	-10.3	-56.5	0.39
	d03	18.2	8	-10.1	-55.8	0.42	8.1	-10	-55.2	0.4	8.4	-9.8	-53.9	0.35	7.7	-10.4	-57.3	0.4
glie	d01	14.6	8.6	-6	-41.4	0.38	8.4	-6.1	-42.1	0.38	8.7	-5.9	-40.5	0.4	7.6	-7	-47.9	0.31
	d02	14.6	8.4	-6.1	-42.1	0.46	8.4	-6.2	-42.2	0.45	8.8	-5.8	-39.9	0.42	8	-6.6	-45.4	0.44
	d03	14.6	8.1	-6.4	-44.2	0.49	8.2	-6.4	-43.9	0.49	8.5	-6.1	-41.6	0.46	7.8	-6.8	-46.7	0.47
amst	d01	14.8	9.1	-5.7	-38.4	0.46	9.1	-5.7	-38.6	0.39	9.4	-5.4	-36.7	0.49	7.9	-6.9	-46.9	0.34
	d02	14.8	9.2	-5.6	-37.5	0.51	9.3	-5.5	-37.2	0.45	9.6	-5.2	-35	0.5	9.3	-5.5	-37.4	0.47
	d03	14.8	9	-5.8	-39.2	0.56	9.1	-5.7	-38.4	0.5	9.5	-5.3	-36	0.53	9.1	-5.7	-38.5	0.51
brue	d01	19.4	9.5	-9.8	-50.8	0.37	9.5	-9.9	-51	0.36	9.8	-9.5	-49.2	0.41	8.4	-10.9	-56.6	0.32
	d02	19.4	9.4	-9.9	-51.3	0.43	9.5	-9.8	-50.8	0.39	9.7	-9.7	-49.9	0.37	9.3	-10	-51.7	0.39
	d03	19.4	9.1	-10.2	-52.9	0.47	9.2	-10.1	-52.3	0.44	9.5	-9.9	-51	0.4	9.1	-10.3	-53	0.44
nans	d01	19.1	9.5	-9.6	-50.1	0.37	9.5	-9.6	-50.3	0.36	9.8	-9.2	-48.4	0.39	8.4	-10.7	-55.9	0.31
	d02	19.1	9.4	-9.7	-50.6	0.41	9.5	-9.6	-50.1	0.38	9.7	-9.4	-49.2	0.35	9.3	-9.7	-51	0.38
	d03	19.1	9.1	-10	-52.4	0.45	9.2	-9.9	-51.8	0.43	9.5	-9.6	-50.5	0.4	9.2	-9.9	-51.9	0.43
pots	d01	16.6	8.6	-8	-48.4	0.32	8.4	-8.1	-49	0.29	8.7	-7.9	-47.6	0.32	7.6	-9	-54.1	0.21
	d02	16.6	8.2	-8.4	-50.4	0.36	8.2	-8.4	-50.8	0.35	8.5	-8	-48.5	0.31	8	-8.6	-51.8	0.34
	d03	16.6	8.1	-8.5	-51.3	0.4	8.1	-8.5	-51.4	0.4	8.4	-8.2	-49.5	0.36	7.9	-8.7	-52.5	0.36

Table S9. Statistics of daily $PM_{2.5}$ for JJA. „Obs" refers to the JJA observed mean, „mod" refers to the JJA modeled mean for the respective grid cell. MB is the mean bias for JJA, NMB refers to the normalized mean bias and r is the correlation of hourly values. Obs, Mod and MB are given in $\mu g\,m^{-3}$ and NMB is given in %.

St.		Obs	base Mod	MB	NMB	r	S1_urb Mod	MB	NMB	r	S2_mos Mod	MB	NMB	r	S3_emi Mod	MB	NMB	r
blan	d01	11.2	7.8	-3.4	-30.4	0.47	7.6	-3.6	-32	0.42	7.8	-3.4	-30.1	0.48	6.7	-4.4	-39.8	0.35
	d02	11.2	7.8	-3.4	-30.5	0.48	7.8	-3.3	-29.8	0.46	8.2	-3	-26.6	0.45	7.3	-3.9	-34.7	0.45
	d03	11.2	7.5	-3.7	-33	0.5	7.6	-3.6	-32.3	0.5	8	-3.2	-28.5	0.45	7.1	-4.1	-36.3	0.48
amst	d01	11.6	9.5	-2.1	-18.1	0.26	9.4	-2.3	-19.6	0.1	10.3	-1.4	-12.2	0.08	7.7	-3.9	-33.4	0.17
	d02	11.6	9.7	-1.9	-16.8	0.17	9.9	-1.7	-14.8	0.2	10.6	-1.1	-9.6	0.13	9.8	-1.9	-16.2	0.14
	d03	11.6	9.4	-2.2	-18.8	0.22	9.7	-1.9	-16.7	0.19	10.4	-1.2	-10.6	0.15	9.8	-1.9	-16.4	0.17
brue	d01	12.1	10.2	-2.2	-17.9	0.19	10	-2.3	-19.1	0.02	11	-1.2	-10	0.15	8.6	-3.6	-29.7	0.08
	d02	12.1	9.9	-2.3	-18.7	0.18	10.1	-2.2	-17.9	0.13	10.5	-1.7	-14.3	0.07	9.6	-2.6	-21.8	0.09
	d03	12.1	9.4	-2.7	-22.7	0.17	9.8	-2.4	-19.9	0.15	10.2	-2.1	-17.1	0.1	9.5	-2.8	-23.4	0.13
nans	d01	10.5	8.5	-2.1	-19.6	0.36	8.3	-2.2	-20.7	0.32	8.8	-1.7	-16.6	0.39	7.3	-3.2	-30.6	0.28
	d02	10.5	8.3	-2.2	-21	0.37	8.4	-2.2	-20.4	0.28	8.6	-2	-18.7	0.29	8.1	-2.4	-22.8	0.34
	d03	10.5	8	-2.6	-24.3	0.44	8	-2.5	-23.6	0.35	8.3	-2.2	-20.9	0.32	7.9	-2.6	-25	0.38
pots	d01	10.9	7.7	-3.2	-29.7	0.4	7.6	-3.3	-30.5	0.35	7.8	-3.1	-28.5	0.4	6.7	-4.2	-38.5	0.3
	d02	10.9	7.4	-3.5	-32.6	0.45	7.3	-3.6	-32.9	0.41	7.7	-3.2	-29.7	0.36	7.1	-3.8	-34.8	0.41
	d03	10.9	7.2	-3.7	-34.1	0.47	7.2	-3.7	-33.9	0.44	7.5	-3.4	-31.1	0.4	7	-3.9	-35.9	0.42

S3   Base run namelist

```
&time_control
 start_year = 2014, 2014, 2014
 start_month = 05, 05, 05
 start_day = 30, 30, 30
 start_hour                         = 00, 00, 00,
 start_minute                       = 00, 00, 00,
 start_second                       = 00, 00, 00,
 end_year = 2014, 2014, 2014
 end_month = 08, 08, 08
 end_day = 29, 29, 29
 end_hour                           = 00, 00, 00,
 end_minute                         = 00, 00, 00,
 end_second                         = 00, 00, 00,
 interval_seconds                   = 21600
 input_from_file                    = .true., .true., .true.,
 iofields_filename                  = "iofields_d01.txt", "iofields_d02.txt", "iofields_d03
 history_interval                   = 60, 60, 60,
 frames_per_outfile                 = 24, 24, 24,
 frames_per_auxinput5               =   1, 1, 1,
 restart = .true.
 restart_interval                   = 1440,
 io_form_history                    = 2,
 io_form_input                      = 2,
 io_form_boundary                   = 2,
 debug_level                        = 0,
 auxinput4_inname                   = 'wrflowinp_d<domain>',
 auxinput5_inname                   = 'wrfchemi_d<domain>_<date>',
 auxinput6_inname                   = 'wrfbiochemi_d<domain>',
 auxinput4_interval                 = 360, 360, 360,
 auxinput5_interval_m               = 60, 60, 60,
 io_form_auxinput2                  = 2,
 io_form_auxinput4                  = 2,
 io_form_auxinput5                  = 2,
 io_form_auxinput6                  = 2,
 auxhist3_outname        = "wrfxtrm_d<domain>_<date>",
 auxhist3_interval       = 1440,      1440,      1440,
 frames_per_auxhist3     = 1,         1,         1,
 io_form_auxhist3        = 2,
 write_hist_at_0h_rst               = .true.,

 /

&dfi_control
 /

&domains
```

```
     time_step                   = 75,
     time_step_fract_num         = 0,
     time_step_fract_den         = 1,
     max_dom                     = 3,
 5   e_we                        = 150,  146,  154,
     e_sn                        = 150,  156,  154,
     e_vert                      = 35,        35,        35,
     p_top_requested             = 5000,
     num_metgrid_levels          = 38,
10   eta_levels                  = 1.0,  0.993,  0.983,  0.97,
                                   0.954,  0.934,  0.909,  0.88,  0.845,
                                   0.807,  0.765,  0.719,  0.672,  0.622,
                                   0.571,  0.52,  0.468,  0.42,  0.376,
                                   0.335,  0.298,  0.263,  0.231,  0.202,
15                                 0.175,  0.15,  0.127,  0.106,  0.088,
                                   0.07,  0.055,  0.04,  0.026,  0.013,
                                   0.0,
     num_metgrid_soil_levels     = 4,
     dx                          = 15000,      3000,      1000,
20   dy                          = 15000,      3000,      1000,
     grid_id                     = 1,         2,         3,
     parent_id                   = 1,         1,         2,
     i_parent_start              = 1,        61,        43,
     j_parent_start              = 1,        60,        55,
25   parent_grid_ratio           = 1,         5,         3,
     parent_time_step_ratio      = 1,         5,         3,
     feedback                    = 0,
     smooth_option               = 0,
     /
30
     &physics
      mp_physics                 = 10,       10,       10,
      ra_lw_physics              = 4,        4,        4,
      ra_sw_physics              = 4,        4,        4,
35    radt                       = 15,       15,       15,
      sf_sfclay_physics          = 1,        1,        1,
      sf_surface_physics         = 2,        2,        2,
      bl_pbl_physics             = 1,        1,        1,
      bldt                       = 0,        0,        0,
40    cu_physics                 = 3,        3,        3,
      cu_rad_feedback            = .true.,
      cudt                       = 0,        0,        0,
      isfflx                     = 1,
      icloud                     = 1,
45    num_soil_layers            = 4,
      mp_zero_out                = 2,
      mp_zero_out_thresh         = 1.e-12,
      sf_urban_physics           = 1,        1,        1,
      sst_update                 = 1,
```

```
   sf_urban_physics                = 1,      1,        1,
   usemonalb                       = .true.,
   progn                           = 1,      1,        1,
   cu_diag                         = 1,      1,        1,
 5 num_land_cat                    = 33,
   /

   &fdda
   /
10
   &dynamics
   rk_ord                          = 3,
   w_damping                       = 0,
   diff_opt                        = 1,1,1,
15 km_opt                          = 4,4,4,
   diff_6th_opt                    = 0, 0, 0,
   diff_6th_factor                 = 0.12, 0.12, 0.12,
   base_temp                       = 290.
   damp_opt                        = 0,
20 zdamp                           = 5000.,   5000.,   5000.,
   dampcoef                        = 0.01,    0.01,    0.01
   khdif                           = 0,       0,       0,
   kvdif                           = 0,       0,       0,
   non_hydrostatic                 = .true., .true., .true.,
25 moist_adv_opt                   = 2,       2,       2,
   scalar_adv_opt                  = 2,       2,       2,
   chem_adv_opt                    = 2,       2,       2,
   tke_adv_opt                     = 2,       2,       2,
   time_step_sound                 = 4,       4,       4,
30 h_mom_adv_order                 = 5,       5,       5,
   v_mom_adv_order                 = 3,       3,       3,
   h_sca_adv_order                 = 5,       5,       5,
   v_sca_adv_order                 = 3,       3,       3,
   /
35
   &bdy_control
   spec_bdy_width                  = 5,
   spec_zone                       = 1,
   relax_zone                      = 4,
40 specified                       = .true., .false., .false.,
   nested                          = .false., .true., .true.,
   /

   &grib2
45 /

   &namelist_quilt
   nio_tasks_per_group = 0,
   nio_groups = 1,
```

```
    /

    &chem
    kemit                      = 1,
 5  ne_area                    = 100,
    chem_opt                   = 106, 106, 106,
    bioemdt                    = 15., 15., 15.,
    photdt                     = 15, 15, 15,
    chemdt                     = 2.5, 2.5, 2.5,
10  io_style_emissions         = 2,
    emiss_inpt_opt             = 1, 1, 1,
    emiss_opt                  = 3, 3, 3,
    chem_in_opt                = 1, 1, 1,
    phot_opt                   = 3, 3, 3,
15  gas_drydep_opt             = 1, 1, 1,
    aer_drydep_opt             = 1, 1, 1,
    bio_emiss_opt              = 3, 3, 3,
    gas_bc_opt                 = 1, 1, 1,
    gas_ic_opt                 = 1, 1, 1,
20  aer_bc_opt                 = 1, 1, 1,
    aer_ic_opt                 = 1, 1, 1,
    gaschem_onoff              = 1, 1, 1,
    aerchem_onoff              = 1, 1, 1,
    wetscav_onoff              = 0, 0, 0,
25  cldchem_onoff              = 0, 0, 0,
    vertmix_onoff              = 1, 1, 1,
    chem_conv_tr               = 1, 1, 1,
    seas_opt                   = 2,
    dust_opt                   = 3,
30  biomass_burn_opt           = 0, 0, 0,
    plumerisefire_frq          = 30, 30, 30,
    have_bcs_chem              = .true., .false., .false.,
    aer_ra_feedback            = 1, 1, 1,
    aer_op_opt                 = 1, 1, 1,
35  opt_pars_out               = 1,
    diagnostic_chem            = 1, 1, 1,
    chemdiag                   = 1, 1, 1,
    diagnostic_dep             = 1,1,1,
    /
```

C.2. Top-down quantification of NO$_x$ emissions from traffic in an urban area using a high resolution regional atmospheric chemistry model

Atmospheric
Chemistry
and Physics

Supplement of

Top–down quantification of NO$_x$ emissions from traffic in an urban area using a high-resolution regional atmospheric chemistry model

Friderike Kuik et al.

Correspondence to: Friderike Kuik (friderike.kuik@gmail.com)

S1   Changes to the model code and impact on results

S1.1   Code changes

The WRF-Chem code file dry_dep_driver.F (v.3.8.1) was changed in order to also allow for increased nighttime mixing in grid cells with high emissions in case an urban physics scheme is used (starting from line 685):

```
5        if  ( p_e_co >=  param_first_scalar  ) then
! if (sf_urban_physics .eq. 0 ) then
           if  ( emis_ant ( i , kts , j , p_e_co )  . gt .  0)  then
            ekmfull ( kts : kts +10)  =  max( ekmfull ( kts : kts +10) ,1.)
           endif
10         if  ( emis_ant ( i , kts , j , p_e_co )  . gt .  200)  then
            ekmfull ( kts : kte /2)  =  max( ekmfull ( kts : kte /2) ,2.)
           endif
           if  ( p_e_pm25i >  param_first_scalar  ) then
            if  ( emis_ant ( i , kts , j , p_e_pm25i )+  emis_ant ( i , kts , j , p_e_pm25j )
15          .GT.  8.19e −4∗200)  then
            ekmfull ( kts : kte /2)  =  max( ekmfull ( kts : kte /2) ,2.)
            endif
           endif
           if  ( p_e_pm_25 >  param_first_scalar  ) then
20          if  ( emis_ant ( i , kts , j , p_e_pm_25 )  .GT.  8.19e −4∗200)  then
            ekmfull ( kts : kte /2)  =  max( ekmfull ( kts : kte /2) ,2.)
            endif
! endif
           endif
```

### 25   S1.2   Impact of code changes

Two test simulations illustrate the impact of some of the modifications made to this model setup with respect to Kuik et al., 2016. The differences between the two model simulations shown in this section are the application of the above-described modification or not, and the use of default (TNO) diurnal cycles of traffic emissions and a diurnal cycle calculated based on traffic counts in Berlin. The latter is expected to mainly impact the results during daytime for urban background stations and,
30 to a smaller extent, suburban background stations. The figures show results for simulated and observed NO_2 concentrations.

1
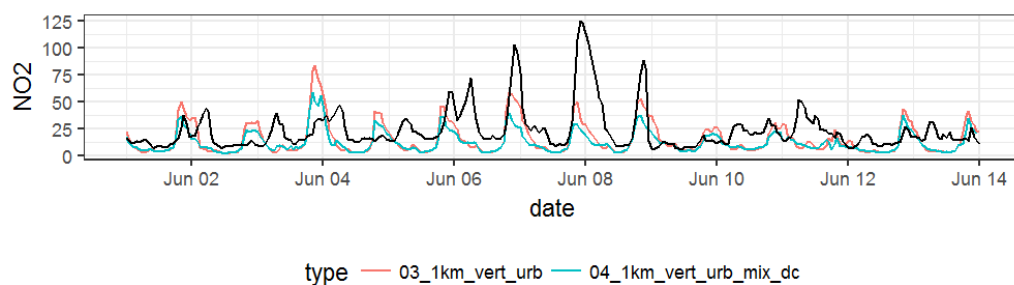
Figure S1. Comparison of modelled NO$_2$ concentrations of simulations without modified mixing routine and default diurnal cycle of traffic emissions (03_1km_vert_urb) and with modified mixing routine and a diurnal cycle of traffic emissions calculated based on traffic counts in Berlin (04_km_vert_urb_mix_dc). The black line shows observations. Results are averaged over all urban background stations used in this study.
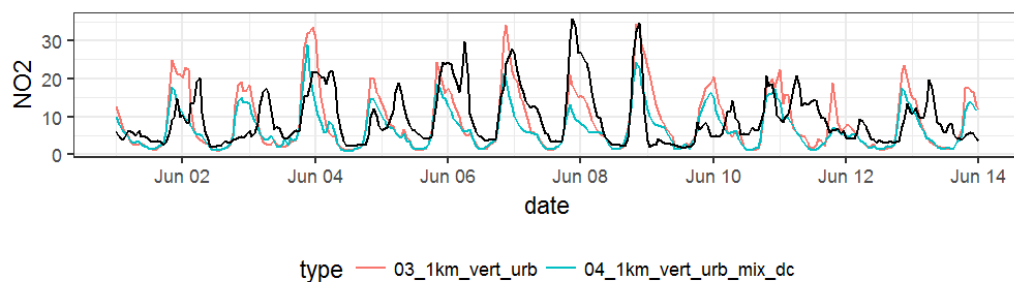
Figure S2. As Fig. S1, but for suburban background stations.
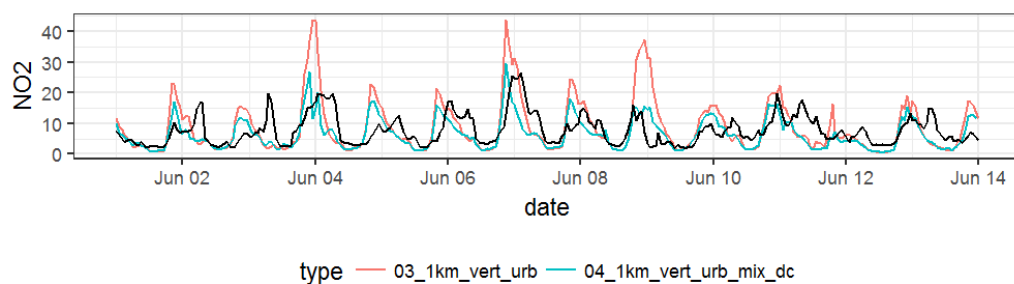
Figure S3. As Fig. S1, but for rural background stations.

S2 Emission processing

S2.1 Downscaling

We used TNO-MACC III emission data and in cooperation with TNO downscaled the data from a horizontal resolution of ca. 7kmx7km to a ca. 1kmx1km. We based the downscaling on proxy data, including population density (Environment Database of the Berlin Senate Department for the Environment, Transport and Climate Protection, Landscan 2010 data), traffic density

for the area of Berlin (Environment Database of the Berlin Senate Department for the Environment, Transport and Climate Protection) and the road network of Brandenburg (OpenStreetMap). Population data is used to downscale emissions from residential combustion (SNAP2) and product use (SNAP6), traffic data is used to downscale emissions from traffic (SNAP 71-75). The 1kmx1km emission grid is defined so that each coarse grid cell of 7kmx7km is divided into 7x7 parts. From each of the proxy datasets a factor is then calculated indicating the proportion of each proxy data type in one high resolution grid cell within one coarse grid cell. These factors are used in order to downscale the respective emissions in the respective area.

**S2.2   Modification of airport emissions for Berlin**

Airport emissions in Berlin, designated by point sources within non-road transport emissions in the TNO-MACC III inventory, are split into airport emissions into emissions on the ground and emissions from the LTO-cycle. We attribute 60% of the emissions to emissions on the ground, and the remaining emissions to emissions from the LTO cycle, where we distribute the emissions equally into all layers below 900m. The LTO-cycle includes emissions from takeoff, landing and aircraft cruise up to ca. 900m. Furthermore, the TNO-MACC III inventory still includes emissions from the Berlin-Tempelhof airport, which has been closed to air traffic in 2008. In addition, emissions from Tegel airport seemed unrealistically larger than emissions from Schönefeld airport. Thus we summed the emissions from all three major airports in the Berlin-Brandenburg region included in the TNO-MACC III inventory and re-distributed them onto the two airports active in 2014, based on activity data, attributing 75% of the emissions to Tegel and 25% to Schönefeld.

S3   Model evaluation

S3.1   Observations

Table S1. Coordinates, names, codes (airbase) and station types of measurement stations used in this paper. Different from what is indicated in the airbase metadata, the station DEBE066 has been defined as suburban background station in this paper, as its characteristics and location are more in line with suburban background conditions in Berlin than with urban background conditions.

Station code	Station name	Station type	Longitude	Latitude
DEBE027	Schichauweg	rural-nearcity background	13.368	52.398
DEBE032	Grunewald	rural-nearcity background	13.225	52.473
DEBE056	Mueggelseedamm	rural-nearcity background	13.647	52.448
DEBE062	Frohnau	rural-nearcity background	13.296	52.653
DEBB075	Gross Glienicke	suburban background	13.124	52.484
DEBB086	Blankenfelde-Mahlow	suburban background	13.424	52.35
DEBE051	Buch	suburban background	13.49	52.644
DEBE066	J. u. W. Brauer Platz	suburban background	13.53	52.485
DEBE010	Amrumer Str.	urban background	13.349	52.543
DEBE018	Belziger Str.	urban background	13.349	52.486
DEBE034	Nansenstr.	urban background	13.431	52.489
DEBE068	Brueckenstr.	urban background	13.419	52.514
DEBE061	Schildhornstr.	urban traffic	13.318	52.464
DEBE063	Silbersteinstr	urban traffic	13.442	52.468
DEBE064	Karl Marx Str.	urban traffic	13.434	52.482
DEBE065	Frankfurter Allee	urban traffic	13.47	52.514
DEBE069	Mariendorfer Damm	urban traffic	13.388	52.438
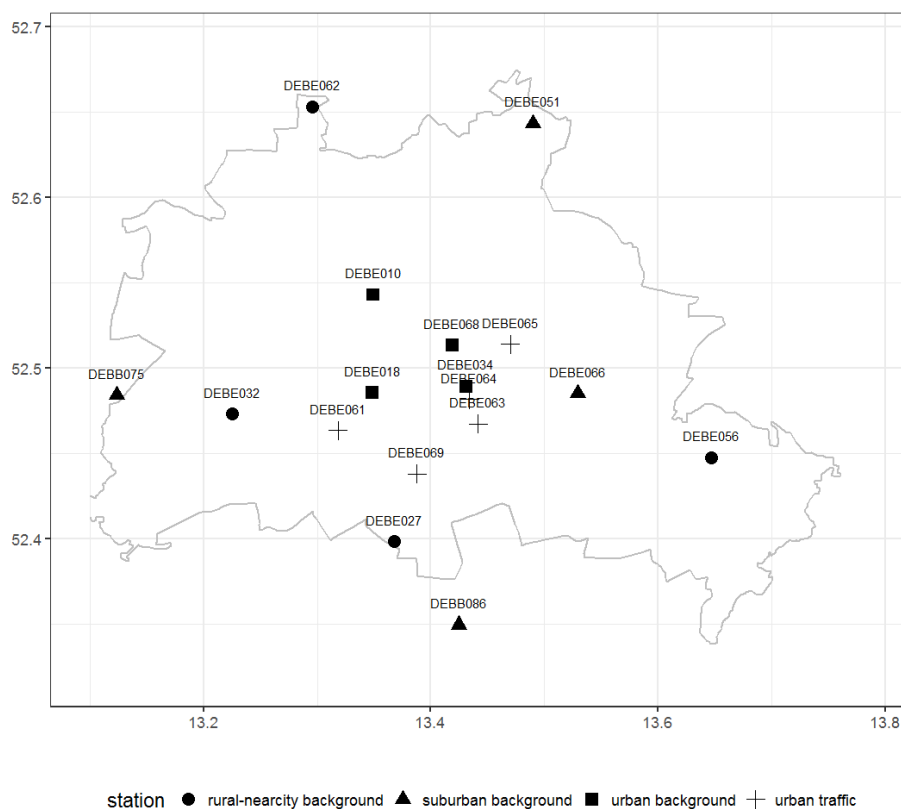
Figure S4. Locations of measurement stations used in this paper including their station type and airbase code.

S3.2 Statistical indicators

The statistical indicators used in this study include the mean bias (MB), normalized mean bias (NMB), root mean square error (RMSE) and Pearson correlation coefficient (R) and are defined as follows, with the model results M, observations O, number of model-observations pairs N and standard deviation σ:

$$MB \quad = \quad \sum_{i=1}^{N}(M_i - O_i) \tag{1}$$

$$NMB \quad = \quad \frac{\sum_{i=1}^{N}(M_i - O_i)}{\sum_{i=1}^{N} O_i} \tag{2}$$

$$RMSE \quad = \quad \sqrt{\frac{1}{N}\sum_{i=1}^{N}(M_i - O_i)} \tag{3}$$

$$R \quad = \quad \frac{\frac{1}{N}\sum_{i=1}^{N}(M_i - \overline{M})(O_i - \overline{O})}{\sigma_M \sigma_O} \tag{4}$$

S3.3   Additional model performance indicators

In addition to the model quality objective (MQO), performance indicators for the mean bias and normalized mean bias are indicated in the manuscript and defined as follows, following Pernigotti et al. (2013):

$$|NMB| \quad < \quad \frac{2RMS_U}{\overline{O}} \tag{5}$$

$$|MB| \quad < \quad 2U(\overline{O}) \tag{6}$$

With the root mean square of the measurement uncertainty

$$RMS_U \quad = \quad \sqrt{\frac{1}{N}\sum_{i=1}^{N} U_{O_i}^2} \tag{7}$$

and $U(\overline{O})$ the uncertainty of the mean of the observed time series.

S4   Spectral decomposition

Observed and modelled time series are spectrally decomposed into a long term (LT), synoptic (SY), diurnal (DU) and intra-diurnal (ID) component, following Hogrefe et al. (2000), and Galmarini et al. (2013). A Kolmogorov-Zurbenko filter $kz_{m,k}$ was used with the time windows m and smoothing parameter k, time series x and time t:

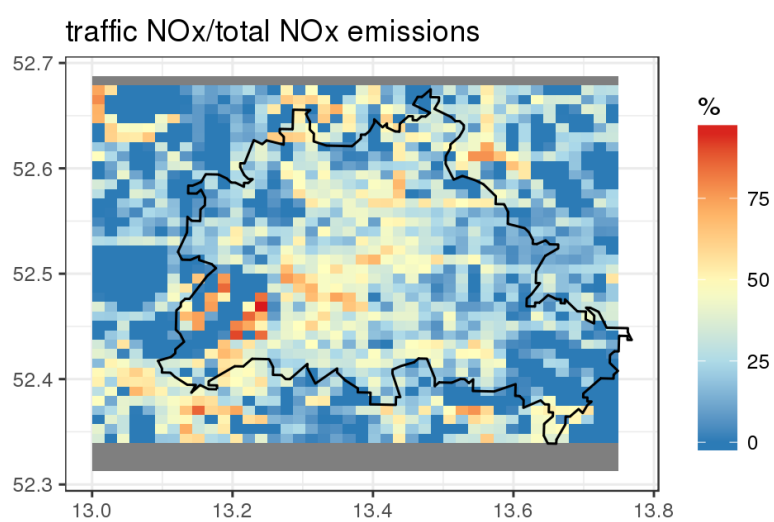$$ID(t) \quad = \quad x(t) - kz_{3,3}(x(t)) \tag{8}$$

$$DU(t) \quad = \quad kz_{3,3}(x(t)) - kz_{13,5}(x(t)) \tag{9}$$

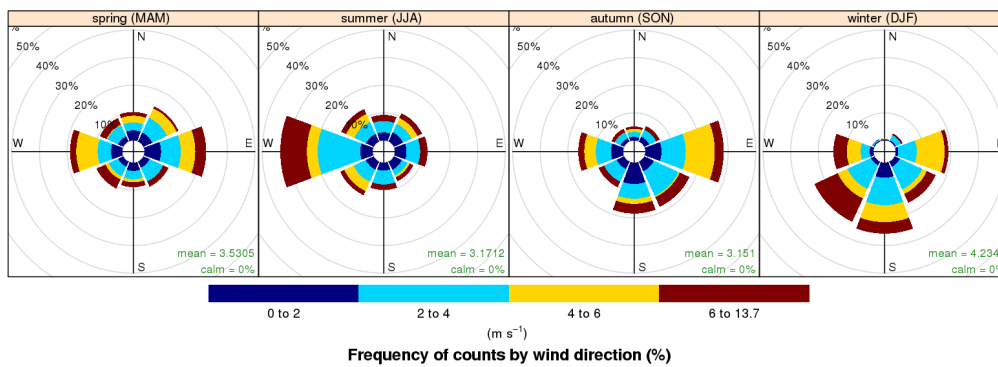$$SY(t) \quad = \quad kz_{13,5}(x(t)) - kz_{103,5}(x(t)) \tag{10}$$

$$LT(t) \quad = \quad kz_{103,5}(x(t)) \tag{11}$$

The decomposition was done in R, using the library *kza*.

S5   Supplementary figures

Figure S5. Contribution of traffic NOx emissions to total annual surface NOx emissions in the Berlin-Brandenburg area, based on the downscaled version of TNO-MACC III.

Figure S6. Wind rose showing the frequency distribution of wind speed and direction for the Berlin DWD stations, observations.
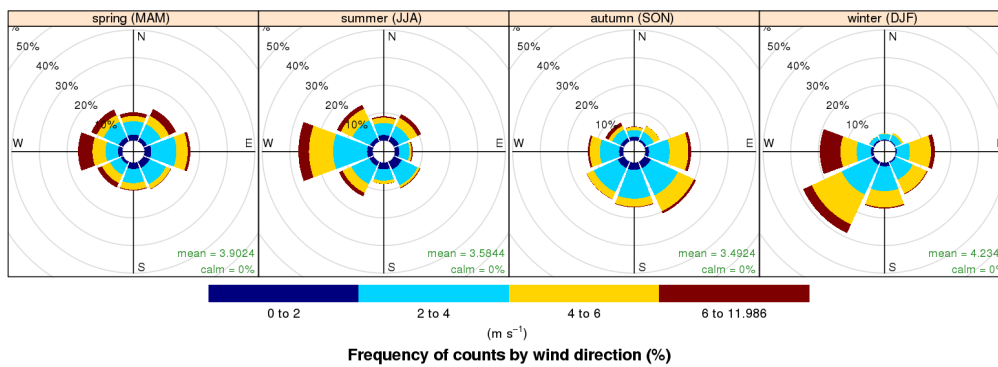
Figure S7. Wind rose showing the frequency distribution of wind speed and direction for the Berlin DWD stations, model results.
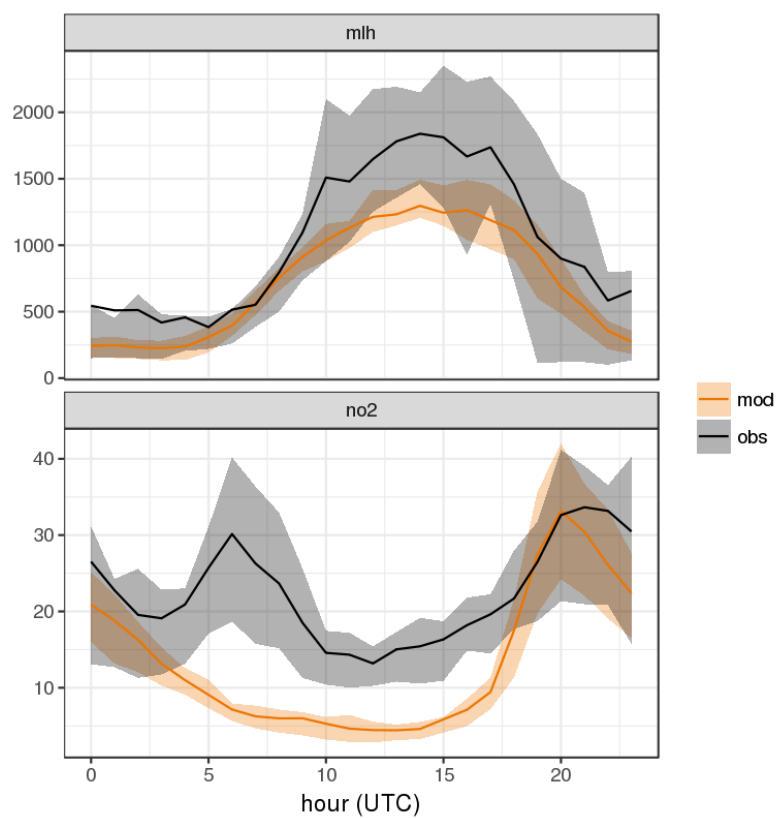
Figure S8. Mean diurnal cycles of observed (obs) and modelled (mod) mixing layer height (MLH) and NO₂ concentrations at Nansenstraße. All data are only averaged over times when MLH observed with a ceilometer is available. This includes between 24-57 hourly values between 20 June and 27 August 2014. The shaded areas show the 25th and 75th percentiles of the data. MLH is given in m, NO₂ concentrations are given in μg m^{-3}.
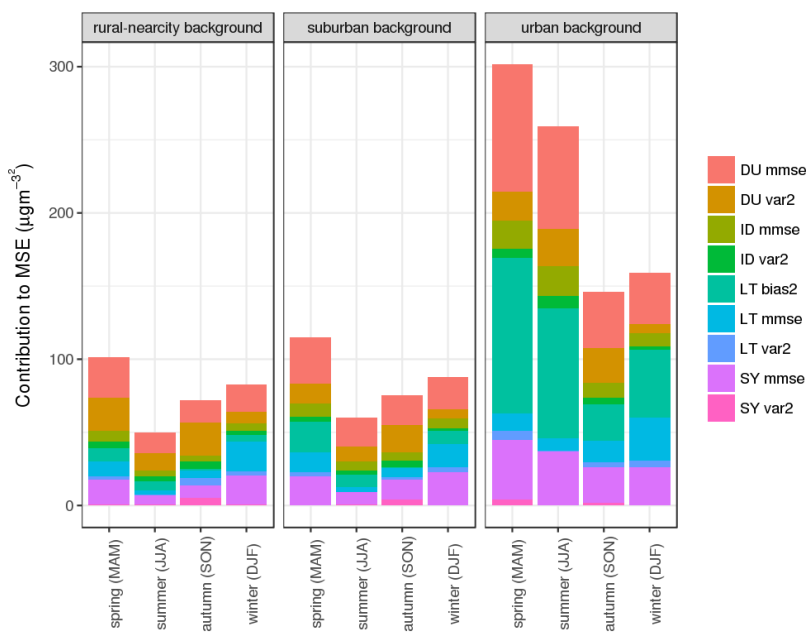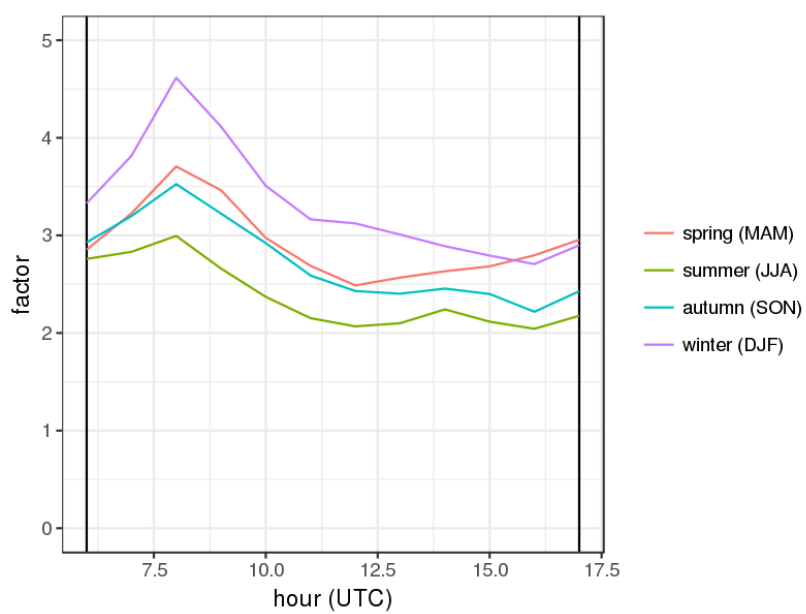
Figure S9. Contribution to mean square error of model results per season and station class.

Figure S10. Time- and season-dependent NO$_x$-emission correction factor.

C.3. Potential reduction in ambient NO$_2$ concentrations from meeting diesel vehicle emission standards

Supplementary Information:

Potential reductions in ambient NO$_2$ concentrations from meeting diesel vehicle emissions standards

Erika von Schneidemesser*, Friderike Kuik, Kathleen A. Mar, Tim Butler

S1. Model Simulations

S1.1. European simulations

The setup for the European simulation has been described in Mar et al. (2016) with a small number of changes, described here. The horizontal resolution was 22.5 km x 22.5 km; the model domain had 230 and 186 grid points in the west-east and south-north directions, respectively. Given the short duration of the simulation, no four-dimensional data assimilation was applied. Emissions for the base simulation were taken from the TNO-MACCIII inventory for 2011 and prepared as described in Mar et al. (2016), except that all emissions were emitted at the surface rather than into higher vertical levels, as the model results for this setup showed little sensitivity to the distribution of emissions above the surface layer (see Mar et al, 2016).For the US EPA scenario, NO$_x$ emissions were calculated as described in Section 2.4, namely, the reduction factor for going from HBEFA to US EPA emission factors for LDVs was applied to diesel exhaust emissions for road transport based on the ratio of LDVs to LDVs+HDVs for each country (Kuenen, 2015). Application of these diesel LDV emission reductions led to a reduction of domain-total NOx emissions of 12% for the US EPA scenario compared to the base scenario. WRF-Chem simulations were performed using both the MOZART-4 and RADM2 gas-phase chemical mechanisms. In the text results from the simulations done with the RADM2-mechanism are discussed to parallel the Berlin simulations. Results from both mechanisms are presented in Table 3.

S1.2. Berlin simulations

The setup focusing on the greater Berlin area is described in Kuik et al., (2016), and uses the same settings as the European simulations, limited to the RADM2 chemical mechanism. The setup has three nested domains with 15 km x 15 km, 3 km x 3 km and 1 km x 1 km horizontal resolution. The coarsest domain covers large parts of Europe, but only the results from the 1 km x 1 km domain covering the greater Berlin area are discussed here. Results at this resolution should be considered representative of the urban background environment for urban areas. A consistency check showed that the results from the 15 km x 15 km domain are consistent with the results obtained with the European simulation setup. As the setup is focused on the urban area of Berlin, it includes three urban land use classes as well as updated input parameters to the urban scheme (Kuik et al., 2016). In order to match the resolution of the emission input data with the model resolution, the emissions for Berlin were downscaled to a horizontal resolution of ca. 1 km as described in Kuik et al., (2016). In addition, the emissions were distributed vertically into seven model layers. The setup mainly covers Germany and thus the fraction of diesel LDV in Germany (43%) has been used in the US EPA scenario simulation.

Table S1. Summary of WRF-Chem model simulations for the European simulation and the Berlin simulation.

	European simulations	Berlin simulations
Main reference	Mar et al., 2016	Kuik et al., 2016
Chemical mechanism	MOZART and RADM2	RADM2
Horizontal resolution	22.5 km x 22.5 km	15 km x 15 km 3 km x 3 km 1 km x 1 km
Emissions	TNO-MACC III (7 km x 7 km hor. res.) No vertical distribution	TNO-MACC III (7 km x 7 km hor. res.) Distributed vertically into 7 model layers Downscaled to 1 km x 1 km over 1 km x 1 km domain
EPA scenario emissions	Using country-specific LDV/HDV ratios (TNO – add reference)	Using LDV/HDV ratio for Germany (TNO – add reference)
Urban processes		Single-layer urban canopy model with modified input parameters (Kuik et al., 2016) 3 urban land use categories
Further changes with respect to main reference	No FDDA applied	Using physics options of Mar et al., 2016

Table S2. Comparison of modeled (Berlin simulation, 1km x 1km resolution) and measured surface NO_2 concentrations. The statistics include the mean bias and normalized mean bias over the whole month of July 2011, as well as the correlation coefficient (R) of daily mean NO_2 concentrations. FAC2 denotes the fraction of modeled concentrations within a factor of 2 of the observations.

Station	Code	Mean bias (ug/m3)	Normalized mean bias (%)	R	FAC2 (%)
Urban background					
Amrumer Str.	DEBE010	-6.1	-31	0.63	77
Belziger Straße	DEBE018	-4.1	-23	0.74	90
Brückenstraße	DEBE068	-5.5	-28	0.44	80
Johanna und Willi Brauer Platz	DEBE066	-3.4	-25	0.06	80
Nansenstraße	DEBE034	-6.5	-30	0.56	84
Suburban/rural background					
Buch	DEBE051	-0.05	-1	0.56	77
Grunewald	DEBE032	0.4	6	0.50	90
Müggelseedamm	DEBE056	-0.2	-3	0.13	87
Frohnau	DEBE062	-0.4	-5	0.44	71

*S2. Observation-based calculations*

Table S3. Estimated reduction in ambient concentrations of daily mean NO_2 at the roadside and for the urban background of Berlin from the observation-based calculations. Estimates for both the national and city level fraction of LDV diesel are included. Values are (top) monthly average daily mean values and (bottom) annual average daily mean values, both with standard deviation. All units are in $\mu g\ m^{-3}$.

	National fleet (43% LDV)		City fleet (80% LDV)	
	Roadside	Urban background	Roadside	Urban background
	Monthly Average (July)			
Euro 5	10 ± 2.5	1.3 ± 0.43	19 ± 4.6	2.3 ± 0.80
Euro 6 (conformity factor, Sept 2017)	11 ± 2.5	1.3 ± 0.44	20 ± 4.6	2.4 ± 0.81
Euro 6	12 ± 2.9	1.5 ± 0.50	23 ± 5.3	2.7 ± 0.94
US EPA	14 ± 3.3	1.6 ± 0.53	26 ± 6.2	2.9 ± 0.99
	Monthly Average (January)			
Euro 5	8.3 ± 2.3	0.94 ± 0.49	15 ± 4.3	1.7 ± 0.92
US EPA	11 ± 3.1	1.1 ± 0.60	21 ± 5.8	2.1 ± 1.1
	Annual Average			
Euro 5	9.0 ± 2.8	1.2 ± 0.65	17 ± 5.2	2.2 ± 1.2
Euro 6 (conformity factor, Sept 2017)	9.1 ± 2.8	1.2 ± 0.66	17 ± 5.2	2.2 ± 1.2
Euro 6	11 ± 3.2	1.4 ± 0.76	20 ± 6.0	2.6 ± 1.4
US EPA	12 ± 3.8	1.5 ± 0.80	23 ± 7.0	2.7 ± 1.5

Table S4. The relationship between NO_2 and NOx concentrations. The slope of the linear fit (NO_2:NOx) and r^2 values are provided.

	Site type	Slope	r^2
Annual		0.35	0.88
July	traffic	0.48	0.94
January		0.31	0.90
Annual	urban background	0.55	0.85
July		0.82	0.98
January		0.56	0.89

Figure S1. Hourly NOx versus NO$_2$ concentrations in µg m^{-3} by site type for July 2014. Station names are listed in the legend. Linear fits to the lines shown are included in Table S4.
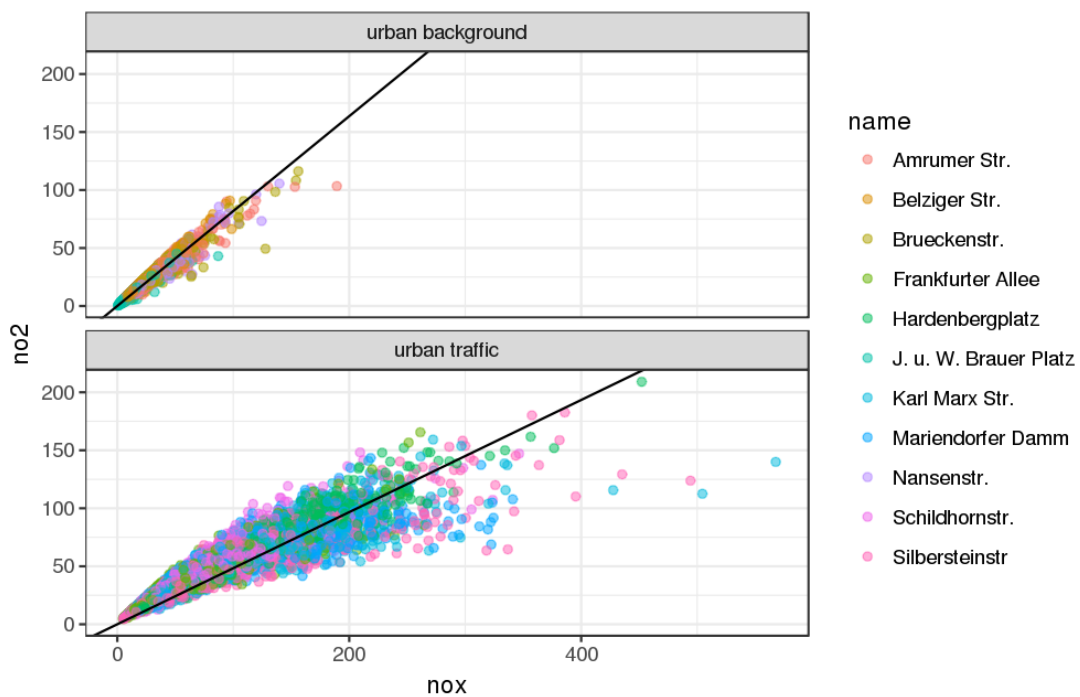
C.4. Effect of VOC emissions from vegetation on air quality in Berlin during a heatwave

The supplementary material can be found online: `https://pubs.acs.org/doi/suppl/10.1021/acs.est.6b06514`.

D. Technical Appendix

D.1. Most recent namelist

```
&time_control
 start_year = 2014, 2014, 2014
 start_month = 02, 02, 02
 start_day = 06, 06, 06
 start_hour                            = 00, 00, 00,
 start_minute                          = 00, 00, 00,
 start_second                          = 00, 00, 00,
 end_year = 2014, 2014, 2014
 end_month = 02, 02, 02
 end_day = 08, 08, 08
 end_hour                              = 00, 00, 00,
 end_minute                            = 00, 00, 00,
 end_second                            = 00, 00, 00,
 interval_seconds                      = 21600
 input_from_file                       = .true., .true., .true.,
 history_interval                      = 60, 60, 60,
 frames_per_outfile                    = 24, 24, 24,
 frames_per_auxinput5                  =   1, 1, 1,
 restart = .true.
 restart_interval                      = 2880,
 io_form_history                       = 2,
 io_form_input                         = 2,
 io_form_boundary                      = 2,
 debug_level                           = 0,
 auxinput4_inname                      = 'wrflowinp_d<domain>',
 auxinput5_inname                      = 'wrfchemi_d<domain>_<date>',
 auxinput6_inname                      = 'wrfbiochemi_d<domain>',
 auxinput4_interval                    = 360, 360, 360,
 auxinput5_interval_m                  = 60, 60, 60,
 io_form_auxinput2                     = 2,
 io_form_auxinput4                     = 2,
 io_form_auxinput5                     = 2,
 io_form_auxinput6                     = 2,
 history_outname              = "wrfout_d<domain>_<date>",
```

```
 auxhist3_outname          = "wrfxtrm_d<domain>_<date>",
 auxhist3_interval         = 1440,      1440,      1440,
 frames_per_auxhist3       = 1,         1,         1,
 io_form_auxhist3          = 2,
 write_hist_at_0h_rst                   = .true.,

/

&dfi_control
/

&domains
 time_step                 = 90,
 time_step_fract_num       = 0,
 time_step_fract_den       = 1,
 max_dom                   = 2,
 e_we                      = 150,  146,  154,
 e_sn                      = 150,  156,  154,
 e_vert                    = 35,          35,          35,
 p_top_requested           = 5000,
 num_metgrid_levels        = 38,
 eta_levels                = 1.0,  0.993,  0.983,  0.97,
                0.954,  0.934,  0.909,  0.88,  0.845,
                0.807,  0.765,  0.719,  0.672,  0.622,
                0.571,  0.52,  0.468,  0.42,  0.376,
                0.335,  0.298,  0.263,  0.231,  0.202,
                0.175,  0.15,  0.127,  0.106,  0.088,
                0.07,  0.055,  0.04,  0.026,  0.013,
                0.0,
 num_metgrid_soil_levels   = 4,
 dx                        = 15000,      3000,      1000,
 dy                        = 15000,      3000,      1000,
 grid_id                   = 1,          2,          3,
 parent_id                 = 1,          1,          2,
 i_parent_start            = 1,          61,          43,
 j_parent_start            = 1,          60,          55,
 parent_grid_ratio         = 1,          5,          3,
 parent_time_step_ratio    = 1,          5,          3,
```

```
feedback                          = 0 ,
smooth_option                     = 0 ,
/

&physics
 mp_physics                                = 10 ,      10 ,      10 ,
 ra_lw_physics                             = 4 ,       4 ,       4 ,
 ra_sw_physics                             = 4 ,       4 ,       4 ,
 radt                                      = 15 ,      15 ,      15 ,
 sf_sfclay_physics                         = 5 ,       5 ,       5 ,
 sf_surface_physics                        = 2 ,       2 ,       2 ,
 bl_pbl_physics                            = 6 ,       6 ,       6 ,
 bldt                                      = 0 ,       0 ,       0 ,
 cu_physics                                = 3 ,       3 ,       3 ,
 cu_rad_feedback                           = .true. ,
 cudt                                      = 0 ,       0 ,       0 ,
 isfflx                                    = 1 ,
 icloud                                    = 1 ,
 num_soil_layers                           = 4 ,
 mp_zero_out                               = 2 ,
 mp_zero_out_thresh                        = 1.e−12 ,
 sf_urban_physics                          = 1 ,       1 ,       1 ,
 sst_update                                = 1 ,
 sf_urban_physics                          = 1 ,       1 ,       1 ,
 usemonalb                                 = .true. ,
 progn                                     = 1 ,       1 ,       1 ,
 cu_diag                                   = 1 ,       1 ,       1 ,
 num_land_cat                              = 33 ,
/

&fdda
/

&dynamics
rk_ord                            = 3 ,
w_damping                         = 0 ,
diff_opt                          = 1 ,1 ,1 ,
km_opt                            = 4 ,4 ,4 ,
```

```
diff_6th_opt                          = 0, 0, 0,
diff_6th_factor                       = 0.12, 0.12, 0.12,
base_temp                             = 290.
damp_opt                              = 0,
zdamp                                 = 5000.,   5000.,   5000.,
dampcoef                              = 0.01,    0.01,    0.01
khdif                                 = 0,       0,       0,
kvdif                                 = 0,       0,       0,
non_hydrostatic                       = .true., .true., .true.,
moist_adv_opt                         = 2,       2,       2,
scalar_adv_opt                        = 2,       2,       2,
chem_adv_opt                          = 2,       2,       2,
tke_adv_opt                           = 2,       2,       2,
time_step_sound                       = 4,       4,       4,
h_mom_adv_order                       = 5,       5,       5,
v_mom_adv_order                       = 3,       3,       3,
h_sca_adv_order                       = 5,       5,       5,
v_sca_adv_order                       = 3,       3,       3,
/

&bdy_control
spec_bdy_width                        = 5,
spec_zone                             = 1,
relax_zone                            = 4,
specified                             = .true., .false., .false.,
nested                                = .false., .true., .true.,
/

&grib2
/

&namelist_quilt
nio_tasks_per_group = 0,
nio_groups = 1,
/

&chem
kemit                                 = 7,
```

```
ne_area                             = 100,
chem_opt                            = 106, 106, 106,
bioemdt                             = 15., 15., 15.,
photdt                              = 15, 15, 15,
chemdt                              = 0, 0, 0,
io_style_emissions                  = 2,
emiss_inpt_opt                      = 1, 1, 1,
emiss_opt                           = 3, 3, 3,
chem_in_opt                         = 1, 1, 1,
phot_opt                            = 3, 3, 3,
gas_drydep_opt                      = 1, 1, 1,
aer_drydep_opt                      = 1, 1, 1,
bio_emiss_opt                       = 3, 3, 3,
gas_bc_opt                          = 1, 1, 1,
gas_ic_opt                          = 1, 1, 1,
aer_bc_opt                          = 1, 1, 1,
aer_ic_opt                          = 1, 1, 1,
gaschem_onoff                       = 1, 1, 1,
aerchem_onoff                       = 1, 1, 1,
wetscav_onoff                       = 0, 0, 0,
cldchem_onoff                       = 0, 0, 0,
vertmix_onoff                       = 1, 1, 1,
chem_conv_tr                        = 1, 1, 1,
seas_opt                            = 2,
dust_opt                            = 3,
biomass_burn_opt                    = 0, 0, 0,
plumerisefire_frq                   = 30, 30, 30,
have_bcs_chem                       = .true., .false., .false.,
aer_ra_feedback                     = 1, 1, 1,
aer_op_opt                          = 1, 1, 1,
!opt_pars_out                        = 1,
!diagnostic_chem                     = 1, 1, 1,
!chemdiag                            = 1, 1, 1,
!diagnostic_dep                      = 1,1,1,
/
```

D.2. Modifications to module_dep_simple.F

From line 1900:

```
if( trim(mminlu_loc) == 'USGS' .and. &
config_flags%num_land_cat .ne. 33) then
        luse2usgs(:) = (/ (iland,iland= &
        1,config_flags%num_land_cat) /)
elseif( trim(mminlu_loc) == 'USGS' .and. &
config_flags%num_land_cat == 33) then
        luse2usgs(:) = (/ 1,2,3,4,5,6,7,8,9,10, &
        11,12,13,14,15,16,17,18,19,20, &
        21,22,23,24,25,25,25,25,25,25, &
        1,1,1 /)
elseif( trim(mminlu_loc) == 'MODIFIED_IGBP_MODIS_NOAH' ) then
        luse2usgs(:) = (/ 14,13,12,11,15,8,9,10,10,7, &
        17,4,1,5,24,19,16,21,22,23 /)
endif
```

D.3. Modifications to dry_dep_driver.F

See the Supplementary Material to Article 2.

D.4. Changes to URBPARM.TBL

In the following, changes made to the input parameters to the single-layer urban canopy
model (sf_urban_physics=1) are listed.

```
# The parameters in this table may
# vary greatly from city to city.
# The default values are probably
# not appropriate for any given city.
# Users should adapt these values
# based on the city they are working with.


# Urban Parameters depending on Urban type
# USGS


Number of urban categories: 3


#
#  Where there are multiple columns of values,
#  the values refer, in order, to:
# 1) Low density residential,
# 2) High density residential,
# 3) Commercial
#
#  Index:     1            2            3
#  Type:  Low-dens Res, Hi-dens Res, Commercial
#


#
# ZR:   Roof level (building height)  [ m ]
#       ( sf_urban_physics=1)

# default: ZR: 5.0,   7.5,   10.0
ZR: 5.3,   13.3, 6.0


#
# SIGMA_ZED:   Standard Deviation of roof height   [ m ]
#       ( sf_urban_physics=1)
```

```
# default : SIGMA_ZED: 1.0,   3.0,   4.0
SIGMA_ZED:  4.4 ,  6.3 ,  5.2


#
# ROOF_WIDTH:   Roof ( i . e . ,  building )  width   [ m ]
#       ( sf_urban_physics =1)


# default : ROOF_WIDTH:  8.3 ,  9.4 ,  10.0
ROOF_WIDTH:  9.7 ,  17.2 ,  17.9


#
# ROAD_WIDTH:   road  width   [ m ]
#       ( sf_urban_physics =1)
#

# default : ROAD_WIDTH:  8.3 ,  9.4 ,  10.0
ROAD_WIDTH:  17.5 ,  17.5 ,  17.5


#
# FRC_URB:   Fraction  of  the  urban  landscape  which  does  not  have  natural
#            vegetation . [ Fraction ]
#       ( sf_urban_physics =1,2,3)
#

# default : FRC_URB:  0.5 ,  0.9 ,  0.95
FRC_URB:  0.46 ,  0.72 ,  0.54


#
# CAPR:   Heat  capacity  of  roof   [ J m{−3} K{−1} ]
#       ( sf_urban_physics =1,2,3)
#

# default : CAPR:  1.0E6 ,  1.0E6 ,  1.0E6,
CAPR:  1.32E6 ,  1.32E6 ,  1.32E6


#
# CAPB:   Heat  capacity  of  building  wall  [ J m{−3} K{−1} ]
#       ( sf_urban_physics =1,2,3)
```

```
#

# default : CAPB:  1.0E6,  1.0E6,  1.0E6,
CAPB:  1.32E6,  1.32E6,  1.32E6


#
# AKSR:   Thermal  conductivity  of  roof  [  J  m{−1}  s{−1}  K{−1}  ]
#       ( sf_urban_physics =1,2,3)
#

# default . AKSR:   0.67,  0.67,  0.67,
AKSR:   0.695,  0.695,  0.695


#
# AKSB:   Thermal  conductivity  of  building  wall  [  J  m{−1}  s{−1}  K{−1}  ]
#       ( sf_urban_physics =1,2,3)
#

# default ; AKSB:   0.67,  0.67,  0.67,
AKSB:   0.695,  0.695,  0.695
```

D.5. Example R function for spectral decomposition of air pollutant time series

```
# timestamp: array with time and date of observation
# (best: POSIXct-format)
# timeseries: array with observations corresponding
# to the respective entry in the timestamp array
# output: data.frame with 3 columns (values, component, date)
# naming of components:
# 01_TS: original time series
# 02_LT: long term component
# 03_SY: synoptic component
# 04_DU: diurnal componont
# 05_ID: intra-diurnal component

decompose_function <- function(timestamp, timeseries){
library(kza)

# timeseries needs to be ordered by date
        id <- timeseries - kz(timeseries, 3,3)
        du <- kz(timeseries, 3,3) - kz(timeseries, 13,5)
        sy <- kz(timeseries, 13,5) - kz(timeseries, 103,5)
        lt <- kz(timeseries, 103,5)

        dat <- data.frame(values = c(timeseries, id, du, sy, lt),
                component = c(rep("01_TS", length(timeseries)),
                rep("05_ID", length(timeseries)),
                rep("04_DU", length(timeseries)),
                rep("03_SY", length(timeseries)),
                rep("02_LT", length(timeseries))
                ),
                date = rep(timestamp, 5)
                )

        return(dat)
}
```

Acknowledgements

Selbstständigkeitserklärung

Hiermit erkläre ich, dass ich diese Arbeit selbständig verfasst und keine anderen als die von mir angegebenen Hilfsmittel genutzt habe. Ich versichere weiterhin, die Arbeit nicht schon einmal in einem fr'uheren Promotionsverfahren eingereicht zu haben.

Frankfurt, im August 2018,

Friderike Kuik